IMPERIAL COLLEGE OF SCIENCE AND TECHNOLOGY

(University of London)

DEPARTMENT OF CHEMISTRY

EFFECT OF PRETREATMENT ON THE STATE AND REACTIVITY OF ALUMINA-SUPPORTED PLATINUM-IRIDIUM CATALYSTS

by

Christopher Charles Arthur Riley, B.Sc., ARCS

Submitted for the Degree of Doctor of Philosophy

and for the Diploma of Imperial College

MARCH, 1987

ABSTRACT

Alumina-supported platinum-iridium bimetallic catalysts and their monometallic counterparts have been subjected to various oxidation-reduction pretreatments at selected temperatures up to 740K. The effect of each pretreatment has been assessed with the aid of the following techniques: Temperature-Programmed Reduction (TPR), Temperature-Programmed Oxidation (TPO), Hydrogen Thermal Desorption, Hexane Thermal Desorption, Transmission Electron Microscopy (TEM) and X-ray Photoelectron Spectroscopy (XPS). All temperature-programmed experiments were performed in a micro-reactor system equipped with a computer-interfaced quadrupole mass spectrometer for time-resolved multiple product analysis. It was found that highly dispersed (< 2nm in size) bimetallic clusters were produced after the supported precursor salts were reduced at a temperature of 610K. Catalysts prepared in this way showed an improved aromatisation activity when compared to monometallic platinum catalysts. The increased resistance of such alloys to catalyst fouling has been shown to be due largely to the residual hydrogenolysis activity of the iridium component. However, it was found that the hydrogenolysis activity of the bimetallic clusters was suppressed following reduction at 740K, possibly as a result of the formation of a Strong Metal-Support Interaction (SMSI). An initial oxidation at a temperature of 740K followed by reduction at 610K caused the formation of large (~10nm) iridium-rich crystallites with a surface enriched in platinum, as well as a highly dispersed (< 2nm) platinum-rich phase. A limited redispersion of the large particles occurred during reduction, producing dispersed clusters with an iridium-enriched exterior. This might account for the higher catalyst hydrogenolysis activity observed following this pretreatment. Such increased activity was not observed when the subsequent reduction was performed at a temperature of 740K. Under these conditions the dispersed clusters are thought to form an SMSI state whilst the larger crystallites undergo thermal annealing.

ACKNOWLEDGEMENTS

I would like to thank the SERC for the award of a research studentship and Professor W.J. Albery for the use of the facilities of the Department of Physical Chemistry, Imperial College.

I wish to thank especially my supervisor, Dr. D.O. Hayward, for his advice and support throughout the course of this work.

I am also grateful to Dr. K. Senkiw for his assistance with computing matters and Dr. H. Flower for providing the TEM micrographs.

I would also like to express my gratitude to Mrs. O. Hopkins for her accurate typing of the manuscript and finally I would like to thank Ruth for her continuous encouragement during the past four years.

CONTENTS

PAGE

CHAPTER ONE

General Introduction

Catalytic reforming is one of the major conversion processes operating in a modern oil refinery where it is used to increase the octane number of petroleum naptha feedstocks. When the process was first introduced by Universal Oil Products in 1949 the catalyst employed was alumina-supported platinum in which the metal exists on the oxide support as small crystallites with the majority of the metal atoms lying in the surface of the particles. However, over the intervening years the original monometallic platinum catalysts have been largely superceded by various bimetallic and multimetallic systems in which platinum still remains the major metal constituent. The active centres in these catalysts may well be highly dispersed alloy clusters. One combination which has made a particularly major industrial impact in reforming is the Pt-Ir/alumina system discovered by Sinfelt and coworkers at Exxon in 1976.

Despite the importance of this combination many aspects of the Pt-Ir/alumina system remain incompletely understood. In particular, the way in which the performance of the catalyst is influenced by the pretreatment conditions used during catalyst manufacture and activation have not been reported in detail. With this in mind, the objective of this thesis has been to characterise the effects of various pretreatment conditions on the state and reactivity of Pt-Ir/alumina catalysts through the utilisation of several chemical and physical probes. In this context the phrase 'catalyst state' will be used as a general term for the physical nature of the supported metal particles, whilst the expression 'catalyst reactivity' will be used in preference to 'catalyst activity' since this designation emphasises the interaction of the catalyst with all the reactant molecules employed in each part of this study.

The details of the apparatus used for this examination are contained in Chapter Two, the major part being devoted to a description of the micro-reactor system in which most of the pretreatments were performed. Chapter Three describes the method of application of the metals onto the alumina support and also details

the various pretreatment conditions investigated. Catalyst manufacture and activation frequently employ an initial oxidation step followed by a reduction pretreatment and these are discussed in Chapter Four where the results of temperature-programmed reduction and oxidation experiments are described. The influence of the conditions of reduction are then assessed in Chapter Five using hydrogen temperature-programmed desorption, whilst the effects of the pretreatments are further investigated in Chapter Six by the use of transmission electron microscopy and X-ray photoelectron spectroscopy. Chapter Seven is concerned with the influence of the pretreatment conditions on the performance of the catalyst through the use of hexane temperature-programmed desorption. The results are interpreted in terms of the information gathered in the preceding Chapters.

It should be noted that whilst the Chapters containing the results necessarily combine to produce a unified investigation, in format each Chapter is essentially self-contained. Hence each of these Chapters is subdivided into Introduction, Experimental, Results and Interpretation, Discussion and Summary sections, and the appropriate literature surveys are presented in each Chapter when necessary. Furthermore, the Results and Interpretation sections do not merely list the results obtained, but also evaluate them in a wider context. It should be noted that each Discussion section forms a part of an ongoing discussion which serves to unify the separate Chapters. Finally, the main findings of this investigation are discussed in general terms in Chapter Eight.

The aim of this study has been to improve the level of our understanding of the Pt-Ir/alumina system in the hope that such knowledge will assist in the development of new, improved catalysts and conversion processes.

CHAPTER TWO

Apparatus

This Chapter contains a description of the micro-reactor system in which temperature-programmed reactions were studied, together with a brief account of the ESCALAB system used to obtain X-ray photoelectron spectra. Specific points of experimental procedure will not be covered here but these can be found in the appropriate Introduction and Experimental sections contained in subsequent Chapters.

2.1 The Micro-Reactor System

2.1.1 General Outline

A schematic diagram of the micro-reactor system is shown in Fig. 2.1. In general, the system allows the following types of experiment to be carried out:

a) Insitu catalyst pretreatment using gas pressures of around 1 atm. and temperatures from 298K to ~900K.

b) Catalyst characterisation using adsorbate-pulse and temperature-programmed techniques.

c) Reaction studies using feedstock either pulsed or continuously fed over the catalyst sample, in either a single pass or recycled manner.

The apparatus can be dividied into four sections as outlined below.

i) The Carrier-Gas Flow System which allows a constant flow of inert gas to be maintained over the catalyst. Provision is made for reactant gases to be either fed continuously, or pulsed, into the carrier-gas stream.

ii) The Reactant Gas Handling System which is used for the preparation of reactant gas mixtures that can then be injected as pulses into the carrier-gas stream.

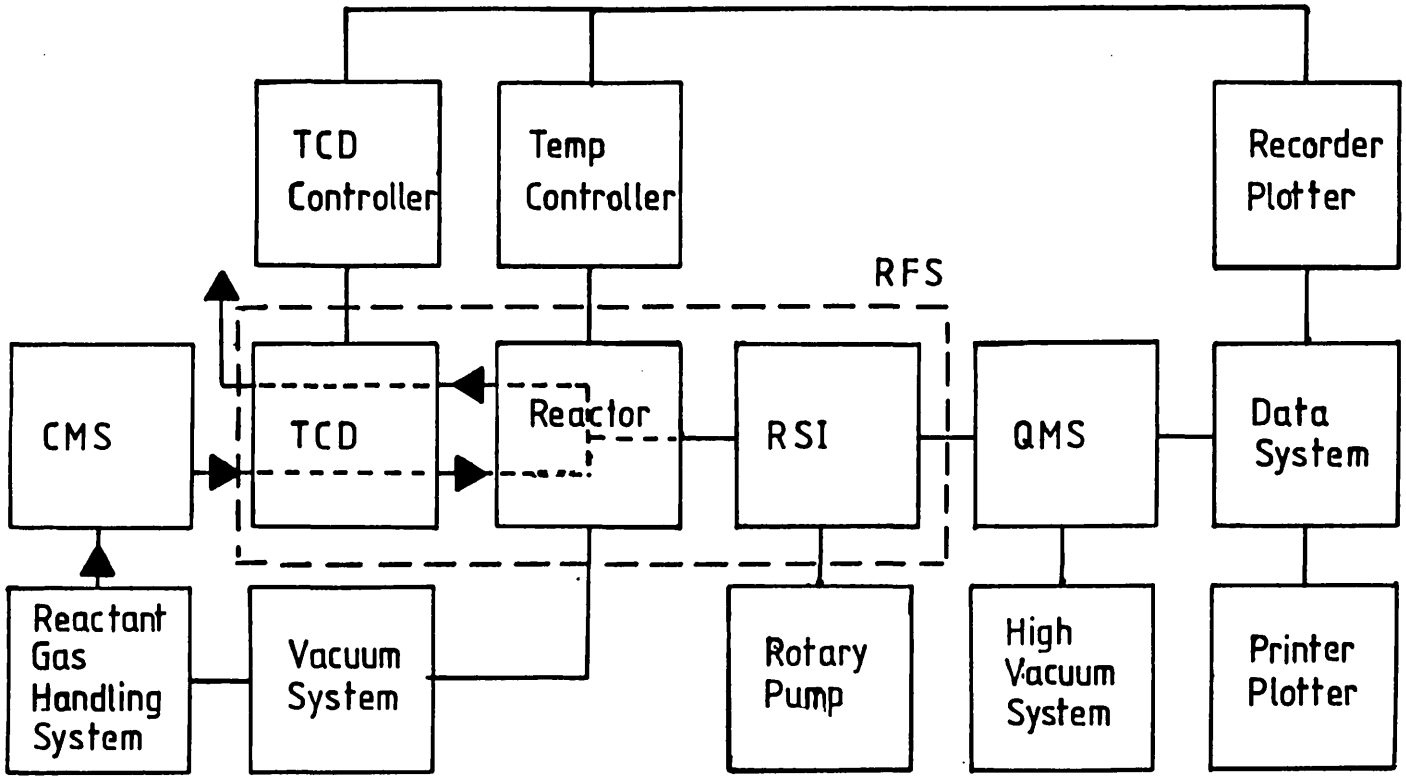

CMS Carrier-Gas Manipulation Section
RSI Reactor-Mass Spectrometer Interface
TCD Thermal Conductivity Detector
QMS Quadropole Mass Spectrometer
RFS Reactor Feed Section

Fig. 2.1: The Micro-Reactor System - Schematic

iii) The Reactor.

iv) The Quadrupole Mass Spectrometer Detector.

2.1.2 The Carrier-Gas Flow System (CFS)

A schematic diagram of the CFS is shown in Fig. 2.2. For the purposes of discussion the system can be conveniently sub-divided into two sections, namely the Carrier-Gas Manipulation Section and the Reactor Feed Section.

i) Carrier-Gas Manipulation Section (CMS)

The CMS controls the flow rate of the carrier-gas as well as allowing reactants, such as hydrogen or oxygen, to be continuously fed into the carrier stream.

The flow lines for this section are constructed from $\frac{1}{8}$in.o.d. copper tubing supplied by Phase Separations Limited. All the valves used in the CMS have bodies constructed from brass and were manufactured by the Whitey Valve Company Limited. Two types were used; three-way ball valves allowing selection of one of two flow lines and simple on/off valves. Most valves and couplings were fitted with Swagelok compression fittings, which provide a leak-tight vacuum-compatible seal.

Various hydrogen/argon and oxygen/argon gas mixtures can be obtained from separate cylinder gases (BOC HP grade), by using the appropriate settings of valves V_{24}, V_{25}, V_{26}, V_{27}, V_{22}, V_{23}, V_5, and V_6 and the relative settings of the two Porter mass flow controllers. The gases are purified in situ by passage over moisture traps containing activated zeolite beds and oxygen traps, both supplied by Phase Separations Limited. The traps were regenerated each month. Valves V_{27} and V_{23} are used to prevent oxygen feed contacting oxygen traps O_1 and O_2. The Quadrupole Mass Spectrometer (QMS) (see Section 2.1.5) was used to monitor impurity levels in the carrier stream.

Flow meters F_1 and F_2 (located in the RFS) were supplied by Jencons (Scientific) Limited and were calibrated using soap bubble flow meters. The former is primarily used for the measurement of the carrier stream flow rate during trap regeneration and is only suitable for measuring flow rates in excess of 30 ml min^{-1}. The

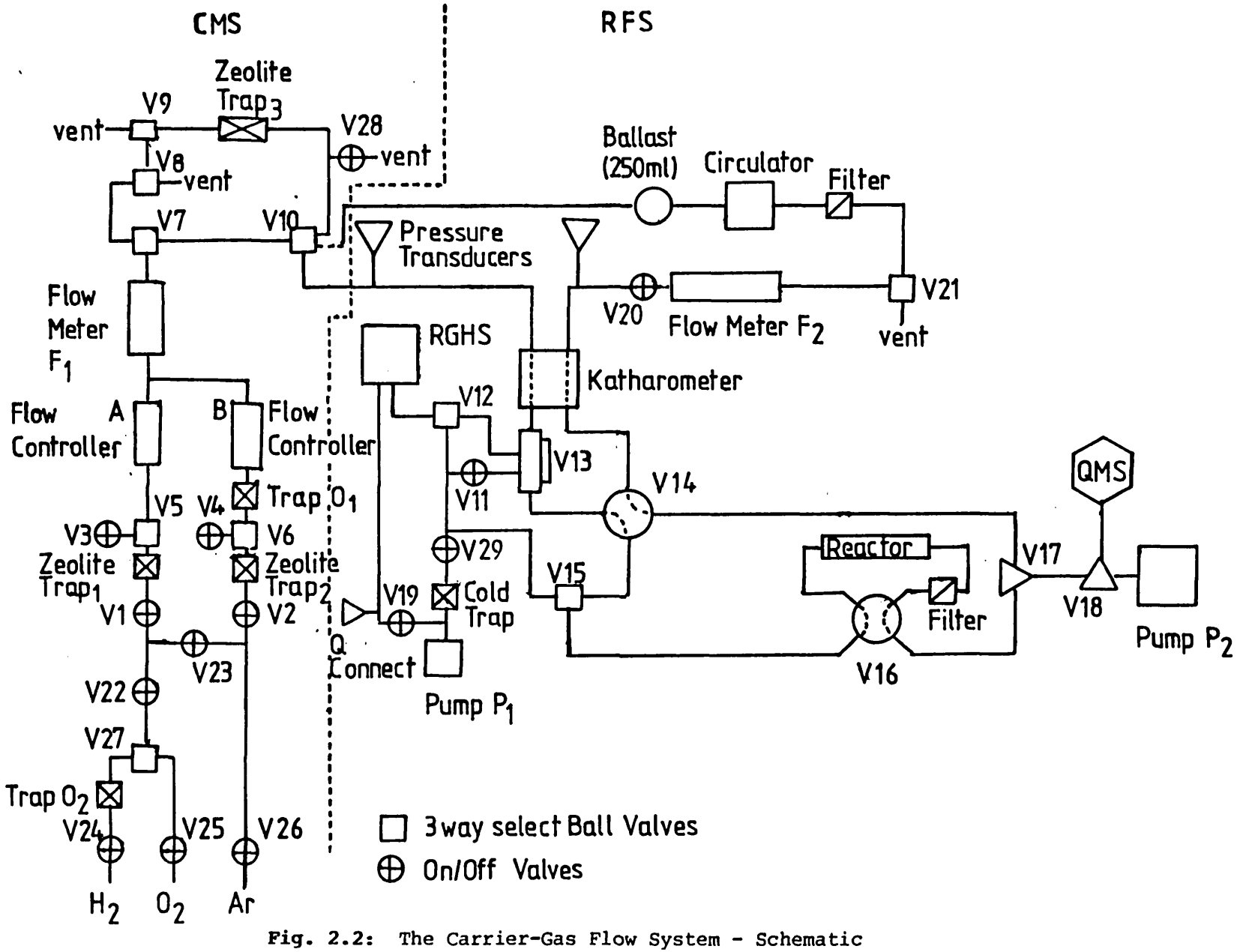

Fig. 2.2: The Carrier-Gas Flow System - Schematic

latter is used for monitoring the lower flow rates ($\leq$ 30 ml min^{-1}) used for most experiments.

ii) Reactor Feed Section (RFS)

This contains the gas sample inject valve, V_{13}, the reactor, the various reactor bypass circuits and the Reactor-Mass Spectrometer Interface (RSI). In addition, this section also contains a katharometer detector and facilities for reactant/product recirculation experiments. However, these were not used in the present study and the system was operated with valve V_{21} set to the vent position.

To reduce the reaction of injected gases or products with the walls of the flow lines or valve bodies, the components in this section were constructed from stainless steel. The dead volume of this part of the system was kept to a minimum by using $\frac{1}{16}$in. o.d., 0.5mm i.d. tubing for the flow lines linking V_{13}, V_{14}, V_{15}, V_{16}, the reactor, V_{17} and V_{18} and the length was kept as short as possible.

The gas sample inject valve, V_{13} and the two bypass valves V_{14} and V_{16} were manufactured by Condyne Valves Limited. The valves consist of a central rod fitted with Viton o-rings which allow the interconnection of various ports on the outside of the valve body by altering the rod position. The gas sample inject valve was fitted with a dose volume loop (0.25 ml) which permitted known amounts of reactant to be introduced into the gas stream. The reactor bypass valve enabled the reactor to be bypassed which was necessary for control experiments or for replacing catalyst samples. The other bypass valve, V_{14}, allowed both the reactor and the mass spectrometer to be bypassed, thus permitting the reactor tube to be evacuated by the E2M2 Edwards rotary pump, P_1, with the appropriate settings of valves V_{29} and V_{15}.

The Reactor Spectrometer Interface produces the pressure drop ($1000 \rightarrow 1 \times 10^{-6}$ mbar) required for the operation of the QMS. The interface consists of two micro-needle valves supplied by SGE Limited which are differentially pumped by the E2M2 Edwards rotary pump, P_2. Like P_1 this pump was fitted with an alumina-charged foreline trap to minimise back streaming of pump oil. The primary needle valve, V_{17}, was set to produce a pressure of around 2×10^{-2} mbar in this pumped region whilst the needle valve adjacent to the high vacuum

chamber was adjusted to give a pressure in the chamber of around 1 x 10^{-6} mbar. To prevent product (e.g. H_2O) condensation, the entire RSI from the reactor outlet to the QMS vacuum chamber was heated by an electrical heating tape to a temperature of around 330K. By keeping the length of the interconnecting tubing to a minimum (~10cm) the response time from the reactor to the detector was kept small at about one second. The total response time from the gas sample inject valve to the QMS was around three seconds.

Two pressure transducers supplied by Foxboro Instruments Limited enabled the reactor inlet and outlet pressures to be measured. These pressure transducers allowed the condition of the sample bed to be monitored since the pressure difference across the sample was much reduced when undesirable 'cracks' were present in the catalyst bed.

2.1.3 The Reactant Gas Handling System (RGHS)

A schematic diagram of the RGHS is shown in Fig. 2.3. The system enables a gaseous reactant, or a mixture of gaseous reactants, to be prepared and then passed over the catalyst sample. Vapours from liquids (e.g. hexane) can also be injected into the carrier stream provided the liquid exerts a sufficient vapour pressure at around room temperature. Furthermore, the system allows different gases to be passed sequentially over the sample, a common requirement for gas titration studies (e.g. H_2/O_2).

The RGHS is mainly constructed from glass (Pyrex) and uses conventional greased ground-glass taps as well as greaseless taps. The latter were supplied by Youngs and consist of an external glass barrel surrounding a glass piston fitted with Viton o-rings to create the vacuum-tight seal. The greaseless taps were used where the presence of a reactive gas (e.g. hydrocarbons) would attack and dissolve the vacuum grease.

The RGHS is pumped by a mercury diffusion pump backed by a rotary pump. Several cold traps are provided to ensure that reactant contamination by either mercury or pump oil vapour does not occur. Base pressures of less than 1 x 10^{-3} mbar were routinely obtained, as measured by an Edwards PR10K Pirani Gauge.

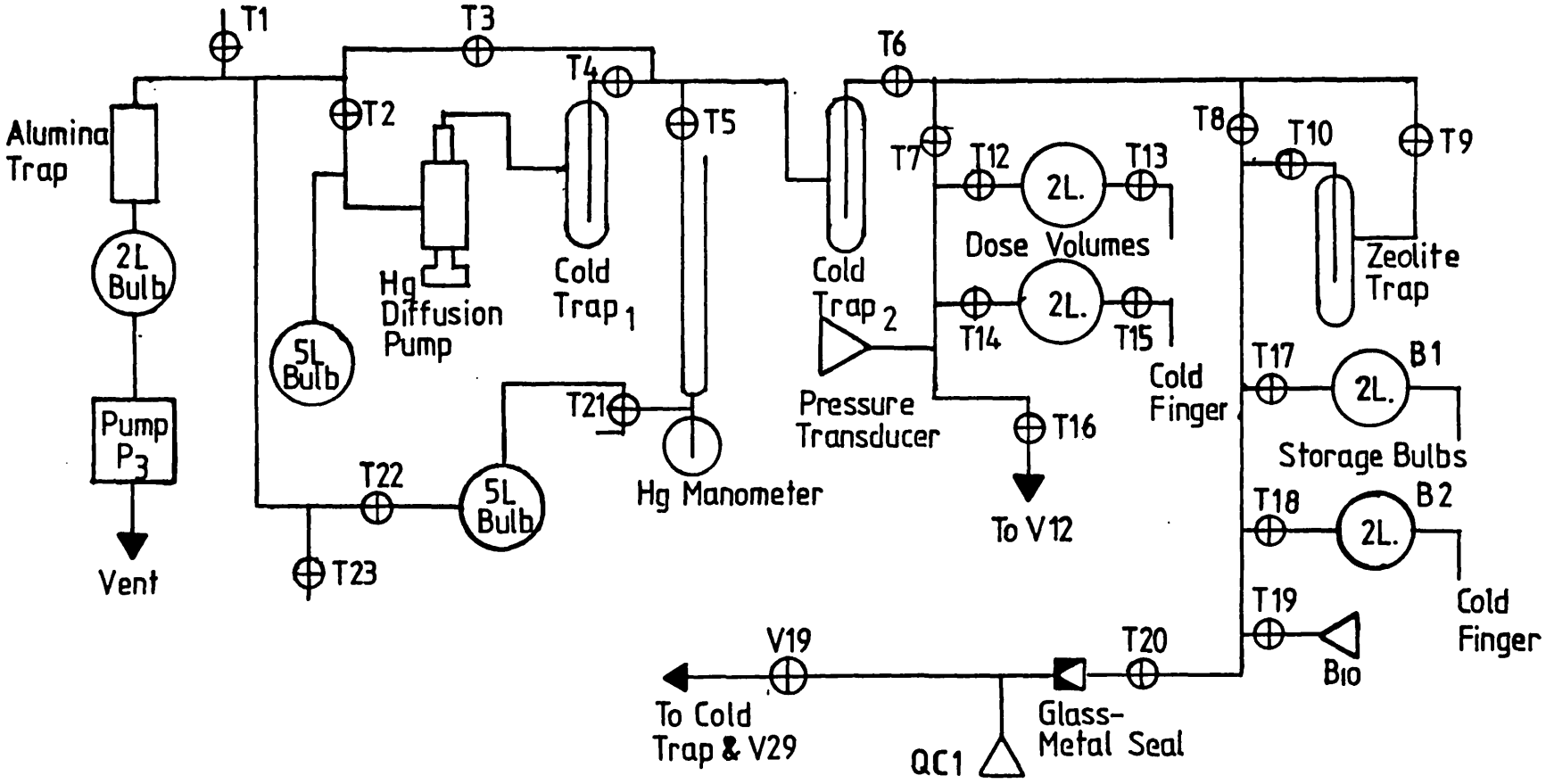

Fig. 2.3: The Reactant Gas Handling System - Schematic

Admission of gas samples from lecture bottles and gas cylinders could be made via the quick connection socket, QC1. The glass-metal seals used were of the Kovar-Pyrex type supplied by Jencons (Scientific) Limited. Gas samples obtained from sufficiently volatile liquids (e.g. hexane) were admitted via the B10 port. These samples were purified by subjecting them to several freezing-pumping-thawing cycles before they were stored in the storage bulbs, B_1 and B_2. Condensable samples were transferred from the various storage bulbs to the dose volumes by freezing them out in the appropriate cold finger.

Reactant sample gas pressures in the range ~1 mbar to 1000 mbar were measured with a Foxboro pressure transducer which was calibrated for various reactant gases against a mercury manometer. The response was found to vary linearly with pressure and was virtually independent of the gas used. The quantity of reactant gas injected was calculated from a knowledge of the reactant pressure and the volume of the sample loop on valve, V_{13} (0.25 ml), assuming ideal gas behaviour. The large dose volumes (2000 ml) allowed a fairly constant amount of reactant to be dosed into the carrier-gas stream for large numbers of reactant pulses.

2.1.4 The Reactor

A diagram of the reactor furnace and its holder is shown in Fig. 2.4. The furnace consists of three concentric tubes held in place by aluminium end caps. These are locked in position by three tie rods running the length of the tubes. The innermost tube is made from fused quartz and has nichrome heating tape wrapped around the central 6 cms of the tube. The tape is held in position by heat resistant asbestos-substitute cloth which is wrapped around the quartz. This arrangement constitutes the heating section of the furnace. The second tube is made from copper and the space between this and the inner tube is packed with silica wool. The outermost tube is made from heavy gauge steel and the space between this and the central tube is filled with glass wool. The two outermost sections serve to insulate the furnace windings. The whole tube arrangement is supported on an aluminium frame.

A proportional band temperature programmer/controller supplied by Newtronic Controls International Limited was used to control the

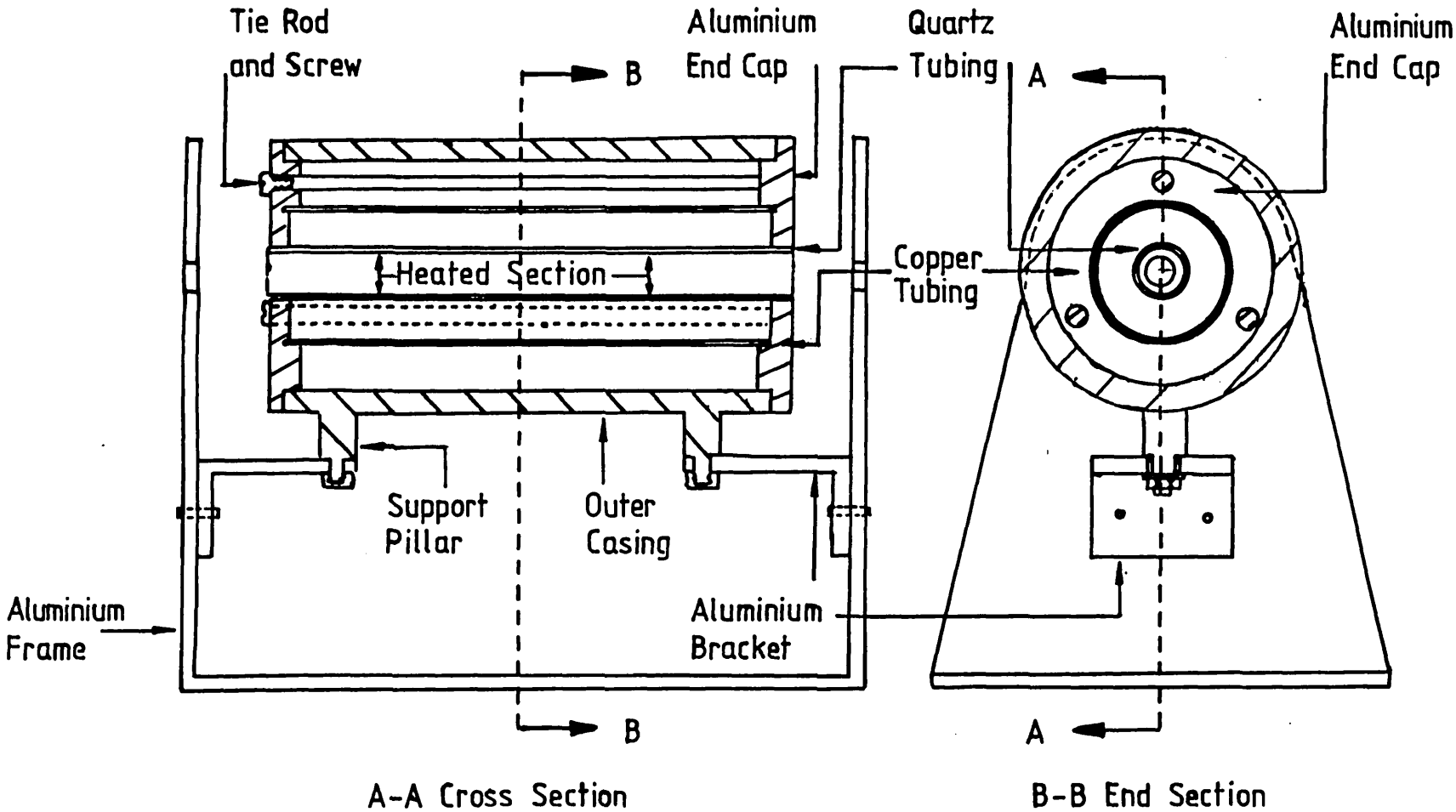

Fig. 2.4: The Reactor Furnace

furnace temperature. Linear heating rates from 0.1 to ~100Kmin^{-1} could be obtained with a maximum temperature of ~900K. The controller was used to maintain the catalyst sample at a constant temperature. The furnace thermocouple, used to control the temperature programmer, was made from 0.125 mm diameter chromel/alumel wire and was placed between the innermost quartz furnace tube and the reactor tube. The junction was located adjacent to the central section of the furnace windings.

The reactor assembly is shown in Fig. 2.5. The reactor tube consists of a precision ground quartz tube (1/4 in. o.d., 4 mm i.d.) supplied by Jencons (Scientific) Limited. This fits inside the inner quartz furnace tube and a gas tight seal to the Swagelok end fittings is made with disposable 1/4 in. Teflon ferrules, supplied by The North London Valve and Fitting Company Limited. The ferrule seals were helium leak tested using the QMS. The reactor tube outlet is joined to the 1/16 in. o.d. stainless steel tubing using a 1/4 in. to 1/16 in. reducing union. A 5μm Teflon filter plug, supplied by Phase Separations Limited, was placed in the machined well in this fitting to prevent catalyst particles damaging the delicate needle valves downstream.

The catalyst sample (50 mg) was placed at the centre of the reactor tube using a preweighed loading tube, and was held in place with silica wool plugs. Care was taken to ensure that cracks were not present in the sample bed. The catalyst thermocouple was made from 0.125 mm dia. chromel/alumel wire which entered the tube via one arm of the stainless steel tee-piece. The thermocouple junction was located at the front of the catalyst bed. The reactor tube dead volume was reduced to a minimum by the ceramic insulator rod of the catalyst thermocouple on the one side of the catalyst and by inserting a quartz rod on the other side.

2.1.5 The Quadrupole Mass Spectrometer (QMS) Detector

The QMS detector supplied by V.G. Quadrupoles Limited (model Spectralab SX200) was contained in a stainless steel high vacuum chamber of standard design. The chamber was pumped by a combination of an E2M5 Edwards rotary pump and an Edwards Diffstak 63/150 polyphenyl ether diffusion pump. The latter has a high efficiency water cooled baffle which permitted high vacuum (~3 x 10^{-9} mbar) to be

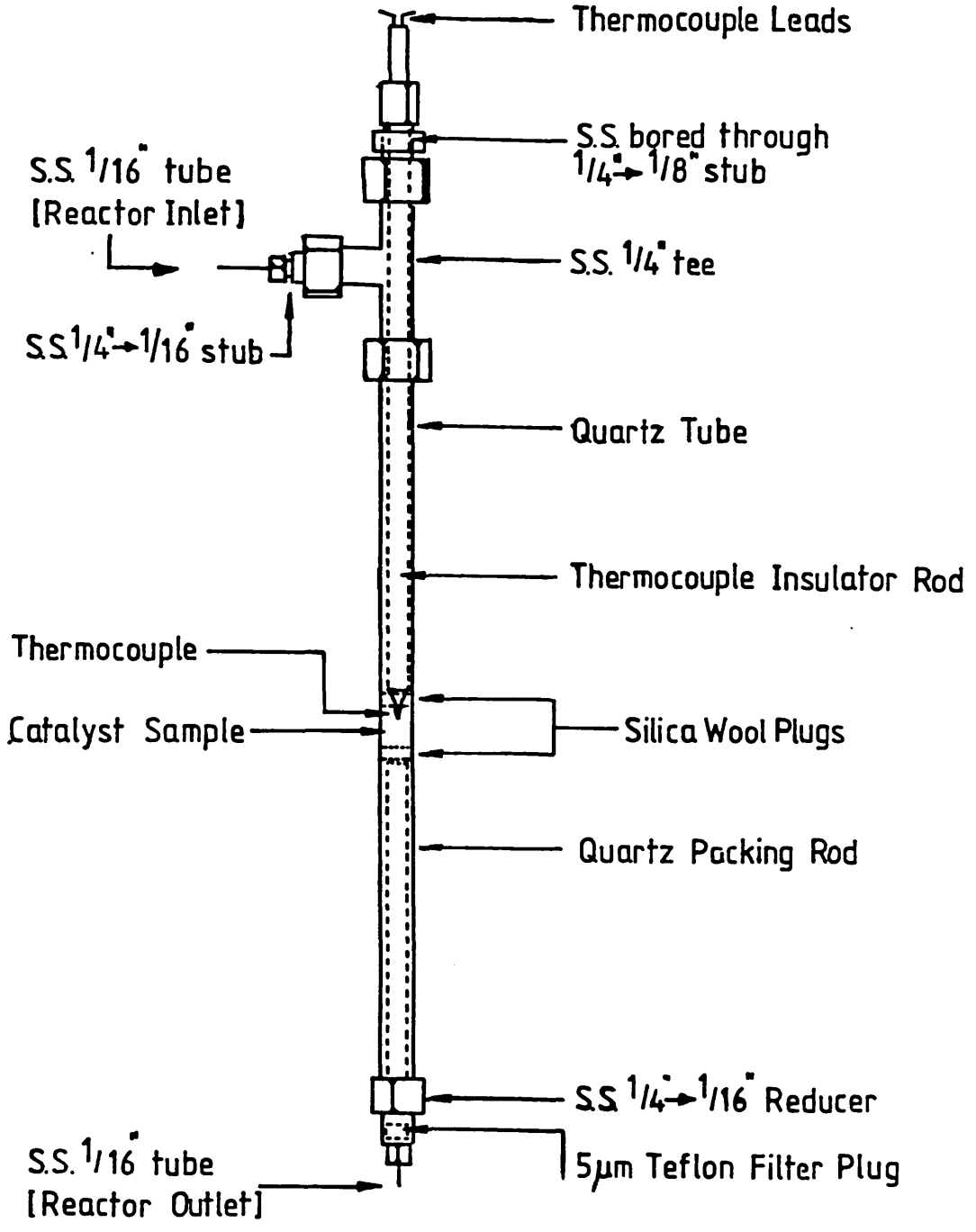

Approx. scale 1: 1·5

Fig. 2.5: Reactor Tube Assembly

obtained without a liquid nitrogen cooled trap. The vacuum chamber is connected to the reactor outlet by the RSI described in section 2.1.2.

The QMS is controlled by a microcomputer (Apple IIe) fitted with a real time clock. This combination allowed time-resolved monitoring of up to sixteen different gaseous species to be performed at the same time. Experimental data stored on disks were displayed graphically using software produced by V.G. Quadrupoles Limited and processed using more specifically devised software. The latter also enabled data to be plotted out on a Rikadenki RY-101 digilogue plotter.

One drawback of the detection system arose from the use of the mass 5 signal as a zero setting for the QMS FET amplifier. This effectively precluded the use of helium as a carrier gas since large mass 4 signals produced a large negative background over the entire mass range as a result of the large mass 4 signal 'tailing' into the mass 5 signal region. For this reason, argon had to be used as the inert carrier gas. However, this had one advantage in that it allowed helium to be used for leak detection in the micro-reactor system.

2.2 The ESCALAB System

2.2.1 General Outline

The ESCALAB-MKII (made by Vacuum Generators Limited) is a surface analysis sytem which has facilities for X-ray Photoelectron Spectroscopy (XPS), Auger Electron Spectroscopy (AES), Ultraviolet Photoelectron Spectroscopy (UPS), Secondary Ion Mass Spectroscopy (SIMS), Ion Scattering Spectroscopy (ISS) and Low Energy Electron Diffraction (LEED).

A diagrammatic plan view of the instrument is shown in Fig. 2.6. The ESCALAB can be divided into three main sections, namely:

i) The analysis chamber.
ii) The preparation chamber (prepchamber).
iii) The fast entry air-lock.

The analysis chamber contains all the surface analytical techniques apart from LEED which is carried out in the prepchamber.

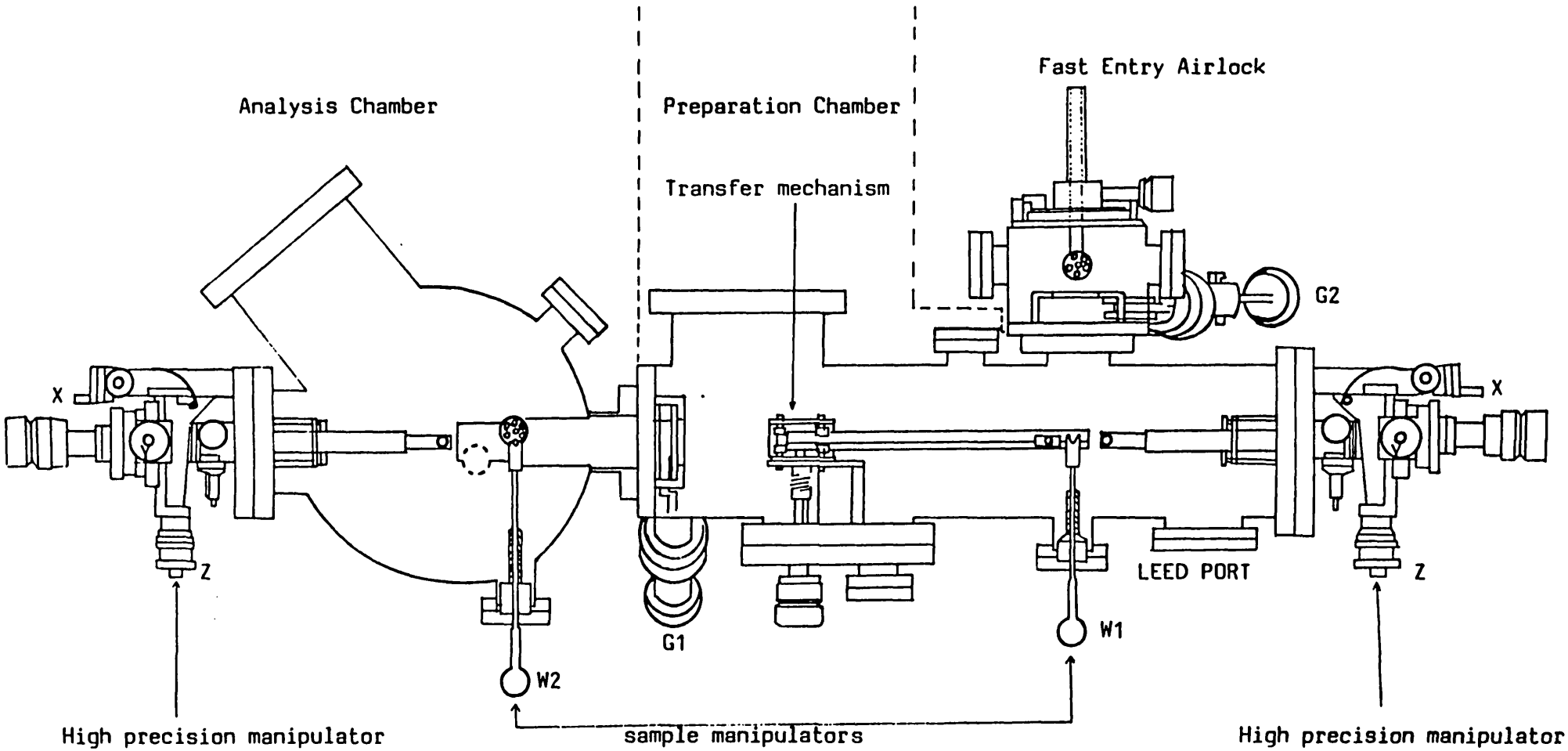

Fig. 2.6: Plan View of the ESCALAB

The fast entry air-lock enables samples to be introduced into the apparatus without breaking the vacuum. It also contains a reaction cell which allows high pressure (~1000 mbar) sample pretreatments to be performed. However, at the time that the experiments were carried out this cell contained a leak and hence all catalyst pretreatments were carried out inside the prepchamber. A transfer mechanism in the prepchamber enables samples to be moved between the various sections of the instrument, whilst two UHV compatible gate valves, G1 and G2 isolate the prepchamber from the rest of the apparatus.

The analysis chamber is pumped by an Edwards E04 diffusion pump containing polyphenyl ether pumping fluid and incorporating a CCT100 liquid nitrogen trap. Additional pumping is provided by a titanium sublimation pump and the line is backed by an E2M5 Edwards rotary pump. The prepchamber has a similar pumping line although the diffusion pump is valved so that it can be used for differentially pumping the UV source, the SIMS gun and the ISS gun. The system can be baked at 150-180°C without the X-ray monochromator and at 80-100°C with the monochromator. The pressure in the analysis chamber was routinely maintained in the 10^{-10} mbar region whilst the pressure in the prepchamber tended to be higher, in the 10^{-9} mbar region, because of the use of this chamber for performing sample pretreatments.

2.2.2 Sample Mounting and Pretreatment

To prevent spillage during sample manipulation the powder catalyst samples were contained in a specially constructed tantalum box which is shown in Fig. 2.7. The box was constructed by spot-welding tantalum foil (0.2 mm thick) on to a V.G. stainless steel sample-mounting stub. The hinged lid was opened for catalyst pretreatments and closed using the bellows mounted wobble stick, W1, when the sample was transferred around the apparatus.

With the aid of the wobble stick the sample box could be placed on to the P8 probe which could then be used to heat the sample during the insitu catalyst pretreatments. The probe, which consists of a stainless steel cylinder terminated by a short end-piece made of nickel, contains two stainless steel tubes for cooling by liquid nitrogen, a resistance heater and chromel-alumel thermocouple. The heating, cooling and temperature measurement takes

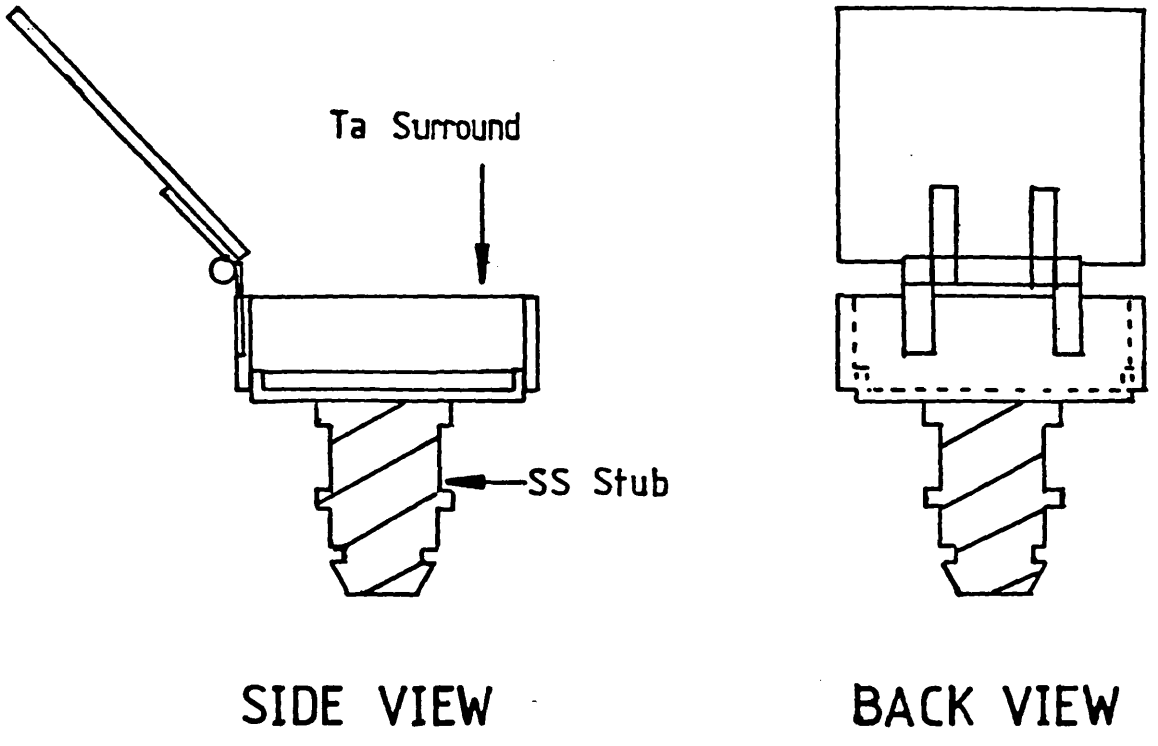

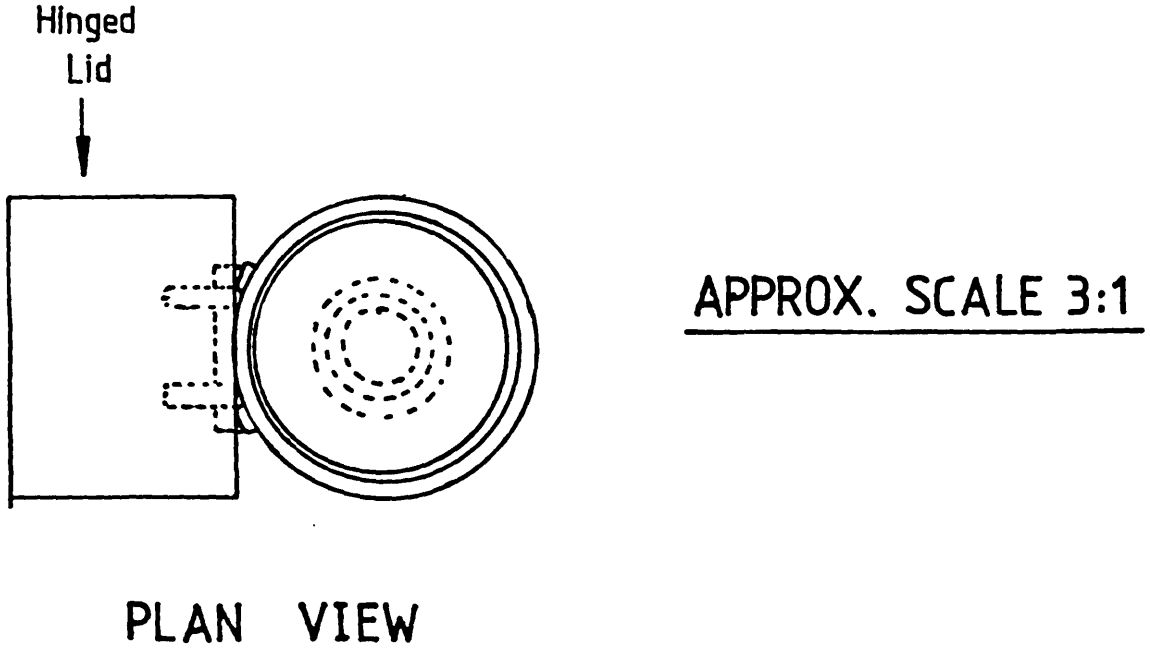

Fig. 2.7: Tantalum Box Sample Holder

place inside the nickel end-piece which had a locating socket for the sample box. The temperature of the sample was measured more accurately using a 0.125 mm diameter chromel-alumel thermocouple mounted vertically on a z-shift above the sample.

During catalyst pretreatment the prepchamber was isolated and filled with the appropriate gas by dosing from the gas-handling section, which is shown schematically in Fig. 2.8. This section consists of two manifolds each with connections for four gas bottles. The system was rough pumped by an Edwards E2M5 rotary pump but lower pressures could be obtained by using the prepchamber diffusion pump. Each manifold has a mixing volume and it is also possible to transfer gas from one manifold to the other. The upper manifold is generally used to handle gases required for the SIMS and ISS guns whilst the lower is reserved for gases used in adsorption and sample pretreatments. The latter manifold is connected to the analysis chamber and prepchamber by high precision leak valves.

2.2.3 XPS Analysis

ESCALAB has facilities for both monochromated and achromatic XPS, but the low levels of metal loading in the samples permitted only the former to be performed. The Mg/Al twin anode X-ray source produced two independent X-ray lines at 1253.6 eV (Mg $K\alpha_1$, α_2) or 1486.6 eV (Al $K\alpha_1$, α_2). The source was operated with an emission current of around 20 mA, the filament being at earth potential and the anode at a potential of 10 kV. The X-ray gun is mounted on a linear motion drive which allows it to be positioned very close to the sample when taking an XPS spectrum. The sample was held on a high precision manipulator which allowed the sample to be moved in the x, y and z directions until the maximum XPS signal was obtained. Two general orientations of the sample are possible; in the 'normal emission' position the analyser collects all the photoelectrons ejected normal to the surface whilst in the 'grazing emission' position, only photoelectrons ejected at an angle of 5-15° to the surface are collected. Only the former method of photoelectron collection was used in this study.

The electron spectrometer consists of a 150° spherical sector analyser which acts as a narrow pass energy filter allowing only electrons with a particular energy to pass through it, this energy

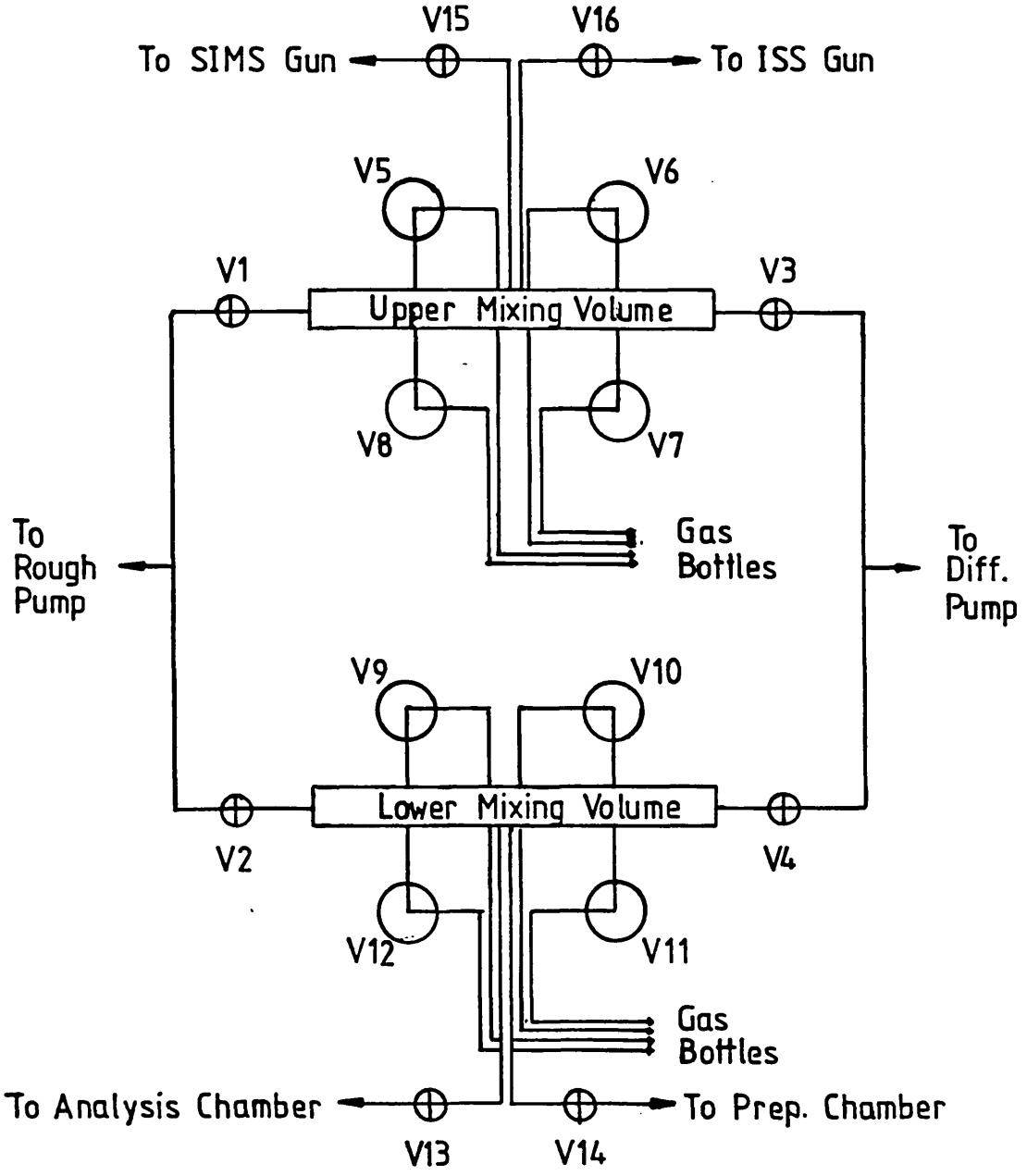

Fig. 2.8: Gas Handling Section of ESCALAB

being controlled by the potential difference between the inner and outer hemispheres of the analyser. The extremely small currents ($\sim 10^{-15}$A) which have to be measured are detected by a Mullard B419AL channel electron-multiplier. The pulses from the channeltron are passed through a series of pulse shaping amplifying and discriminating circuits before being fed into a ratemeter which records the signal. The analyser may be operated in one of two modes. The first employs a Constant Analyser Energy (CAE) and results in a constant peak resolution, ΔE, which is determined by the analyser pass energy setting. The second employs a Constant Retard Ratio (CRR), i.e the ratio of electron kinetic energy to pass energy is held constant. In this mode ΔE is not constant but increases at the higher kinetic energies. The latter mode produces a flatter background at low kinetic energies and is therefore preferred for AES whilst the CAE mode is more useful for XPS. The spectrometer can be operated manually or under computer control using an Apple IIe microcomputer equipped with a VGS 1000 data system.

CHAPTER THREE

Catalyst Preparation and Activation

The aim of this Chapter is to outline the method and results of the catalyst production and give the conditions of the various catalyst pretreatments investigated in this study.

3.1 Catalyst Preparation

This section contains an account of the way in which the catalyst samples were prepared. In this context, the term catalyst preparation is reserved for the incorporation of the platinum and/or iridium component onto the alumina support and does not encompass the various thermal pretreatments which were subsequently applied to obtain the active catalyst system.

The preparation of supported-metal catalysts has received widespread attention in both industrial and academic research groups. Reviews on the subject include those by Moss (1976) and Acres et al. (1981) as well as specialist volumes in many journals; see for example the volume edited by Poncelet et al. (1983). Despite the appearence of many novel catalyst preparation methods there are only three widely used ways by which a metal component can be applied onto a separately produced carrier, namely:

- adsorption from solution
- impregnation and drying
- precipitation of metal in the presence of suspended support.

As discussed by Geus (1983) the adsorption method tends to lead to a more homogeneous metal distribution than the latter two methods, especially when the support is saturated with metal. The main drawback of the adsorption method being the lower quantity of metal which can be deposited. However, since catalyst metal loadings of less than 2% are frequently utilised in the reforming process it is envisaged that the extent of metal adsorption obtained using adsorption will be comparable to that found in industrial reforming catalysts. Therefore, in this study the adsorption technique was employed for the production of the platinum/alumina, iridium/alumina and platinum-iridium/alumina catalysts.

3.1.1 Preparation of the Monometallic Samples

The platinum/alumina and iridium/alumina samples were prepared by the adsorption technique using aqueous solutions of hexachloroplatinic and hexachloroiridic acids, respectively. The metal salts were supplied by Johnson Matthey Chemicals Limited and the alumina used as the support material was a high purity, γ-alumina powder of surface area $90 m^2 g^{-1}$ (BET), supplied by BDH Limited. In all future discussions the γ-alumina will be referred to as alumina.

To obtain reproducible metal loadings the initial concentration of the aqueous metal complex was chosen to be above that required to give a saturation coverage of the alumina. This concentration was determined from adsorption isotherms for the aqueous hexachloroplatinic acid/alumina and hexachloroiridic acid/alumina systems at 293K, which are both shown in Fig. 3.1. The adsorption was carried out with an initial aqueous metal ion concentration in the range $(1.25 - 12.5) \times 10^{-3}$ mol dm^{-3} by placing $20 cm^3$ of each solution in contact with 1g of alumina for 16 hrs. The metal uptakes were determined by filtering off the solid material and analysing the solutions using u.v./visible spectrophotometry (Perkin Elmer Double Beam Spectrometer). Both acids were found to obey Beer's Law over the concentration range of platinum and iridium used at wavelengths of 450nm and 488nm respectively.

Fig. 3.1 shows that the limiting coverage n_m/mol g^{-1} of the iridium adsorbing complex is slightly greater than for the platinum complex indicating an increased degree of interaction of the iridium with the support. On the basis of the data shown in Fig. 3.1 the monometallic catalysts used in this study were produced by contacting 1g of alumina with $20 cm^3$ of 0.01 mol dm^{-3} hexachlorometal solution for 16 hrs at 293K. Following this, the catalyst powder was filtered off, dried and finally stored in a silica gel desiccator. The saturated platinum and iridium catalysts contained 1.48 wt% and 1.61 wt% metal respectively. It was not considered feasible to have equal loadings of the two metals because this would entail having the iridium at below saturation coverage. The sharpness of the 'knee' in the iridium isotherm shows that a very small change in solution concentration could result in a significant difference in the amount of iridium adsorbed and could thereby lead to irreducibility of results. For this reason saturation coverages were always used.

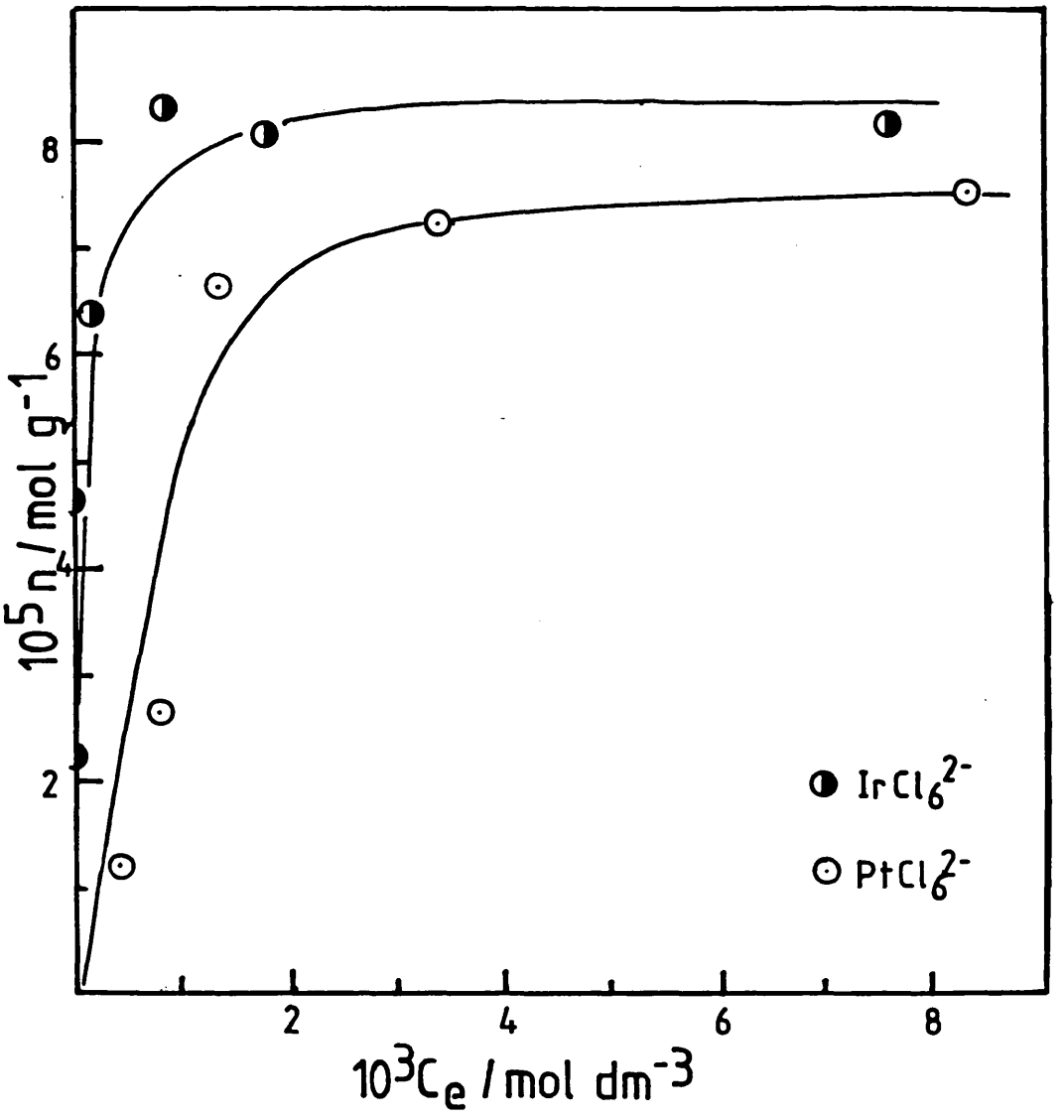

Fig. 3.1: Adsorption Isotherms for $PtCl_6^{2-}$/Alumina and $IrCl_6^{2-}$/Alumina

One way of assessing the relative strengths of adsorption of the platinum and iridium on the oxide is as follows. Assuming that the adsorption of both complexes is described by a Langmuir Isotherm then the equilibrium aqueous metal ion concentration, c_e/mol dm^{-3} is related to the amount adsorbed n/mol g^{-1} by the following relationship:

$$c_e/n = c_e/n_m + 1/bn_m \qquad (3.1)$$

where n_m/mol g^{-1} is the limiting coverage found using the Langmuir Adsorption Isotherm and b/dm^3 mol^{-1} is the adsorption equilibrium constant. If this is applicable then the concentration, $c_{1/2}$, that gives half the saturation coverage is equal to 1/b. For the adsorbing platinum complex $c_{1/2}$ is approximately 0.7 x 10^{-3} mol dm^{-3} and therefore b is approximately 1.4 x 10^3 dm^3 mol^{-1}, whilst for the iridium complex $c_{1/2}$ is only 0.05 x 10^{-3} mol dm^{-3} which results in a value for b of 2.0 x 10^4 dm^3 mol^{-1}.

Santacesaria et al. (1977) have obtained similar results for the $H_2PtCl_{6(aq)}$/alumina system and suggested that the adsorption of the acid occurs at a single site. This was thought to have been preceeded by an acid attack on the alumina with dissolution of aluminium into solution to form hydrolysed aluminium ions. Furthermore, a kinetic analysis suggested that the hexachloroplatinate anion formed an ion pair with these hydrolysed aluminium ions, the resulting complex then being adsorbed onto the support in the following manner:

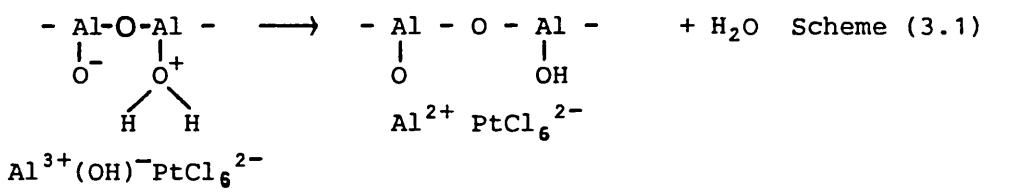

Scheme (3.1)

However, it is questionable whether Al-O^- species are present under the highly acidic conditions used for adsorption from solution.

A further possibility for the adsorption mechanism for the $PtCl_6^{2-}$ complex has been suggested by Summers and Ausen (1978). These workers propose that anionic chloride complexes react with alumina surfaces by a ligand displacement reaction as follows:

$$\equiv \text{Al-O}^- + Cl_5PtCl^{2-} \rightarrow \equiv \text{Al-O-}PtCl_5^{2-} + Cl^- \qquad \text{Scheme (3.2)}$$

However, under the conditions used in this study such a mechanism is also open to doubt. As mentioned above, Al-O$^-$ species are probably not present under highly acidic conditions and, furthermore, the reaction of two similarly charged species is expected to be slow.

It is most likely that under the highly acidic conditions present (pH ~2) the adsorption occurs via protonated hydroxyl groups attached to the alumina surface; a process described by Brunelle (1978) and D'Aniello (1981):

$$2 \equiv Al\text{-}OH_2^+ + PtCl_6^{2-} \rightarrow (\equiv Al\text{-}OH_2^+)_2\ PtCl_6^{2-} \quad \text{Scheme (3.3)}$$

Undoubtedly the iridium complex may initially adsorb by the above mechanism. However, once filtered and stored in a desiccator the iridium samples underwent the following series of colour changes over a month or so:

brown → green → blue → grey → grey/green

This is in contrast to the behaviour of the platinum sample which remained a pale yellow colour. This difference in behaviour between the two monometallic samples must reflect the greater lability of the $Ir^{IV}Cl_6^{2-}$ complex compared to the $Pt^{IV}Cl_6^{2-}$ complex. In fact several workers have observed an interaction between adsorbed iridium complexes and alumina using u.v./visible spectroscopy (UVS). Thus, Escard et al. (1973), have interpreted their results in terms of the reduction of $Ir^{IV}Cl_6^{2-}$ on the alumina surface to an $Ir^{III}Cl_6^{3-}$ species. Similarly, Bureau-Tardy et al. (1978) observed that the Ir(IV) oxidation state was only stabilised when adsorption of $Ir^{IV}Cl_6^{2-}$ anions was carried out in strongly acidic solutions. More recently, Engels et al. (1984) proposed that $Ir^{III}Cl_6^{3-}$ is hydroxylated to form $[Ir^{III}Cl_x(H_2O)_y]^{(3-x)+}$ complexes on the alumina surface. Furthermore, Fine (1970) has obtained blue-coloured, polymeric iridium species from aqueous solutions of $Ir^{IV}Cl_6^{2-}$ complexes under acidic conditions.

Therefore, the colour changes observed in this study are most likely to be due to hydroxylation, polymerisation and reduction of the adsorbed iridium complex on the alumina surface.

A reaction network which accounts for these changes is shown below and is based on a scheme proposed by Fine (1970) for the reaction of Ir(IV) and Ir(III) chloride species in acid solution:

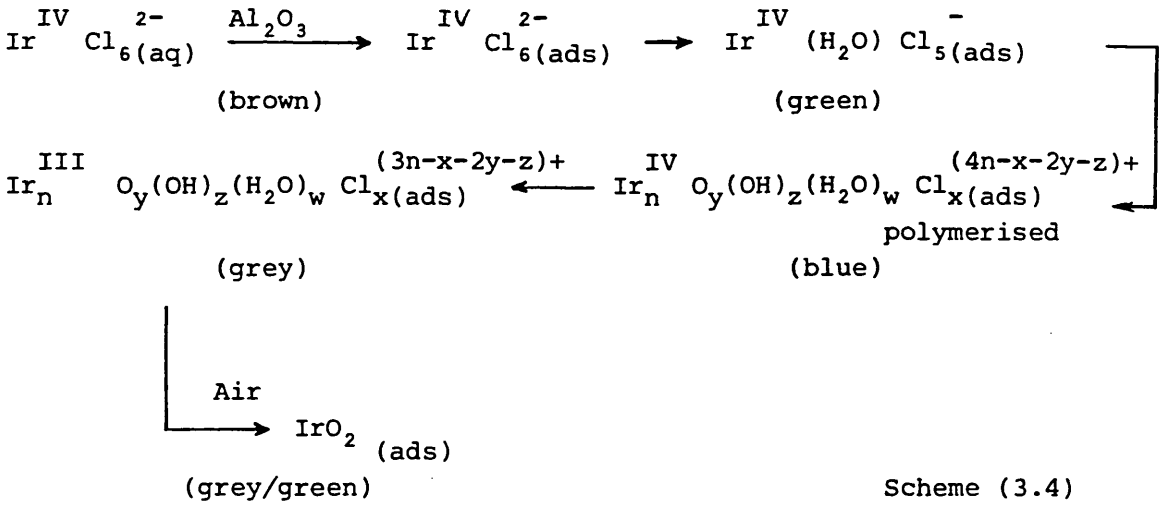

Scheme (3.4)

In this scheme brown hexachloroiridate (IV) anions initially adsorb onto the alumina and are subsequently hydroxylated by surface hydroxyl or surface bound water groups to give the green $Ir^{IV}(H_2O)Cl_5^-$ species. This green species probably does not contain Ir(III) entities since the colour of the sample was too intense. In general, the colour of Ir(III) species is much paler than that of their Ir(IV) counterparts. The difference arises because the adsorption bands of the Ir(III) species come from metal d-d transitions with molar extinction coefficients (ε_m) $\leqslant$ 100, whilst the colour of Ir(IV) compounds is due to charge transfer processes involving the surrounding ligands ($\varepsilon_m \leqslant 4000$). At a later stage the green species convert into the blue, polymeric $Ir_n^{IV}O_y(OH)_z(H_2O)_w\,Cl_x^{(4n-x-2y-z)+}$ species, possibly containing -O- and -Cl- bridges. The polymerisation is likely to be facilitated by the hydroxyl groups on the alumina surface. The blue species may then be reduced by water (either from the atmosphere or the support) according to the scheme:

$$Ir_n^{IV}O_y(OH)_z(H_2O)_w\,Cl_x^{(4n-x-2y-z)+} + \frac{n}{2}H_2O \rightarrow Ir_n^{III}O_y(OH)_z(H_2O)_w\,Cl_x^{(3n-x-2y-z)+} + \frac{n}{4}O_2 + n\,H^+$$

Scheme (3.5)

Thus, upon reduction the blue colour fades to the pale grey colour the intensity of which is indicative of an Ir(III) species. The Ir(III) polymeric species are possibly air sensitive and upon standing undergo oxidation to iridic oxide, which may account for the final grey-green colour. The oxidation state of several of the coloured iridium samples was investigated further using a temperature-programmed reduction analysis, the results of which are contained in Chapter Four.

3.1.2 Preparation of the Bimetallic Samples

A series of Pt-Ir/alumina catalysts were produced by coadsorption of the hexachlorometal(IV) salts from aqueous solution ($20cm^3$) onto γ-alumina (1g), using the method described for the production of the monometallic samples. Five catalysts with different Pt:Ir ratios were obtained by contacting the alumina with solutions containing different relative amounts of the two metals. However, to maintain a saturated alumina surface, the total initial metal complex concentration was always made up to 0.01 mol dm^{-3}. Once filtered, the samples were stored in a desiccator until required. No colour changes were observed for the stored bimetallic samples.

The extent of metal uptake was measured by Plasma Emission Spectroscopy since the u.v./vis. adsorption bands of the two metal complexes overlap. The compositions of the five bimetallic catalysts together with the monometallic samples are given in Table 3.1. To aid identification a simple catalyst coding system has been employed. The bimetallic samples are identified by the code PtIrX; where PtIr signifies the platinum-iridium bimetallic nature of the sample and X is the atomic percentage of platinum, relative to iridium, present. For instance, a bimetallic catalyst containing 43 at.%Pt, 57 at.%Ir is coded PtIr43. Similarly, the monometallic platinum and iridium samples are coded Pt100 and Ir100 respectively.

Table 3.1: Catalyst Compositions

Sample	wt.% metal[a]		at.% Pt[b]
	Pt	Ir	
Ir100	0.00	1.61	0
PtIr15	0.24	1.36	15
PtIr27	0.43	1.14	27
PtIr43	0.67	0.87	43
PtIr58	0.88	0.63	58
PtIr78	1.18	0.32	78
Pt100	1.48	0.00	100

(a) error = $\pm$ 0.10 wt.%; (b) at.% Pt = mols Pt adsorbed/total mols metal adsorbed.

The complete set of adsorption data used to calculate the catalyst loadings is given in Table 3.2. The following treatment shows that the adsorption behaviour of each of the two metal components in the adsorption mixture can be described by a simple Langmuir adsorption model involving competitive adsorption.

The adsorption rate of each metal component can be described by equations of the following form:

$$R_{Pta} = k'_{Pt}\, c_{Pt} \left\{A - n_{Pt}a_{Pt} - n_{Ir}a_{Ir}\right\} \qquad (3.2)$$

$$R_{Ira} = k'_{Ir}\, c_{Ir} \left\{A - n_{Ir}a_{Ir} - n_{Pt}a_{Pt}\right\} \qquad (3.3)$$

where R_{ia}/mol s^{-1} g^{-1} is the rate of adsorption of component i, $k'_i/s^{-1}\ m^{-2}\ dm^3$ is the adsorption rate constant of component i, c_i/mol dm^{-3} is the concentration of i in solution, $A/m^2\ g^{-1}$ is the total surface area available for adsorption, n_i/mol g^{-1} is the amount of component i adsorbed and a_i/m^2 mol^{-1} is the effective surface area of each component i.

The rate of desorption is given by

$$R_{Ptd} = k''_{Pt}\, n_{Pt} \qquad (3.4)$$

$$R_{Ird} = k''_{Ir}\, n_{Ir} \qquad (3.5)$$

where R_{id}/mol s^{-1} g^{-1} is the rate of desorption of component i and k_i''/s^{-1} is the desorption rate constant for i.

At equilibrium, the rates of adsorption and desorption are equal for each component, thus

$$R_{Pta} = R_{Ptd} \qquad (3.6)$$

$$R_{Ira} = R_{Ird} \qquad (3.7)$$

Hence, by equating expressions (3.2) and (3.4), and (3.3) and (3.5) the following expressions for the amount of Pt and Ir adsorbed are obtained.

$$n_{Pt} = k_{Pt}\, c_{Pte}\, A \Big/ \left\{1 + a_{Pt}\, c_{Pte}\, k_{Pt} + a_{Ir}\, c_{Ire}\, k_{Ir}\right\} \qquad (3.8)$$

$$n_{Ir} = k_{Ir}\, c_{Ire}\, A \Big/ \left\{1 + a_{Ir}\, c_{Ire}\, k_{Ir} + a_{Pt}\, c_{Pte}\, k_{Pt}\right\} \qquad (3.9)$$

where $k_i/m^2 dm^3$ is the adsorption equilibrium constant, k_i'/k_i'' and c_{ie}/mol dm^{-3} is the equilibrium concentration of i in solution.

Table 3.2: Adsorption Data for the Bimetallic Samples

Sample	$10^3 c_{Pti}$ mol dm^{-3}	$10^3 c_{Iri}$ mol dm^{-3}	$10^3 c_{Pte}$ mol dm^{-3}	$10^3 c_{Ire}$ mol dm^{-3}	$10^5 n_{Pt}$ mol g^{-1}	$10^5 n_{Ir}$ mol g^{-1}
Ir100	0.00	10.00	0.00	5.81	0.00	8.39
PtIr15	1.67	8.33	1.05	4.79	1.23	7.08
PtIr27	3.33	6.67	2.23	3.70	2.21	5.94
PtIr43	5.00	5.00	3.28	2.73	3.44	4.53
PtIr58	6.67	3.33	4.41	1.69	4.51	3.28
PtIr78	8.33	1.67	5.30	0.84	6.05	1.67
Pt100	10.00	0.00	6.20	0.00	7.59	0.00

Notes:

i) c_{Pti}, C_{Iri} are the initial concentrations of the platinum and iridium complexes in the contacting solution, respectively.

ii) c_{Pte}, c_{Ire} are the equilibrium concentrations of the platinum and iridium complexes in solution after contact with the alumina, respectively.

iii) n_{Pt}, n_{Ir} are the amounts of platinum and iridium adsorbed on the alumina.

All adsorptions were performed at total metal concentrations which were sufficient to saturate the alumina surface, therefore

$$\theta_{pt} + \theta_{Ir} = 1 \qquad (3.10)$$

where θ_i is the fractional coverage of component i, each given by the following expressions:

$$\theta_{Pt} = n_{Pt}/n_{Ptm} \qquad (3.11)$$

$$\theta_{Ir} = n_{Ir}/n_{Irm} \qquad (3.12)$$

where n_{im}/mols g^{-1} is the limiting amount of component i adsorbed at equilibrium.

Insertion of equations (3.11) and (3.12) into (3.10) followed by rearrangement for n_{Pt} gives

$$n_{Pt} = n_{Ptm}\left\{1 - n_{Ir}/n_{Irm}\right\} \qquad (3.13)$$

Therefore, a plot of n_{Pt} against n_{Ir} should give a straight line of slope, $s = -n_{Ptm}/n_{Irm}$ and intercept, $i = n_{Ptm}$, which is clearly the case as shown by Fig. 3.2. Now a combination of expressions (3.13) and (3.8) leads to the following equation:

$$n_{Ptm}\left\{1 - n_{Ir}/n_{Irm}\right\} = k_{Pt}c_{Pte}A/\left\{1 + a_{Pt}c_{Pte}k_{Pt} + a_{Ir}c_{Ire}k_{Ir}\right\} \qquad (3.14)$$

However, according to equation (3.9)

$$A = n_{Ir}\left\{1 + a_{Ir}\,c_{Ire}\,k_{Ir} + a_{Pt}\,c_{Pte}\,k_{Pt}\right\}/k_{Ir}\,c_{Ire} \qquad (3.15)$$

Substitution of this expression for A in (3.14), followed by rearrangement, gives

$$1/n_{Ir} = (K/n_{Ptm})(c_{Pte}/c_{Ire}) + 1/n_{Irm} \qquad (3.16)$$

where $K = k_{Pt}/k_{Ir}$.

Hence, a plot of $1/n_{Ir}$ against c_{Pte}/c_{Ire} should give a straight line of slope, K/n_{Ptm} and intercept, $1/n_{Irm}$. Such a plot is shown in Fig. 3.3 and results in a value for K of 0.58. The plot clearly confirms the validity of the above analysis for the chloroplatinic acid-chloroiridic acid/alumina system.

There was not time in this study to make a systematic study of the relationship between catalytic activity and composition of the bimetallic catalyst. Instead the effects of various pretreat-

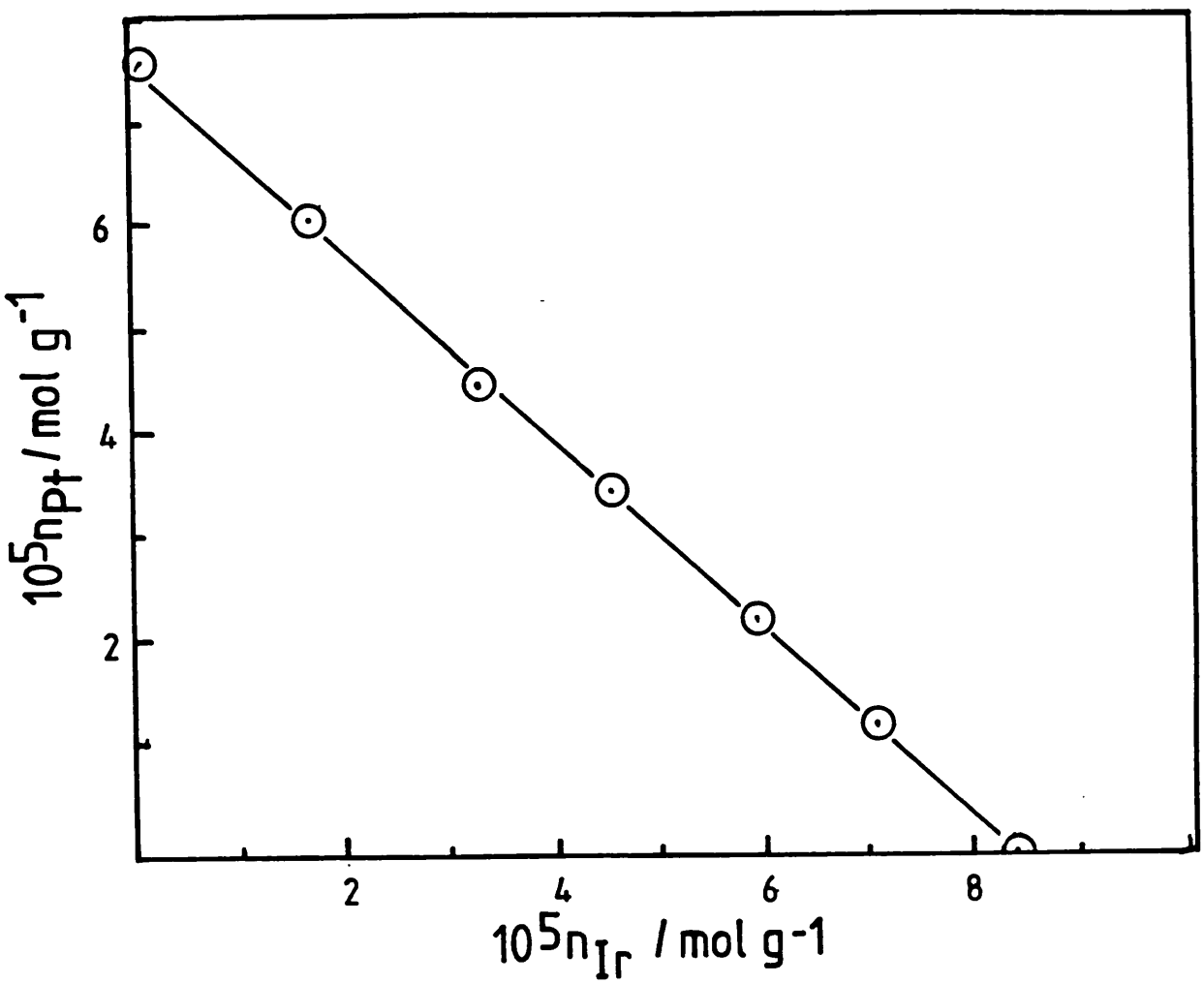

Fig. 3.2: Plot of n_{Pt} Against n_{Ir} for the Bimetallic $PtCl_6^{2-}$-$IrCl_6^{2-}$/ Alumina System

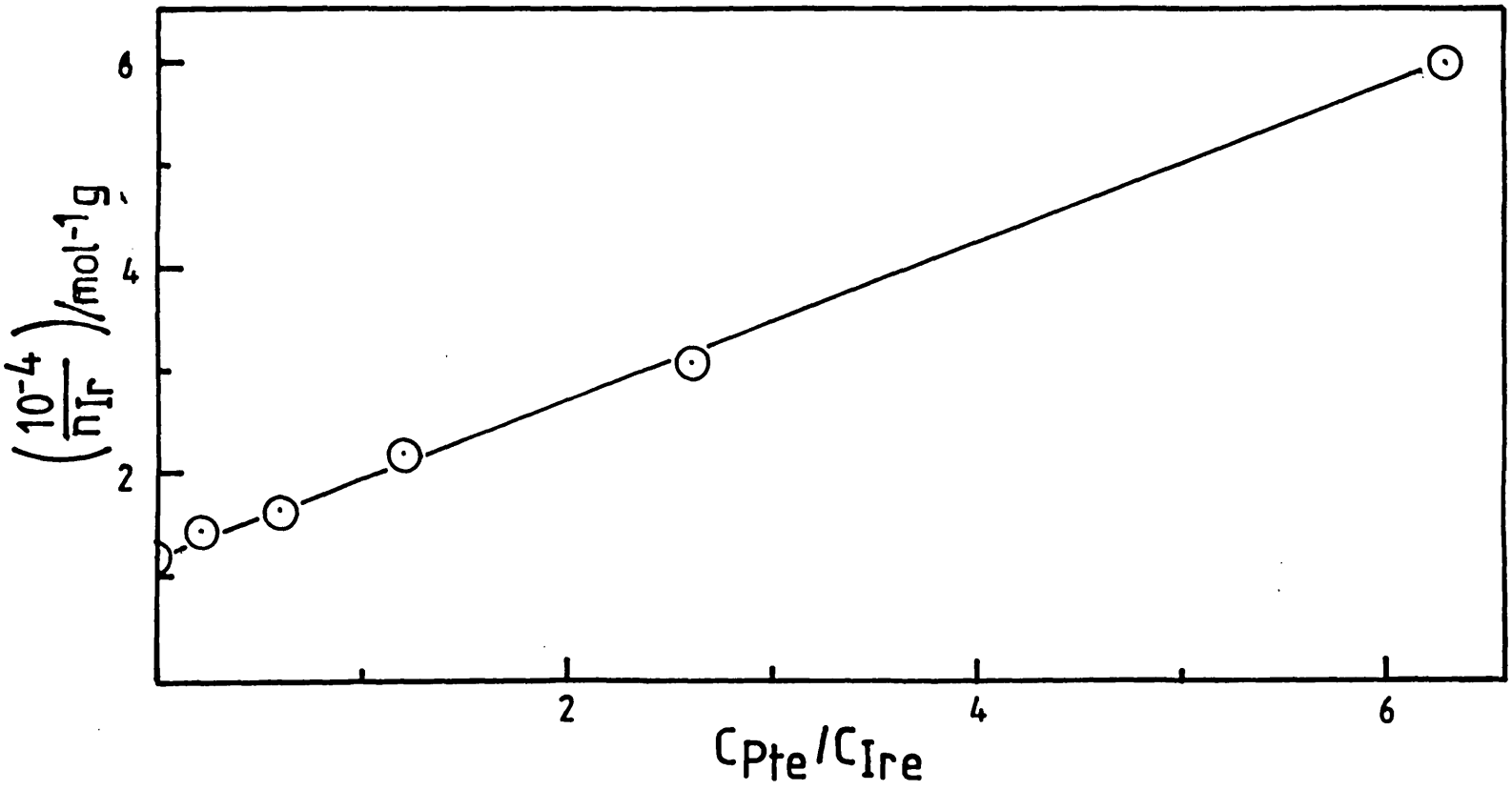

Fig. 3.3: $PtCl_6^{2-}$-$IrCl_6^{2-}$/Alumina Adsorption Plot

ment conditions have been evaluated for a single bimetallic catalyst (PtIr43) together with the two monometallic samples for comparative purposes. In addition, several experiments have been performed using a physical mixture of the monometallic samples (coded M50) which was produced by thoroughly mixing together equal weights (100mg) of the two monometallic samples.

3.2 Catalyst Pretreatment Conditions

This section contains a detailed description of the pretreatments carried out in the micro-reactor system. These can be divided into four main groups, each of which is described in detail below. They are:

i) Pretreatments involving only an oxidation step.
ii) Pretreatments involving only a reduction step.
iii) Pretreatments involving a combination of both oxidation and reduction.
iv) Thermal pretreatments involving no oxidation or reduction step.

3.2.1 Oxidation Pretreatments

Oxidation pretreatments are identified by the code OT_O; where O signifies the oxidation step and T_O/K is the temperature at which the oxidation was performed. In general, the effects of three oxidation pretreatments have been studied, namely, pretreatment O0, O560 and O740. The former actually corresponds to no pretreatment other than metal complex adsorption and drying in a desiccator, whilst the second and third represent oxidation at temperatures of 560K and 740K respectively.

The oxidising gas mixture was prepared by mixing BOC HP grade oxygen with BOC HP grade argon. Two flow control valves were employed to regulate mixing and were set to give a 10% oxygen-in-argon mixture. The oxidising gas mixture was passed over the catalyst sample at a flow rate of 12ml. min^{-1} and a pressure of 1.0-1.1 atm. The catalyst sample was heated under the oxidising gas mix to the required oxidation temperature in a linear manner using a Newtronic temperature programmer. For the low temperature O560 oxidation a heating rate of 12K min^{-1} was used, whilst for the high temperature O740 pretreatment a heating rate of 24K min^{-1} was

applied. The required oxidation temperature was maintained for twenty minutes before the reactor was allowed to cool to 350K. At this temperature the oxygen supply was cut off and the system was left to allow the oxygen to flush away as the sample cooled to 298K.

3.2.2 Reduction Pretreatments

Reduction pretreatments are identified by a code format which is consistent with that used for oxidation pretreatments, namely RT_R; where R signifies reduction and T_R/K indicates the temperature at which the reduction was carried out. Reduction has been carried out mainly at temperatures of 610K (R610) and 740K (R740). The reducing gas was a 3% hydrogen-in-argon mixture, the preparation of which is described in Section 4.2. The reduction procedure was similar to that described for the oxidation pretreatments. However, following the isothermal reduction period the sample was cooled to 298K before the hydrogen was removed from the argon carrier-gas.

Reduction experiments performed without an isothermal reduction stage are coded $TPRT_H$; where TPR signifies the temperature-programmed, non-isothermal nature of the pretreatment and T_H/K is the temperature to which the sample was heated before being immediately cooled. Apart from the absence of an isothermal reduction period at T_H the methods of performing the two types of reduction pretreatments were the same.

3.2.3 Oxidation-Reduction Combinations

Pretreatments involving a sequence of oxidation and reduction steps are denoted by the appropriate catenation of the individual oxidation and reduction components. For example, oxidation at 740K followed by reduction at 610K is coded O740 R610. The individual oxidation and reduction steps were carried out consecutively in the manner outlined in Sections 3.2.1 and 3.2.2 respectively without exposing the sample to air.

3.2.4 Thermal Pretreatments Without Oxidation/Reduction

Thermal pretreatments were carried out in the absence of oxygen or hydrogen and are coded DT_D; where D signifies the desorption/drying nature of the pretreatment and T_D/K is the temperature at which the drying was carried out. The catalyst tempera-

ture was raised to T_D in the same manner as for the oxidation and reduction pretreatments. Thermal pretreatments in which the temperature increased linearly with time are coded $TPDT_p$; where TPD signifies the temperature-programmed desorption nature of the pretreatment and T_p/K is the maximum temperature reached before the heating was switched off and the sample allowed to cool. Combinations of oxidation/reduction/drying steps are coded by catenation of the individual pretreatment codes. However, pretreatments involving a drying step were not investigated in a systematic manner.

3.2.5 Summary of Pretreatment Conditions

The principal pretreatments used are summarised in Table 3.3.

Table 3.3: Summary of Principal Pretreatments Investigated.

Code	Pretreatment/Comments
O0	No pretreatment performed in micro-reactor.
O560	Heated to 560K in 10% O_2/Ar (12K min^{-1}), sample held at 560K for 20 mins, cooled to 350K, O_2 removed, cooled to 298K.
O740	As for O560 but heated to 740K (24K min^{-1}).
R610	Heated to 610K in 3% H_2/Ar (12K min^{-1}), sample held at 610K for 20mins, cooled to 298K, H_2 removed.
R740	As for R610 but heated to 740K (24K min^{-1}).
O740 R610	Pretreatment O740 followed by R610.
O740 R740	Pretreatment O740 followed by R740.

CHAPTER FOUR

Temperature-Programmed Reduction and Temperature-Programmed Oxidation Studies

4.1 Introduction

4.1.1 Aim

The aim of this Chapter is to determine the effects of various oxidation pretreatment temperatures on the state of alumina-supported platinum-iridium catalysts. Temperature-Programmed Oxidation (TPO) has been used to directly follow oxidation processes occurring on the catalyst samples whilst the complementary technique of Temperature-Programmed Reduction (TPR) has been used to determine the number and nature of oxidised species in the catalysts. In addition, the above techniques have been extended to follow oxidation or reduction processes occurring on the catalyst samples which are not due to the reaction of the supported metal species. This has been carried out by the use of a computer-interfaced quadrupole mass spectrometer for product detection during the temperature-programmed experiment.

The effects of three different oxidation temperatures has been investigated. TPR and TPO experiments have been performed on samples subjected to no oxidation pretreatment, to provide information on the reaction of the alumina-supported metal impregnating complexes in oxygen and hydrogen atmospheres. The effects of a mild oxidation, carried out at a temperature of 560K and a more severe oxidation, performed at 740K, have also been investigated. In order to fully understand the processes occurring in the bimetallic samples, the pretreatments and temperature-programmed experiments were also performed on the monometallic samples. In addition, experiments have been carried out on samples which have been previously oxidised and reduced insitu.

Hence this study should identify the oxidation pretreatments which result in alloy formation following reduction and, additionally, will provide information on the reactivity and stability of such alloy species in oxygen, at various temperatures.

4.1.2 Temperature-Programmed Reduction

TPR has become widely established as a routine method for the determination of the state of the metal in supported metal catalysts. Reviews on the subject have been published by Jenkins et al. (1977) and Hurst et al. (1982). The only requirement for the TPR technique is that the metal must be present in a reducible form.

In the TPR experiment a carrier gas containing a low concentration of hydrogen is passed over the sample, whilst the temperature of the sample is programmed to rise in a linear manner. As the temperature increases, reduction processes occur producing changes in the hydrogen gas concentration. Such changes are usually detected in an apparatus using a Thermal Conductivity Detector (TCD), as described by Robertson et al. (1975) and Boer et al. (1982). The resulting plot of hydrogen signal (or uptake) against temperature is known as a reduction profile. Calibration of the peak areas in such profiles allows the change in oxidation state of the metal to be determined and this information combined with the reduction peak position enables a distinction to be made between different reducible species. Therefore, the technique can be used to examine whether alloy formation has occurred during catalyst preparation by comparing the reduction profiles of samples containing more than one metal component with the profiles for the corresponding monometallic systems.

Robertson et al. (1975) were first to use the TPR technique in such a manner to identify alloy formation in the bimetallic Cu-Ni/silica system. Since then this technique has been widely used to study other bimetallic systems and the following brief review outlines the results of several of these investigations including studies of supported Pt-Ir catalysts.

Bolivar et al. (1975), McNicol (1977), Wagstaff and Prins (1979a), Isaacs and Petersen (1982) and Mieville (1984) have all investigated whether alloy formation occurs in the Pt-Re/alumina system using TPR. These workers showed that alloy formation occurred when samples were reduced following an initial oxidation step at temperatures around 570K, whilst oxidation at around 770K prevented alloy formation following reduction.

Burch (1981), Sexton et al. (1984) and Lieske and Voelter (1984) have examined metal interactions in the Pt-Sn/alumina system using TPR. These workers found that most of the tin existed in the II oxidation state following reduction and was unalloyed with the platinum.

The Pt-Ir/alumina system was first investigated, using TPR, by Wagstaff and Prins (1979b). These workers performed an initial catalyst oxidation in air at 770K and found no particular evidence for bimetallic interactions during the subsequent TPR experiment. The effects of other initial oxidation pretreatment temperatures were not determined although these workers did perform a catalyst reoxidation at 620K, before carrying out a second TPR experiment, in which some evidence of alloy formation was obtained. However, the effect of varying the second oxidation temperature was not investigated. Foger and Jaeger (1981a) have also examined this system and the silica-supported system (1981b) using TPR. Similarly, these workers did not investigate the effect of the initial oxidation temperature, although they did vary the reoxidation temperature following the first reduction step. Alloy formation was only observed for samples reoxidised below around 700K.

Faro et al. (1983) have also investigated alloy formation in Pt-Ir/alumina samples using TPR. Whilst these workers did carry out reoxidation at several temperatures, all the experiments were performed on samples subjected to an initial oxidation at 753K, followed by reduction at 693K. It was concluded that the initial oxidation temperature did not effect alloy formation whilst reoxidation above 770K caused the breakup of alloy particles. Furthermore, these workers observed a high temperature reduction uptake around 650K, which was not due to the reduction of an oxidised metal species. Since a TCD was used to monitor changes in gas composition by these workers, the assignment of this peak to a hydrogen spillover reaction is speculative. Wang and Schwarz (1985) have used a mass spectrometer to try and follow the reduction of Pt-Ir/alumina catalysts but these workers could only monitor the water partial pressure during the TPR experiment.

In this present study product analysis has been performed using a computer-interfaced quadrupole mass spectrometer. Hence,

during a temperature-programmed experiment, up to sixteen different gas species can be monitored simultaneously. This powerful extension of the TPR technique allows a more detailed analysis of all the processes observed in the reduction profile to be made through which a better understanding of the alumina-supported Pt-Ir system can be obtained.

Finally, Birke et al. (1985) have investigated the effect of the initial oxidation pretreatment temperature and observed the formation of a separate IrO_2 phase following oxidation above 673K. However, these workers did not carry out TPR experiments on any reoxidised samples.

To summarise, several TPR investigations of the Pt-Ir/alumina system have been carried out which have identified some pretreatments which affect Pt-Ir alloy formation. In general, oxidation performed above a temperature of around 700K causes the breakdown of alloy particles. However, in none of the previous studies of the Pt-Ir/alumina system have the effects of different oxidation and reoxidation temperatures been studied in a systematic and comprehensive manner. The effect of the initial oxidation pretreatment remains especially unclear and hence this study extends previous investigations by examining in detail the effects of initial and reoxidation temperatures to fully determine the factors which control alloy formation and stability in Pt-Ir/alumina catalysts

4.1.3 Temperature-Programmed Oxidation

In the TPO experiment the hydrogen component in the carrier is replaced by oxygen. The technique requires that the metal must be present in an oxidisable state. The mass spectrometer was used to follow the reaction in oxygen and the experiment was carried out in a similar manner to the TPR experiment.

The technique has not received as much widespread attention as its TPR counterpart. This may be due to experimental difficulties associated with the stability of the TCD filaments in oxygen containing gases. However, Huizinga et al. (1984) have performed TPO experiments on alumina-and titania-supported platinum using such a detection system, whilst Vis et al. (1985) have studied the morphology of rhodium on titania and alumina, using TPO and TPR. The technique

has also been applied to the characterisation of supported bimetallic systems. Tauszik et al. (1984) have studied magnesia and silica-supported ruthenium-gold catalysts using the technique, whilst more recently Van't Blik et al. have used TPR and TPO experiments to study colbalt-rhodium supported on alumina (1986a), titania (1986b) and silica (1986c). However, to date, no TPO study of the Pt-Ir/alumina system has been reported.

The experiment is especially important since the technique directly monitors the formation of oxygen-containing species on the catalyst surface. Hence the technique is complementary to the TPR experiment, in which the reduction of the oxidised species is followed.

4.2 Experimental

TPR and TPO experiments were carried out in the micro-reactor system described in Chapter Two. The gas mixture used in the TPR experiments was prepared by mixing a commercial 10% hydrogen-in-argon mixture (BOC HP grade) with argon (BOC HP grade). Helium could not be used as a carrier because of the effect it had on the mass spectrometer readings (see Chapter Two). Two flow control valves were used to regulate mixing and these were set to give a 3% hydrogen-in-argon mixture. The gases were purified by passage over oxygen traps and zeolite-containing moisture traps, both obtained from Phase Separations Limited. The gas mixture was passed over the catalyst sample at a flow rate of 12ml. min^{-1} and a pressure of 1-1.1 atm. The pressure at the front and rear of the catalyst bed was monitored with two pressure transducers, supplied by Foxboro Instruments.

The catalyst sample (50mg) was held in a quartz tube reactor ($^1/_4$inch o.d.; 4mm. i.d.) with silica wool plugs at either end as described in Chapter Two. The temperature programmer was set to give an approximately linear temperature rise of 12Kmin^{-1} and was halted at a temperature of 740K unless otherwise stated. The catalyst temperature was measured with a chromel-alumel thermocouple, made from 0.125mm. diameter wires, which was placed in the silica wool plug in contact with the front of the catalyst bed.

During a temperature-programmed run up to sixteen different mass numbers could be monitored simultaneously by the quadrupole mass

spectrometer (Spectralab SX200). The mass number is defined as the ratio of the relative molecular mass, m, to the number of positive electronic charges, n, carried by the ionised species. For instance, singly charged argon has a mass number of 40, whilst doubly charged argon has a mass number of 20. More concisely, the latter species is said to give rise to a signal at mass 20. Ion currents were measured with an electron multiplier which was calibrated against a Faraday cup detector. The mass numbers monitored in a typical experiment are summarised in Table 4.1. It took approximately 10 seconds to scan through all the peaks and this time was accurately determined using a stopwatch. This enabled peak positions to be converted to temperatures, using the thermocouple output recorded on a y-t chart bed recorder.

Table 4.1: Mass Numbers Monitored During the Temperature-Programmed Reduction and Oxidation Experiments.

Mass Number	Species
2	Hydrogen
12	C-containing species
15	Methane
16	Methane and water
18	Water
26	C_2 hydrocarbons
28	Carbon monoxide and nitrogen
29	C_2 hydrocarbons
32	Oxygen
35	Chlorine-containing species
40	Argon carrier
43	C_3 and higher hydrocarbons
44	Carbon dioxide and C_3 hydrocarbons

Quantitative estimates of the hydrogen uptakes observed during TPR experiments were obtained by comparison with temperature-programmed reduction of bulk NiO and CuO samples.

For temperature-programmed oxidation the reducing gas mixture was replaced by a 1% oxygen-in-argon mixture, prepared by mixing pure oxygen with argon. Otherwise the conditions for temperature-programmed oxidation and reduction were similar. Oxygen uptakes were

calibrated against the TPO spectrum of a reduced Ni (75wt%)/alumina catalyst. Additionally, the instrument was calibrated using pulses of known amounts of gas. This calibration was performed for oxygen, hydrogen, carbon dioxide and methane. Temperature-Programmed Desorption (TPD) experiments were also performed using pure argon as the carrier-gas.

The alumina-supported catalyst samples were prepared by the methods outlined in Chapter Three, and included pure platinum (Pt100), pure iridium (Ir100) and a bimetallic catalyst containing 43at.% platinum and 57at.% iridium (PtIr43). A physical mixture (M50) was also prepared by thoroughly mixing equal weights of samples Pt100 and Ir100. The catalysts were subjected to a variety of insitu treatments prior to examination by temperature-programmed methods. A summary of the treatments used prior to examination by TPR is given in Table 4.2. A more detailed description of all the pretreatments used can be found in Chapter Three.

Table 4.2: Summary* of Pretreatments used in TPR Experiments

Code	Pretreatment/Comments
O0	No pretreatment, experiment carried out on alumina-supported precursor salts
O560	Oxidation at 560K
O560 TPR740 O560	Oxidation at 560K, followed by TPR to 740K then reoxidised at 560K
O560 TPR740 O740	As for O560 TPR740 O560 but reoxidised at 740K
O740	Oxidation at 740K
O740 TPR740 O560	Oxidation at 740K followed by TPR to 740K then reoxidised at 560K
O740 TPR740 O740	As for O740 TPR740 O560 but reoxidised at 740K

*Note: more detailed descriptions can be found in Chapter Three.

4.3 Results and Interpretation

4.3.1 Temperature-Programmed Reduction

In the forthcoming descriptions the term hydrogen profile, or reduction profile, will be used to describe the variation of hydrogen signal with temperature. The variation of other mass numbers will be similarly expressed e.g. methane profile. The term TPR profile refers to the collection of individual profiles. Reduction profiles

in the literature are frequently plotted showing hydrogen consumption as a function of temperature. In such cases it is necessary to invert the reduction profiles for a direct comparison to be made with the results presented in this study.

a) Samples Subjected to No Oxidation Pretreatment

In order to fully understand the reduction processes observed in the bimetallic samples it is first necessary to investigate the reduction behaviour of the monometallic catalysts. For ease of comprehension, in this section the results for the pure metals are discussed first followed by those for the bimetallic samples.

i) Platinum

Fig. 4.1 shows the TPR profile for sample Pt100 subjected to no oxidation pretreatment (coded 00). The hydrogen, methane, water and carbon dioxide profiles are represented by curves A-D respectively. Included in the figure are the amounts of methane and carbon dioxide produced together with the total amount of hydrogen consumed. The mass 15 signal has been chosen to represent methane as the mass 16 signal is complicated by a component arising from the cracking of water. The hydrogen profile shows the presence of two reduction processes and it will be convenient to discuss these separately.

The low temperature reduction process.

Calibration of the hydrogen consumed in the low temperature process, centred at a temperature of 453K, indicated that two hydrogen molecules are taken up per Pt atom, corresponding to complete reduction of a Pt(IV) species to Pt metal. Similar results have been obtained recently by Hoyle et al. (1985). The sharpness and symmetry of the reduction peak shows that the surface platinum complex formed by adsorption exists as a single species on the alumina support. This result should be compared with the TPR profile of bulk, unsupported chloroplatinic acid which produced a sharp reduction uptake at a temperature of 350K. The higher reduction temperature for the supported samples is clear evidence that the platinum salt interacts with the support, thereby stabilising the surface species towards reduction. The nature of the species formed is unclear; a $Al^{2+}PtCl_6^{2-}$ complex has been proposed by Santacesaria et al. (1977) and a $[PtCl_5(OH)]^{2-}$ surface complex by Summers and Ausen (1978).

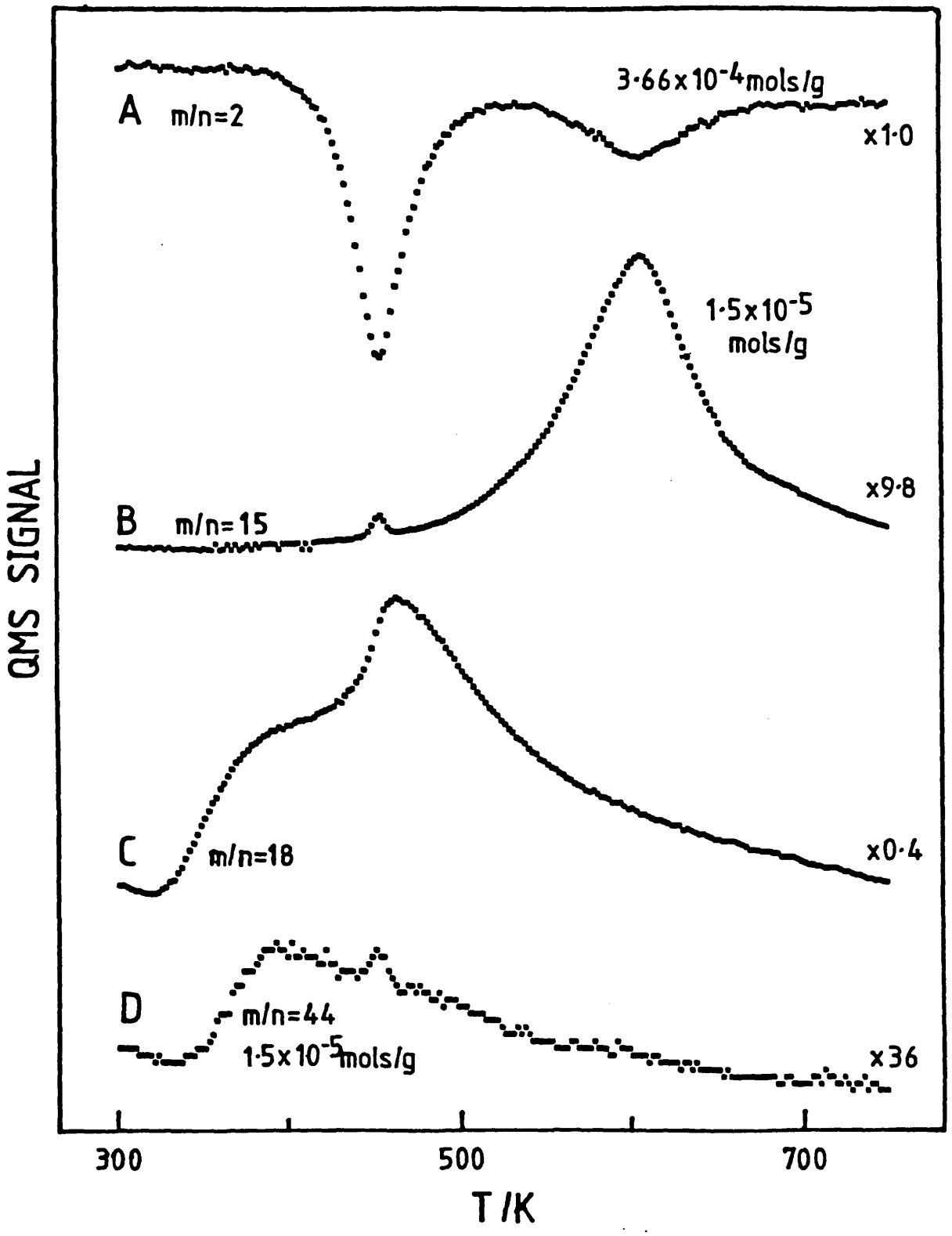

Fig. 4.1: TPR Profile for Sample Pt 100 Subjected to Pretreatment OO.

Since no chlorine containing species were observed during the reduction process any HCl formed must react with the support. Evidence for such a reaction is obtained from the water signal which shows a fairly sharp peak superimposed on a broader peak occurring just after the maximum in the hydrogen uptake. This may be due to an exchange reaction of the following type:-

$$HCl + S\text{-}OH \rightarrow S\text{-}Cl + H_2O \qquad (4.1)$$

Where S-OH represents a surface hydroxyl species on the alumina support and HCl is hydrogen chloride produced during the reduction of the supported metal species. An approximate calibration of the water profile indicated that most of the HCl formed during the reduction underwent reaction (4.1).

The low temperature reduction process was accompanied by small peaks in the mass 15 and 44 signals which are due to the production of hydrocarbon species, since small peaks were also observed in the mass 29 and 26 signals. The small peak in the mass 44 signal which is superimposed on a much broader peak is thought to be caused by a C_3 hydrocarbon rather than carbon dioxide, since a small peak was also observed in the mass 43 signal. These hydrocarbons could arise from hydrogenation of carbonaceous material over the newly formed metal produced by the reduction process. Alternatively, they could arise from a Fischer-Tropsch reaction between carbon dioxide and hydrogen. Carbon dioxide is clearly seen to be present in the broad mass 44 peak on which the small C_3 hydrocarbon peak is superimposed. The amount of C_2 and C_3 hydrocarbons formed amounted to less than 10% of the total amount of hydrocarbons formed.

The high temperature reduction process

The high temperature uptake observed in the hydrogen profile at a temperature of 610K has also been observed by many previous workers (e.g. Faro et al. (1983), Tang et al. (1984) and Hoyle et al. (1985)). This hydrogen uptake has generally been attributed to hydrogen spillover onto the support leading to a partial reduction of the alumina. This in turn has been thought to result in the formation of Pt-Al alloys. An alternative explanation has been proposed by Burch (1981) in which the peak has been associated with the

formation of chlorine for this samaple. The amount of hydrogen involved in the high temperature reduction process was approximately 6.2×10^{-5}mol H_2 g^{-1} catalyst. The amount of methane formed was 1.5×10^{-5} mol g^{-1} catalyst. These quantities are consistent with the following type of reaction:-

$$CO_2 + 4H_2 \rightarrow CH_4 + 2H_2O \qquad (4.2)$$

Evidence that the high temperature methane peak centred at 610K may be connected with desorption of carbon dioxide from the sample surface is obtained from temperature-programmed desorption experiments on a fresh Pt100 sample. Fig. 4.2 (curve A) shows the mass 44 signal produced during such an experiment. The high temperature peak occurs at almost the same temperature as the methane peak in Fig. 1 indicating that desorption of carbon dioxide is probably the primary process. Therefore, it appears that in the presence of hydrogen, carbon dioxide is hydrogenated to methane over the Pt metal sites to form methane and water. The water produced may be too small to be detected or may be strongly adsorbed on the support. Calibration of the carbon dioxide peak in curve A showed that 1.4×10^{-4} mol g^{-1} catalyst were produced. This implies that less carbon material can be thermally removed from the catalyst when hydrogen is present, since the amount of methane formed is only 1.5×10^{-5} mol g^{-1} catalyst.

There is also a desorption of carbon dioxide at a temperature of 416K. This peak is probably due to desorption of carbon dioxide from the support as a similar, but larger, peak is observed during TPD on the alumina support (curve B). Similar results were obtained for the γ-alumina during a TPR experiment. The total amount of carbon dioxide desorbed in curve B was 4.0×10^{-5} mol g^{-1} alumina, which corresponds to 2.7×10^{13} molec. CO_2 cm^{-2}. The low temperature peak, centred at 388K, may contain two components. The high temperature peak is of much reduced intensity for the alumina sample and occurs at 594K. Paryjczak et al. (1982) have obtained three CO_2 desorption peaks for thermally treated aluminas. They attributed (although did not assign) each to surface carboxylate, bicarbonate and carbonate groups.

To determine whether the high temperature state, obtained when Pt was present, resulted from acidication of the alumina support during the metal adsorption process, additional TPD experiments were

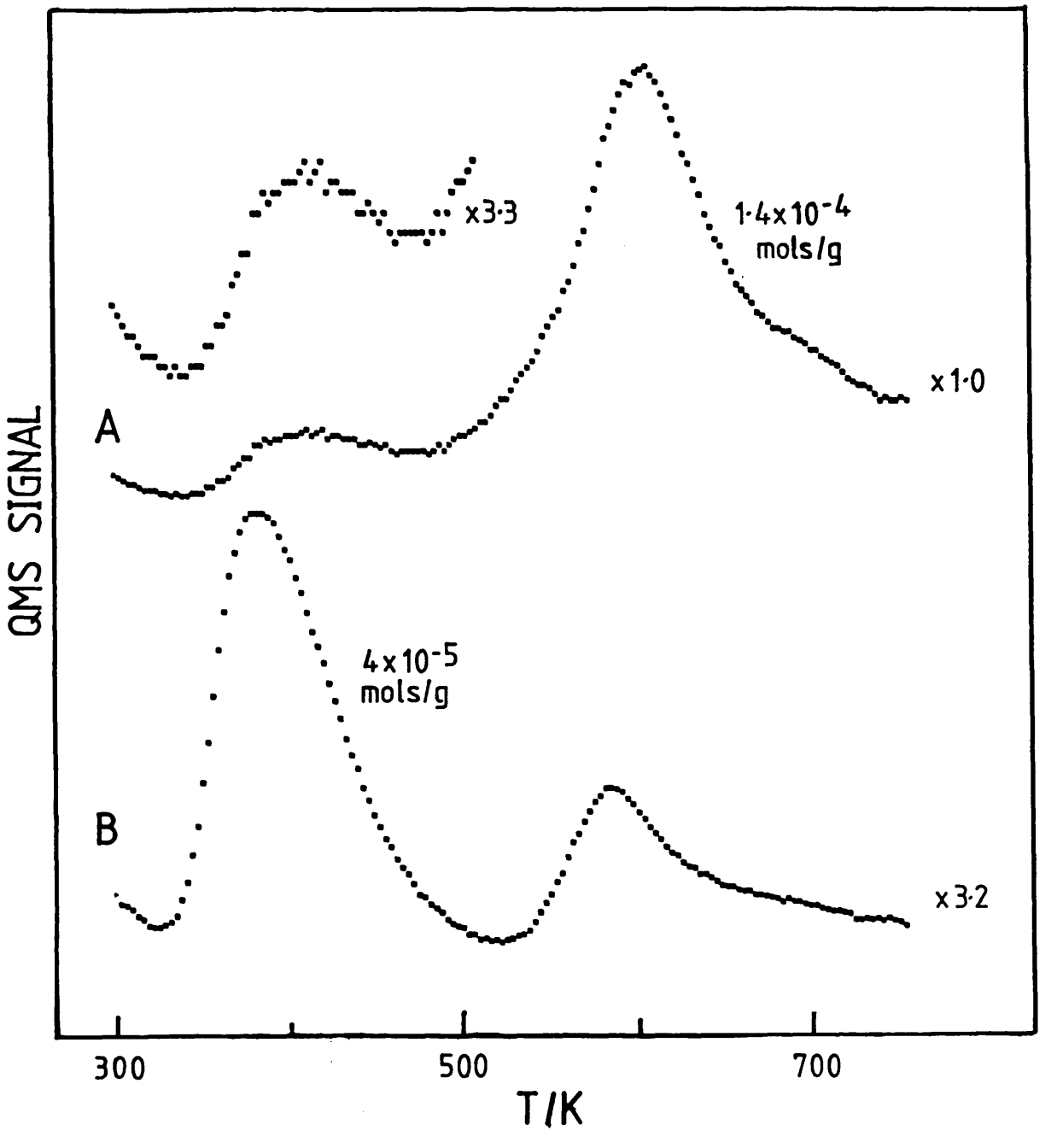

Fig. 4.2: Mass 44 Desorption Profiles for the Pt100 (curve A) and γ-alumina (curve B) Samples Obtained During Temperature-Programmed Desorption.

performed on alumina treated with acidic (2M HCl; $20cm^3\ g^{-1}$; 12hr) or alkali (2M NaOH; $20cm^3\ g^{-1}$; 12hr) solutions. The resulting CO_2 desorption profiles were similar to the untreated alumina. No enhanced high temperature peak was observed. In addition, TPR experiments performed on a Pt100 sample prepared at pH11 (adjusted with NaOH(aq)) produced methane at the normal temperature of 610K. It appears therefore that the CO_2 state desorbing at 610K is associated with the presence of platinum.

Carbon dioxide could be readsorbed onto an alumina surface that had been subjected to temperature-programmed desorption by exposing the surface to air or pulses of carbon dioxide at 298K. During subsequent heating in hydrogen, carbon dioxide peaks similar to those found in Fig. 4.2 (curve B) were produced, but the high temperature peak was absent. By contrast, exposure of a reduced Pt100 sample (previously subjected to TPR) to air or carbon dioxide at 298K resulted in methane production with a peak at 620K, when this sample was subsequently subjected to TPR. These results clearly show that metal must be present to catalyse the hydrogenation of carbon dioxide to methane. It is also evident that carbon dioxide reacts differently with the metal loaded samples. This may be due to carbon dioxide adsorption occurring on the metal sites or on new alumina sites created by the presence of the metal.

From the previous results the source of the carbon dioxide would appear to be adsorption of atmospheric carbon dioxide onto the alumina surface, forming carbon-containing species. The production of a high temperature peak in the presence of platinum may be a result of a metal induced modification of the alumina surface which would enable carbon dioxide to adsorb from the atmosphere, onto the alumina, and exist in a more stable form. This species would then decompose around 610K forming carbon dioxide which is hydrogenated over the metal sites. Alternatively, the results may be due to the methanation of carbon monoxide or formate species formed on the metal as a result of the decomposition of a carbonate-type species associated with the platinum salt. Interaction with the alumina surface may promote the formation of such species. Whatever the exact nature of species involved, the results are significant since they establish that hydrogen uptakes in a TPR profile cannot necessarily be attributed to the reduction of oxidised metal species or the support material.

Fig. 4.3 shows the TPR profiles for Pt100 samples subjected to various drying pretreatments, curves A, B and C relating respectively to pretreatments D700, D560 and D400. The experiments were performed in a nitrogen carrier-gas in the absence of oxygen. The results are important for future analysis of heat treatments in the presence of oxygen, since they allow the effect of oxygen in the carrier-gas to be determined.

It can be seen from curve C that heating at 400K causes an increase in the temperatures at which the two reduction processes occur. The first peak increases from 453K to 465K and the second peak from 610K to 626K. The low temperature uptake appears broader and may have more than one component. However, the overall oxidation state change is still IV to 0 for this peak. Heating at 560K (curve B) greatly diminished the low temperature reduction process whilst the high temperature hydrogen uptake remained largely unaffected. Heating at 700K (curve A) removes the low temperature process. However, some high temperature reduction still occurs at 536K.

Schweizer and Kerr (1978) have shown that bulk chloroplatinic acid thermally decomposes producing platinum chlorides at temperatures above 400K and platinum metal around 800K. From the results obtained here it would appear that a similar process is occurring on the alumina surface. Heating in nitrogen to temperatures around 560K causes the decomposition of the platinum surface complex to platinum metal. The carbon-containing species which gives rise to the second peak appears to decompose at temperatures between 560K and 700K, in keeping with the temperature of the carbon dioxide peak observed in Fig. 4.2 (curve A). This decomposition may result in a metal surface which is partially covered in carbonaceous material. Hydrogenation of this material could result in the small high temperature uptake observed in curve A.

Fig. 4.4 shows the TPR profile of a Pt(0.8wt%)/TiO_2 sample (subjected to pretreatment O0) prepared using the adsorption technique. Comparing Fig. 4.1 with Fig. 4.4 the effect of the support on the state of the metal can be evaluated. Like the alumina-supported platinum sample the titania-supported catalyst shows the presence of two reduction processes. Huizinga et al. (1984) and Hoyle et al. (1985) have obtained similar results.

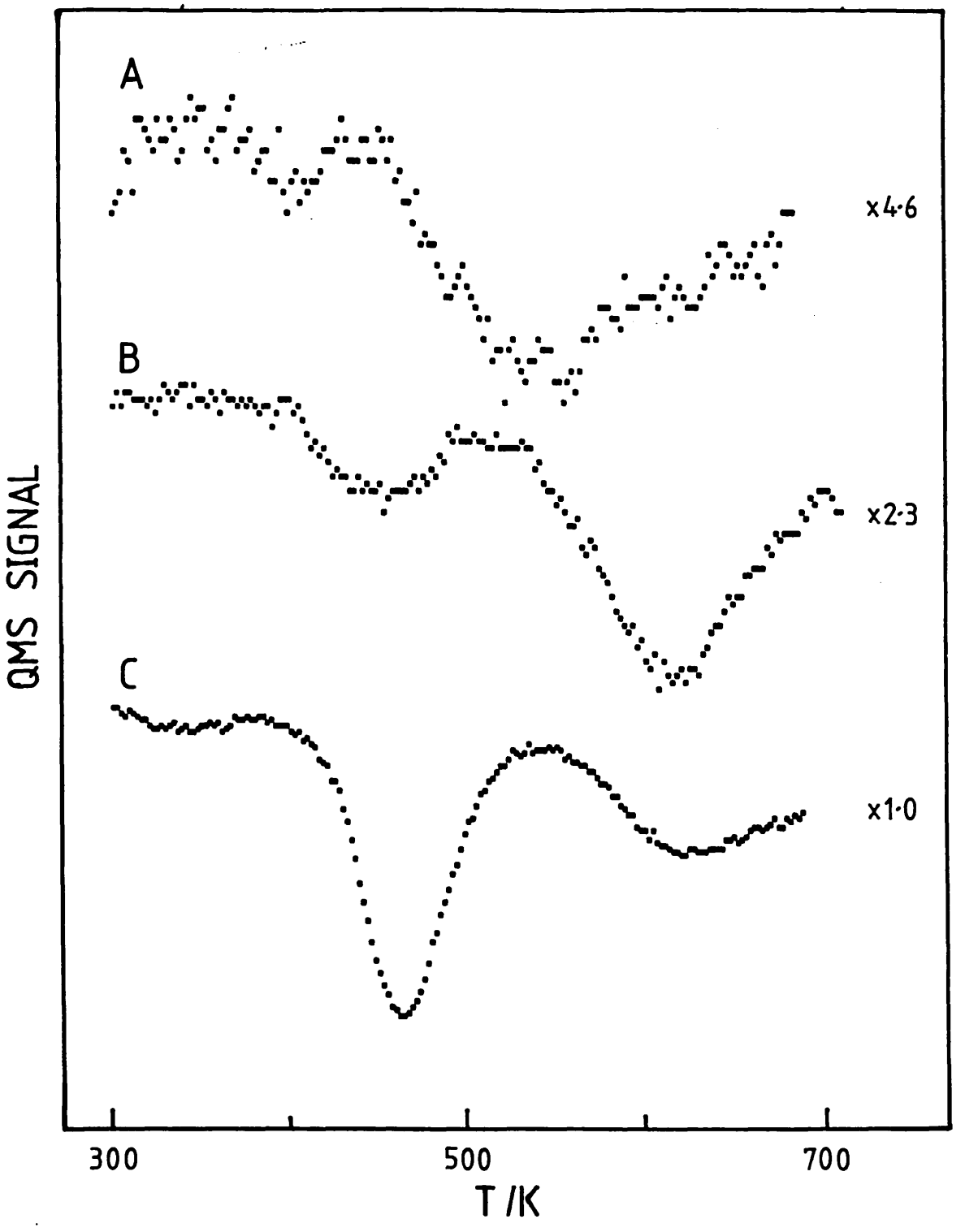

Fig. 4.3: Reduction Profiles for Pt100 Samples Subjected to Heating in N_2 at 700K (curve A), 560K (curve B) and 400K (curve C).

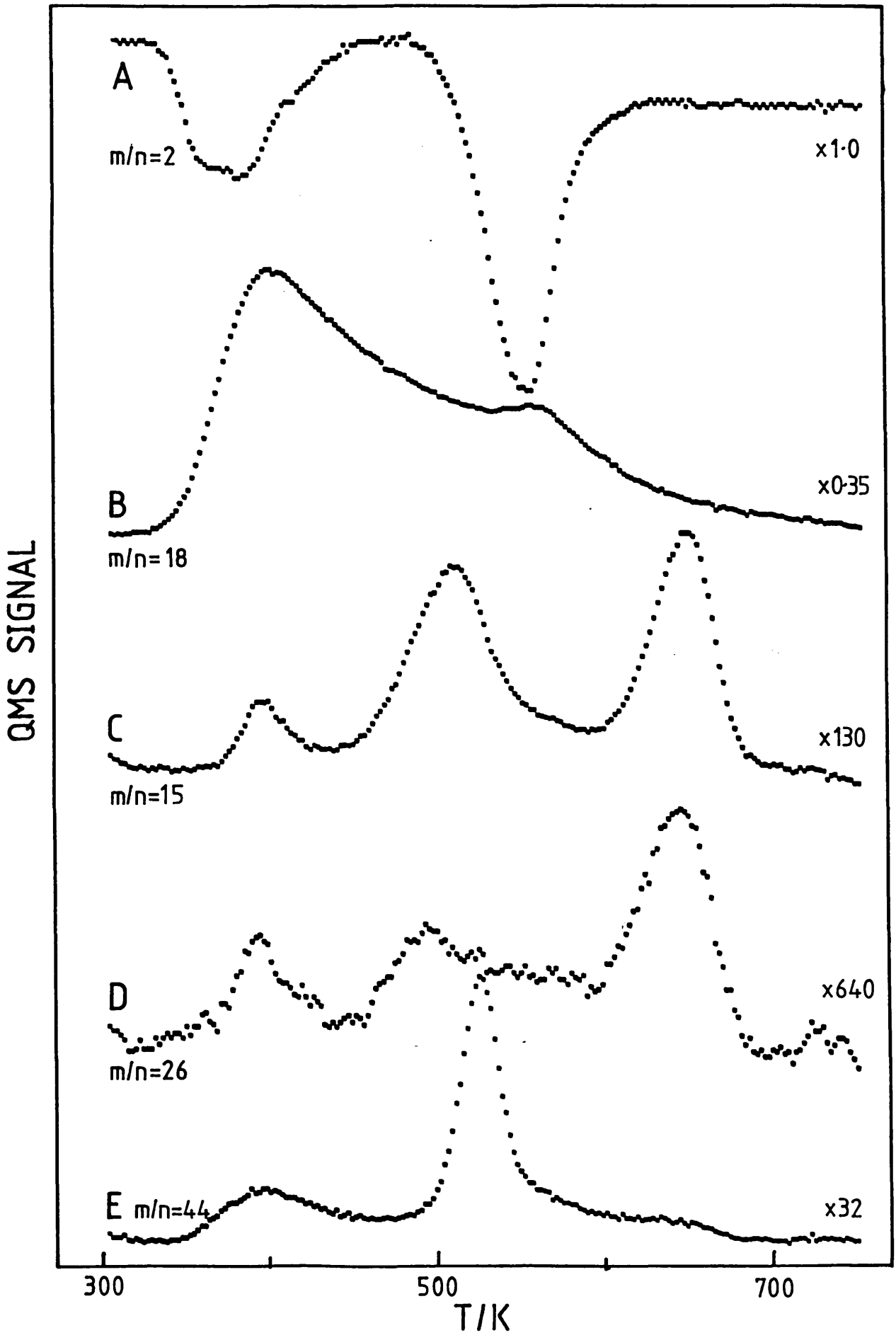

Fig. 4.4: TPR Profile for the Pt (0.8wt%)/TiO_2 Sample Subjected to Pretreatment O0.

Calibration of the low temperature process centred at a temperature of 350K shows that a complete reduction of Pt(IV) species to metal occurs. The shape of this uptake may be suggestive of a two step reduction process or may show the presence of two different reducible species. Contrary to the effects observed in the Pt/alumina system the high temperature reduction peak at 532K is not associated with any particular hydrocarbon formation reaction. However, this uptake does correspond to the production of water, seen as a shoulder on the main water peak. This high temperature uptake may therefore result from a metal catalysed reduction of the titania support. This could lead to the so called Strong Metal-Support Interaction (SMSI) state first observed by Tauster et al. (1978). As with the Pt/alumina sample Fischer-Tropsch products can be observed. However, the process does appear to be much more complex in the titania-supported system.

To summarise, the TPR results for the Pt/alumina sample show that the platinum exists in the IV oxidation state as a species which interacts with the support. Chlorine, liberated during the reduction of the metal, is adsorbed onto the alumina support displacing surface hydroxyl groups. The high temperature reduction process observed in this system is due to the hydrogenation of carbon dioxide. The carbon dioxide results from the decomposition of a carbon-containing species, which may be carbonate or formate-type species associated with the support or the metal. When platinum is supported on titania a high temperature reduction process is also observed but this does not appear to be connected with the hydrogenation of carbonaceous species as no methane is observed. The most likely explanation here is that the metal formed promotes the reduction of the support material.

ii) Iridium

Fig. 4.5 shows the TPR profile for a freshly prepared Ir100 sample that has received no oxidising pretreatment (coded 00). The hydrogen profile (curve A) shows considerable structure with reduction peaks at 350K, 383K and 431K. This is in direct contrast to the simple, single uptake observed for the Pt100 sample at low temperatures. The multiple peaks may result from the reduction of several different surface species on the alumina surface, or from reduction of a single species in several steps or a combination of

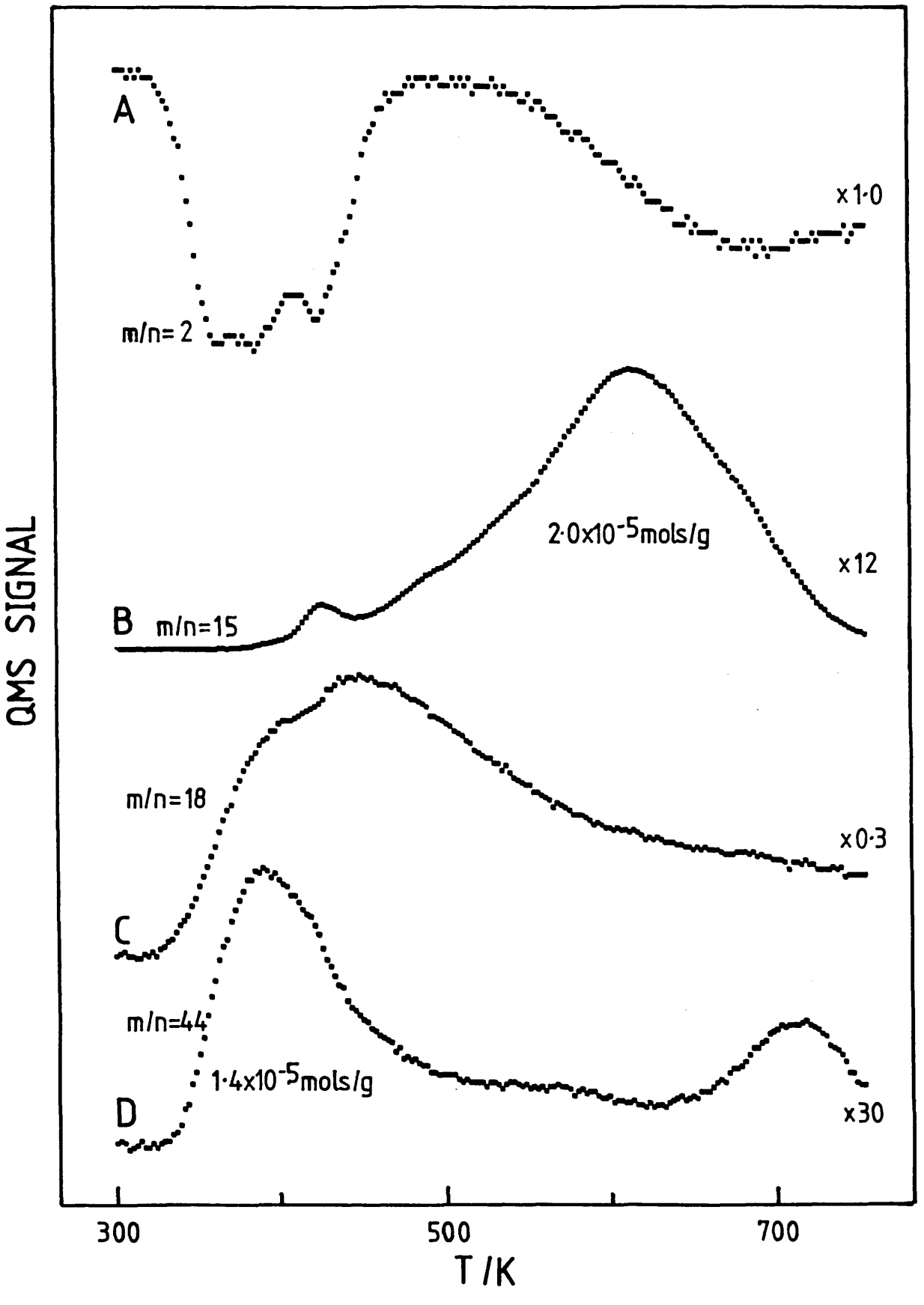

Fig. 4.5: TPR Profile for Sample Ir100 Subjected to Pretreatment O0.

both. The hydrogen uptake over the whole of this region showed that the overall oxidation state of the metal was IV. This is in contrast to the results of Escard et al. (1973) who observed the presence of an Ir(III) species on alumina following reduction at 673K. For comparison, the reduction of bulk chloroiridic acid occurs at a temperature of 425K. Thus the surface complex is less stable than the bulk compound. This is in contrast to the Pt100 sample where the reverse is true.

In agreement with the Pt100 sample no chlorine species were detected. A second peak in the water profile, occurring after the 431K reduction process, could arise from hydroxyl groups that had been displaced from the surface of the alumina by chloride ions. If this is correct chlorine evolution occurs only after the 431K reduction process begins. The size of the water peak is smaller than that found in the Pt100 sample, presumably because there are fewer chloride ions to displace the hydroxyl groups. This may result from extensive hydroxylation of the iridium complex prior to temperature-programmed reduction.

The hydrogen profile shows that at the highest temperatures used in this study (740K) a hydrogen reduction process was still occurring which was not due to methane formation (curve B). Subsequent experiments were performed in which the temperature was held constant upon attaining 740K. The hydrogen signal then returned to the base-line. The water signal (curve C) shows that water formation was also occurring at 740K. The water signal slowly returned to the base-line when the temperature was held constant. This is in contrast to the behaviour of the Pt100 sample in which the hydrogenation of carbonaceous material was predominant at temperatures above 550K.

This additional reduction behaviour for the Ir100 sample may be due to hydrogen spillover onto the support from the metal. The spiltover hydrogen may react with surface hydroxyl groups, producing water, according to the following reaction:-

$$S\text{-}OH + 2Hsp \rightarrow S\text{-}H + H_2O \qquad (4.3)$$

where S-OH and Hsp represent a surface bound hydroxyl group and spiltover hydrogen respectively. More likely, the spiltover

hydrogen may react with the support to produce a partially reduced alumina surface and water. Weller and Montagna (1971) have proposed the following type of reaction for this process:-

$$Al_2O_{3(s)} + Hsp \rightarrow 2AlO_{(s)} + H_2O_{(g)} \qquad (4.4)$$

In this scheme $Al_2O_{3(s)}$ and $AlO_{(s)}$ represent surface alumina and partially reduced alumina respectively.

The hydrogen profile shows a high temperature uptake which maximises at 681K. There is a corresponding shoulder on the methane profile (curve B) but the maximum rate of generation of methane occurs at 615K, a temperature similar to that found for the Pt100 sample. The amount of methane formed (2.0×10^{-5} mol g^{-1} catalyst) was slightly more than the amount formed by the Pt100 sample. This increased quantity may be due to the presence of additional features at 490K, 530K and around 680K. No mass 26, 29 or 43 signals arising from the formation of higher hydrocarbons were observed at these temperatures. Because of the high temperature hydrogen uptake occurring at 740K, estimation of the amount of hydrogen consumed in the methane formation process is difficult. However, an estimate was made by subtracting a linearly sloping background from the profile from 500K to 740K. Calibration of the remaining peak area indicated that 6.6×10^{-5} mol g^{-1} catalyst of hydrogen were consumed. The quantity (H/M = 1.7) is consistent with hydrogenation reaction (4.2). Higher hydrocarbons (C_2 and C_3 species), amounting to less than 10% of the total hydrocarbon formed, were observed accompanying the 431K methane peak. The fact that hydrocarbons were only observed during the 431K reduction process may be evidence for a sequential reduction mechanism producing metal only to this point. Alternatively, metal species formed at 350K and 383K may be in active at such temperatures for CO_2 hydrogenation and Fischer-Tropsch synthesis.

The total amount of carbon dioxide detected (1.4×10^{-5} mol g^{-1} catalyst) was approximately the same as that found for the Pt100 sample (1.5×10^{-5} mol g^{-1} catalyst). However, the mass 44 profile (Curve D) shows the presence of a high temperature peak at 720K. This peak is definitely due to carbon dioxide rather than C_3 hydrocarbons as there were no corresponding signals for hydrocarbon cracking fragments. There are two possible explanations for this

peak. It may be that at temperatures of around 700K the iridium surface no longer catalyses the methanation process, and carbon dioxide rather than methane is generated. However, a more likely explanation is that the carbon dioxide is adsorbed on the alumina support as a carbonate or formate-type complex and is resistant to hydrogenation, being far removed from the active metal sites. TPD experiments on a fresh Ir100 sample produced a carbon dioxide desorption profile with peaks occurring at 380K, 560K and 660K. The 660K peak was the most intense and the total amount of carbon dioxide desorbed amounted to 1.3×10^{-4} mol g^{-1} catalyst, which is roughly equivalent to the amount formed over the Pt100 sample.

The above results indicate that a variety of carbon-containing species may be formed on the samples, the number and nature of these species being dependent upon the nature of the metal present. Interestingly, when the interaction with the support is simple, as with the Pt100 sample, the carbon dioxide hydrogenation is also relatively simple. However, when the interaction is complex, as with the Ir100 sample, then the carbon dioxide hydrogenation also appears to be complex. This may be due to the hydroxylation and polymerisation of the iridium complex as discussed in Chapter Three which could result in the formation of carbonate-type complexes associated with either the metal, the support or both.

In an attempt to determine whether the reduction of the Ir100 sample proceeded by a parallel or sequential mechanism temperature-programmed reduction was performed on some of the coloured Ir100 samples described in Chapter Three and a heavily loaded Ir(10wt%)/alumina sample, prepared by the incipient wetness, impregnation technique. The results are shown in Fig. 4.6. In each case the total amount of hydrogen taken up is equivalent to complete reduction from the IV oxidation state. Reduction of a well aged, blue Ir100 sample (curve C) shows a pre-dominance of the first two peaks at 350K and 383K whereas a less well-aged, blue-green sample (curve B) shows all three reduction peaks at approximately equal intensity. It would appear that ageing decreases the intensity of the 431K peak. Curve A shows the profile of a blue-green sample that was dried overnight in flowing argon, with the reactor held at 300K. Drying reduces the intensity of the centre peak at ~385K and increases the intensity of the 350K peak. The profile for the heavily loaded 10% Ir100 sample

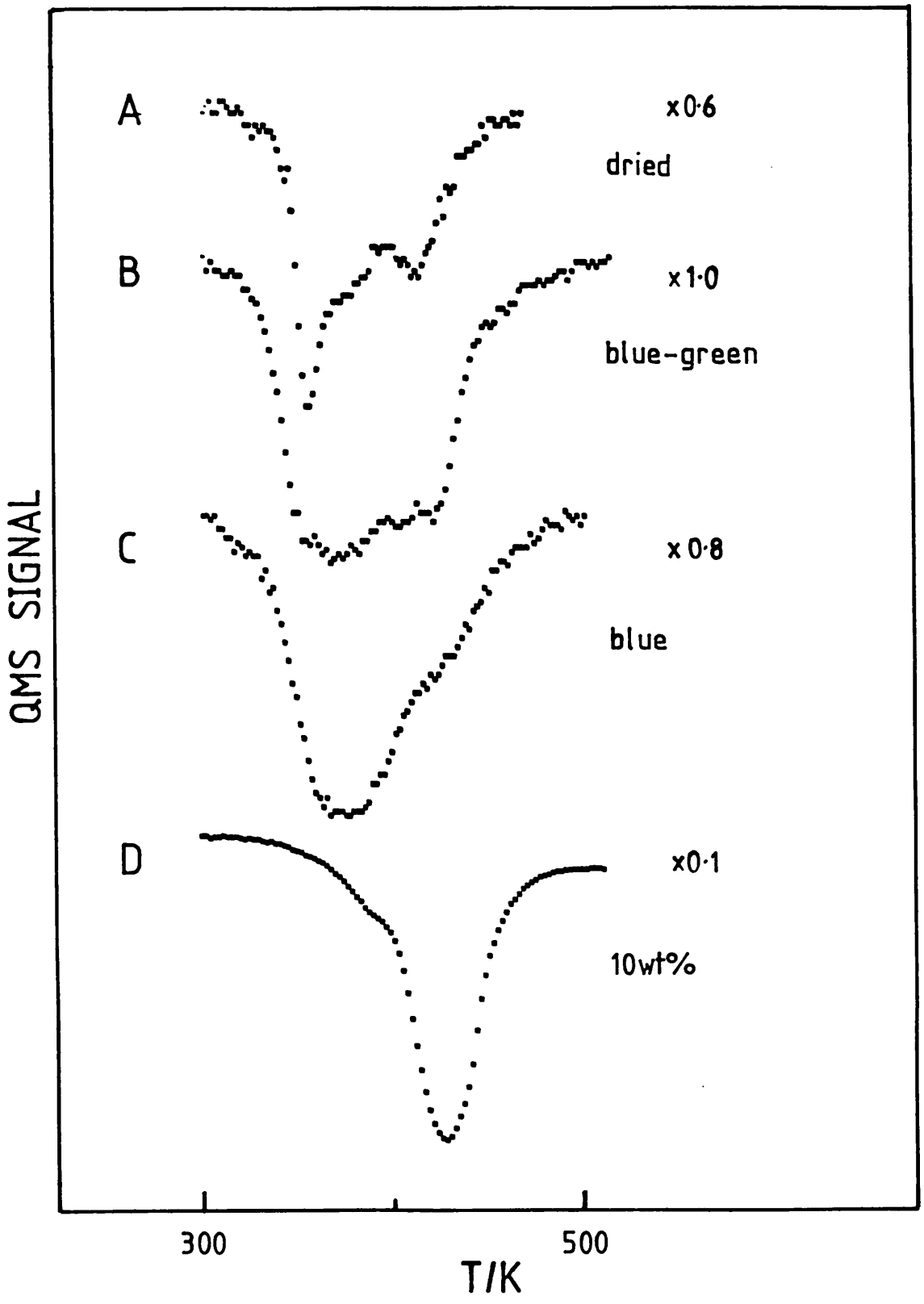

Fig. 4.6: Reduction Profiles for the Coloured Ir100 Samples (curves A to C) and the Ir(10wt%)/alumina sample (curve D)

(curve D) shows a large uptake centred at 431K with only a small shoulder at 350-380K. Although these results are difficult to interpret in detail, the variation in relative intensity of the three reduction peaks is most easily explained if the reduction processes represent the reduction of various iridium species held on the alumina support.

The results for the dried sample may be explained by proposing that drying causes the break up of the various polymeric forms of iridium on the alumina surface, presumably by removal of bridging water on hydroxyl groups. The formation of such species is governed by the number of surface hydroxyl groups on the alumina surface. Hence for the heavily loaded 10wt% Ir100 sample only a fraction (~10%) of the available metal is able to react over the support material. The reduction uptake at 431K may therefore represent the reduction of an $[Ir^{IV}\ Cl_6]^{2-}$ surface species. A tentative assignment of the metal reduction peaks shown in Fig. 4.5 is given in Table 4.3.

Table 4.3: Assignment of Metal Reduction Peaks Observed for the 00 Ir100 Sample.

Reduction Peak Temp/K	Assignment
350	$[Ir^{IV}(OH)_z(H_2O)_yCl_x]_s^{(4-x-z)+}$
383	$[Ir_n{}^{IV}O_y(OH)_z(H_2O)_wCl_x]_s^{(4n-x-2y-z)+}$
431	$[Ir^{IV}Cl_6]_s^{2-}$

Note: i) $[\ ]_s$ denotes an alumina surface complex.
ii) w, x, y and z can all vary.

The full reduction profile for the 10% Ir100 sample also showed methane formation occurring around 620K. The amount was similar to that found for the Ir100 sample. This result suggests that the amount of methane formed is either related to the amount of hydrolysed and polymeric metal species or to the alumina surface in contact with such entities. Therefore some modification of the assignments shown in Table 3 may be required, to include the presence of carbonate, bicarbonate or formate-type complexes.

The fact that hydrocarbon formation was only observed during the 431K reduction process may indicate that the reduction processes observed at 350K and 383K do not produce metal. The reduction may

stop with the formation of partially oxidised iridium chloride species which finally reduce with the hexachloroiridate-type complex at 431K.

To summarise, the TPR profile for the Ir100 sample shows that the iridium-alumina interaction is more complex than that of the platinum, probably because the $IrCl_6^{2-}$ ion is less stable than the $PtCl_6^{2-}$ ion. The complex appears to exist on the alumina surface in at least three different forms, as represented by the TPR profile. However, the fact that methane formation is not observed until the last reduction peak occurs at 431K may suggest that the earlier reductions do not form iridium metal. It may be that these species undergo a sequential reduction.

A high temperature reduction process was also observed which was a result of CO_2 hydrogenation over the metal sites. However, structure observed in the methane peak does show that this process is more complicated than the similar methanation process observed with the Pt100 sample. Furthermore, evidence for a possible partial reduction of the alumina support was obtained which was not apparent for the Pt100 sample.

iii) Platinum-Iridium

Fig. 4.7 shows the TPR profile for the PtIr43 sample which has not been subjected to any oxidation pretreatment. The hydrogen profile (curve A) shows two uptakes in the low temperature region at 383K and 431K. The amount of hydrogen taken up corresponds to the reduction of a metal IV oxidation state completely to the metal.

There is also a high temperature reduction process occurring around 647K which appears to be related to the complicated methane formation peak observed in curve B. The total amount of methane formed was 1.8×10^{-5}mol g^{-1} catalyst. As with pure iridium, the presence of a significant hydrogen uptake at 740K, makes estimation of the amount of hydrogen, necessary for the methane formation, difficult. However, using the same estimation procedure as for iridium, a value of 9.0×10^{-5} mol g^{-1} catalyst was obtained. The probable 20% error in this value associated with the estimation procedure shows that this uptake is consistent with the hydrogenation reaction 4.2. As with pure iridium, the presence of a significant hydrogen uptake, and water evolution at 740K, is indicative of surface

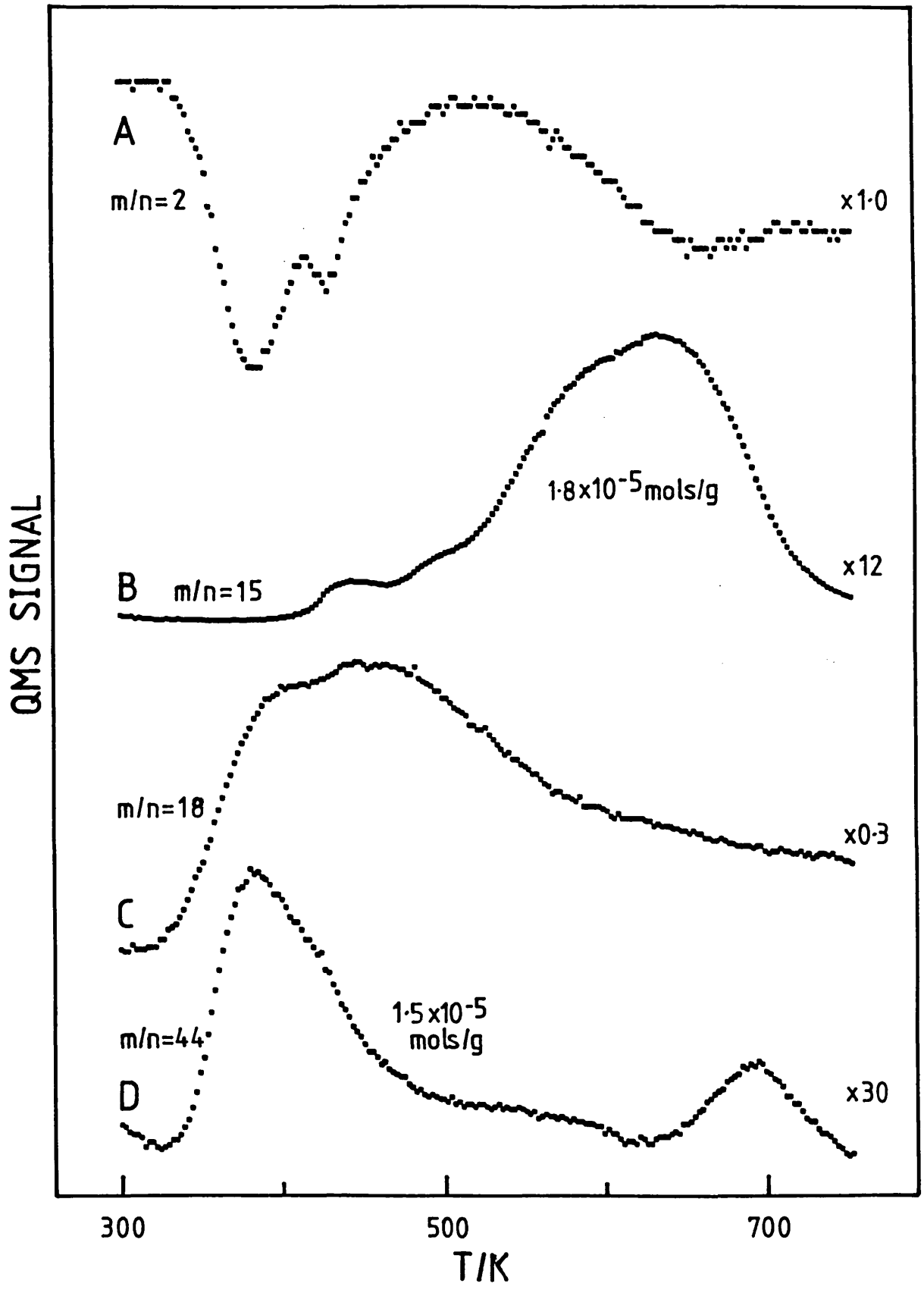

Fig. 4.7: TPR Profile for Sample PtIr43 Subjected to Pretreatment OO.

hydroxyl reduction, or support reduction, via a hydrogen spillover process. One component of the methane profile occurs at a temperature of 610K in broad agreement with the Pt100 and Ir100 samples. The main peak at 630K is also present as a shoulder with the Ir100 sample.

The total amount of carbon dioxide detected (1.5×10^{-5} mol g^{-1} catalyst) was the same as that found for the Pt100 sample. The mass 44 profile (curve D) also shows the presence of a high temperature (685K) state as found for the Ir100 sample.

For comparative purposes Fig. 4.8 shows the hydrogen profiles for the Ir100, Pt100, PtIr43 samples and the physical mix M50, without any oxidation pretreatment (coded O0). The physical mix (curve C) has a profile which is simply the sum of the two monometallic samples (curves A and B). However, the bimetallic sample (PtIr43) has a profile (curve D) closely resembling the Ir100 profile except that the 350K peak is largely missing. Thus the reduction peak at 431K in the PtIr43 sample corresponds to that found in the Ir100 sample. On the other hand, there is little evidence of characteristic Pt features, the 453K peak for the Pt100 sample being present only as a small shoulder in the PtIr43 sample. These results suggest that in the PtIr43 bimetallic catalyst the reduction of the platinum component is activated by the presence of iridium. There are three ways in which this might be brought about:

i) It is possible that metallic iridium, formed by reduction of iridium salts, catalyses the reduction of the platinum species. Alternatively, the presence of partially reduced iridium species may promote the platinum reduction. The presence of reduced platinum does not appear to promote the reduction of the remaining iridium.

ii) An intermetallic compound may be formed on the alumina surface, which has similar properties to those of the pure iridium salts.

iii) The presence of iridium salt may destablise the platinum complex, causing extensive hydroxylation and/or carbonate formation to occur with platinum as well as iridium.

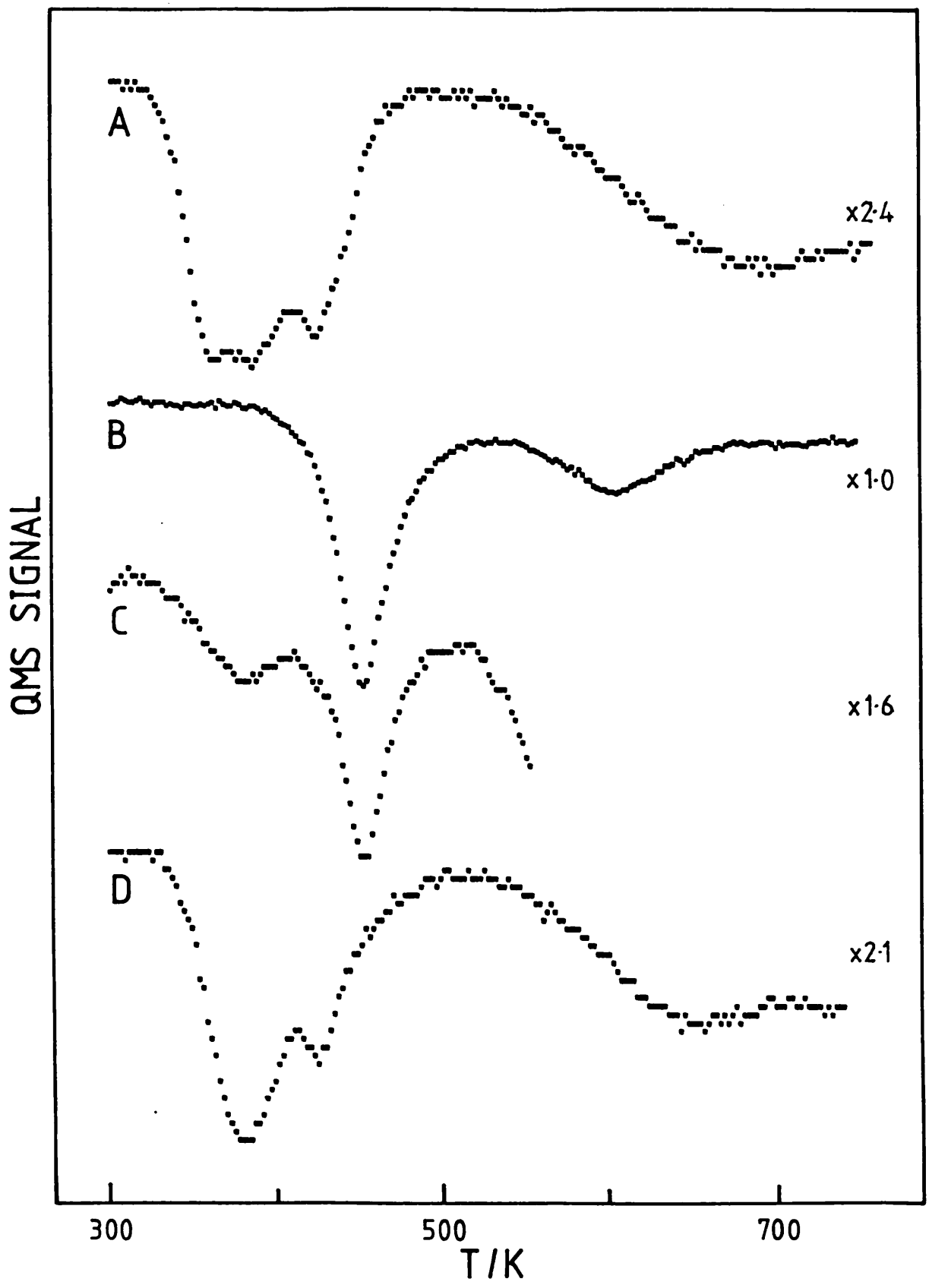

Fig. 4.8: Reduction Profiles for the Ir100 (curve A), Pt100 (curve B), M50 (curve C) and PtIr43 (curve D) Samples Subjected to Pretreatment O0.

Whatever the explanation there must be some form of interaction between the Pt and Ir complexes and it is likely that alloy clusters will be formed upon reduction. The existence of such clusters may explain the enhanced methane peak observed at a temperature of 630K with the PtIr43 sample.

Fig. 4.9 shows the hydrogen profiles obtained during temperature-programmed reduction of PtIr15 (curve A), PtIr27 (curve B), PtIr58 (curve C) and PtIr78 (curve D) samples prior to any oxidation pretreatment. The profiles which are plotted up to temperatures of 520K, show the effect of incorporating various amounts of platinum into the bimetallic samples. Table 4.4 summarises the temperatures for the various hydrogen uptake maxima for the monometallic and bimetallic samples. Also included is the quantity of hydrogen involved in the reduction process, expressed as the ratio of hydrogen atoms required for reduction, H, to metal atoms present, M.

Table 4.4: Temperatures for Maximum Rates of Reduction (Tm/K) and Total Hydrogen Uptakes (H/M) for the Freshly Prepared Bimetallic and Monometallic Samples.

Sample	Tm/K[a]				Total Uptake[b] (H/M)
Pt100	-	-	-	453	4.0
PtIr78	419	-	432	453	4.2
PtIr58	402	-	430	453[c]	4.1
PtIr43	383	-	431	453[c]	4.2
PtIr27	272	-	430	453[c]	4.1
PtIr15	363	-	427	453[c]	3.7
Ir100	350	383	431	-	3.9

Notes: a) error = $\pm$4K; b) error = $\pm$0.4; c) small component.

The results show that as the Pt/Ir ratio increases the low temperature iridium reduction peak shifts from 350K, for 100% iridium, to 419K for 22% iridium. However, the temperature for the uptake at 430K remains unaltered across the composition range. Most of the platinum complex appears to undergo reduction at temperatures within the region of these two peaks, although there is a distinct reduction occurring at 453K, the reduction temperature for pure platinum. This

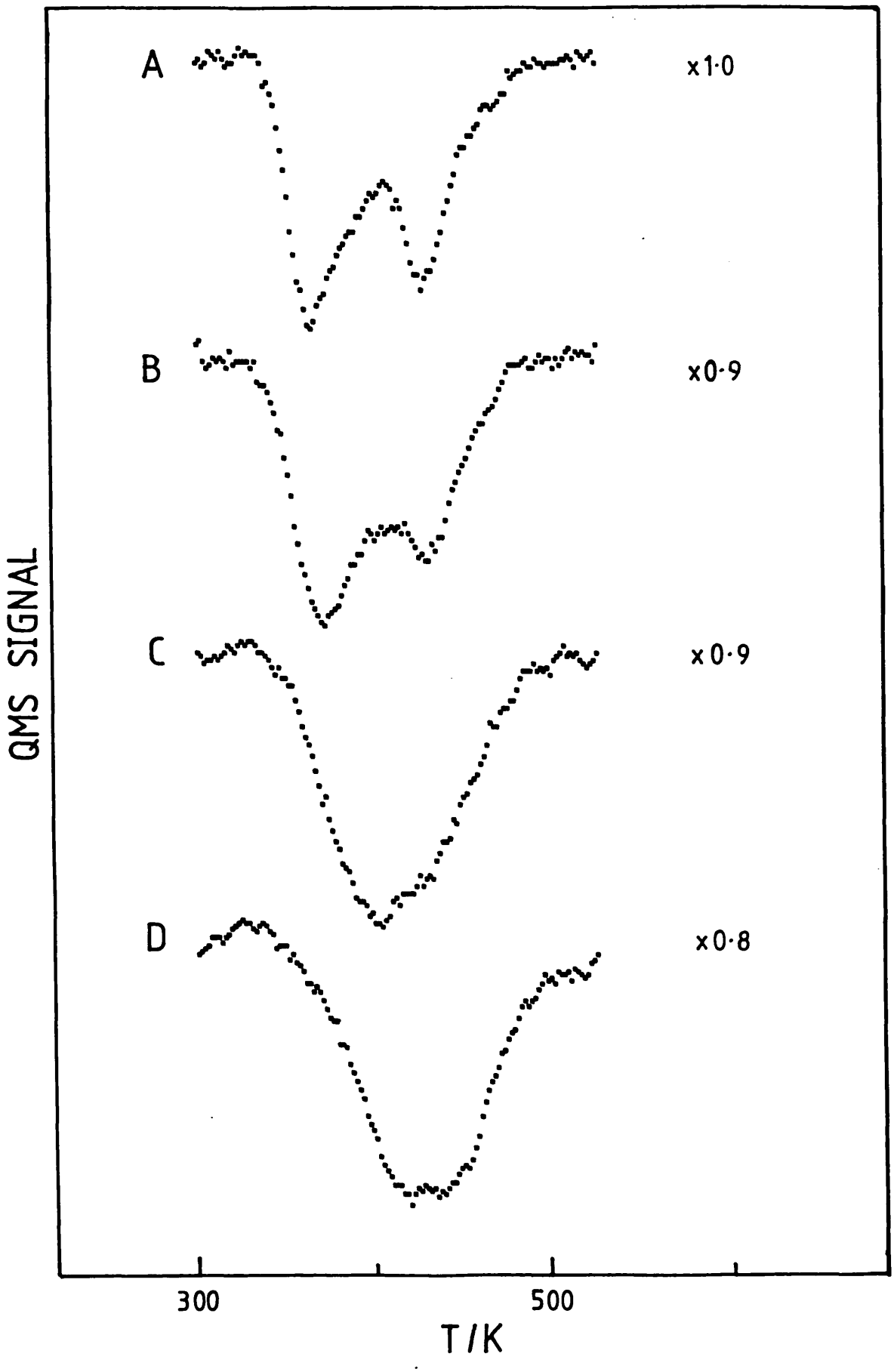

Fig. 4.9: Reduction Profiles for Samples PtIr15 (curve A), PtIr27 (curve B), PtIr58 (curve C) and PtIr78 (curve D) Subjected to Pretreatment O0.

latter peak is quite prominent with the PtIr78 sample (curve D). The results show that decreasing the amount of the more easily reduced iridium leads to an overall increase in the reduction temperature. In addition, curve A shows that incorporation of small quantities of platinum can cause the central peak at 383K to disappear. This peak has been associated with polymeric iridium species on the alumina surface. In this context it is of some interest to note that no colour changes are observed in the bimetallic catalysts when they are stored in a desiccator. With pure iridium colour changes have been associated with polymerisation of iridium on the alumina surface. Thus it may be that the presence of platinum disrupts the polymerisation of the iridium complexes.

To summarise, the reduction behaviour of freshly prepared bimetallic samples exhibit a strong interaction between the two metal species. The effect is two fold; the presence of platinum disrupts the growth of polymeric iridium species across the alumina surface whilst the presence of iridium causes the platinum to reduce at a lower temperature. The results suggest that reduction of bimetallic samples (at moderate temperatures), in the composition range 15%<Pt<78%, results in the formation of alloy clusters.

Furthermore, the presence of iridium appears to promote a high temperature reduction process, which is possibly a partial reduction of the alumina support. Such a process may well affect the properties of the catalyst system. In addition, methane formation, observed with all samples at temperatures above 500K, may be important since possible carbon deposition on the metal at these temperatures may also influence the state and reactivity of the metal clusters formed.

b) Samples Subjected to Oxidation at 740K

This section describes the temperature-programmed reduction of samples oxidised at 740K (coded O740). The section also includes the TPR results for samples reoxidised at 740K (O740 TPR740 O740) or 560K (O740 TPR740 O560) following the initial TPR experiment.

Fig. 4.10 shows the TPR profile for the PtIr43 sample subjected to the O740 pretreatment. The hydrogen profile (curve A) shows an assymmetric uptake maximising at 487K. Similar results have been obtained by Foger and Jaeger (1981a) and Faro et al.

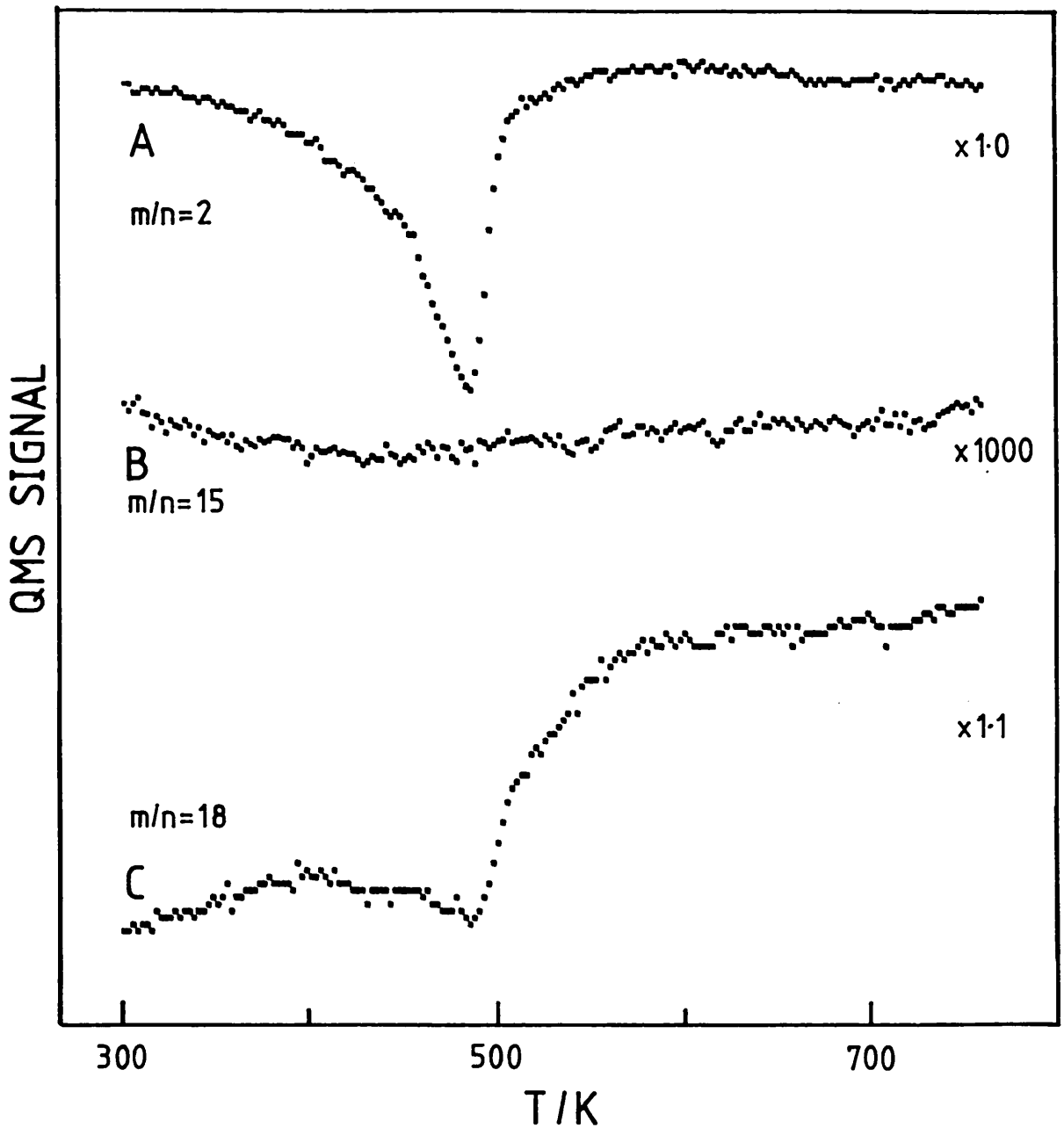

Fig. 4.10: TPR Profile for Sample PtIr43 Subjected to Pretreatment O740.

(1983). Foger and Jaeger (1981b) have also obtained similar results for silica-supported Pt-Ir catalysts.

It is significant that no methane production could be detected (curve B) indicating that the O740 pretreatment removes all the surface carbon containing species. Similarly, there was no evidence of carbon dioxide production. The water signal shows a slight dip as the reduction process maximises, which might imply consumption of water in the reduction process. However, this was an artefact caused by reaction in the mass spectrometer chamber since it was found that the water and hydrogen signals were interdependent. The absence of a water peak shows that water formed during the reduction process readsorbs onto the support. This water may act as a bridge for hydrogen spillover from the metal to the support, as suggest by Ambs and Mitchell (1983). In fact a small hydrogen uptake at temperatures above 600K can be observed and this spillover hydrogen may result in water formation according to reactions (4.3) and (4.4) once metal has formed.

Fig. 4.11 shows the TPR profile for the Pt100 sample. The hydrogen profile (curve A) shows the presence of a high temperature reduction process. This may be due to a spillover effect since water formation (not shown) similar in nature to that shown for the PtIr43 sample was observed. In addition, some methane (curve B) is still formed (3.0×10^{-7} mol g^{-1} catalyst) indicating that surface carbon-containing compounds are still present in this sample, following oxidation at 740K. However, the amount produced is much less (~2%) than for samples not subjected to oxygen pretreatment and therefore the majority of the hydrogen uptake must be caused by the processes given by reactions (4.3) or (4.4). No carbon dioxide formation could be observed, the signal at mass 44 (curve C) remaining constant throughout. These results are significant since the inclusion of the oxidation step appears to allow the support to be partially reduced. This may be related to the reduced amount of carbon on the sample following the O740 pretreatments.

Fig. 4.12 compares the hydrogen profiles obtained during the temperature-programmed reduction of samples Ir100 (curve A), Pt100 (curve B), a physical mix, M50 (curve C) and a bimetallic sample, PtIr43 (curve D) subjected to pretreatment O740. Calibration of the

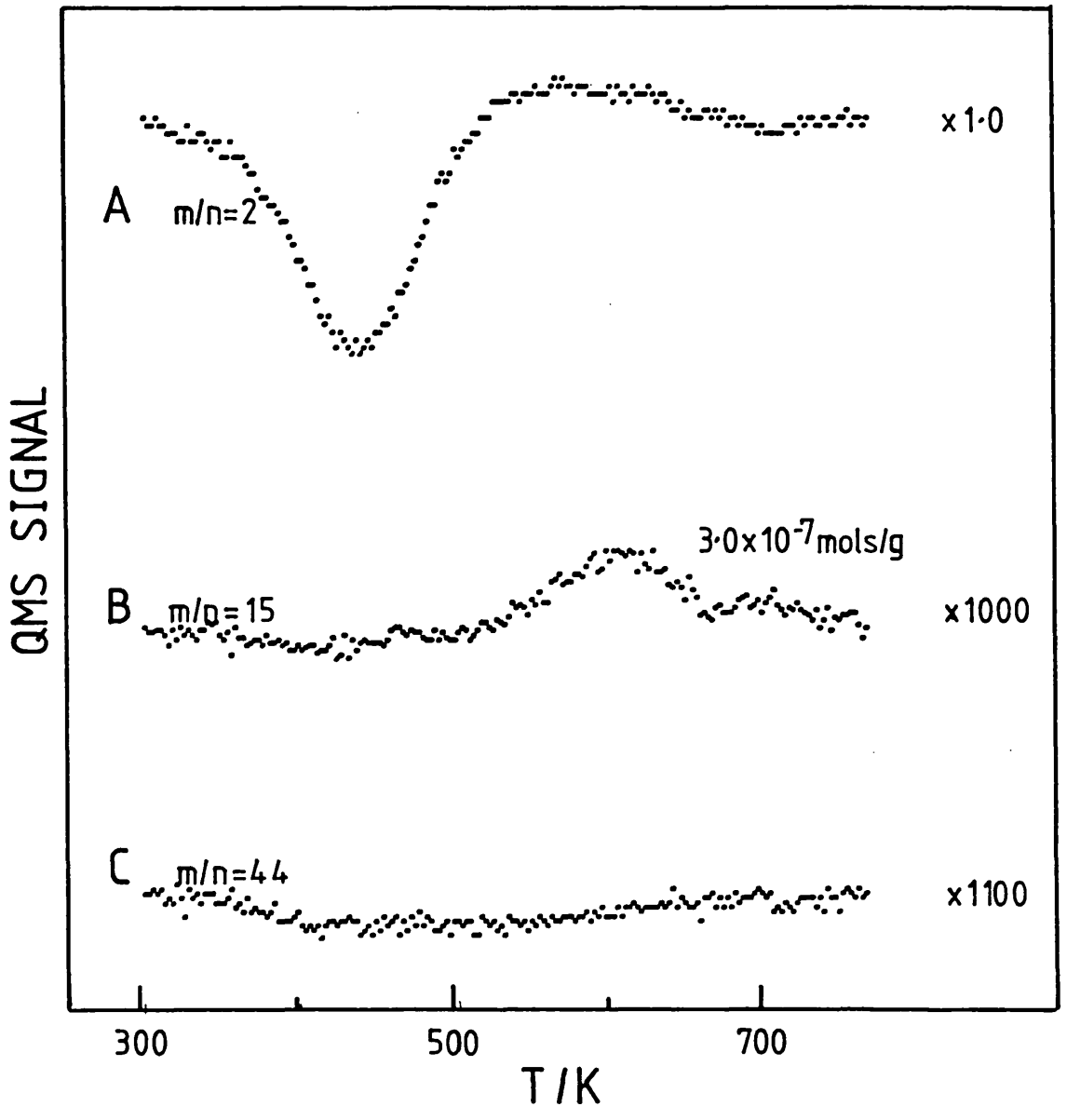

Fig. 4.11: TPR Profile for Sample Pt100 Subjected to Pretreatment O740.

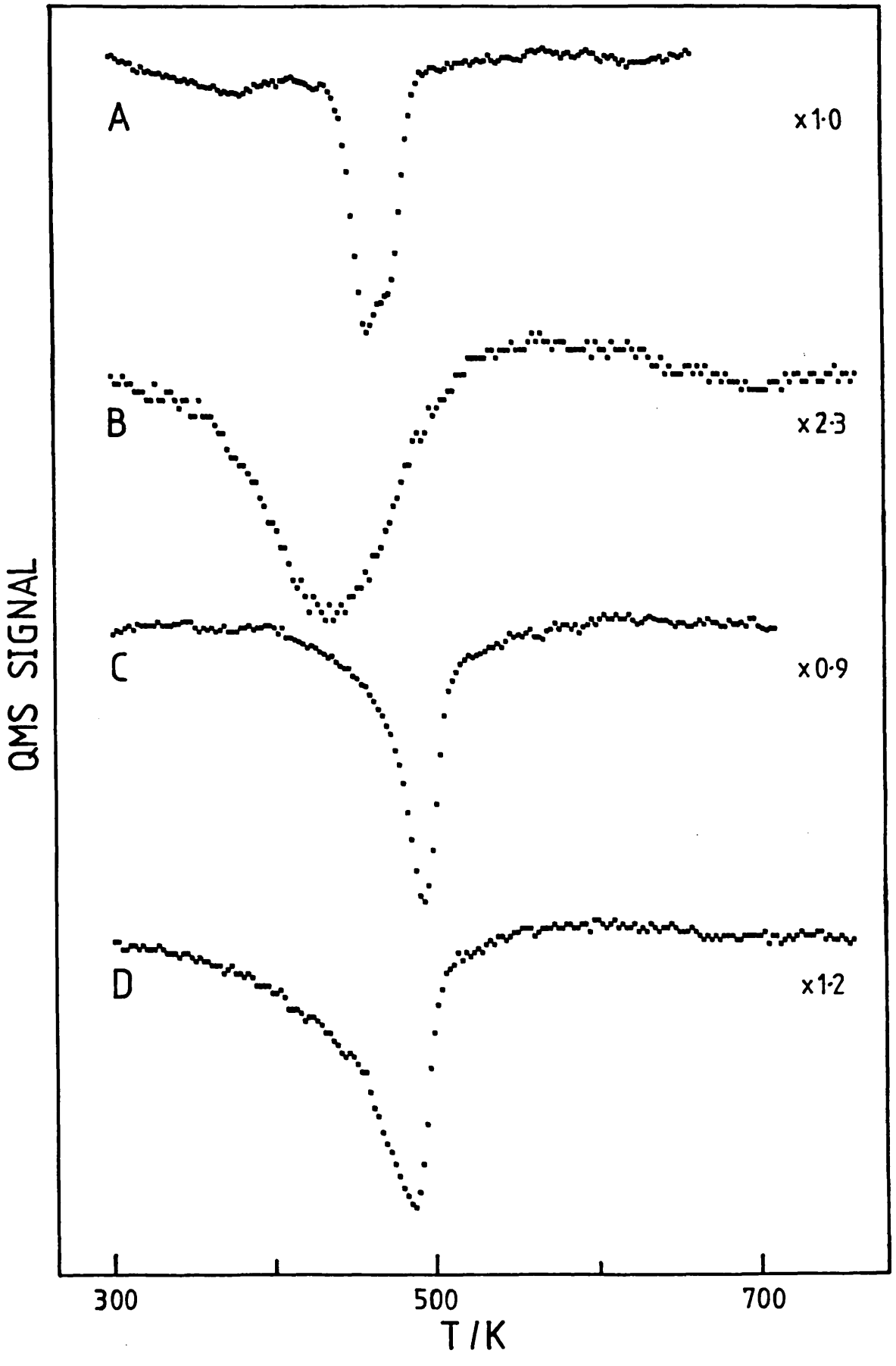

Fig. 4.12: Reduction Profiles for Samples Ir100 (curve A), Pt100 (curve B), M50 (curve C) and PtIr43 Subjected to Oxidation at 740K (Pretreatment O740).

hydrogen uptakes indicate that the metals are in the IV oxidation state following the O740 pretreatment. These species undergo complete reduction to the metal during the TPR experiment. No carbon dioxide was desorbed from any of these samples and methane was observed only with the Pt100 sample. Table 4.5 summarises the results shown in Fig. 4.12.

Table 4.5: Temperatures for Maximum Rates of Reduction (Tm/K) and Total Hydrogen Uptakes (H/M) for the Bimetallic and Monometallic Samples Subjected to Pretreatment O740.

Sample	Tm/K[a]			Uptake (H/M)[b]
Ir100	377	461	472	4.2
Pt100	-	440	-	4.0
PtIr43	-	-	487	4.1
M50	-	-	495	4.1

Note: a) error = $\pm$4K; b) error = $\pm$0.4

The Ir100 sample exhibits a low temperature uptake at 377K and two high temperature uptakes at 461K and 472K. Faro et al. (1983) have obtained similar results, with uptakes at 415K, 490K and 571K. For a silica-supported iridium sample, that had been oxidised at 800K, Foger and Jaeger (1981b) obtained a similar reduction profile with reduction maxima occurring at 348K, 488K and 513K. These workers also observed the formation of bulk IrO_2 crystallites, using XRD and SAED techniques, following this pretreatment.

In order to determine the nature of the reduction process observed for the Ir100 sample a fresh sample was oxidised at 740K. This sample was then subjected to temperature-programmed reduction up to a maximum temperature of 405K. A subsequent temperature-programmed reduction performed on the sample, starting at 298K, resulted in a shift downwards of the 461K and 472K doublet to temperatures of 428K and 437K. This can only be explained if metal formed during the reduction process at 377K catalyses the later reduction. A similar auto-catalytic effect was observed by Foger and Jaeger (1981b) for silica-supported iridium. However, the intermediate reduction temperature in their study was sufficiently high for some of the high temperature species to be reduced.

The sharpness of the Ir100 profile and the results of Foger and Jaeger (1981b) for the silica-supported system, indicates that reduction of a bulk-like oxide phase is occurring. The doublet at 461K and 472K is therefore assigned as the reduction of bulk IrO_2. However, it is not clear whether the two peaks signify two oxide species or whether a single species undergoes sequential reduction. One possibility is that IrO_2 present on the surface and in the pore structure of the alumina reduce differently. The reduction appears to be promoted by the presence of a highly dispensed iridium metal phase formed during the reduction at 377K.

By comparison, the Pt100 hydrogen uptake is very broad indicating the reduction of a highly dispersed, heterogeneous species. Lieske et al. (1983) and Lietz et al. (1983) have assigned this species as a $Pt(IV)O_xCl_y$ surface complex. The variation in x and y producing the heterogeneous character of the reduction profile.

The profile for the bimetallic sample (curve D) indicates that substantial agglomeration of the iridium component has occurred. This could result in the formation of a highly dispersed platinum-rich phase and large iridium-rich crystallites, when the oxide species are reduced. The upwards shift in the reduction temperature of the agglomerated phase to 487K may be due to the presence of some platinum in the IrO_2 crystallites, which has the effect of stabilising the oxide. The appropriate areas contained in the TPR profiles indicate that around 65% and 80% of the iridium had agglomerated in the PtIr43 and Ir100 samples respectively.

The most remarkable result was obtained with the mixed oxide which had a TPR profile quite different from those of the two pure metals. There was little evidence of the platinum peak at 440K and the sharp uptake found with iridium now occurred at the higher temperature of 493K. This is clear evidence that there has been a transfer of iridium and platinum between the alumina particles, possibly by the vapour phase transport of IrO_3 and PtO_2. The absence of a substantial platinum peak at 440K can only be explained if the major part of the platinum has formed a mixed bulk oxide with the IrO_2. This may explain why reduction occurs at 493K rather than 461, 472K with pure iridium.

Fig. 4.13 shows the hydrogen profiles obtained during the TPR of samples subjected to a repeat oxidation at 740K (coded O740 TPR740 O740). Curve A shows the reduction behaviour of the Ir100 sample. A sharp reduction peak at 465K is still present but no longer exists as a doublet. Reduction peaks at 379K and 430K can also be observed. If the latter two peaks are assigned to a reduction of dispersed oxide or oxychloride phases respectively, then it can be concluded that the above pretreatment causes a limited redispersion of the oxide to occur. Wang and Schmidt (1980) have observed such a redispersion phenomena for model Ir/silica catalysts using STEM.

After the second oxidation, the Pt100 sample shows the presence of a new low temperature reduction peak at 383K as well as the high temperature peak at 435K, previously observed. The 383K peak also contains a slight shoulder at around 360K. Using the assignments of Lieske et al. (1983) and Lietz et al. (1983) these peaks can be attributed to the reduction of a dispersed $Pt(IV)O_2$ surface complex (at 383K) and dispersed $Pt(IV)O_xCl_y$ species (at 435K). These workers made their assignments on the basis of results obtained using temperature-programmed reduction and u.v./visible spectrophotometry. The temperatures for maximum rates of reduction obtained by these workers were higher than those obtained in this study. However, this may be due to large quantity of material (1g) used for TPR in their work, resulting in a large thermal lag for their samples.

The 383K and 435K uptakes can also be seen in the profiles for both the physical mixture (curve C) and the PtIr43 sample (curve D). The PtIr43 sample is the sum of the monometallics although the sharp reduction peak is shifted to 474K. The similarity of the M50 and PtIr43 samples is a strong indication that the iridium component does agglomerate by an interparticle mechanism. Table 4.6 summarises the results shown in Fig. 4.13.

The hydrogen uptakes given in Table 4.6 are significantly less than those obtained for the first oxidation (Table 4.5) and most probably correspond to incomplete oxidation of all the metal.

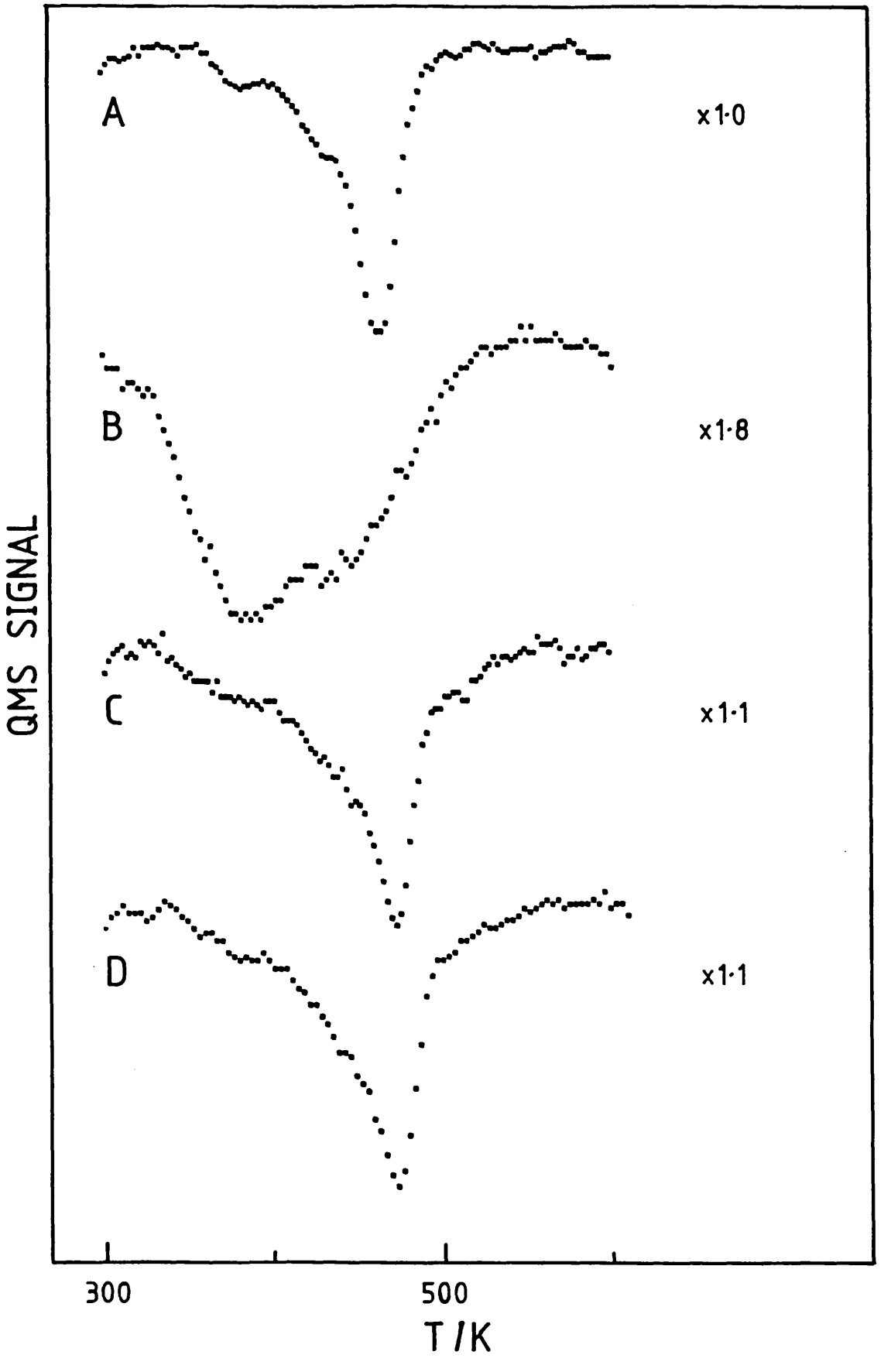

Fig. 4.13: Reduction Profiles for Samples Ir100 (curve A), Pt100 (curve B), M50 (curve C) and PtIr43 (curve D) Subjected to Pretreatment O740 TPR740 O740.

Table 4.6: Reduction Peak Temperatures (Tm) and Hydrogen Uptake Values (H/M) for Samples Subjected to Pretreatment O740 TPR740 O740.

Sample	Tm/K[a]			Uptake (H/M)[b]
Ir100	379	430	465	3.5
Pt100	383[c]	435	-	3.1
PtIr43	383	435	474	3.5
M50	383	435	474	3.5

Note: a) error = ±4K; b) error = ±0.4; c) component present at 360K.

This is particularly evident with the Pt100 sample. It seems likely that Pt(II)O as well as Pt(IV)O_2 is formed, in which case a H/M ratio approaching 3 could easily be obtained. The reduction of the Pt(II)O species may account for the shoulder present at 360K. Alternatively, the low uptake values may be due to loss of metal from the samples, due to vapour phase transport. However, no evidence of condensed metal species could be found in cold sections of tubing downstream from the reactor.

Fig. 4.14 shows the hydrogen profiles obtained during temperature-programmed reduction of samples subjected to a repeat oxidation at 560K (coded O740 TPR740 O560).

The profile for the Ir100 sample (curve A) shows a single reduction peak occurring at 410K, the total amount of hydrogen taken up corresponding to an H/M value of 0.9. It would appear that only the most highly dispersed iridium is oxidised at 560K and larger crystallites remain in the metallic state. The larger crystallites probably form a chemisorbed surface oxide which is removed by exposure to hydrogen at 300K. The hydrogen uptake suggests that approximately 80% of the iridium can be found in the large crystallites, if dispersed Ir(IV) oxide species were present.

By comparison the Pt100 sample shows a much larger hydrogen uptake (H/M ratio = 2.7) centred at 359K, which was only present as a shoulder after the O740 TPR740 O740 pretreatment. The 383K reduction process, which was prominent after the latter pretreatment, is now only present as a shoulder on the 359K uptake. Clearly, reoxidation at 560K results in the formation of increased quantities

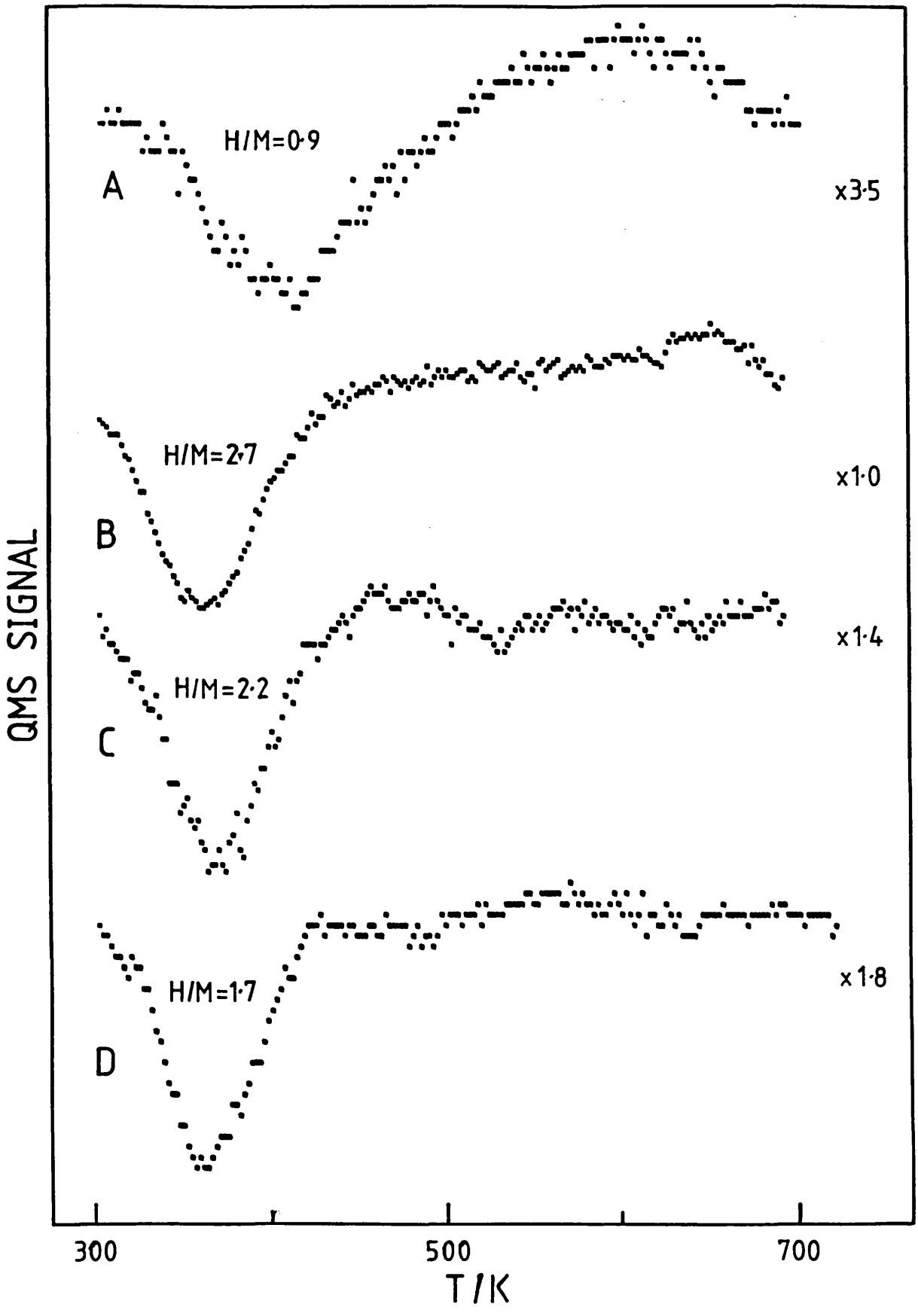

Fig. 4.14: Reduction Profiles for Samples Ir100 (curve A), Pt100 (curve B), M50 (curve C) and PtIr43 (curve D) subjected to Pretreatment O740 TPR740 O560.

of the Pt(II)O phase, relative to reoxidation at 740K. Additionally, no oxychloride-type species can be observed following the 560K reoxidation.

The profiles for the physical mix (curve C) and the PtIr43 samples are very similar. From a comparison with the Pt100 profile it would appear that only the highly dispersed platinum-rich phase has been oxidised to any extent in these samples, the iridium component being largely unaffected by heating in oxygen to 560K. The hydrogen uptakes expressed as H/M ratios are included in Fig. 4.14.

To summarise, the TPR profile for the bimetallic PtIr43 sample subjected to oxidation at 740K, indicates that such pretreatment produces a highly dispersed platinum-rich oxide phase and large iridium-rich oxide crystallites. From a comparison with the results of the monometallic samples it would appear that the iridium-rich phase has the structure of bulk IrO_2 whilst the dispersed platinum-rich phase is most likely to consist of platinum oxychloride surface complexes. Reduction of the oxidised catalyst may result in a limited redispersion of the iridium component. The simplest explanation for the reductive behaviour of the physical mixture is that interparticle transport of iridium, and possibly platinum, is occurring via volatile, or highly mobile oxides.

Reoxidation of the monometallic iridium sample at 560K results in the oxidation of the remaining dispersed metal and the possible formation of a surface oxide on the large iridium crystallites. By contrast the whole of the highly dispersed Pt100 sample becomes oxidised at 560K produçing PtO and PtO_2 surface complexes. Reoxidation of the bimetallic sample at 560K also produced the PtO and PtO_2 type complexes, and presumably a surface oxide on the large iridium-rich crystallites.

Reoxidation of the Pt100 sample at 740K resulted mainly in the formation of PtO_2 with some oxychloride species present as well. These two phases were also apparent in both the physical mixture and the bimetallic samples. For the Ir100 sample reduction/oxidation cycles at 740K may cause some redispersion to occur in agreement with the results of Wang and Schmidt (1980).

Finally, oxidation at 740K appears to effectively remove the carbon-containing species from the iridium and bimetallic samples. However, the TPR of the platinum sample does show a limited pro-

duction of methane, indicating that some carbon is still present in this sample. Furthermore, the insertion of the high temperature oxidation step may allow a partial reduction of the support to occur for the Pt100 sample.

c) Samples Subjected to Initial Oxidation at 560K

Fig. 4.15 shows the TPR profile for the bimetallic PtIr43 sample subjected to pretreatment O560. The hydrogen profile (curve A) shows reduction processes occurring at 430K and 629K, the latter being associated with the production of methane (curve B). The methane profile is less structured than that found after no oxidation (Fig. 4.7). The quantity of methane produced amounted to 1.4×10^{-5} mol g^{-1} catalyst. The amount of hydrogen consumed above 550K (5.5×10^{-5} mol g^{-1} catalyst) is consistent with reaction (4.2). No low temperature carbon dioxide desorption was obtained and no higher hydrocarbons were detected.

The water profile (curve C) starts to rise as the reduction process starts at 388K. This is partly due to water being produced from the reduction of oxidised metal species. However, the water signal remains above the baseline thereby indicating a possible reaction between spiltover hydrogen and the support according to reactions (4.3) or (4.4). This interpretation is open to question, however, since no significant hydrogen uptake can be observed at the highest temperatures. Such water behaviour was also observed for the samples oxidised at 740K. The additional, small rise in the water signal, observed at 550K may result from the hydrogenation reaction. Alternatively, this peak may occur because the temperature is approaching that of the initial oxidation pretreatment. The desorption begins at a slightly lower temperature as a result of readsorption of water produced during the 430K reduction process.

Fig. 4.16 shows the hydrogen profiles for the Ir100 (curve A), Pt100 (curve B), M50 (Curve C) and PtIr43 (curve D) samples, subjected to the pretreatment O560. All samples exhibit a high temperature reduction process that occurs above 550K and is associated with methane formation. Profiles for methane and water were similar to those shown in Fig. 4.15. The results for the high temperature reduction process are summarised in Table 4.7. No carbon dioxide, carbon monoxide or higher hydrocarbons were detected with any sample.

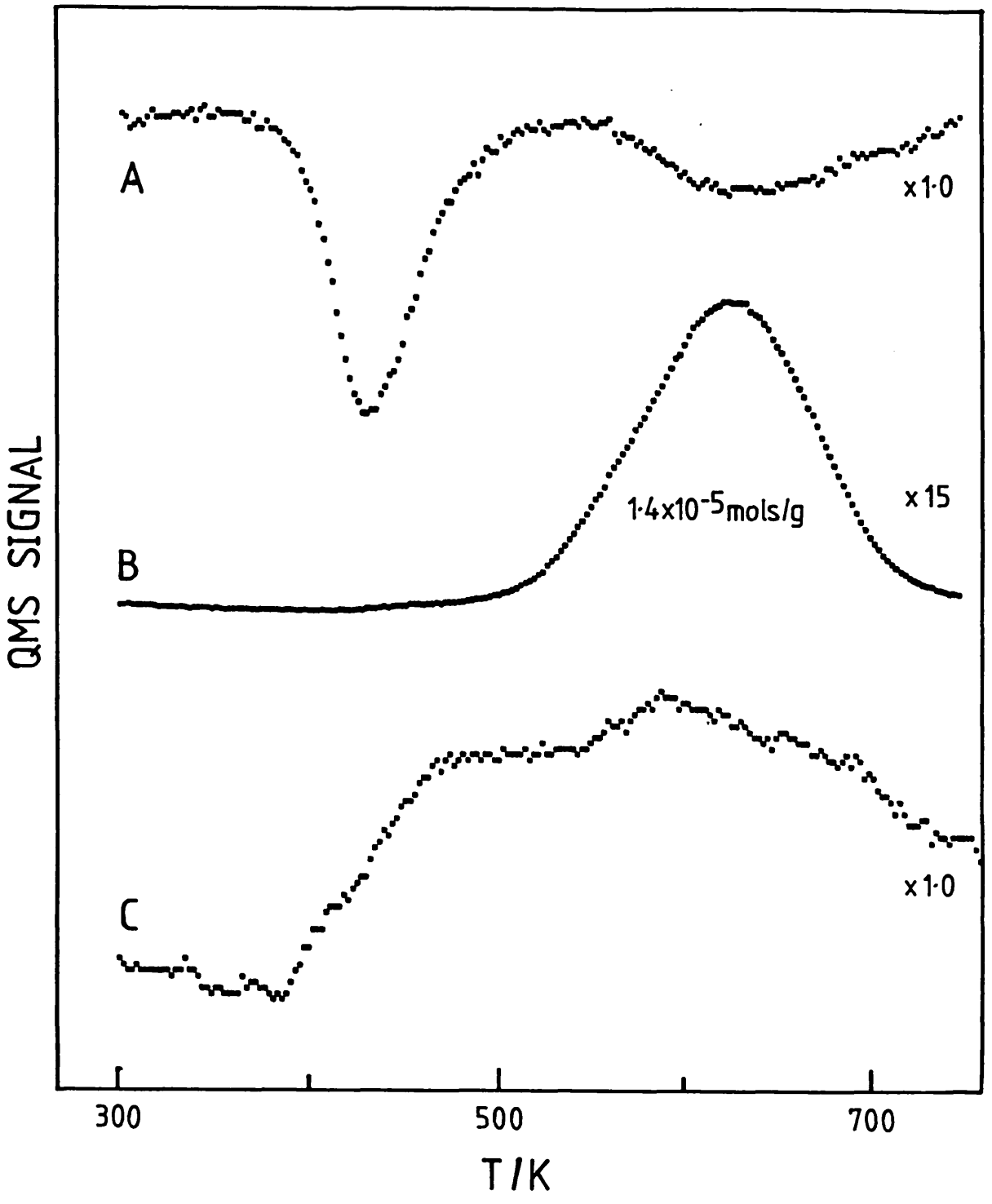

Fig. 4.15: TPR Profile for Sample PtIr43 Subjected to Pretreatment O560

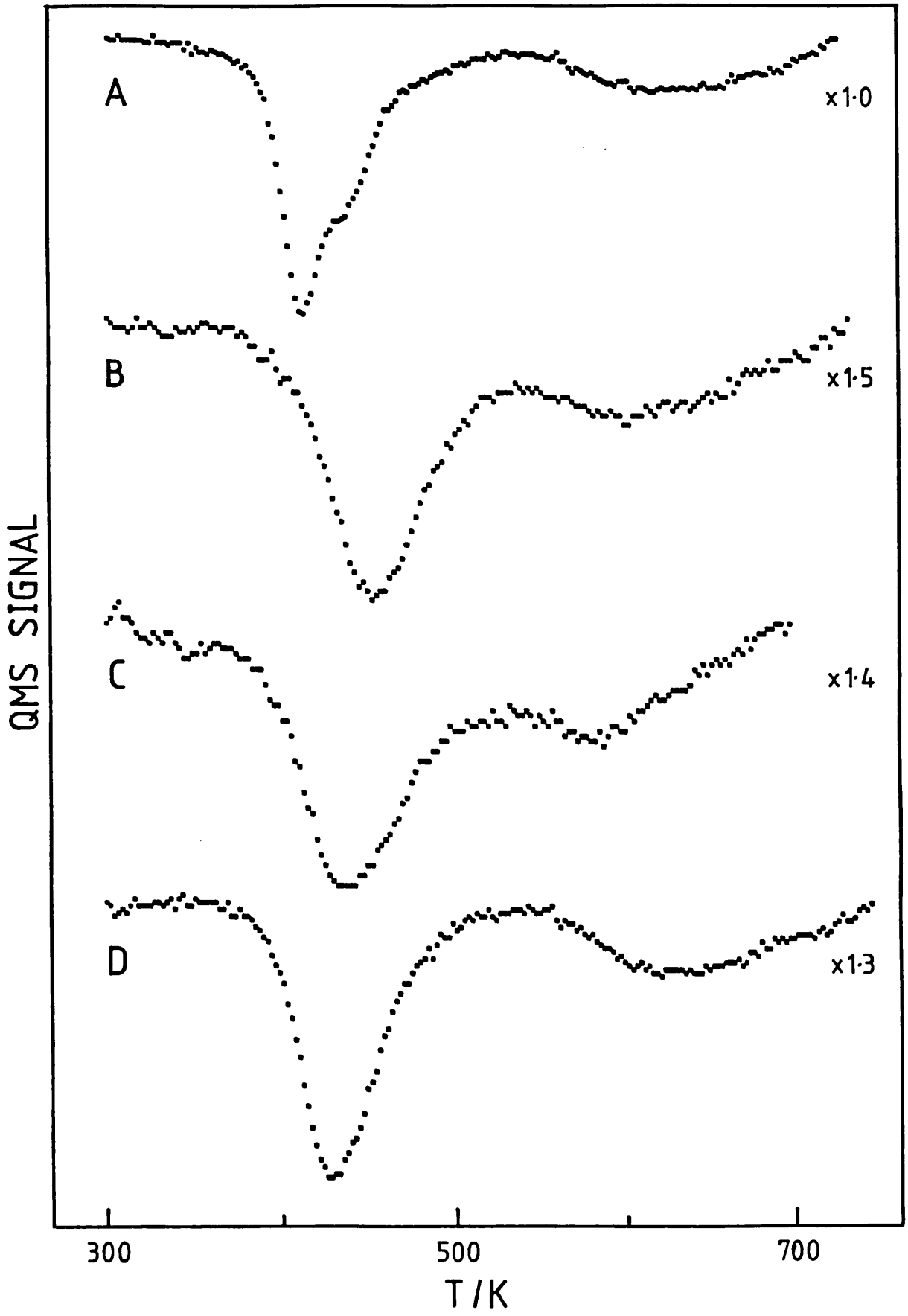

Fig. 4.16: Reduction Profiles for samples Ir100 (curve A), Pt100 (curve B), M50 (curve C) and PtIr43 (curve D) Subjected to Pretreatment O560.

Table 4.7: High Temperature Reduction Peak Temperatures (Tm/K), Hydrogen Uptakes (H/M), Methane Formation Peak Temperatures (Tcm/K) and Amounts of Methane Formed (n/mol g^{-1}) for Samples Subjected to Pretreatment O560.

Sample	Tm/K[a]	H/M[b]	Tcm/K[a]	n^c mol g^{-1}
Ir100	600	1.8	600	1.6
Pt100	594	1.5	594	1.3
PtIr43	629	1.4	629	1.4
M50	595	1.3	601	1.4

Notes: a) error = ±4K; b) error = ±0.2; c) error = ±0.2

The total amount of hydrogen taken up in the low temperature process corresponds to a change in oxidation state for the metal from IV to O in all cases. The low temperature reduction process for the Ir100 sample (curve A) shows the presence of two reduction peaks at 410K and 435K. A reduction peak at 430K was observed in the reduction of the alumina supported precursor salt (Fig. 4.5) and it may be that heating in oxygen at 560K is insufficient to completely decompose the starting complex. However, the shift upwards in temperature to 435K may result from the formation of oxychloride species.

The Pt100 sample (curve B) shows a broad reduction peak centred at 455K. Lieske et al. (1983) and Lietz et al. (1983) have observed the formation of $Pt(IV)(OH)_xCl_y$ species after similar oxidation pretreatments. The variation of x and y would account for the broadness of the uptake. However, it is significant that the 455K uptake does occur at the same temperature as that for a Pt100 sample without any oxidation (Fig. 4.1). Therefore heating in oxygen to 560K leaves a substantial fraction of the $Pt(IV)Cl_6^{2-}$ surface species intact. This is in contrast to oxidation at 740K (Fig. 4.11) which results in a reduction profile with only a slight shoulder at 455K indicating that a substantial fraction of the $Pt(IV)Cl_6^{2-}$ surface species had reacted at this temperature.

The mix M50 gives a profile (curve C) which in some respects is similar to that of the PtIr43 sample (curve D). Neither is the simple addition of the two monometallic profiles. However, the profile of the mixture does show a more pronounced shoulder at 455K which would correspond to separate reduction of the platinum

component. The reduction peak for the PtIr43 sample is narrower showing that interactions between the two metals are important. The behaviour may be due to the formation of an intermetallic surface species. This could consist of a hydroxy chloride species with bridging hydroxyl or chloride groups. Alternatively, the reduction of one metal species may promote the reduction of the other.

The samples were then subjected to reoxidation at 560K (coded O560 TPR740 O560). A slight increase in the background pressure for the carbon dioxide was detected during the isothermal period of the reoxidation. The results of a subsequent temperature-programmed reduction are plotted in Fig. 4.17. Methane formation was observed for all samples during the temperature-programmed reduction experiment. The temperature for the maximum rate of formation was in the range 629-673K. The amount formed, for all the samples, was approximately 7×10^{-7} mol g^{-1} catalyst which is only around 4% of the amount formed after pretreatment O0. Clearly, the O560 TPR740 O560 pretreatment does not remove all the carbon from the samples. The amount remaining is significant, corresponding to a carbon to metal ratio of approximately 0.01. This carbon may well influence the properties of catalysts prepared by oxidation at 560K followed by temperature-programmed reduction to 740K.

The Ir100 sample (curve A) reduces with a broad reduction peak centred at 406K. The amount of hydrogen taken up indicates the reduction of an Ir(IV) species to metal. By comparing Fig. 4.17, Fig. 4.16 and Fig. 4.14 it appears that the same reduction process is being observed at around 410K. This is probably the reduction of a highly dispersed $Ir(IV)O_2$ species. This reduction peak is much smaller in the TPR profile of the O740 TPR740 O560 sample (Fig. 4.14) since most of the iridium agglomerates to form large crystallites of IrO_2 during the high temperature oxidation. The Pt100 profile in Fig. 4.17 (curve B) shows a low temperature reduction peak at 348K. This corresponds quite closely with the reduction peak observed in Fig. 4.14 after treatment O740 TPR740 O560. Both peaks are attributed to reduction of PtO. This interpretation is supported by a H/M ratio of 1.7 for the reduction shown in Fig. 4.17.

The PtIr43 sample (curve C) shows a single reduction peak at 369K although there are slight shoulders at 350K and 405K. The

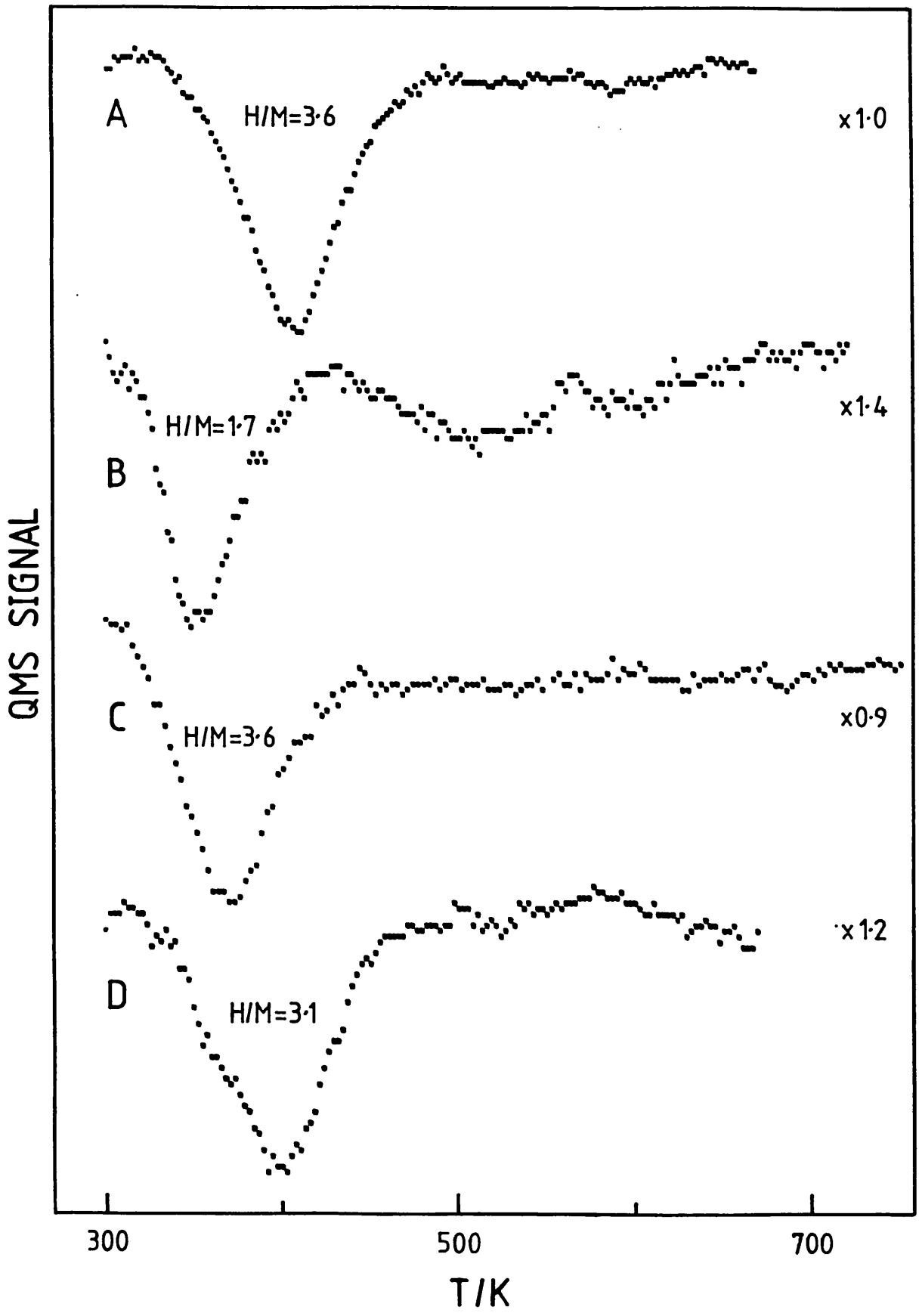

Fig. 4.17: Reduction Profiles for Samples Ir100 (curve A), Pt100 (curve B), PtIr43 (curve C) and M50 (curve D) Subjected to Pretreatment O560 TPR740 O560.

amount of hydrogen consumed corresponds to an oxide composition of $M(IV)O_2$ which may indicate that the presence of iridium promotes the oxidation of the platinum to a higher oxidation state. Hilaire et al. (1984) observed a similar phenomenon in a photoemission study of the oxidation of platinum in bulk Pt-Ir alloys. The profile for the physical mix, M50 (curve D) shows that the reduction behaviour of this sample is described by the addition of the two monometallic profiles. The amount of hydrogen consumed (H/M = 3.1) also shows that no oxidative interaction occurs between the two metals.

A PtIr43 sample subjected to O560 TPR740 O740 produced a TPR profile similar to that found for the O740 TPR740 O740 pretreatment, as shown in Fig. 4.13. This shows that the alloy clusters formed following the reduction step are unstable to oxidation at 740K.

To summarise, oxidation at 560K reduces the number of iridium species present on the alumina surface. The species observed are probably a dispersed oxide phase and oxychloride surface complexes. The platinum impregnating complex is more stable but does react to form some new surface species, which may be various hydroxychlorides. The bimetallic sample may react to form similar species. The oxidised species present exhibit a reductive interaction which suggests the formation of alloy clusters during reduction.

Reoxidation at 560K may result in the formation of separate dispersed oxide species in the PtIr43 sample. The presence of iridium appears to promote the oxidation of platinum. The oxidised species present still show a reductive interaction which indicates the reformation of alloy clusters during reduction. However, reoxidation at 740K produces iridium agglomeration into large oxide crystallites. In this case reduction results in the formation of a dispersed platinum-rich phase and large iridium-rich crystallites.

4.3.2 Temperature-Programmed Oxidation

The description of the TPO results has been divided into three sections. The first section describes the results of TPO experiments performed on the alumina-supported precursor salts (pretreatment O0). The second section describes the oxidation of samples that have already been oxidised at 740K, then reduced at 740K, and finally heated to 620K in an inert carrier gas (pretreat-

ment O740 R740 TPD620). The desorption to 620K removed adsorped hydrogen, which otherwise would have complicated the TPO profile. The final section presents the results for samples previously subjected to reduction at 610K, followed by heating in an inert gas to 630K (pretreatment R610 TPD630). Similar TPO results were obtained for samples initially oxidised at 560K, prior to reduction (coded O560 R610 TPD630).

a) Samples Subjected to No Oxidation Pretreatment

Fig. 4.18 shows the oxygen profiles obtained for the temperature-programmed oxidation of samples Ir100 (curve A), Pt100 (curve B) and PtIr43 (curve C). All the profiles show three regions of oxygen uptake which occur at approximately the same temperatures in each case. The amount of oxygen consumed is included in the figure. The profiles for the platinum-containing samples show a desorption of oxygen at temperatures greater than 740K which is probably due to the decomposition of oxygen-containing Pt species. A comparison of this data with the carbon dioxide profiles illustrated in Fig. 4.19 shows that all the oxygen uptakes are accompanied by the desorption of carbon dioxide. The amounts of carbon dioxide produced are included in the figure and appear to be less than the corresponding amounts of oxygen consumed. However, only with the Pt100 sample is the excess equal to the amount of oxygen required to form a $M(IV)O_2$ species. The probable 20% error in these quantities arising from the calibration procedure could account for the apparent discrepancy for the Ir100 and PtIr43 samples. However, the similar shape of the profiles shown in Figs. 4.19 and 4.18 suggests that if any additional oxygen uptake does occur, then this must take place at the same time as the carbon dioxide is produced.

The temperature-programmed oxidation of an alumina sample produced CO_2 peaks at 390K, 590K and 710K (profile not shown). The profile was similar to that shown in Fig. 4.2 with the additional presence of the 710K peak. The total amount of carbon dioxide produced, over the alumina sample (4.1×10^{-5} mol g^{-1} alumina), was much less than the quantity found with the metal samples. Also, an oxygen uptake was only apparent for the 710K carbon dioxide peak. The first of the alumina carbon dioxide peaks corresponds to a small carbon dioxide peak observed with all the metal samples at 386K. The second and third peaks also correspond roughly to carbon dioxide

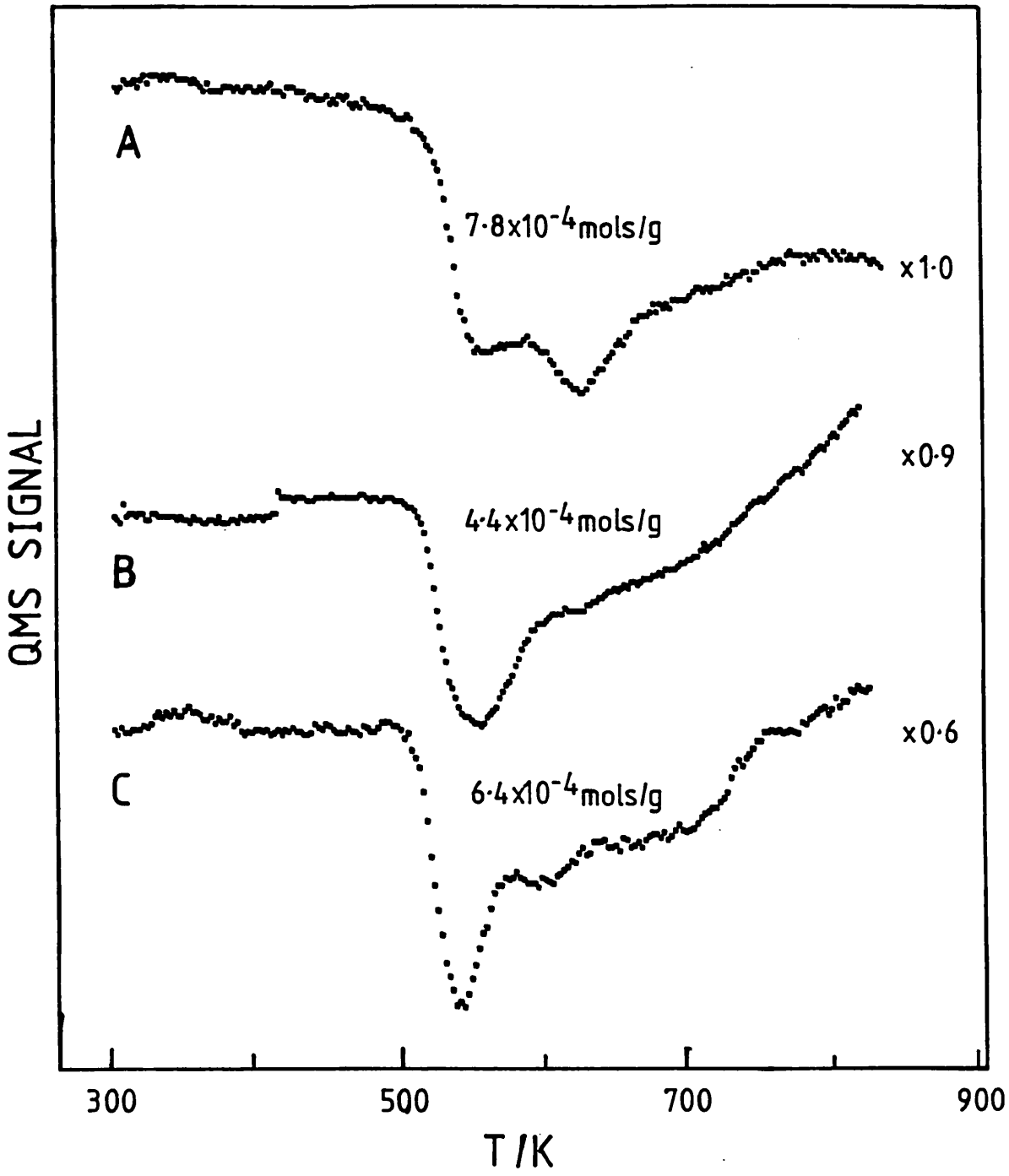

Fig. 4.18: Oxidation Profiles for Samples Ir100 (curve A), Pt100 (curve B) and PtIr43 (curve C) Subjected to Pre-treatment O0.

peaks found with the metal samples at 602-619K and 697-713K, although the second peak was much reduced in intensity for the alumina sample. However, the major peak at 545-560K shown in Fig. 4.19 has no analogue in the temperature-programmed oxidation of pure alumina.

Fig. 4.20 compares the water signals obtained, for the above samples, during the TPO experiments. For the metal-containing samples a small peak can be observed at around 548K which is not present with the alumina sample. Also shown is the mass 35 signal (for chlorine species) obtained for the Pt100 sample (curve E). It can be seen that chlorine is liberated during temperature-programmed oxidation at 432K. Similar profiles were obtained for the Ir100 and PtIr43 samples. This indicates that hydroxychloride, or oxychloride species, may form at such temperatures.

The above results suggest that oxidation of the supported metal complex either occurs at the same time as the production of carbon dioxide or occurs over a broad temperature range and is independent of the carbon dioxide production. The observed liberation of chlorine indicates that this reaction may begin at temperatures as low as 400K. Additionally, if it is assumed that all the observed oxygen uptake is accounted for by the production of carbon dioxide then the metal complex must react with oxygen already on the sample. The source of this oxygen may be support oxygen anions, or hydroxyl groups, or could be oxygen originally found in the carbon-containing species postulated in Section 4.3.1. However, the effect of heating in an inert gas (described in Section 4.3.1a) suggests that the presence of oxygen, in the carrier, enhances this reaction and prevents the decomposition of the salt to the metal.

The production of carbon dioxide at 545-560K was accompanied by the evolution of water. This may be due to the oxidation of a surface formate species as shown in the following reaction:-

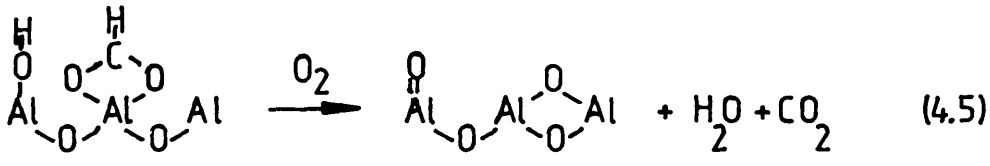

(4.5)

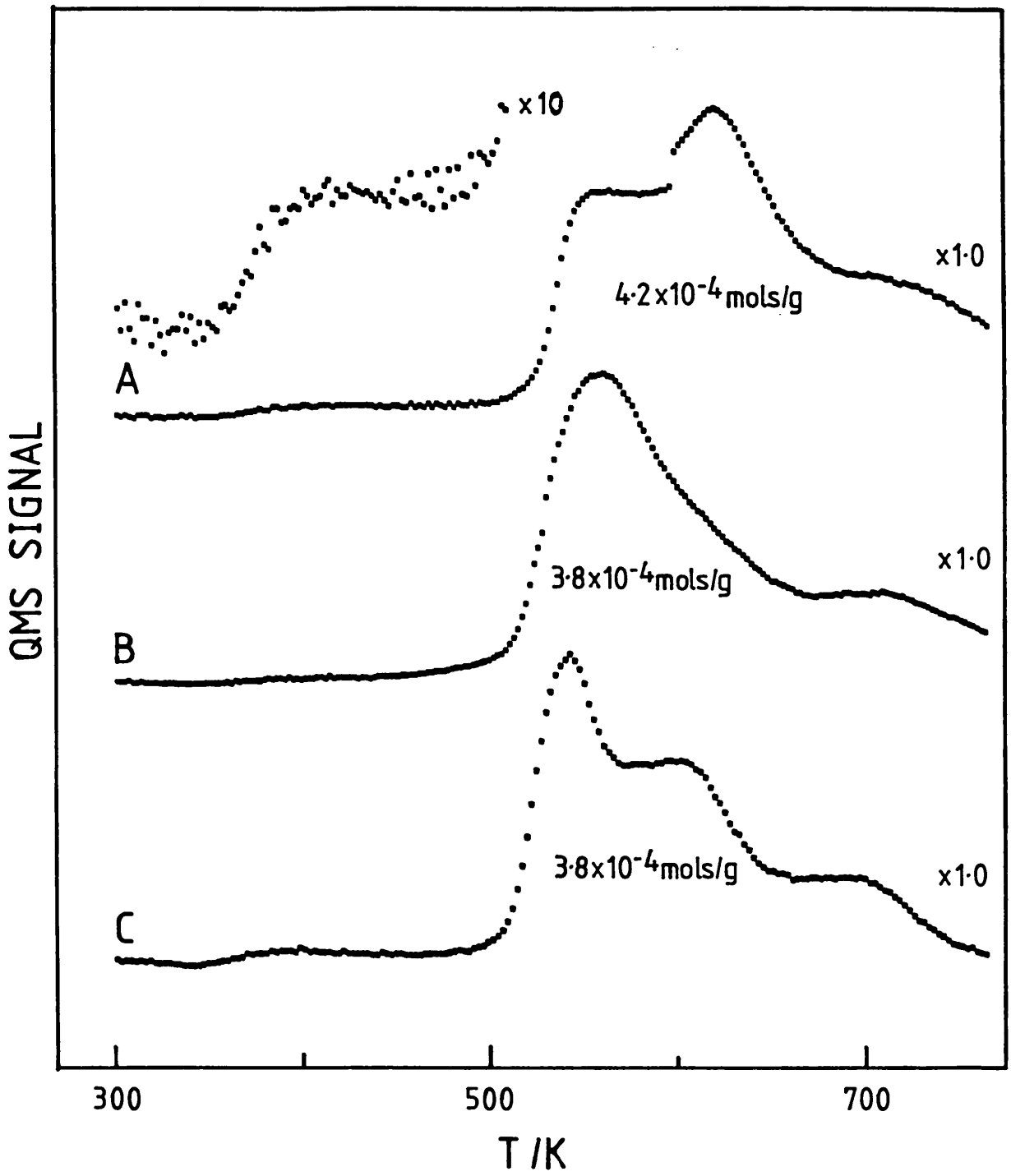

Fig. 4.19: Carbon Dioxide Profiles Obtained During TPO for Samples Ir100 (curve A), Pt100 (curve B) and PtIr43 (curve C) Subjected to Pretreatment O0.

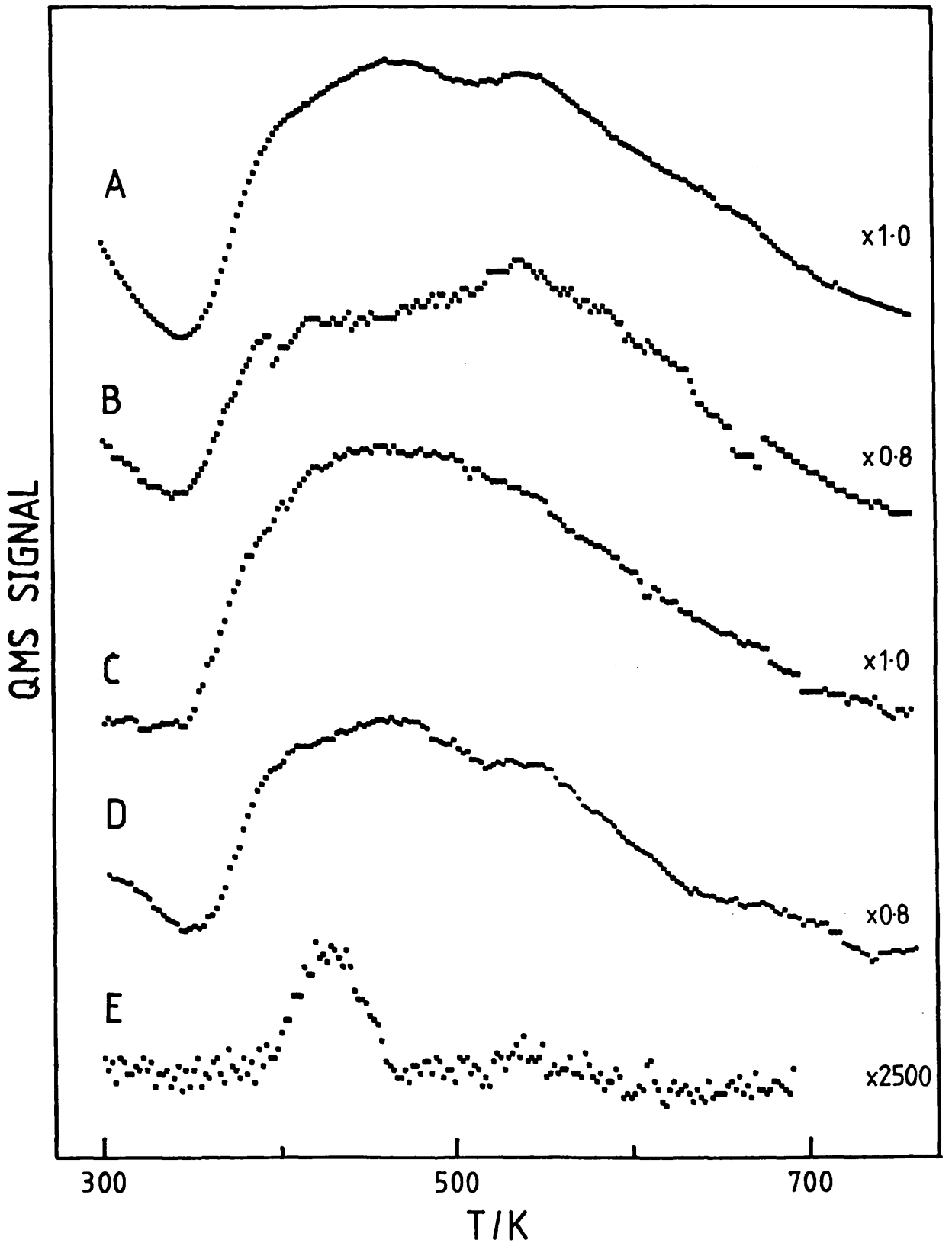

Fig. 4.20: Water Profiles for Samples Ir100 Pt100, γ-Alumina and PtIr43 (curves A-D respectively), and the Chlorine Profile for Sample Pt100 (curve E) Obtained During the TPO of Samples Subjected to Pretreatment O0.

This reaction was only observed with the metal loaded samples. Hence the formate species must be associated with the adsorbed metal complex or the support close to the metal species.

The production of carbon dioxide in the range 602-619K was not associated with water production and may be due to the oxidation of an alumina-held carbonate species as shown in reaction (4.6):-

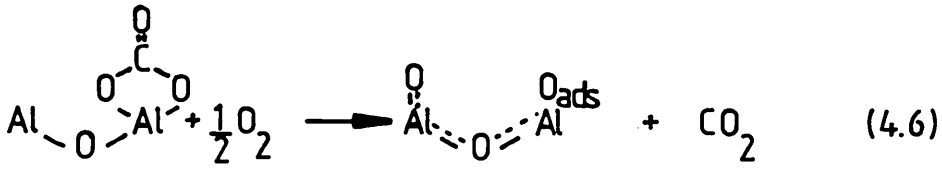

(4.6)

where Oads represents an adsorbed mononuclear oxygen species which may undergo further reaction with the supported metal complex.

The carbon dioxide formation observed above 700K could be due to oxidation of carbon impurities contained in the alumina support. These impurities may originate from the organic starting materials used in the manufacture of the alumina and their importance has been discussed by Bozon-Verundez (1970).

b) Samples Subjected to Pretreatment O740 R740 TPD620

Fig. 4.21 shows the oxygen profiles obtained during the temperature-programmed oxidation of samples subjected to pretreatment O740 R740 TPD620. No water peaks were observed. A very slight increase in the background carbon dioxide signal could be detected above 700K.

The Ir100 sample (curve A) shows a sharp uptake centred at 735K and two smaller uptakes at 372K and 550K. The total amount of oxygen involved is suggestive of a change in oxidation state from O to IV. The process occurring at 735K probably represents the formation of bulk IrO_2 crystallites from large iridium metal crystallites. This uptake was not observed for the Ir100 sample subjected to pretreatment O0. The smaller oxidation peaks at 372K and 550K are due to the oxidation of highly dispersed iridium and may represent respectively the formation of dispersed IrO and IrO_2 species.

The Pt100 sample (curve B) shows a broad uptake maximising at 439K and extending up to 600K. This probably represents the formation of PtO, PtO_2, and oxychloride species, the broadness of the

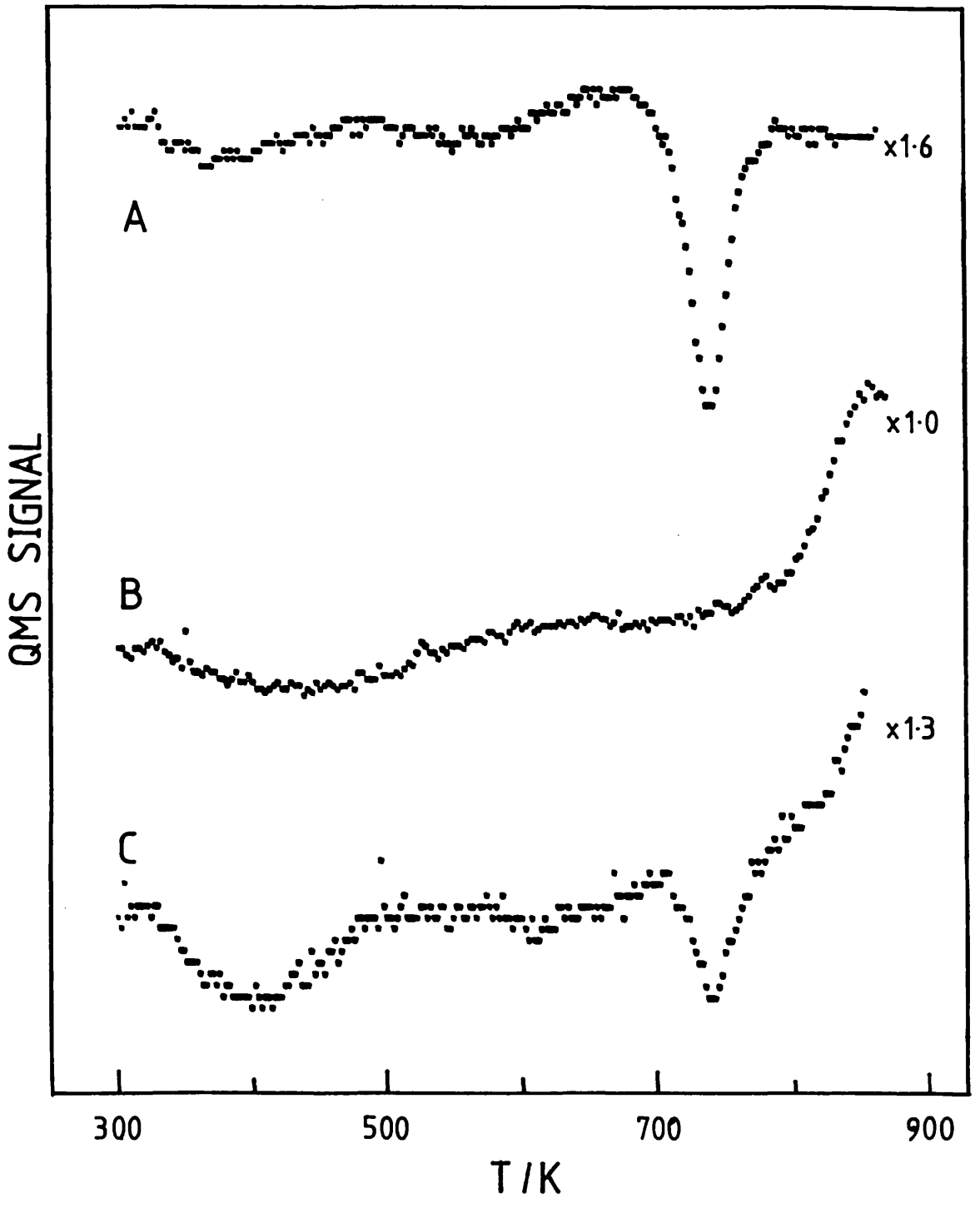

Fig. 4.21: Oxidation Profiles for Samples Ir100 (curve A), Pt100 (curve B) and PtIr43 (curve C) Subjected to Pretreatment O740 R740 TPD620.

peak reflecting the highly dispersed heterogeneous nature of the platinum and the formation of the different species. At temperatures in excess of 740K decomposition of oxidised species occurs.

The PtIr43 sample (curve C) shows three regions of oxygen uptake which broadly correspond with features in the profile of the separate metals. The overall oxygen uptake accounted for the formation of metal in the IV oxidation state. The oxidation process occurring at 402K appears to be considerably larger than would be expected by adding contributions from the separate metals and it may be that the presence of platinum causes a greater dispersion of the iridium, thereby enhancing the uptake observed at 372K for the pure metal.

The Ir100 and PtIr43 oxidation profiles show that reoxidation at 560K, following pretreatment O740 R740, would result in the oxidation of the dispersed phase only. The TPR profiles shown in Fig. 4.14 support this, the sharp uptake due to reduction of large oxide crystallites being absent. These crystallites can only be oxidised at temperatures in excess of 700K. Consequently, the TPR profiles shown in Fig. 4.13, for samples subjected to O740 TPR740 O740, include an uptake due to the reduction of such entities.

Finally, the results of Fig. 4.21 show that oxidation of the various metal entities on the alumina removes oxygen from the carrier-gas. This is in contrast to the oxidation behaviour of the supported metal ions shown in Fig. 4.18, which may only require oxygen to stabilize the replacement of chloride ions by oxygen, or hydroxyl, anions from the support.

c) Samples Subjected to Pretreatment R610 TPD630

Fig. 4.22 shows the TPO profile for the Pt100 sample subjected to reduction at 610K followed by TPD to 630K. Hiuzinga et al. (1984) have obtained a similar oxygen profile but these workers did not calibrate the oxygen uptake. The oxygen profile (curve A) shows a broad oxygen uptake which is associated with the formation of carbon dioxide (curve B). The amount of oxygen consumed (1.7×10^{-4} mol g^{-1} catalyst) was roughly equivalent to the amount of CO_2 formed (2.0×10^{-4} mol g^{-1} catalyst). Interestingly, the water signal (curve C) shows an increase beginning at 580K just after the oxygen uptake starts. This may be due to water arising from the oxidation process

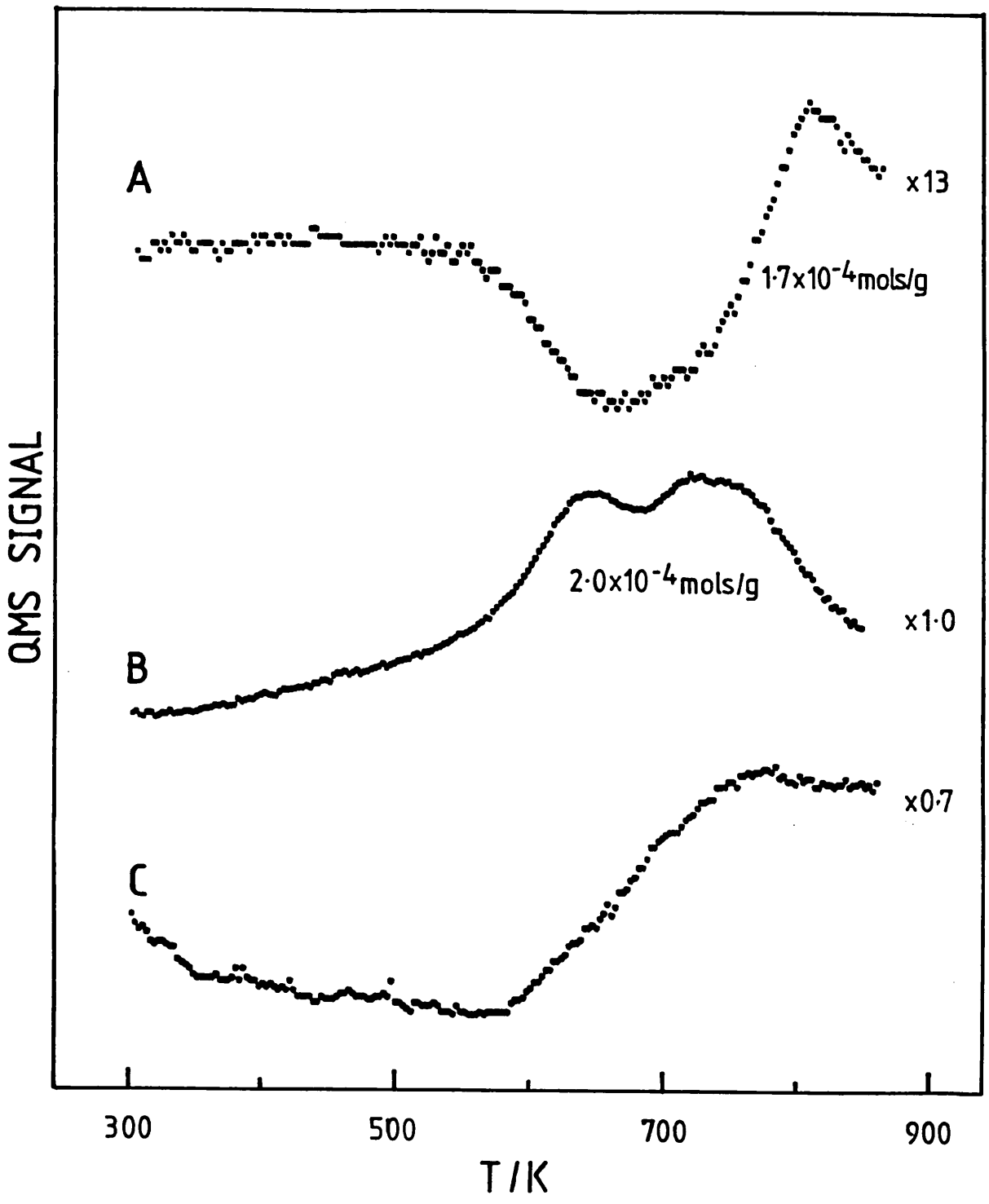

Fig. 4.22: TPO Profile for Sample Pt100 Subjected to Pretreatment R610 TPD620.

and also from desorption of water from the support at temperatures greater than the pretreatment temperatures. The two peaks in the carbon dioxide profile correspond with the second and third carbon dioxide peaks observed in temperature-programmed oxidation of a Pt100 sample subjected to no oxidation pretreatment. Significantly, the first peak is entirely missing and the second much reduced, which shows that these states react with hydrogen during the temperature-programmed reduction of samples previously subjected to pretreatment O0 or O560. The fact that no oxygen uptake is observed at temperatures below 560K suggests that heating a reduced sample in oxygen to 560K is not effective in producing oxide. However, a sample which had been subjected to such a treatment does show a hydrogen uptake in temperature-programmed reduction (see Fig. 4.17). This reduction is probably a reaction with oxygen that has adsorbed on the surface of the platinum clusters at room temperature forming PtO species.

Fig. 4.23 compares the oxygen profiles for samples Ir100 (curve A), Pt100 (curve B) and PtIr43 (curve C) subjected to the R610 TPD630 pretreatment. The water profiles were similar for all samples (see Fig. 4.22). The carbon dioxide profiles showed peaks at 762K and 666K with the Ir100 sample and at 733K with the PtIr43 sample and are compared with the Pt100 sample in Fig. 4.24. The quantity of carbon dioxide produced amounted to 1.8×10^{-4} mol g^{-1} catalyst and 1.2×10^{-4} mol g^{-1} catalyst for the Ir100 sample and PtIr43 sample respectively. Similar profiles were obtained for samples initially oxidised at 560K (coded O560 R610 TPD630).

The Ir100 profile (curve A) in Fig. 4.23 shows three oxygen uptakes which broadly correspond in temperature with the values observed after the pretreatment O740 R740 (Fig. 4.21). Significantly, the carbon dioxide desorption peaks do not occur at these temperatures and it would appear that these oxygen uptakes represent oxidation of iridium. One difference from the TPO profile following pretreatment O740 R740 is that the low temperature peaks are much more prominent. The peaks therefore probably represent oxidation of highly dispersed iridium species whilst the peak at 729K may result from the formation of the bulk IrO_2 phase. Recently Kip et al. (1986a) have published a similar TPO profile for an iridium/alumina sample. They attributed the lowest temperature uptake to the formation of a chemisorbed oxide layer whilst the second and

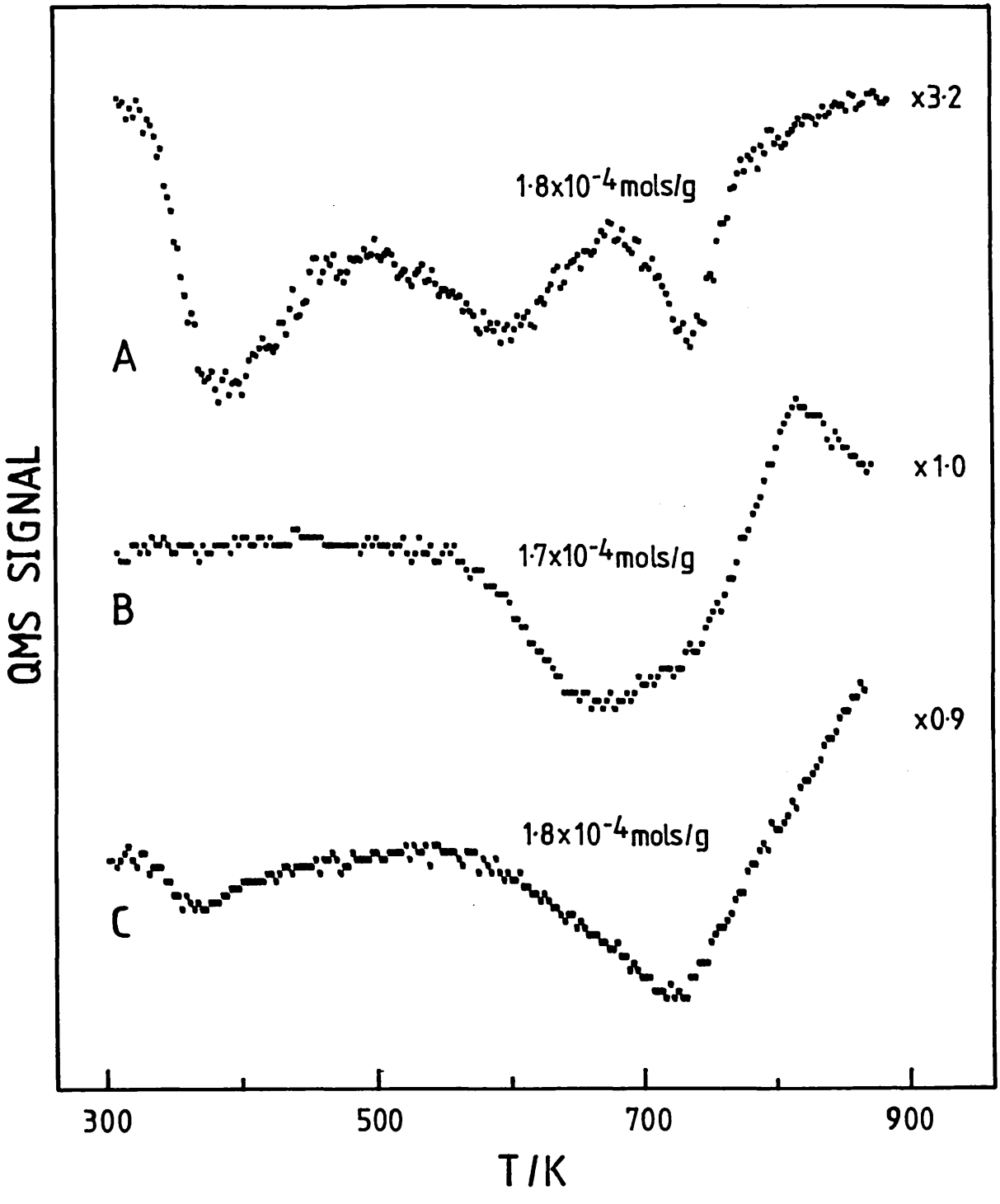

Fig. 4.23: Oxidation Profiles for Samples Ir100 (curve A), Pt100 (curve B) and PtIr43 (curve C) Subjected to Pretreatment R610 TPD630.

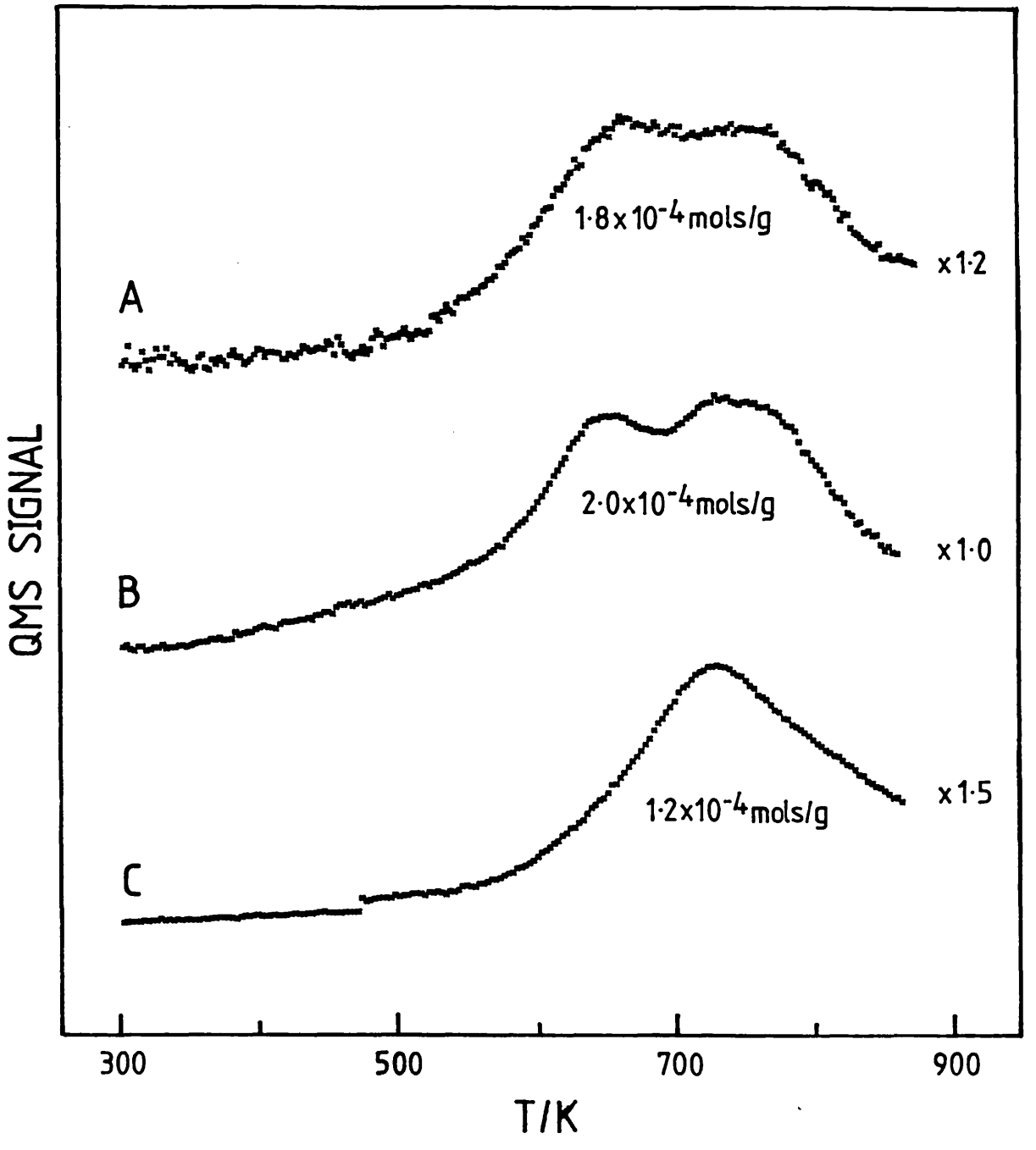

Fig. 4.24: Carbon Dioxide Profiles Obtained During TPO of Samples Ir100 (curve A), Pt100 (Curve B) and PtIr43 (curve C) Subjected to Pretreatment R610 TPD630.

third were assigned to the formation of an oxide film and a bulk oxidation process respectively.

The PtIr43 profile (curve C) appears to be the addition of the two monometallic profiles. This result is unexpected since the results shown in Fig. 4.17 indicate that the presence of iridium does aid the oxidation of the platinum component in such samples.

The above results show that reoxidation, at 560K, of an Ir100 sample, subjected to pretreatment R610 (or O560 TPR740) would produce significant oxidation of the dispersed iridium metal, forming a dispersed IrO_2 species possibly with some IrO. The reduction profiles shown in Fig. 4.17 for samples subjected to pretreatment O560 TPR740 O560 supports this. In addition, reoxidation of samples above 700K would result in the agglomeration of the iridium component. This too was observed using temperature-programmed reduction.

To summarise, temperature-programmed oxidation of samples subjected to pretreatment O0 results in the oxidation of at least three forms of carbon-containing species. Two of these species are associated with the presence of the metal and react with hydrogen at 610K. The high temperature species is largely unaffected by such pretreatment and this may be due to the presence of carbon impurity in the alumina, arising from the decomposition of organic starting materials used in its manufacture.

It is unclear whether the oxidation of the metal ion species, present after pretreatment O0, directly remove oxygen from the carrier-gas. The presence of oxygen could simply stabilise chloride ligand replacement by support oxide, or hydroxide, anions. However, oxidation of metal clusters or larger crystallites does remove oxygen from the carrier. Oxidation of the highly dispersed clusters occurs below 700K, whilst above 700K oxidation of iridium or iridium-rich large crystallites occurs. At temperatures greater than 750K the highly dispersed oxidised platinum, or platinum-rich species, begin to decompose, probably producing metal and oxygen. Finally, the presence of platinum in the bimetallic samples may reduce the agglomeration of the iridium component. However, no evidence was found for the iridium component promoting the oxidation of the platinum component in the highly dispersed bimetallic sample.

4.4 Discussion

It will be convenient to divide this discussion into two sections. The first part deals with the reduction behaviour in the high temperature region, at temperatures above 550K, whilst the second section discusses the reduction and formation of the oxidised metal species formed during the various pretreatments.

4.4.1 The High Temperature Reduction Process

a) The Origin of the Reduction Process

Many workers have observed the presence of a high temperature reduction process in the TPR profiles of supported metal catalysts. Since changes in gas composition have been measured with a thermal conductivity detector, in these studies, it has not been possible to determine the exact nature of the reduction process. The following brief review outlines the main findings of these and related studies.

In a TPR study of Pt supported on alumina Lieske et al. (1983) observed a reduction process at 620K which they stated was not caused by the reduction of platinum species. However, no further explanation was given. Burch (1981), in a study of Pt-Sn/alumina catalysts, observed a reduction peak at 650K and attributed this to loss of chlorine from the support. Recently, Hoyle et al. (1985) have also observed a high temperature reduction process at 593K for alumina-supported chloroplatinic acid, which they attributed to a hydrogen spillover reaction from the metal onto the alumina support. Similarly, Faro et al. (1983) in a TPR study of alumina-supported platinum-iridium bimetallic catalysts observed an uptake in the region of 650K, the exact temperature of which was dependent on catalyst composition. This too was assigned as the result of hydrogen spillover, possibly via the reductive elimination of surface hydroxyl groups, producing aluminium ions in a lower oxidation state. The high temperature reduction process they observed could be substantially eliminated by oxidation at 773K or by heating to 773K in argon. Tang et al. (1984) have observed a similar reduction process for alumina-supported platinum catalysts, but they attribute this to reduction of some active parts of the alumina support. Furthermore, they conclude that the reduction process results in the formation of platinum-aluminium alloys.

The formation of Pt-Al alloy species had previously been suggested by Kunimori et al. (1983) and originally by Den Otter and Dautzenberg (1978) to account for the reduction in hydrogen chemisorption observed at room temperature, following reduction in hydrogen at temperatures greater than 770K. This effect was first observed by Dautzenberg and Wolters (1978) who found that the process could be reversed by an oxidation at 770K followed by a low temperature reduction (~650K). The possibility that the effect was caused by impurities was dismissed by Den Otter and Dautzenberg (1978), whilst Kunimori et al. (1983) ruled out poisoning by sulphur, arising from sulphate reduction on the alumina support, by using X-ray Photoelectron Spectroscopy (XPS). However, in an earlier study Kunimori et al. (1980) did show that the magnitude of the effect was dependent on the type of alumina used.

An alternative explanation of the high temperature reduction effect has been given by Menon and Froment (1979). They propose that high temperature reduction causes some of the chemisorbed hydrogen to become strongly adsorbed on the platinum and inaccessible to oxygen titration at room temperature. In addition, the presence of such strongly chemisorbed hydrogen caused a decrease in the hydrogenolysis activity of the catalyst. However, Burch and Garla (1982) discount this interpretation since they could produce activity changes in platinum catalysts simply by heating in argon. Hence they conclude that loss of activity is not due to Pt-Al alloy formation nor to the retention of strongly adsorbed hydrogen. These workers do not offer an alternative explanation but suggest that transformation of exposed Pt surfaces into Pt(111) planes may be a contributing factor. Previously, Gonzalez-Tejuca et al. (1977) also suggested that the effect was due to changes in platinum metal morphology. However, these workers proposed that formation of atomically dispersed platinum caused the suppression of hydrogen chemisorption.

Tauster et al. (1978) showed that for titania-supported platinum metals alloy formation between the metal and a reduced form of titania could occur. The support was thought to be reduced by hydrogen spillover from the platinum metal. Tauster et al. (1978) suggested that this effect would produce $PtTi_x$ or $PtTiO_x$ species both of which would have a drastically reduced hydrogen chemisorption capacity. Furthermore, these workers found that a high temperature

reduction of alumina-supported metals did not give rise to dramatic changes in the sorption properties. In a further study, Tauster and Fung (1978) propose that a Strong Metal-Support Interaction (SMSI) could only be produced if a reducible support is present. These workers classified titania as such a support whilst alumina was classified as a non-reducible support material.

Clearly, previous explanations given in the literature for both the origin of the high temperature reduction process, observed during temperature-programmed reduction, and the effect of such a pretreatment on the properties of the catalyst are far from agreement. In particular, the proposed formation of Pt-Al alloys is open to question, especially in the light of the results obtained by Burch and Garla (1982) and Tauster and Fung (1978).

The TPR results obtained in this study for titania-supported platinum, shown in Fig. 4.4, support the Pt-titania alloy interpretation of Tauster et al. (1978). The reduction of the titania produces water at 532K. Kunimori et al. (1985) have also detected water during the TPR of titania-supported platinum, at temperatures up to 773K. However, the TPR results obtained in this study clearly show that the situation is more complex for the alumina-supported metals. For the Pt100 sample subjected to pretreatment O0 the high temperature reduction process, observed at temperatures around 610K, is largely accounted for by the production of methane. Therefore, it is tempting to suggest that the high temperature uptakes of hydrogen observed in the TPR studies of the alumina-supported metals discussed above would also have produced methane. Subsequently, the presence of a high temperature reduction peak in the TPR profiles of alumina-supported platinum catalysts would not be evidence for the reduction of the alumina, leading to the formation of Pt-Al alloys. In addition, the production of methane points to surface poisoning, or incorporation of carbon into the metal clusters, as possible alternative explanations for the reduced hydrogen chemisorption capacity of alumina-supported systems, following heating in hydrogen at elevated temperatures.

However, for the iridium-containing samples subjected to pretreatment O0 and the Pt100 sample subjected to pretreatment O740, a high temperature hydrogen uptake was observed which cannot be

totally accounted for by the production of methane. In addition, water formation was observed at these temperatures and, therefore, it is reasonable to suggest that some reduction of the support material had occurred which may lead to the formation of metal-support alloy species for these samples.

This significant difference in behaviour may be due to the metal in the iridium-containing samples adopting a different structural relationship with the oxide support which enables reduction to occur. On this basis, the oxidation of the Pt100 sample may cause the nature of the contact between the platinum and the oxide to change. However, a more likely explanation is that the reduction behaviour is linked to the carbon contained in the samples. More precisely, the high carbon content of the Pt100 sample following pretreament O0 is likely to prevent the metal catalysing the reduction of the support, whilst this process can occur following pretreatment O740, since most of the carbon has been removed. This inhibition effect may be caused by the presence of a carbon barrier between the metal and the support. The support reduction for the iridium-containing samples appears to be less susceptible to the effect of the carbonaceous material. This is probably related to the higher hydrogenolysis activity of iridium (see Chapter Seven) which could result in the absence of the carbon barrier.

Such a role for the carbon 'contaminent' could help explain the inconsistencies in the literature regarding the effect of high temperature reduction of alumina-supported platinum catalysts, since the amount of carbon is likely to be dependent on the method of catalyst production, the type of alumina used and the exact form of the pretreatment carried out.

Unfortunately, Den Otter and Dautzenberg (1978) dismissed the presence of impurities as being the cause of the high temperature reduction effect for the alumina-supported system. These workers state that high purity gases and starting materials were used in their work and hence assert that no impurities were present. However, the results obtained in this study show that adsorption of the metal complex onto the alumina support, enhances the adsorption of carbon dioxide from the atmosphere leading to the formation of several carbon-containing species.

There now follows a detailed discussion of the nature of these carbon-containing species the presence of which may have pronounced effects on the properties of supported metal catalyst samples.

b) The Nature of the Carbon-Containing Species

Many workers have studied the interaction of carbon dioxide with alumina surfaces. Such studies have been carried out in order to obtain information on the nature of the alumina surface and to obtain mechanistic details for various reactions, such as the Water-Gas Shift reaction. These studies usually employ isotope exchange reactions and Infra-Red Spectroscopy (IRS) to obtain such information.

Using oxygen exchange between $C^{18}O_2$ and γ-alumina Peri (1975) showed that the exchange required the formation and decomposition of surface carbonate, bicarbonate or carboxyl species. It was concluded that the exchange probably proceeded by the formation of an unstable bridge (I) or bidentate (II) carbonate as shown in reaction (4.7):-

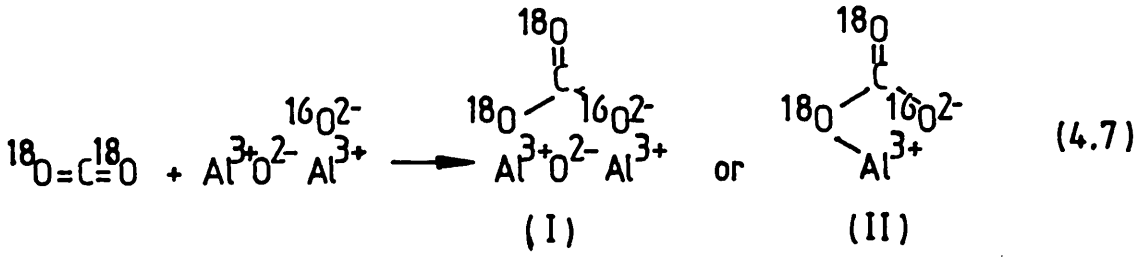

(4.7)

It was postulated that I and II were in equilibrium with a stable unidentate species (III). This species along with those proposed by other workers are included in Fig. 4.25.

Previously Gregg and Ramsay (1969) had also observed the formation of species II and III, using IRS. Earlier Little and Amberg (1962), also on the basis of infra-red spectra, had suggested the presence of species I and III, when carbon monoxide and carbon dioxide are adsorbed on an alumina surface. In addition, a carboxylate species (IV) was suggested.

However, Parkyns (1969) dismissed species IV on the grounds that the electron transition required would be energetically unfavourable. He accounted for most of the reactions which occur between carbon dioxide and alumina by proposing the formation of a

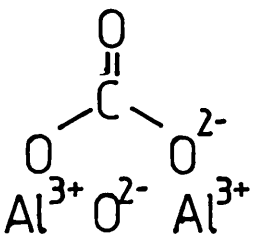

(I)

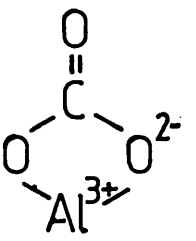

(II)

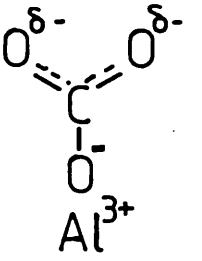

(III)

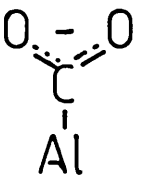

(IV)

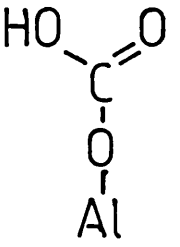

(V)

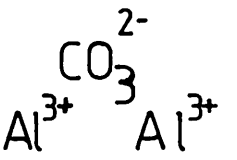

(VI)

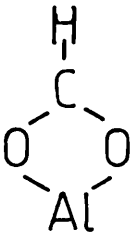

(VII)

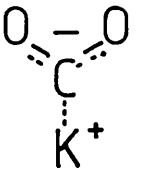

(VIII)

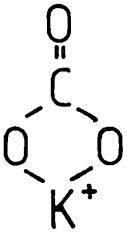

(IX)

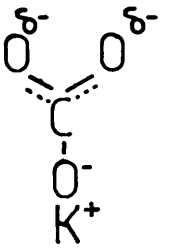

(X)

Fig. 4.25: Carbon-Containing Species Formed During the Adsorption of Carbon Dioxide on Various Alumina and K^+/Alumina Samples.

monodentate bicarbonate species (V), via interaction of adsorbed carbon dioxide with surface hydroxyl groups. Initial carbon dioxide adsorption occurring at an aluminium cation site. Species V is simply the result of protonation of species III, observed by Peri (1975). Parkyns (1971) provided further support for his proposal in a later study of the influence of thermal pretreatments on the infrared spectra of carbon dioxide on alumina. He confirmed that in the presence of surface hydroxyl groups bicarbonate species are formed. However, if the alumina surface had been dehydroxylated then carbon dioxide reacts with the oxide anions to produce carbonate species in various degrees of coordination. In addition to the unidentate species III and the bidentate species II, proposed by Peri (1975), Parkyns also detected an uncoordinated species (VI), presumably formed by reaction (4.8):-

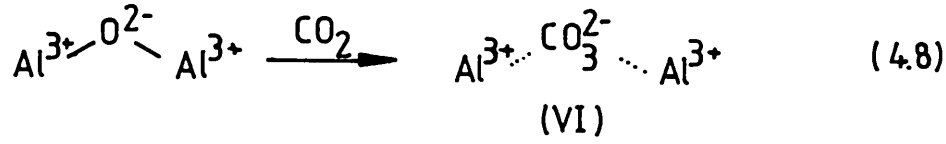

(4.8)

Parkyns concluded that species formed on the alumina surface were dependent on the number of hydroxyl groups present on the surface. Hence different studies using different pretreatments and aluminas, produce varying amounts of the carbon-containing species, although the formation of bicarbonate is proposed to take precedence over that of any other species.

Confirming this, using IRS, Amenomiya et al. (1977) deduced that bridge carbonate (I), bidentate carbonate (II), unidentate carbonate (III), bicarbonate (V) and free carbonate (VI) species were all present to some degree on the alumina surface.

Recently, Rethwisch and Dumesic (1986), using IRS, have observed the formation of a formate species (VII), in addition to bicarbonate and carbonate species, when alumina was exposed to CO/CO_2 mixtures. The formate was observed to form directly from the reaction of adsorbed carbon monoxide with a surface hydroxyl group. It was proposed that the formate could interact further with a surface hydroxyl group, or oxygen anion, to produce bicarbonate or carbonate species. These species were formed directly following the

adsorption of carbon dioxide. Extraction of oxygen, from such species, resulting in the production of formate. These workers concluded that the relative amounts of the adsorbed species was dependent on the metal-O bond strength. A weak bond, such as that found in magnesia, favoured carbonate and bicarbonate formation, whilst an intermediate bond strength, found with alumina and titania, favoured formate species. However, a strong bond, as found with silica, inhibited the adsorption of carbon monoxide and carbon dioxide. Finally, these workers found that thermal treatment at 660K, in vacuo, reduced the carbonate infra-red bands more than the formate, but did not totally remove them. Additionally, treatment in hydrogen at 660K removed the infra-red bands associated with both sets of species leaving bands which could not be assigned.

The effects of thermal treatment on the adsorbed species has also been investigated by Krupay and Amenomiya (1981) who obtained TPD profiles for carbon dioxide adsorbed on both potassium promoted and potassium-free alumina. For the potassium-free sample a single assymmetric peak was found at 470K. This temperature is considerably higher than that found in this work (387K). However, these authors do point out that the temperature recorded was that of the furnace. The alumina disc, which was under vacuum, will be at a considerably lower temperature. Krupay and Amenomiya attribute this peak to the desorption or decomposition of the various carbon containing species identified in an earlier study by Amenomiya et al. (1977). For the K^+/alumina sample two new peaks were observed at 720K and 880K. These were attributed to the desorption of carbon dioxide from complexes coordinated to potassium ions. The low temperature peak was assigned as the decomposition of a carboxylate species (VIII). The high temperature peak was thought to be due to the decomposition of a bidentate carbonate species (IX).

Kantschewa et al. (1983) have investigated the temperature-programmed decomposition of potassium carbonate on alumina. They attribute carbon dioxide desorption between 520K and 570K to the decomposition of a monodentate carbonate (X), but they also observe a second, bidentate species which was stable up to 770K. Both the monodentate and bidentate species were considered to be coordinated to the potassium.

Paryjczak et al. (1982) performed temperature-programmed desorption from γ-alumina and obtained three peaks at 390K, 485K and 670K. They stated that individual desorption peaks may arise from decomposition of surface carboxylate, bicarbonate and carbonate groups. However, they did not attribute any particular peak to a particular species. These workers also investigated the effect of water on the adsorptive-desorptive properties of carbon dioxide on the alumina surface. As the degree of wetting of the surface was increased the high temperature form diminished, whilst the low temperature state increased. It would be expected that the surface concentration of hydroxyl groups would increase as the degree of wetting grew, whereas the concentration of alumina cations and oxygen anions would decrease. Combining these observations with the proposals forwarded by Parkyns (1971), indicates that the low temperature process, observed by Paryjczak et al., is due to the decomposition of bicarbonate species (V). In addition Rethwisch and Dumesic (1986) have shown that the presence of water inhibits the formation of carbonates on alumina. Hence the peak at 485K may represent the decomposition of the bridged carbonate species (I) or the unidentate species (III). Furthermore, by comparison with the results obtained for potassium-promoted alumina, it is likely that the high temperature carbon dioxide desorption process was due to the decomposition of the bidentate carbonate (II) species.

Using the above tentative assignment the origins of the carbon dioxide peaks, shown in Fig. 4.2 (curve B), for the alumina sample, can be identified. With the inclusion of the shoulder on the side of the first peak there are three desorption processes occurring at 380K, 410K and 594K. These are assigned respectively to decomposition of surface bicarbonate (V), decompositiion of a unidentate carbonate species (III) and/or the bridged carbonate (I), and decomposition of the bidentate carbonate species (II).

Additionally, the TPO profile for γ-alumina, described in section 4.3.2.a, indicates that elemental carbon impurity is also present. This probably arises from the use of organic solvents or organometallic aluminium compounds in the manufacture of the γ-alumina.

The TPD profile for alumina impregnated with chloroplatinic acid (Fig. 4.2, curve A) shows that incorporation of a metal chloride complex onto the alumina surface alters the carbon dioxide desorption profile. The peak at 380K is almost eliminated whilst a large peak appears at 613K. If the 380K peak is associated with decomposition of bicarbonate its removal is expected if adsorption of the hexachloroplatinate (II) ion from solution requires an interaction with surface hydroxyl groups. Such an interaction may be dipolar or may involve a ligand replacement reaction, as discussed by Summers and Ausen (1978). Hence the carbon dioxide bound to the alumina surface in the bicarbonate form (V) would be replaced by the metal salt. Species I, and III, which require surface oxygen anion sites only, remain largely unaffected by the adsorption of the metal salt and hence are observed to decompose in the TPD profile.

The large carbon dioxide peak observed at 613K could result from the decomposition of an alumina-bound bidentate carbonate species (II). The presence of the metal complex appears to enhance its formation. This may result from a modification of the support during the metal adsorption step or it may result from a stabilizing interaction with the metal complex itself, possibly by the formation of a metal carbonate complex.

The TPO profiles for metal loaded samples, shown in Fig. 4.19, show the presence of three oxidisable carbon species. The high temperature species is probably due to oxidation of carbon impurity from the alumina support. The low temperature process at around 560K is accompanied by the production of water. This may be due to oxidation of a formate-type species (VII) according to reaction (4.5). The middle peak may represent the reaction of a bidentate carbonate species (II), according to reaction (4.6) which is seen decomposing in the TPD profile. The relative amount of each species appears to be dependent on the metal salt present. In the Pt100 sample the formate appears to be the dominant species. Increasing the iridium content of these samples increased the amount of carbonate present, whilst decreasing the amount of formate species. The total amount of both species remains approximately constant. This shows that the formation of such species could occur at the same site, and the presence of iridium promotes the formation of the carbonate. Rethwisch and Dumesic (1986) have shown that decreasing the metal-

oxygen bond strength, in oxides, leads to an increase in the amount of carbonate species formed on the surface, relative to the amount of formate present. Hence the presence of the iridium complex could weaken the Al-O bond strength in the alumina surface. This may be due to the reaction of the iridium complex with the alumina surface. The hydroxylation and polymerisation of the iridium on the alumina producing this bond weakening. The formate or carbonate species may coordinate to both the iridium and the support. Cherngaev and Novozhenyuk (1966) have observed the formation of a formate-iridium species, $H[Ir(OOCH)_2Cl_2]$ as a product of the reaction of formic acid with hexachloroiridic acid in ethanol and hydrochloric acid.

The TPD results show the decomposition of the carbonate species, with only a shoulder present where the decomposition of the formate should occur. Rethwisch and Dumesic (1986) similarly found that thermal treatment at 660K removes the carbonate species and not the formate. The amount of carbonate formed also indicates that more carbonate can be removed in the presence of oxygen.

The TPR results show the formation of methane at temperatures around 620K. The amount produced was approximately an order of magnitude less than the amount of carbon dioxide formed in a TPD experiment. This shows that thermal treatment in hydrogen is not as effective at removing carbon-containing species, as heating in oxygen (the most effective), or simply heating in an inert atmosphere. Hence heating in hydrogen may lead to some thermal desorption of carbonate which is subsequently hydrogenated over the metal sites. However, heating in hydrogen must cause a conversion of the formate and some of the carbonate species into a highly stable carbon-containing species which, according to the TPO results shown in Fig. 4.24, is resistant to oxidation below 800K. The presence of the metal may aid the conversion by providing spillover hydrogen onto the support which is able to promote the reaction of the formates and carbonates. Rethwisch and Dumesic (1986) have found that heating an alumina sample, containing formate and carbonate species, in hydrogen leads to a reduction in the intensity of the infra-red bands associated with these species, leaving bands which could not be assigned.

The observed structure in the methane profiles for the iridium-containing samples, during TPR, may result from the decomposition of some formate from the support and various carbonate species which were previously associated with the metal. The apparent high spillover capacity of these samples may promote the formation of methane from the species still bound to this support. Heating in oxygen at 560K removes most of the structure in the methane profile produced in a subsequent TPR experiment, which indicates that most of the structure is associated with the surface formate.

The formation of methane and higher hydrocarbons, at temperatures around 430K-460K, is probably due to hydrogenation and Fischer-Tropsch conversion of carbon dioxide produced by the decomposition of the alumina bound bicarbonate (V) and carbonate species (I and III). The carbon dioxide probably undergoes a dissociative adsorption on the newly formed metal, producing CO and O fragments. The hydrocarbon reactions may proceed by the formation of formate species on the metal surface. Additionally, formate and carbonate previously associated with the metal salt may adsorb on the cluster surface, once metal formation begins.

Whilst it is difficult to entirely rationalise all the data concerning the nature of the carbon-containing species on the alumina-supported metal samples, some general conclusions can be drawn, namely:

1) Impregnation of γ-alumina with a metal salt leads to a removal of bicabonate species from the alumina surface.

2) The presence of a metal complex leads to the formation of a formate species and carbonate species which may interact with the metal complex. Iridium seems to favour the formation of the carbonate species, probably as a result of the hydroxylation of the hexachloride complex. The total amount of carbon is large corresponding to a carbon-to-metal ratio of around 5.

3) The formate species appears to be thermally stable. Some decomposition of the carbonate does occur, whilst oxidation removes both species. The additional uptake of oxygen observed during the carbonate oxidation may be involved with

oxidation of the metal salt, although this process remains uncertain.

4) Heating in hydrogen leads to some thermal decomposition of the carbonate species. The carbon dioxide produced being hydrogenated over the metal sites to methane. However, both the formate and the majority of the carbonate react, possibly with spillover hydrogen, to form an unidentified species which is resistant to oxidation below 800K.

5) Hydrogen spillover, apparently prominent in the iridium-containing samples, may also result in the methanation of some of the formate species bound to the support leading to additional structure in the methane profile. Alternatively, the methane profile may arise from the hydrogenation of formates found on the metal surface, which form from the carbonates originally bound to the metal complex.

To conclude, alumina-supported platinum metal catalysts contain a number of carbon-containing species, which form as a result of the impregnation of the alumina with the starting metal complex. The hydrogenation of such species may influence the properties of the metal entities formed during reduction at elevated temperatures. Furthermore, the presence of such species may be an important factor in determining whether a metal catalysed reduction of the oxide support can occur.

4.4.2 The Oxidation Behaviour of Pt-Ir/Alumina Catalysts

The results of sections 4.3.1 and 4.3.2 show that the choice of the oxidation temperature is important in determining the extent of alloy formation in the Pt-Ir/alumina system.

If a high temperature oxidation temperature of 740K is chosen then substantial agglomeration of the iridium component occurs, resulting in the formation of an iridium-rich bulk-type oxide. Sinfelt and Via (1979) observed such an effect, using hydrogen chemisorption and XRD, for silica- and alumina-supported samples heated in oxygen to 770K. Garten and Sinfelt (1980), using Mossbauer Spectroscopy of alumina-supported samples doped with ^{57}Fe, also observed a similar oxidation effect. This effect has also been observed by Graham and Wanke (1981), using hydrogen chemisorption,

and by Pick et al. (1983) who utilized TEM, XRD and hydrogen chemisorption. Foger and Jaeger (1981b) also detected the formation of large iridium rich crystallites in the silica-supported system by employing TPR, XRD, TEM and SAED (Selected-Area Electron Diffraction).

In all of the above studies the high temperature oxidation was performed on samples which had already been reduced. In this study similar agglomeration effects have been observed for the oxidation of the supported metal starting complexes. These results are in contrast to the interpretation of TPR results forwarded by Faro et al. (1983). These workers state that an initial oxidation, at such temperatures, does not result in the agglomeration of the iridium component. However, no TPR experiments were carried out to prove this assertion.

The iridium agglomeration also occurs in the monometallic iridium sample. The presence of platinum may reduce the sintering tendency in the bimetallic sample. Hydrogen chemisorption has been used by Fiedorow et al. (1978) to detect the agglomeration of alumina-supported iridium catalysts in oxygen at 770K. These workers propose that the iridium is susceptible to sintering because of the formation of a volatile IrO_3 species, at elevated temperatures. This species could produce a bulk oxide either by vapour phase transport or by a mechanism involving molecular migration across the alumina surface. However, Chaston (1965) in a review of the oxidation mechanism of bulk iridium metal stated that IrO_3 species only form at temperatures in excess of 1200K. In agreement, Krier and Jaffee (1973) observed the growth of bulk IrO_2 at 1500K, which they attributed to the formation and transport of IrO_3 through the gas phase. Additionally, Wimber and Kraus (1974), using a mass spectrometer detector, observed the formation of volatile oxides only above 1400K. Therefore, if vapour phase transport is responsible for the iridium sintering then supporting the metal on the alumina must promote the formation of the IrO_3 species.

Alternatively, the iridium could sinter by a molecular migration model of the type proposed by Flynn and Wanke (1974). In such a model sintering occurs by the surface transport of molecular species which collide with, and are captured by larger stationary

crystallites. Since the formation of IrO_3 species was not detected using the TPO technique, it may be that the molecular IrO_2 species reacts with alumina oxygen anions. The mobility of this species would result from the movement of the IrO_2 species from one oxygen anion site to another. The reduction behaviour of the physical mixture shows that this species must be able to undergo inter-particle transport.

Using hydrogen chemisorption, XRD and TEM McVicker et al. (1978) studied the agglomeration of alumina-supported iridium in the presence of GpIIA oxides. These workers found that addition of CaO, SrO or BaO inhibited the sintering of the iridium. These workers proposed that capture of the mobile iridium species, by the well dispersed GpIIA oxides, resulted in the formation of stable, immobilised surface iridates. Similarly, the presence of platinum in the bimetallic samples may reduce the sintering of the iridium component by the formation of a dispersed intermetallic oxide species.

The platinum component in the bimetallic sample does not sinter as readily as the iridium component. This may be due to the much lower vapour pressure of PtO_2 compared to the IrO_3 species, as discussed by Chaston (1965). Alternatively, this may result from an increased interaction with the alumina support, for the platinum species, which reduces the surface mobility of the complex. Yao et al. (1979), using TPR and TEM, have observed the formation of a dispersed platinum oxide phase, which interacts strongly with the alumina support. In addition, the concentration of this dispersed phase was found to increase proportionally with platinum loading until a saturation concentration of 2.2 μmol Pt/m^2 (BET) was reached. Beyond this concentration, the excess oxide aggregates to form a bulk-like particulate phase. For the Pt100 samples used in this work the platinum loading corresponded to a concentration of 0.9 μmol Pt/m^2. Hence all the oxidised platinum phase must interact strongly with the support in the platinum-containing samples.

The TPR results of Lieske et al. (1983) and the U.V./visible spectrophotometric results of Lietz et al. (1983) have shown that various chlorine-containing oxidised platinum species form under oxidising pretreatments. The presence of such species was also

observed in this present study. These species could interact strongly with the alumina support preventing agglomeration from occurring. The above workers also show that the formation of the chlorine-containing species causes redispersion of platinum to occur. The mechanism proposed by these workers involves the attack of oxidised platinum crystallites by chlorine, forming an oxychloride species. This species is mobile and migrates on the surface of the alumina where it becomes anchored at special alumina sites. These sites may be acidic centres on the support since Lee and Kim (1984) have shown that silica-supported samples do not exhibit such redispersion effects.

Heating in oxygen to temperatures greater than 740K, results in the decomposition of the oxidised platinum phase. Huizinga et al. (1984), obtained similar results, and these workers argued that the supported oxide interacted with the alumina, since bulk PtO_2 would have decomposed at around 600K under similar conditions. Fiedorow and Wanke (1976), using hydrogen chemisorption, showed that heating in oxygen, above 900K, resulted in the formation of large crystallites of platinum. These workers argue that sintering of platinum was produced by the vapour phase transport of PtO_2 species. Upon agglomeration the oxide decomposed to form platinum metal. Dautzenberg and Wolters (1978) have also observed the sintering of platinum in oxygen, at temperatures in excess of 770K. However, these workers propose that the sintering occurs either by the molecular migration model or the crystallite migration model developed by Ruchenstein and Pulvermacher (1973). In the latter process migration of crystallites occurs over the surface. Such crystallites eventually collide and fuse to form large metal particles. A further possibility is a mechanism proposed by Ruchenstein and Dadyburjor (1977) whereby a combination of the above processes occurs and particle growth takes place by the coalescence of single atoms and multiatom particles.

Pt-Ir/alumina samples subjected to an initial oxidation at 560K, or to no oxidation at all, appear to reduce to form samples containing bimetallic alloy clusters. Alloy formation has been observed by Sinfelt and Via (1979), Garten and Sinfelt (1980) and Pick et al. (1983) after similar pretreatments. Alloy formation was identified in this present work by the reductive interaction between

the metal components observed during the TPR experiments. The reduction of the platinum component may be aided by either the presence of fully reduced iridium, or alternatively, by partially reduced iridium species. The platinum could exist as a surface mobile species which migrates to these nuclei, where it becomes reduced. Such a mechanism was prepared for the reduction of Re_2O_7 in the Pt-Re/alumina system by Wagstaff and Prins (1979a) and Isaacs and Petersen (1982). Alternatively, hydrogen may be activated by the iridium species, which spills over as hydrogen atoms, into the alumina support. A partially reduced iridium species may promote such a process since the work of Escard et al. (1973) showed that Ir(III) species were present in reduced alumina-supported catalysts. This spillover mechanism has been proposed by Mieville (1984) to account for the reduction of Re_2O_7 in the Pt-Re/alumina system. This mechanism could result in platinum being reduced remote from the site of hydrogen adsorption. Additionally, the platinum and iridium species in close proximity could exist as an intermetallic species on the alumina surface. Chloride or oxygen anions may link the metal ions. The iridium nucleation centres would then activate hydrogen for the reduction of the surrounding platinum species.

Of the above considered mechanisms the one including the mobile platinum species may be the most inappropriate. This can be discarded since it is unlikely that the platinum complex is mobile at such temperatures. The reduction of the platinum component probably proceeds by a combination of the hydrogen spillover and intimate contact mechanisms. The results for the physical mixture shows that the activated reduction process is limited to metal species in the same alumina particles. Similar results have been observed for the reduction of loose mixtures of alumina-supported Pt and Re catalysts by Mieville (1984).

4.5 Summary

The TPR profiles for samples subjected to no oxidation pre-treatment show that the reduction behaviour of the platinum and the iridium are linked. The results suggest that the formation of partially reduced, or fully reduced, iridium aids the reduction of platinum ions. Such interactive behaviour of the two components indicates that reduction results in the formation of metal alloy

clusters. Similarly, samples previously oxidised at 560K also show a reductive interaction. This suggests that alloy clusters also form in these samples. Alloy formation was also seen to occur following reduction of samples which had been reoxidised at 560K.

However, for samples oxidised at 740K, the TPR profiles show that oxidative agglomeration of the iridium occurs to form an iridium-rich bulk oxide phase. The presence of platinum may effectively reduce the tendency for the iridium to agglomerate under such conditions. Reoxidation of these samples at 560K results in the reoxidation of the dispersed platinum-rich phase only. These results were confirmed using the TPO technique, in which the formation of bulk IrO_2 was observed at around 730K.

A high temperature reduction process was observed for samples not subjected to the high temperature oxidation step which was not due to the reduction of an oxidised metal phase. For the mono-metallic platinum sample this was largely due to the hydrogenation of carbon-containing species to form methane. TPO and TPD experiments provided additional evidence for the existance of carbonate and formate-type complexes associated with the metal ion complex and the alumina support. However, for the iridium-containing samples subjected to no oxidation pretreatment and the Pt100 sample oxidised at a temperature of 740K, a high temperature reduction process was observed which could not be solely accounted for by methane production. Furthermore, the production of water indicated that this uptake was due to a metal catalysed reduction of the oxide support. It appears most likely that the presence of carbon-containing species prevent such a reaction occurring for the Pt100 sample subjected to pretreatment OO, whilst the iridium-containing samples are less susceptible to the effect of the carbonaceous material. The reduction of the support and exposure of the metal centres to the carbonaceous material at elevated temperatures in hydrogen may have pronounced effects on the sorption characteristics of the catalyst samples. The next Chapter investigates such effects using the temperature-programmed desorption of hydrogen from the catalyst samples.

CHAPTER FIVE

Hydrogen Thermal Desorption Studies

5.1 Introduction

5.1.1 Aim

The aim of this Chapter is to determine the effects of reduction at different temperatures on the state of the alumina-supported platinium-iridium catalysts. Temperature-Programmed Desorption (TPD) of adsorbed hydrogen from the catalyst surface has been used to determine the nature of the metal species formed during the reduction step. Since hydrogen adsorption is known to be sensitive to surface structure it is envisaged that changes in the metal surface composition, resulting from alloy cluster formation, will produce an alteration in the desorption profile.

The reduction behaviour described in Chapter Four indicated that direct reduction of the precursor salts resulted in the formation of alloy clusters. Hence TPD experiments have been carried out on samples subjected to reduction at 610K in order to detect such clusters. The reduction behaviour of samples initially oxidised at 740K was different, in particular there was evidence that such oxidation pretreatments produced an agglomeration of the iridium component into large iridium-rich oxide crystallites. In order to determine the extent of this phase separation, TPD experiments have been performed on samples oxidised at 740K, prior to reduction at 610K. Finally, as described in Section 4.4.1 the interaction of hydrogen with supported platinum catalysts at temperatures above 650K is known to produce a modification of catalysts properties in many instances which cannot necessarily be attributed to sintering. The results of Chapter Four suggested that the presence of carbon-containing species could be a significant factor in the nature of any such alteration. To determine whether iridium and platinum-iridium catalysts can be similarly modified TPD experiments have been performed on both unoxidised and oxidised samples following high temperature reduction at 740K. It was hoped that the TPD spectra would also provide an insight into the nature and origin of such a possible modification.

Before presenting the experimental results it is necessary to discuss the TPD technique and review previous work done on both single crystals and supported metal surfaces.

5.1.2 Temperature-Programmed Desorption

The Temperature-Programmed Desorption (TPD) technique is in principle similar to the flash desorption method used for desorption from filaments, foils and metal single crystals. The flash desorption technique has been reviewed by Ehrlich (1963). One of the major differences between the two thermodesorption methods is that heating rates employed in a flash desorption experiment are much greater (approx. $> 1K\,s^{-1}$) than those used for the temperature programming of porous catalyst samples (approx. $< 1K\,s^{-1}$). Hence the term temperature-programmed desorption will be reserved for thermodesorption from catalyst samples whilst the term flash desorption will be used to describe thermodesorption from bulk metal samples.

TPD is an extensively used method for the characterisation of supported metal catalysts. Reviews on the subject have been published by Cvetanovic and Amenomiya (1967, 1972) and more recently by Falconer and Schwartz (1983). A theoretical analysis of the desorption process has also been presented by Smutek et al. (1975). In a typical TPD experiment a steady flow of inert gas is established over a pretreated sample and the reactant gas is then added to the carrier stream. Once adsorption of the reactant gas on the catalyst surface is complete, and all the non-adsorbed reactant gas has been flushed away, the temperature of the sample is gradually raised, usually in a linear manner, so that the desorption profile can be obtained. In this study desorbed gases have been detected with a computer-interfaced mass spectrometer. At a sufficiently high flow rate the mass spectrometer signal is directly proportional to the rate of desorption of the adsorbed species. As the temperature increases the rate of desorption increases, goes through a maximum and then eventually drops to zero as the surface is depleted of adsorbate. Besides the reversible adsorption/desorption of the reactant gas, the mass spectrometer will detect any gaseous products produced by reaction of the adsorbed gas with the sample, or with impurities found on the sample.

A desorption profile, or desorption spectrum, is a plot of the concentration of desorbed gas as a function of temperature. The position, shape and number of peaks in such profiles provides information on the nature of the adsorbate species with the sample. The number of peaks generally establishes the number of adsorbed species (states) although multiple peaks may occasionally result from lateral interactions within an homogeneous chemisorbed layer, as discussed by King (1975). The population of a state can be calculated from the peak area and an analysis of the peak shape and position provides information on the kinetics of the desorption process. First and second order processes can usually be distinguished by analysing changes in the desorption profile when the heating rate or initial coverage is varied. The methods used for such an analysis have been reviewed by Falconer and Schwartz (1983).

First-order kinetics indicates molecular adsorption (or a non rate-limiting recombination) whilst second-order kinetics corresponds to dissociative adsorption. However, readsorption and diffusional phenomena can alter the desorption profile resulting in an incorrect evaluation of the parameters of interest. Demmin and Gorte (1984) and Ibok and Ollis (1980) have developed experimental parameters which can be used to select appropriate experimental conditions which limit such effects. Once a full kinetic analysis has been achieved the activation energy for desorption can be calculated and hence, for a non-activated process, the heat of adsorption.

Rasser (1977) has obtained information on the kinetics and energetics of hydrogen adsorption on unsupported platinium-iridium alloy powders and various supported platinum-iridium catalysts. However, this author did not investigate the effects of catalyst pretreatment conditions on the state of the supported metals.

One of the objectives of the present study is to obtain a characterisation of the catalyst samples by analysing changes in hydrogen desorption profiles as catalyst pretreatment conditions are altered. However, a detailed analysis of the adsorption/desorption kinetics following such pretreatments has not been attempted. Hydrogen desorption peaks have been attributed to desorption from various sites on the catalyst and, in some cases, populations of the states have been calculated from the areas under the desorption

peaks. Furthermore, the quantity of hydrogen desorbed in peaks assigned to desorption from the metal surface can be used to calculate the degree of dispersion of the metal. Such results can be compared with results obtained using hydrogen adsorption/desorption experiments performed under isothermal conditions. Menon and Froment (1979, 1981) have used such an approach to determine the effects of high temperature reduction pretreatments on the state of alumina-supported platinum catalysts. However similar experiments performed on iridium-containing catalysts have not been previously reported.

5.1.3 Hydrogen Desorption from Single Crystal Surfaces

This section contains a brief introduction to hydrogen desorption from platinum and iridium single crystal surfaces. Although it is not an exhaustive review of the interaction of hydrogen with metal surfaces it will establish a firm basis for the interpretation of the hydrogen desorption profiles from the supported metal samples.

a) Platinum Surfaces

Lang et al. (1972) studied the adsorption of hydrogen on Pt(111) at elevated temperatures and concluded that dissociative adsorption of hydrogen did not occur on this surface in the temperature range studied. However, Christmann et al. (1976) did observe dissociative adsorption of hydrogen at 150K. The thermal desorption profile consisted of two peaks occurring at around 300K and 230K. The respective activation energies for desorption were calculated to be 39 and 27 kJ mol^{-1}. It was also found that the low temperature state was populated only after the first peak was saturated. The maximum coverage on this surface amounted to approximately a monolayer of hydrogen atoms. No ordered superstructures were observed in the Low Energy Electron Diffraction (LEED) patterns. These workers interpret the formation of the two states in terms of lateral interactions between hydrogen atoms adsorbed on identical sites. In addition, these workers found that sputtering in argon produced an additional state, desorbing at 390K, which was associated with surface imperfections.

Baro et al. (1979) have used Electron Energy Loss Spectroscopy (EELS) to ascertain the type of adsite occupied by hydrogen on

Pt(111). From the vibrational frequencies observed they conclude that hydrogen is adsorbed in the three fold hollow sites only, a conclusion also reached indirectly by Christmann et al. More recently, Sayers (1984) using EELS, has observed vibrational frequencies corresponding to the presence of hydrogen adsorbed on Pt(111) at both 2- and 3-coordinate sites.

A further state of adsorption has been found by McCabe and Schmidt (1976a) who observed three desorption peaks at 140, 230 and 310K following adsorption at 78K. Similarly Norton and Goodale (1979) observed three states but these workers attribute the lowest temperature peak to desorption from the crystal support leads.

Christmann and Ertl (1976) has observed peaks at around 230 and 300K for hydrogen desorbing from a stepped Pt(S) -[9(111) x (111)] surface following adsorption at 120K. This surface consists of (111) terraces 9 atoms wide and (111) steps 1 atom high between each terrace. Surprisingly, the desorption spectrum is similar to that for the smooth (111) surface. An additional state could be produced by argon ion bombardment but this state was no different from the one produced by argon ion bombardment of the smooth Pt(111) surface.

Collins and Spicer (1977) have studied the desorption of hydrogen from Pt(S) -[6(111) x (100)] and Pt(S) -[6(111) x (111)] surfaces. The surface with the (111) steps produced a desorption profile similar to that of the Pt(S) -[9(111) x (111)] surface whereas the surface with (100) steps produced a different desorption profile with peaks at 290 and 410K. These workers considered that the low temperature peak represents desorption from terrace sites while the high temperature peak represents desorption from step sites. This interpretation has been confirmed by Baro and Ibach (1980) who have observed vibrational frequencies in EELS corresponding to two different ad-sites for hydrogen on Pt(S) -[6(111) x (111)] surfaces. These workers identified a 3-fold hollow site on the (111) terrace and a 2-fold bridge site on the inner corner of the step.

A further state of adsorption has been observed by Davis and Somorjai (1980) for hydrogen desorbing from a kinked Pt(12,9,8) surface. In addition to two peaks arising from desorption from terrace and step sites, these workers observed an additional peak at around 500K which was attributed to desorption from sites adjacent

to kink atoms. Furthermore, following adsorption and reaction of various hydrocarbons on this surface a new hydrogen desorption peak was observed at around 600K. A similar high temperature hydrogen desorption peak was observed when hydrogen and carbon monoxide were co-adsorbed on both a polycrystalline platinium surface by Kawasaki et al. (1977) and a Pt(111) surface by Baldwin and Hudson (1971). The latter workers associate this peak with the decomposition of a surface formaldehyde species.

Lu and Rye (1974) have performed hydrogen thermal desorption from the less densely packed Pt(100), (211) and (110) surfaces following adsorption at 125K. The (100) surface produced five peaks in the desorption profile. Three of these peaks occurred around 250K with heats of desorption of approximately 54 kJ mol^{-1}, whilst the other two peaks occurred around 430K with heats of desorption of approximately 113 kJ mol^{-1}. Thermal desorption from a (211) plane produced a profile similar to the sum of the profiles from the (111) and (100) planes. This was expected since the (211) surfaces consist of (111) and (100) ledges. The profile for the (110) plane was composed of two poorly resolved peaks at 260K and 350K. However, McCabe and Schmidt (1976b) observed desorption peaks at 170K and 200K following adsorption of hydrogen on Pt(110) at 78K. Only in the presence of a partially oxidised surface was a desorption peak observed at 350K. This peak was thought to arise either from a change in the electronic structure of the metal caused by the presence of oxygen or from the decomposition of a hydroxide species.

To summarise, hydrogen desorption from various Pt(111) surfaces generally results in the production of three peaks. The lowest temperature state may be due to molecularly bound hydrogen or is alternatively caused by an experimental artefact. Desorption from clean surfaces is usually complete at a temperature of 400K with the highest temperature peak occurring around 300K. However, in the presence of surface imperfections, such as kink sites, some hydrogen does not desorb until around 500K.

Desorption from the less densely packed surfaces, such as the (100) plane, produces a more complex desorption profile. In addition, the highest temperature peak occurs at a temperature approximately 100K higher than that found for the corresponding peak

from the Pt(111) surface. Finally, in the presence of adsorbed hydrocarbon fragments, or carbon monoxide, hydrogen desorption can be extended to temperatures above 600K.

b) Iridium Surfaces

The interaction of hydrogen with iridium single crystal surfaces has not been studied as extensively as the interaction with platinum surfaces.

Nieuwenhuys et al. (1976) have studied the desorption of hydrogen from the Ir(111) and stepped Ir(S) -[6(111) x (100)] surfaces. Following hydrogen adsorption at 293K, the two surfaces gave similar desorption profiles with a maximum around 400K, although the stepped surface did exhibit an extended high temperature tail, indicating that part of the hydrogen was bound more strongly on the stepped surface. These workers also observed the production of a new hydrogen peak around 620K when desorption occurred from surfaces that had been exposed to hydrocarbon species.

Desorption from the Ir(110) surface was shown by Nieuwenhuys and Somorjai (1978) to be similar to desorption from the (111) surface. Once again the production of a new desorption peak, around 600K was observed from surfaces that had been exposed to ethene and benzene.

In the above study hydrogen was adsorbed at 293K. Ibbotson et al. (1980) have extended this work by adsorbing hydrogen at 130K. The desorption profile observed contained peaks at 200K and 400K, the area under the peaks being in the approximate ratio of 2:1. These authors propose that the 400K peak results from the desorption of hydrogen atoms bound to the top rows of iridium atoms or bound in trough sites resulting from the reconstruction of the Ir(110) surface to a (1 x 2) structure. This reconstruction also occurs for the Pt(110) surface and is not a result of the adsorption of hydrogen. In this reconstruction alternate close-packed rows are missing which exposes close-packed (111) microfacets on the inclined terraces of the reconstructed surface. The low temperature peak was proposed to arise from desorption from a combination of 2-fold bridge and 3-fold hollow sites found on the microfacets.

The general conclusion arrived at from single crystal work is that hydrogen desorbs from clean platinum and iridium single crystal surfaces predominantly at temperatures below 500K. However, in the presence of hydrocarbon fragments, or adsorbed carbon monoxide a hydrogen desorption peak can occur in the region of 550-650K.

5.1.4 Hydrogen Desorption from Supported Metal Catalysts

This section contains a review of the literature concerning hydrogen desorption from supported platinum and iridium-containing catalysts together with the results of desorption from polycrystalline filaments, foils and unsupported powders. The basic aim is to catalogue the results and interpretations offered in the literature in order to provide the background information required to interpret the hydrogen desorption results for the Pt-Ir/alumina samples.

a) Platinum Samples

Komers et al. (1969) were among the first to use the TPD technique to investigate the nature of hydrogen on silica-supported platinum at 298K. These workers found that desorption produced a peak at a temperature between 370K and 570K, the position of which depended upon the hydrogen coverage.

In order to eliminate support effects Tsuchiya et al. (1970) studied hydrogen desorption from platinum black and found that a sample, previously reduced at 770K, produced peaks at 170, 250, 360 and 570K. The low temperature peaks agree quite closely with the peaks observed by Stephan et al. (1975) for the desorption of hydrogen from a platinum film (120, 200, 330K). Tsuchiya and co-workers attribute the 170K and 250K species to molecularly adsorbed hydrogen, in bridged and linear forms respectively. The 360K and 570K forms were assigned to hydrogen atoms chemisorbed on top of metal atoms and in interstices, respectively. Such an assignment is inconsistent with the results obtained with the single crystal surfaces, which show that both the 250K and 360K peaks arise from desorption of dissociatively adsorbed atoms, although the 170K peak may arise from a weakly held molecular species. The 570K peak has no analogue in work on clean single crystal surfaces but it does correspond roughly to hydrogen desorption from single crystal surfaces covered by hydrocarbon deposits. It is possible, therefore, that the 570K peak

found with these powders results from the dehydrogenation of a hydrocarbon residue, formed perhaps from the carbon dioxide originally used to measure the catalyst surface area. As an alternative to their final assignment Tsuchiya et al. (1970) propose that the 570K peak could arise from the desorption of hydrogen occluded in the metal.

Verbeek and Sachtler (1976) have obtained a desorption profile containing four peaks at temperatures of 153, 263, 323 and 623K for a series of platinum-tin alloys. Their results suggest that the Pt-H bond was weakened as the platinum became surrounded by tin. Like Tsuchiya et al. (1970) these workers assigned the high temperature peak to desorption of hydrogen from inside the metal. However, they additionally carried out carbon monoxide adsorption to characterise the alloy surface, which may have contaminated the surface.

Tardy et al. (1979) have studied the desorption of hydrogen from a platinum filament exposed to high temperatures and high pressures of hydrogen. These workers found that hydrogen desorbed in a single peak around 415K. However, in conditions where carbon monoxide and water contaminents were present, heating in hydrogen to 773K produced two additional hydrogen desorption peaks at 520K and 610K. The first peak was coupled with desorption of carbon monoxide and the second peak with desorption of water vapour. Decomposition of a surface H-CO complex was suggested for the production of the 520K peak.

Further evidence for a strongly bound form of hydrogen comes from the work of Paal and Thomson (1973) who found that tritium was retained by platinum black at 630K. Although this tritium exchanged with hydrogen it did not exchange with hydrogen in hydrocarbon species, nor react with oxygen. These workers propose the existence of two types of hydrogen; an adsorbed $H_a(I)$ species, which does not react with the above species and an adsorbed $H_a(II)$ species which accounts for the retained tritium. Wells (1978) has also produced evidence for the occlusion of hydrogen in several Group VIII metals, including platinum and iridium. Wells observed that 10% of a monolayer of hydrogen was readily available for H_2/D_2 exchange or butene hydrogenation in platinum powders after evacuation at 373K. However, a further 40% of a monolayer became available over a period of several days. A cavity model was proposed to explain these results.

Therefore, whilst the high temperature desorption process can be explained by the dehydrogenation of hydrocarbon fragments some evidence does exist for the retention, possibly by occlusion of hydrogen in the platinum metal. Alternatively, the occluded hydrogen may exist as hydrogen bound to carbon impurity on the metal, which then behaves similarly to Paal and Thomson's H_a(II) species.

Konvalinka et al. (1981) have studied hydrogen desorption from Raney Nickel and Ni/silica catalysts that had been reduced at 773K and then cooled in hydrogen to 130K. Seven adsorbed states of hydrogen were observed with desorption occurring at temperatures of around 190, 280, 340, 410, 530, 650 and 750K. The desorption of the two lowest temperature states was found to follow first order desorption kinetics. These workers attribute such kinetics to desorption of a surface hydrogen atom with a subsurface atom present in an octahedral hole.

This mechanism was first proposed by Konvalinka and Scholten (1977) to account for similar kinetics observed for the desorption of hydrogen from unsupported and carbon-supported palladium. For these systems four desorption peaks were obtained at temperatures of 293, 407, 643 and 780K. The peak at 293K followed first order kinetics whilst the remainder followed second order kinetics. The mechanism preferred by these authors involved the combination of surface and subsurface pairs of hydrogen atoms leading to desorption at 293K. The subsurface hydrogen involved in this breakthrough mechanism would need to exist in an octahedral site between the first and second layers of palladium atoms. Rasser (1977) obtained similar low temperature peaks to Konvalinka and Scholten (1977) for desorption from both supported and unsupported platinum and iridium samples. The low temperature peak, which occurred at 186K followed second order kinetics but was attributed to a similar breakthrough mechanism, in which diffusion of hydrogen from the bulk to the surface became rate-determining. Thus, whilst some workers suggest that hydrogen, found in the metal, desorbs at temperatures above 500K others propose that this type of hydrogen can be removed at temperatures as low as 186K. This may be rationalised by suggesting that hydrogen which is dissolved in the metal desorbs at low temperatures whilst hydrogen which is occluded in cavities does not desorb until higher temperatures are reached.

Foger and Anderson (1978) obtained a hydrogen desorption peak at around 400K using Pt/silica catalysts with an average particle size of 4nm. However, reducing the particle size to approximately 1.2nm resulted in an additional high temperature desorption process which revealed itself as a tail on the desorption peak. These workers concluded that there is a substantially greater proportion of higher energy binding states for hydrogen on platinum particles in the size range of 1.0-1.2nm than there is on particles with diameters greater than 4nm. Such an effect may be caused by an influence of the support material.

Anderson et al. (1979) have carried out hydrogen desorption from alumina-supported platinum and a series of platinum-gold alloys supported on silica. For the 100 at% Pt samples a broad peak was obtained around 400K. These workers found that gold acted as an inert diluent reducing the amount desorbed but did not affect the shape of the desorption profile. No desorption profile was obtained for the 100 at% gold sample. These workers concluded that Group VIII metal orbitals are largely unaffected by alloying with a Group IB metal, and that all the platinum was available for bonding with hydrogen even if it was in an isolated form. These isolated sites were believed to be filled by a spillover transfer, via gold atoms, from larger ensembles of platinum. Alternatively, it was proposed that hydrogen adsorption could occur directly on the platinum if the other hydrogen atom adsorbs on the gold. A further alternative would be that small platinum aggregates, or isolated atoms, could adsorb two hydrogen atoms per metal atom.

This last interpretation is supported by the work of Candy et al. (1980) who studied the adsorption and desorption of hydrogen from various platinum catalysts. On Pt-silica the surface stoichiometry for hydrogen was found to be nearly twice the number of surface platinum atoms. These workers performed thermal desorption between 77K and 900K, and found that adsorption at 300K led to the formation of two states, β_1 and β_2 which desorbed at temperatures around 150-300K and 250-300K respectively. The formation of the β_2 species was found to be an activated process since adsorption at higher temperatures increased the amount in this state. Exposure of the sample to hydrogen at 900K, followed by cooling in hydrogen, resulted in the formation of a new state, β_3 which desorbed around 750K.

Tsuchiya et al. (1970) observed a similar activated formation for the species responsible for their 360K and 570K peaks. Candy et al. (1980) associate their low temperature peaks with similar peaks observed for desorption from Pt(111) except they preferred a distinct site model for the two states because of the activated formation of the β_2 species. They attribute the β_2 and β_1 species to the partial filling of hollow sites and atop positions respectively. Two alternative mechanisms were proposed for the formation of the β_3 state. The first involved population of more energetic, possibly subsurface sites by high temperature migration of hydrogen atoms. In this model the hydrogen would sit between the first and second layers in octahedral sites. Alternatively, the β_2 state may convert to a bridged species, Si-O-H-Pt, in which the hydrogen was bound to both the metal and the support.

Weatherbee and Bartholomew (1984) have also observed additional activated states on alumina-supported nickel catalysts which were not observed on unsupported samples. It was proposed that these additional peaks arose from an electronic modification of the small nickel crystallites, probably due to an interaction with the support.

Hoyle et al. (1985) have obtained four peaks in the desorption profile for alumina-supported platinum at 320, 373, 400 and 573K. Frennet and Wells (1985) have also observed several peaks in the hydrogen desorption profile from the standard silica-supported platinum catalyst EUROPT-1. These workers associated peaks occurring at temperatures of around 200K and 400K with desorption from the metal surface. However, a peak at 600K was attributed to a combination of the platinum with the support which produced hydrogen as shown in reaction (5.1):

$$2(\equiv Si\text{-}OH) + Pt\text{-}Pt \rightarrow 2(\equiv Si\text{-}O\text{-}Pt) + H_2 \qquad (5.1)$$

Such a reaction was based on the results of Extended X-ray Adsorption Fine Structure (EXAFS) experiments reported by Joyner and Meehan (1983). An additional peak at 770K was attributed to spillover hydrogen, located before desorption on the support.

Kramer and Andre (1979) had previously established that spillover hydrogen desorbed from alumina surfaces in the presence of platinum at temperatures of 750K. This high temperature desorption is not found with metal-free alumina surfaces for which Amenomiya (1971) observed desorption peaks at temperatures of 230, 293, 373, 473 and 590K. These peaks were attributed to desorption from surface defects on the alumina surface although Charcosset et al. (1979a) have attributed similar peaks to the presence of iron or other impurities in the alumina.

Beck and White (1984a, 1984b) have observed peaks at temperatures around 700K for the desorption of hydrogen from Pt/titania samples. By the use of sequential dosing of hydrogen and deuterium these workers were able to show that desorption of spillover hydrogen proceeds by a mechanism which involves back migration to the platinum metal, rather than recombination and desorption directly from the oxide.

Chen and White (1986) have investigated deuterium desorption from alumina-supported platinum. In addition to a peak at 320K, attributed to desorption from the metal, four other states occurring at temperatures around 190, 310, 410 and above 600K were also observed. The lowest temperature peak was assigned as desorption from the support which did not depend on the presence of the metal. However, the remaining peaks were assigned as states populated mainly by spillover from the platinum.

Several workers have investigated the influence of reduction temperature on supported platinum catalysts using temperature-programmed desorption of hydrogen.

Charcosset et al. (1976) performed hydrogen desorption from various supported platinum samples after reduction at temperatures up to 770K. Whilst exposure to hydrogen at temperatures around 570K leads to the production of hydrogen in a single peak at 420K, reduction at 770K resulted in the diminution of this peak and the production of further hydrogen desorption up to temperatures of 770K. The hydrogen desorbing at high temperatures was only partially active towards oxygen at room temperature and hence may be associated with the Ha(II) species observed by Paal and Thomson (1973).

This work was followed by an extensive study of hydrogen desorption from Pt black, Pt/silica, Pt/alumina, Pt/magnesia and Pt/carbon catalysts by Charcosset et al. (1979a). These workers attempted to determine the factors which result in hydrogen desorbing from such samples at elevated temperatures. The initial hydrogen adsorption was carried out at temperatures in the range 300 to 770K and desorption was started at room temperature. Samples exposed to hydrogen at 300K produced a desorption peak around 420K. However, reduction at 770K lead to a diminution of this peak and the growth of a high temperature desorption process up to 770K. The low temperature peak could also be removed by exposing the samples to sulphur. The desorption of carbon monoxide was detected around 600K and hence it was deduced that carbon may be the cause of the high temperature desorption process. Correspondingly, a large high temperature peak was observed with the carbon supported sample. On the basis of these results these workers propose that the high temperature process may be due to the decomposition of a surface bound H-CO species. Alternatives also considered were readsorption phenomena or formation of Pt-H-support species in the supported samples.

Menon and Froment (1979) have also studied the modification of the properties of alumina-supported platinum and Pt black catalysts by hydrogen at high temperatures. These workers used TPD of hydrogen and hydrogenolysis of hydrocarbons to determine such reduction effects. It was found that reduction below 670K resulted in the production of three desorption peaks at temperatures of around 350, 400 and 600K. However reduction of temperatures above 770K reduced the size of the two low temperature peaks and increased the population of the high temperature state whilst keeping the total amount of hydrogen desorbed approximately constant. Addition of carbon disulphide and carbon tetrachloride caused a similar effect although it was not clear whether this arose from poisoning by carbon. Only a small fraction of the strongly bound hydrogen reacted with oxygen at room temperature. In addition reduction at 770K reduced the hydrogenolysis activity of the catalyst. However, oxidation at 770K followed by reduction at 670K restored most of the original activity and characteristics of the catalyst. These workers proposed that hydrogen accessible to hydrocarbons and oxygen converts into an inaccessible form during reduction at 770K. The presence of the

inaccessible species which must inhibit the formation of the accessible species, was thought to be due to some property of the platinum since similar effects were observed for Pt black samples.

This work was extended in a further study by Menon and Froment (1981) who performed TPD and temperature-programmed re-uptake experiments on various supported platinum catalysts. These workers conclude that high temperature reduction may result in chemisorbed hydrogen penetrating into the sublayers of platinum. However, spillover phenomena or the effects of metal-support interactions and metal surface reconstruction were not entirely excluded, significantly effects arising from the presence of carbon contaminents were not considered.

b) Iridium Samples

Mimeault and Hansen (1966) carried out flash desorption of hydrogen from an iridium filament and observed two peaks at 280K and 420K. These results are consistent with the results for the single crystal surfaces. Contour and Pannetier (1972) performed TPD of hydrogen from a 36 wt% Ir/alumina catalyst following adsorption at room temperature. Two hydrogen states were observed desorbing at temperatures of 350 and 900K with activation energies of 44 and 105 kJ mol^{-1} respectively. The low temperature species was attributed to desorption from an iridium-alumina complex.

Escard et al. (1973) in a similar study of a 36 wt% Ir/alumina catalyst obtained desorption peaks at temperatures of 220, 320, 390 and 770K. These workers proposed that the 220K state was due to molecularly bound hydrogen, whilst the 320K and 770K states were due to atomically bound hydrogen. However, the results for hydrogen adsorption on iridium single crystals show that the 220K state is atomically bound hydrogen. Experiments performed on unsupported iridium powders gave similar desorption profiles to those obtained with the supported metal except that the 390K peak was absent. The peak at 390K found for the supported metal was attributed to desorption of spillover hydrogen, but this interpretation is inconsistent with the results of Kramer and Andre (1979) who only observed desorption of spillover hydrogen at temperatures around 750K.

Foger and Anderson (1979) have studied hydrogen desorption from silica- and alumina-supported 1 wt% iridium catalysts. Starting the desorption experiment at 293K these workers observed a desorption peak at around 420K with a shoulder at 370K and a tail extending to approximately 750K. Increasing the dispersion of the samples tended to increase the population of the higher binding energy sites.

Hydrogen desorption from titania-supported iridium has been studied by Foger (1982) who found that reduction at 473K resulted in the production of a single asymmetric peak at 485K. Significantly, reduction at 673K reduced the amount of hydrogen desorbed by 90% and was attributed to the formation of an SMSI state between the metal and the support. The hydrogen desorption profile could only be partially restored following reoxidation and reduction at 473K and it was concluded that the SMSI state for the larger iridium clusters could only be reversed by reoxidation at higher temperatures.

Foger and Anderson (1980) have also performed hydrogen desorption from silica-supported iridium-gold clusters. The samples were reduced at 620K, cooled in hydrogen and desorption was performed in the presence of hydrogen. These workers found that the presence of 19 atom % gold reduced the temperature of the desorption peak from 509K to 438K. It was concluded that the presence of gold led to a significant reduction in the binding energy of adsorbed hydrogen. This was in contrast to the platinum-gold system where gold acted as an inert diluent.

Krishnamurthy et al. (1982) have also studied hydrogen thermal desorption from Ir/alumina samples. These workers reduced their samples at temperatures around 720K, then cooled in hydrogen to room temperature before performing a TPD experiment. For a 1 wt% iridium sample two peaks were observed at 330K and 420K. The low temperature peak was attributed to physisorbed hydrogen which is clearly inconsistent with the single crystal data. The second peak exhibited second order desorption kinetics with an activation energy of desorption in the range 63-75 kJ mol^{-1}. The commencement of a third peak around 600K was attributed to desorption of spillover hydrogen. The fact that the total amount of hydrogen desorbed corresponded to two hydrogen atoms per surface iridium atom may be indicative of atomically dispersed iridium.

c) Platinum-Iridium Samples

There is little information in the literature concerning TPD experiments performed with the H_2/Pt-Ir system.

Faro et al. (1983) have performed hydrogen desorption from bimetallic Pt-Ir/alumina catalysts that had been oxidised at 753K prior to a variety of oxidation/reduction treatments. These workers performed desorption in the presence of hydrogen in a similar manner as Menon and Froment (1981). The desorption profiles were not published but were described as being fairly symmetric and narrow. Tabulated data showed that the desorption peak position varied in temperature from 442K to 579K and increased with increasing iridium content. Furthermore, these workers observed an uptake of hydrogen above 600K which was associated with a spillover reaction of hydrogen with the alumina.

Earlier, Rasser (1977) performed a hydrogen desorption study of supported Pt-Ir catalysts and powders. The effects of using different pretreatment conditions were not examined in any detailed manner. Supported samples were generally oxidised and reduced at 700K before being outgassed under helium at 750K. Hydrogen adsorption was carried out at 298K and then the sample was cooled under hydrogen to 80K. For alumina-supported bimetallic samples desorption peaks were obtained at temperatures of 190, 300, 500 and 700K. The 700K peak was not detected for the powder samples since desorption was halted at 600K for these samples. The 190K peak was assigned to the desorption of dissolved hydrogen by the breakthrough mechanism of Konvalinka and Scholten (1977) whilst the 300K and 500K peaks were assigned to desorption from the metal surface, probably imperfect (111) and (100) planes. Because of the indistinctness of the peaks it was impossible to deduce whether alloy formation had occurred. However the samples had been subjected to oxidation and reduction at elevated temperatures. In this study experiments have been performed both on samples subjected to similar pretreatments as those used by Rasser (1977) and on samples subjected to less vigorous pretreatment conditions.

d) Summary

On the basis of the results just presented it would seem that hydrogen desorption from supported metal catalysts does show some

similarity to desorption from bulk surfaces, especially at temperatures below 500K. However, there are additional features in the desorption profile which are not found with bulk metals. These could arise from a variety of reasons which include the small size of the metal clusters, electronic or chemical interactions between the metal and the support or hydrogen spillover effects. However, there is considerable evidence that the presence of contaminents may often be responsible for the modification of the desorption profile. This is especially evident for catalysts employing carbon as a support. A further factor to be considered is the penetration of hydrogen into the metal clusters. Reduction at elevated temperatures appears to promote these additional phenomena whilst simultaneously suppressing the normal bulk-like desorption characteristics.

The following study attempts to clarify the effects of the reduction step on alumina-supported platinum-iridium catalysts whilst identifying which, if any, of the above phenomena are important in this system.

5.2 Experimental

Hydrogen thermal desorption experiments were performed in the micro-reactor system described in Chapter Two. Desorption experiments were carried out using an argon carrier gas of flow rate 12ml min^{-1} and pressure 1-1.1 atm. Additional desorption experiments were performed using a 3% hydrogen-in-argon carrier mixture, prepared according to the method outlined in Section 4.2. Approximately linear temperature ramps of 24K min^{-1} were used for all temperature-programmed experiments. Desorption was carried out over the temperature range 298K to ~750K.

The computer interfaced mass spectrometer was used to detect adsorption/desorption processes as outlined in Section 4.2. The mass numbers monitored were generally those shown in Table 4.1. No changes in the oxygen signal (mass 32) were detected when experiments were performed under leak-free or impurity-free conditions. Hydrogen desorption profiles were not obtained when leaks were present in the flow lines or impure (oxygen-containing) carrier gases were used. The high background partial pressure of carbon monoxide in the mass spectrometer vacuum chamber restricted the detection limit for this gas to quantities greater than ~50ppm. When carbon monoxide

production was detected this was always accompanied by the production of carbon dioxide. The relative sizes of the mass 44 and 28 signals confirmed that the latter signal arose from the cracking products of carbon dioxide caused by the mass spectrometer ion source.

The catalysts used in this study were prepared as outlined in Chapter Three and consisted of the two monometallic samples, Pt100 and Ir100 and the bimetallic sample PtIr43. Samples (50mg) of these catalysts were loaded into the reactor and subjected to an insitu pretreatment which consisted of either no oxidation treatment or oxidation at a temperature of 740K before the reduction step. The samples were then reduced at either 610K or 740K for 20 mins before being cooled to 298K in the hydrogen-containing carrier gas. At this temperature the hydrogen was no longer added to carrier-gas and the system was left (40 mins) to allow the non-absorbed hydrogen to flush away before the desorption experiment was started. Fresh samples were used to investigate the effect of each pretreatment. A summary of the pretreatments used prior to examination by TPD is given in Table 5.1. A more detailed description of all the pretreatments used can be found in Chapter Three.

Table 5.1 Summary of Pretreatments Used in TPD Experiments

Code	Pretreatment/Comments
R610	TPR to 610K, sample then held at this temperature for 20 mins
R740	As for R610 but reduction temperature held at 740K
O740 R610	Oxidation at 740K followed by pretreatment R610
O740 R740	Oxidation at 740K followed by pretreatment R740

Desorption peaks and hydrogen uptakes were calibrated in the manner described previously in Section 4.2. In addition, the hydrogen desorption peaks could be calibrated from the hydrogen uptake observed during the TPR experiment performed during the catalyst reduction pretreatment.

The hydrogen desorption profiles have not been used to obtain information on the adsorption/desorption kinetics. Instead changes in the desorption profiles, resulting from exchanging the catalyst samples and altering the pretreatment conditions, have been used to determine the presence of alloy interactions and general pretreatment

effects on the supported metal systems. Therefore, absence of diffusional effects is not critical. An evaluation of the parameters of Demmin and Gorte (1984) and Ibok and Ollis (1980) would have shown whether such effects were occurring. However, the parameters require a knowledge of quantities such as the particle and bed porosity, and diffusion coefficients. These quantities were not measured and hence the parameters could not be determined. However, experiments performed using different carrier flow rates and sample sizes indicated that interphase diffusional limitations were negligable, as outlined by Falconer and Schwartz (1983). Also, the hydrogen pulse test of Anderson et al. (1979) resulted in only slight pulse broadening and delay compared to pulses passed through the sample bypass loop. This shows that diffusion effects and lag times are of minor importance under the chosen experimental conditions.

5.3 Results and Interpretation

In the following description of the thermal desorption experiments the term hydrogen desorption profile will be used to describe the variation of the mass 2 signal with temperature. The variation of the mass signal corresponding to other gases will be similarly described. The methane desorption profile has been obtained from the mass 15 signal for reasons previously outlined in Section 4.2. The entire collection of all the mass profiles will be referred to as the desorption profile. The individual profiles have been offset for clarity and particular desorption peaks are referred to by the temperature at which the peak maximum occurred.

The results have been divided into two parts. The first section is concerned with samples that have received no oxidation pretreatment prior to reduction. The results of Chapter Four showed that reduction of such samples probably resulted in alloy formation. The second section is concerned with samples that have been subjected to an initial oxidation pretreatment at 740K, which produced an agglomeration of the iridium component into large IrO_2 crystallites. The effect of a high temperature reduction at 740K and a mild reduction at 610K have been assessed on both sets of samples.

5.3.1 Samples Subjected to No Oxidation Pretreatment

a) Samples Reduced at 610K

Figs. 5.1, 5.2 and 5.3 show the desorption profiles for samples Pt100, Ir100 and PtIr43 respectively that had been subjected to pretreatment R610. In all cases three hydrogen desorption processes (curve A) can be discerned, occurring at temperatures around 340, 410 and 600K. The total amount of hydrogen desorbed is given in the figures in the form of a ratio between the number of hydrogen atoms desorbed, H, to the number of metal atoms present, M. Blank experiments performed on the alumina support material produced no hydrogen desorption peaks below 800K.

It may be significant that the two desorption processes occurring at the lowest temperatures correspond quite well to desorption peaks observed with metal single crystals, filaments and films. Thus the 340K peak observed with the Pt100 sample is close in temperature to the desorption peak found with Pt(111) single crystals and a similar correlation exists between the 410K peak and desorption from Pt(100) single crystals. It is tempting to assume that these crystal faces are present in the supported catalyst and indeed small metal clusters containing more than 13-55 atoms are likely to have a cubo-octahedral geometry in which (111) and (100) faces are both exposed, as discussed by van Hardeveld and Hartog (1969). The higher temperature peak could also represent desorption from the so-called B_5 sites formed when incomplete cubo-octahedral faces are present, as discussed by Hardeveld and Hartog (1969) and Perez et al. (1983). However, the H/M ratio for the Pt100 sample was found to be 0.94, a value which seems to show that a very high proportion of the metal atoms are in the surface. Similar high values have been obtained by other workers in isothermal gas adsorption studies. These results would appear to limit the clusters to no more than approximately 20 atoms in size and it is doubtful whether well developed crystal planes could be present. Furthermore, as discussed by Jackson et al. (1981), the icosahedral structure has been calculated to be the most stable arrangement for highly dispersed metal clusters containing thirteen, or fewer, atoms. However, particle morphology may be influenced by the presence of the support as outlined by Anderson (1985) and therefore it is unclear whether imperfect cubo-octahedral or icosahedral clusters would be present.

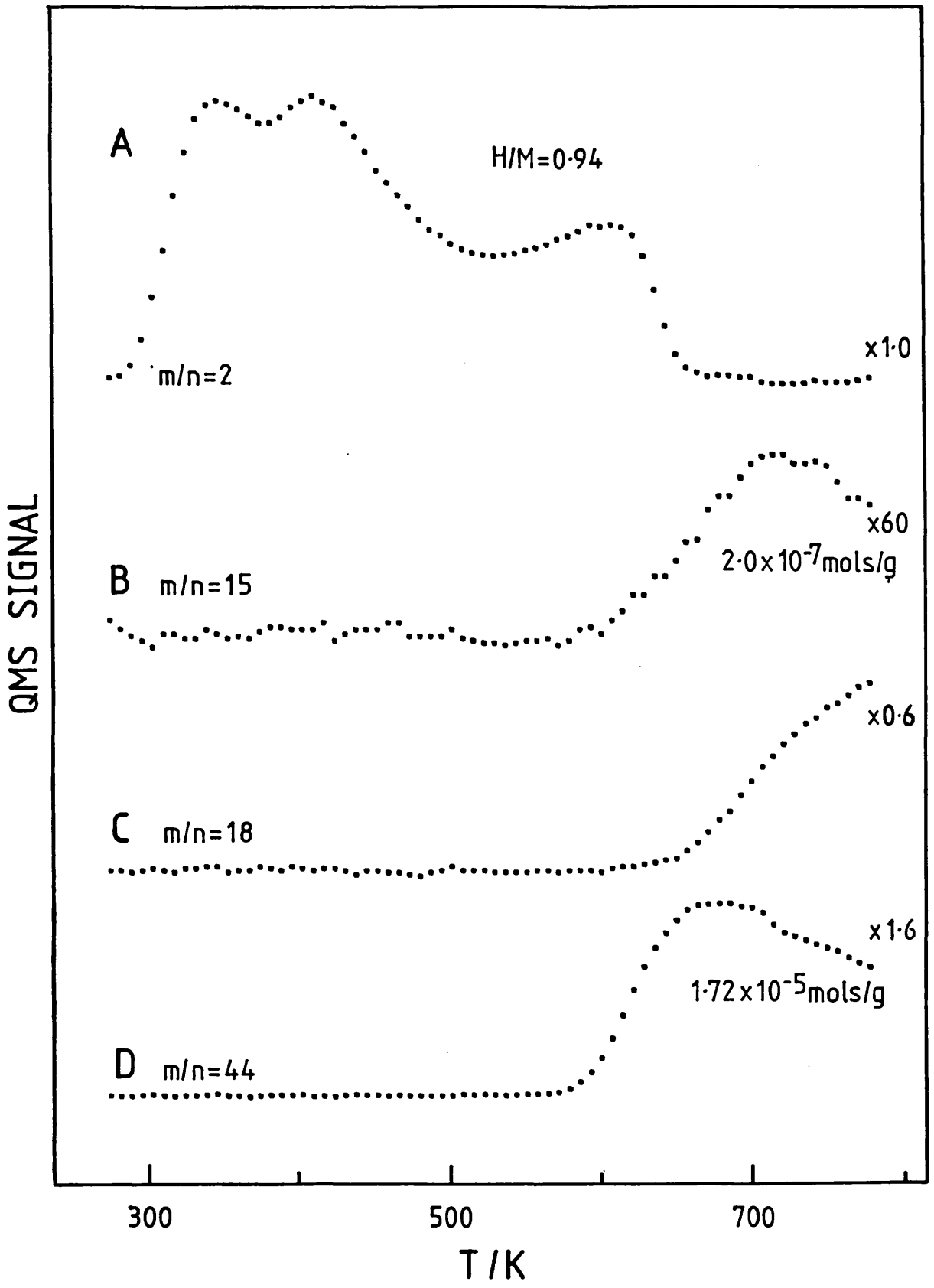

Fig. 5.1: Desorption Profile for Sample Pt100 Subjected to Pretreatment R610.

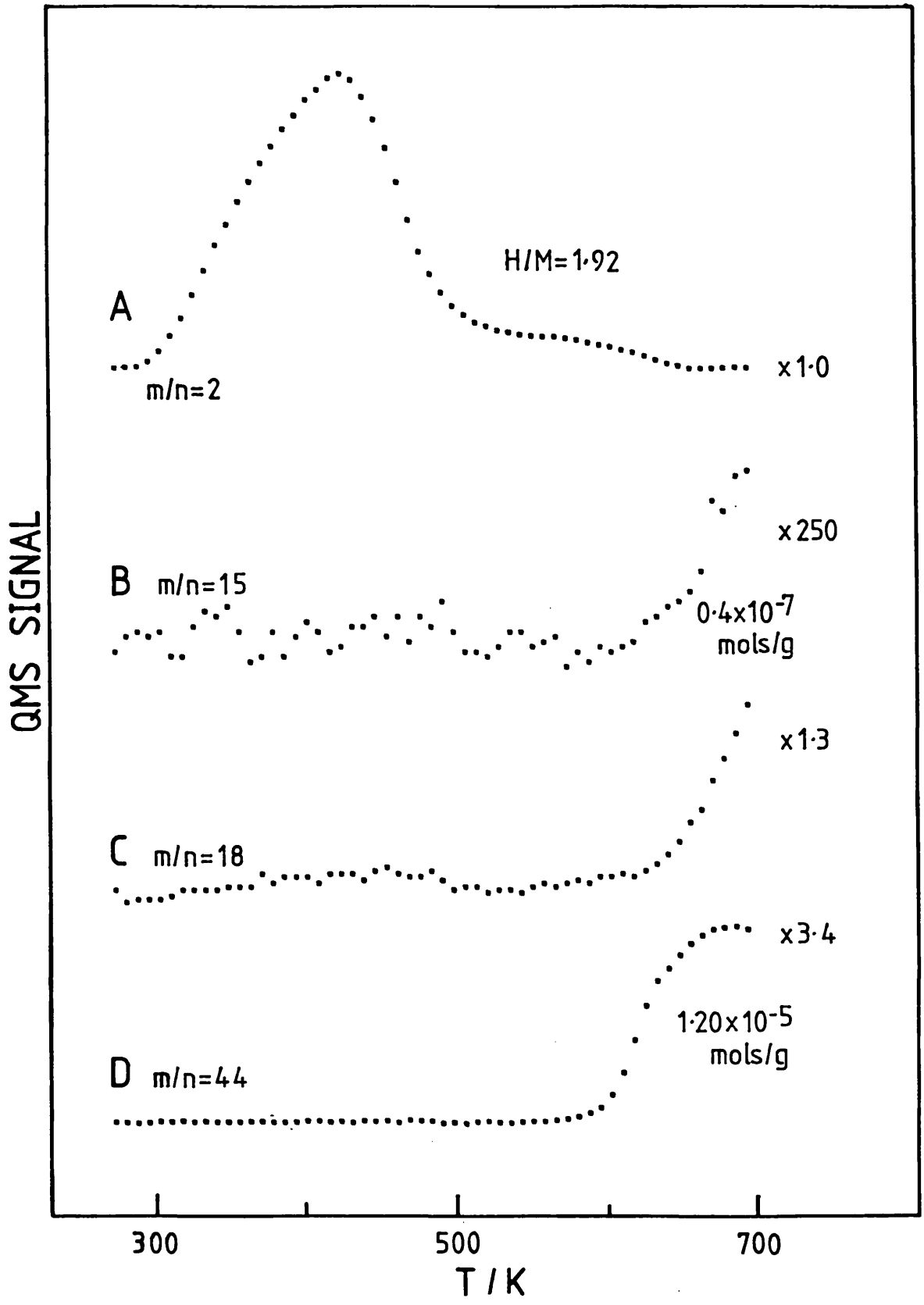

Fig. 5.2: Desorption Profile for Sample Ir100 Subjected to Pretreatment R610

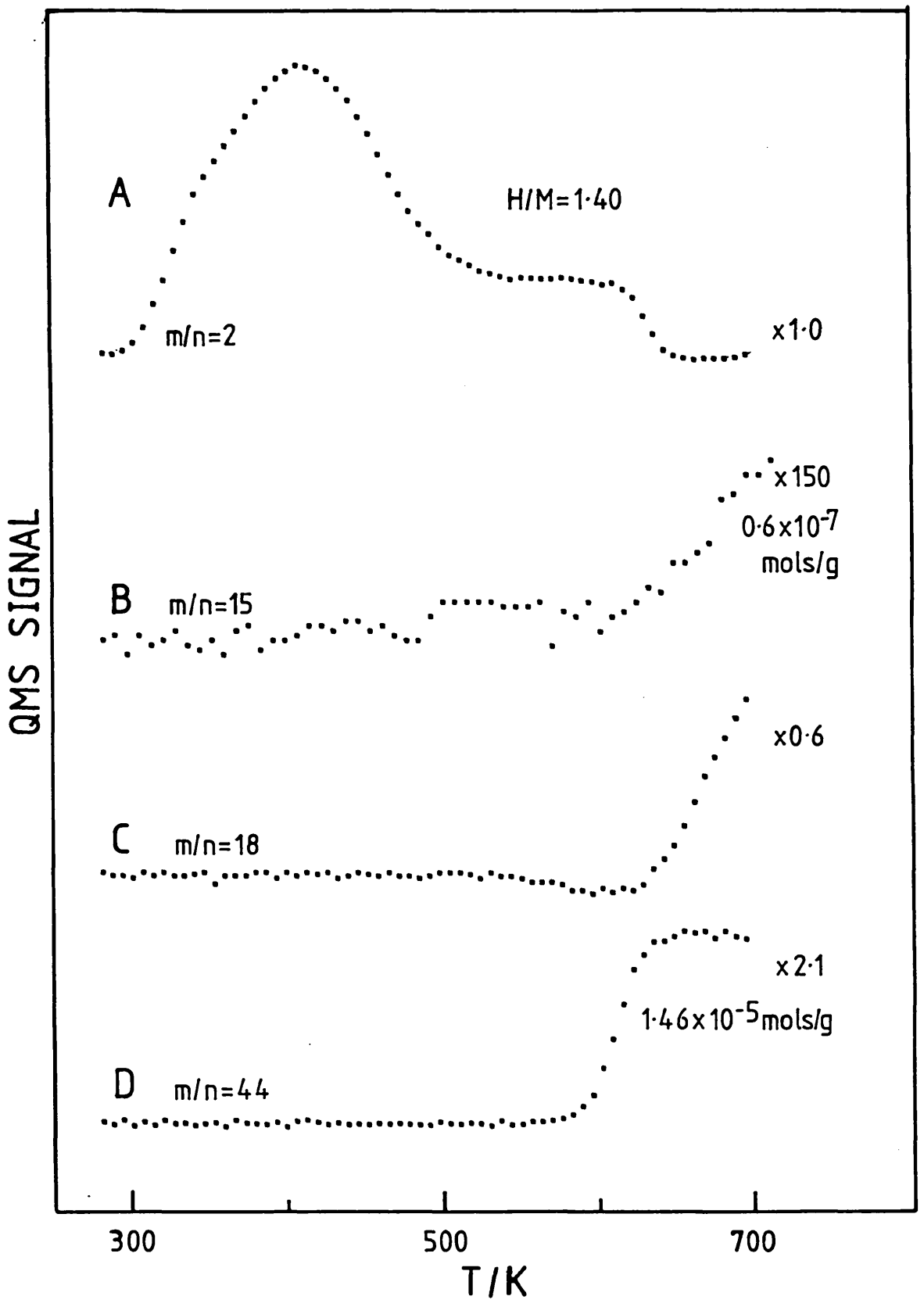

Fig. 5.3: Desorption Profile for Sample PtIr43 Subjected to Pretreatment R610.

An alternative explanation for the correlation with desorption profiles from single crystal surfaces would be that the hydrogen atoms are bound to the same type of local site as found on these surfaces. Thus hydrogen desorbing from surface metal atoms of similar coordinative saturation as those found in the (111) surface give rise to the 340K peak whereas hydrogen adsorbed on less coordinatively saturated metal atoms produces the 410K peak.

The 347K and 420K desorption peaks for the Ir100 sample are comparable to the two Pt100 peaks just discussed. However, the 420K peak is much larger than the corresponding peak in the Pt100 sample and the H/M ratio has risen to 1.92. Similar desorption profiles and H/M ratios have been obtained by Krishnamurthy et al. (1982) for iridium samples reduced at 770K. McVicker et al. (1980) have also obtained H/M ratios of around 2.0 for the hydrogen irreversibly adsorbed at room temperature in a conventional hydrogen adsorption apparatus. These workers propose that this strongly bound hydrogen is bound to iridium atoms on the alumina surface, with each atom adsorbing two hydrogen atoms.

Whilst the profile shown in Fig. 5.2 does not run counter to this proposal it is significant that the 420K peak occurs at temperatures found for desorption from the single crystal surfaces. Therefore it may not be necessary to restrict this particular type of desorption to hydrogen bound to isolated iridium atoms. It is possible that hydrogen adsorbed on linear chains and small clusters of iridium atoms might also give a desorption peak at this temperature. Furthermore, the work by Ibbotson et al. (1980) for hydrogen desorption from the reconstructed Ir (110) surface showed that hydrogen adsorption could occur on both bridged and atop positions. Hence H/M ratios approaching two could easily be obtained. Thus iridium may form highly dispersed clusters which predominantly contain atoms of low coordination number which can adsorb up to two hydrogen atoms per metal atoms. At this stage the major difference between platinum and iridium appears to be that the latter metal is capable of adsorbing two hydrogen atoms per metal atom when the iridium is in a low coordination number site. Thus the highly dispersed iridium is able to adsorb twice as much hydrogen as similarly dispersed platinum and this accounts for the different desorption profiles observed.

Additional experiments performed on a more heavily loaded 10 wt% Ir/alumina sample, produced a similar hydrogen desorption profile to the one shown in Fig. 5.2. However, the relative height of the 420K peak was reduced and the total amount of hydrogen desorbed produced a H/M value of 0.54. Escard et al. (1973) obtained a similar profile for a 36 wt% Ir/alumina catalyst. These results show that increasing the loading leads to the production of larger crystallites with a relatively smaller proportion of metal atoms present in small clusters or as isolated atoms.

The bimetallic PtIr43 sample (Fig. 5.3) also has a H/M value in excess of unity. Engels et al. (1976) obtained similar values using a conventional adsorption system and attributed the excess to hydrogen spillover onto the support. McVicker and Ziemiack (1985) have also obtained similar values for platinum-iridium samples not subjected to oxidative agglomeration pretreatments. The H/M ratio is intermediate between those found for the monometallic systems. The additional uptake relative to the Pt100 sample is due to an increase in the 405K peak, although this peak is reduced relative to the Ir100 sample. The hydrogen desorption profile shown in Fig. 5.3 is therefore not particularly indicative of alloy formation since it can be considered to be the addition of the two monometallic profiles.

The high temperature tails observed on these peaks probably indicates a distribution of sites for isolated metal atoms or for very small clusters. Similar desorption tails have been observed for a stepped Pt(111) surface by Christmann and Ertl (1976) and a stepped Ir(111) surface by Nieuwenhuys et al. (1976). Foger and Anderson (1978) have observed a similar tail for silica-supported platinum particles that had a mean diameter around 1.0-1.2nm.

In addition to the two low temperature peaks each profile contains a high temperature peak around 600K. This peak was approximately the same size for all samples, although it was slightly reduced for the Ir100 sample (height relative to the Pt100 sample ~0.7). For direct comparison of the hydrogen desorption profiles shown in Figs. 5.1-5.3 each profile should be magnified by a factor proportional to the size of the H/M ratio.

Peaks in the region of 600K are not observed for hydrogen desorption from clean single crystal surfaces. Any one of the

following possibilities, previously discussed in the literature, may account for the high temperature peaks:

i) Reaction of the dispersed metal with support hydroxyl groups according to reaction (5.1); a model proposed by Frennet and Wells (1985).

ii) Desorption of dissolved, or occluded hydrogen as suggested by Menon and Froment (1979, 1981) and Tsuchiya et al. (1970).

iii) Desorption of spillover hydrogen.

iv) Decomposition of a bridged M-H-O-Al species, suggested by Candy et al. (1980).

v) Desorption of hydrogen from metal atoms in close interaction with the support.

vi) Desorption of hydrogen from a contaminated surface as proposed by Charcosset et al. (1979a).

It should be noted that a high temperature desorption peak has also been observed for desorption of hydrogen from unsupported platinum black samples, where a support effect cannot be invoked. In this case the possible explanations are restricted to ii) or vi) above. Furthermore, hydrogen desorption has been observed in this region from single crystal surfaces when previously exposed to various hydrocarbons as discussed in Section 5.1.3. In this present study similar experiments have been carried out on catalyst samples. The results are presented in Chapter Seven and in general also show an enhanced formation of hydrogen around 600K following exposure to hexane. Therefore possibility vi) cannot be excluded as the cause of the hydrogen peak around 600K.

Charcosset et al. (1979a) suggested that high temperature desorption peaks were due to a decomposition of surface H-CO complexes. In the light of this it is important to note that all samples shown in Figs. 5.1-5.3 show desorption of methane (curve B), water (curve C) and carbon dioxide (curve D) occurring at high temperatures. The amounts of methane and carbon dioxide produced are included in the figures. However, the calibration procedure was not carried out for the water signal and hence the amount of water formed is unknown, although the magnification factor included in the

figure indicates the relative size of this signal. No carbon monoxide other than that arising from the cracking pattern of carbon dioxide was detected.

Water desorption occurs most probably as a result of the temperature exceeding the initial reduction temperature. This water represents desorption from the support. Methane and carbon dioxide production starts to occur as the hydrogen peak maximises. The carbon dioxide arises from the decomposition of the carbonate species described in Chapter Four. The more unstable formate and carbonate species have already decomposed during reduction at 610K, hence the carbon dioxide signal begins to rise once the temperature is exceeded. The methane may be produced by reaction of carbon dioxide with hydrogen, still present on the catalyst, above 600K as described by equation (4.2) in Chapter Four. This suggests that the high temperature peak is actually a cut-off caused by the onset of this reaction. However, the amount of methane produced is too small to result in such a dramatic drop and therefore the reaction must occur between carbon dioxide and small quantities of hydrogen remaining on the catalyst above 600K.

It has already been observed in Chapter Four that reduction of non-oxidised samples resulted in the production of methane at temperatures in excess of 500K. This methane resulted from the hydrogenation of carbonate and possibly formate species as described by reaction (4.2). Clearly, the metal surfaces may become partially covered in hydrocarbon material during reduction at 610K, which may be the source of the contamination required for explanation vi) to account for the desorption of hydrogen around 600K. However, the high H/M ratios observed with these catalysts indicates that either a large proportion of the metal is not contaminated or that the presence of the carbonaceous material does not greatly affect the hydrogen adsorption capacity of the metal. A further possibility to explain the high temperature desorption process would be that the hydrogen resulted from the dehydrogenation of carbonaceous material held on the support.

To examine the thermal stability of the metal clusters (and the effect of exposing the samples to carbon dioxide and methane) samples were held at 740K in argon, following the desorption run.

These samples were then re-reduced at 610K (coded R610 D740 R610). The hydrogen desorption profiles from a subsequent desorption experiment performed on sample Ir100 (curve A), Pt100 (curve B) and PtIr43 (curve C) are shown in Fig. 5.4.

All samples still exhibit three desorption peaks. However the peaks around 340K and 410K are reduced in height compared to those shown in Figs. 5.1-5.3. Correspondingly, the quantity of hydrogen desorbed is reduced in all cases. These results can be interpreted as arising from a thermal sintering effect, in which heating in argon causes the metal clusters to grow in size. Possibly some of the reduction in size of the peaks may be due to a partial poisoning of the cluster surfaces produced by carbon deposition, above 600K. The high temperature peaks around 500K are approximately the same magnitude as those shown in Figs. 5.1-5.3. Hence the high temperature hydrogen desorption peak is unaffected by the thermal pretreatment. The entire desorption profile is shown for sample Pt100 in Fig. 5.5. Similar impurity profiles were obtained for the Ir100 and PtIr43 samples. The results confirm that the peak around 500K is not caused by a cut off due to conversion of carbon dioxide to methane over the catalyst.

To summarise, reduction of samples at 610K results in the formation of highly dispersed metal clusters which expose metal atoms in both high and low coordination sites. Large clusters may have a cubo-octahedral structure exposing incomplete (111) and (100) planes. For iridium-containing samples H/M ratios in excess of unity have been obtained. This may result from the production of highly dispersed iridium atoms which are each able to adsorb two hydrogen atoms. Additionally, an increased adsorption capacity on the more open cluster surfaces may contribute to the high hydrogen uptake. Previous explanations in the literature attributing a hydrogen desorption peak around 600K, to a support effect or desorption of dissolved, or occluded hydrogen have been considered. Whilst none of these possibilities can be dismissed, the production of methane by the samples during the reduction step, signifies that desorption of hydrogen from carbonaceous material is a plausible alternative cause of the hydrogen desorption peak at temperatures around 600K.

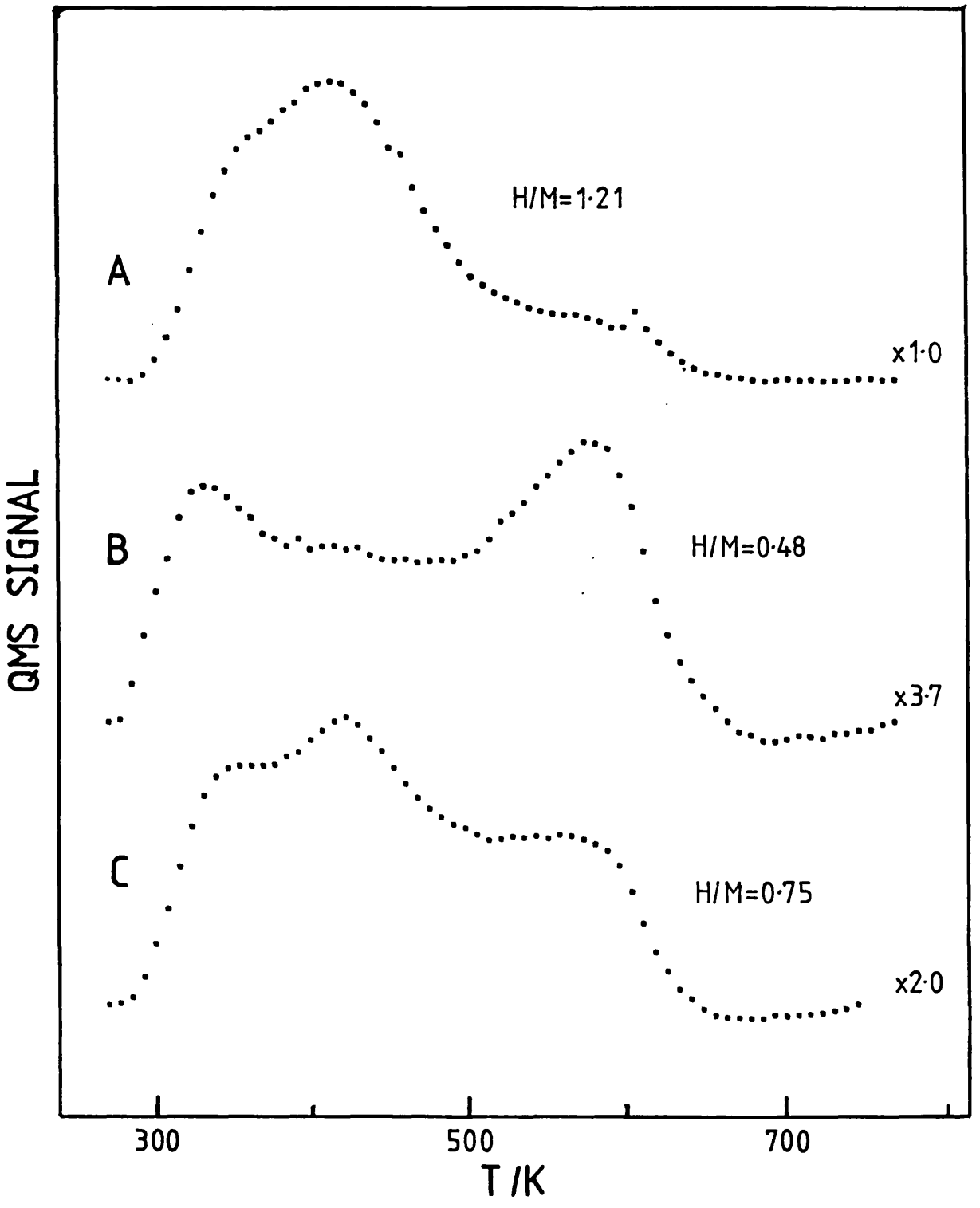

Fig. 5.4: Hydrogen Desorption Profiles for Samples Ir100 (curve A), Pt100 (curve B) and PtIr43 (curve C) Subjected to Pretreatment R610 D740 R610

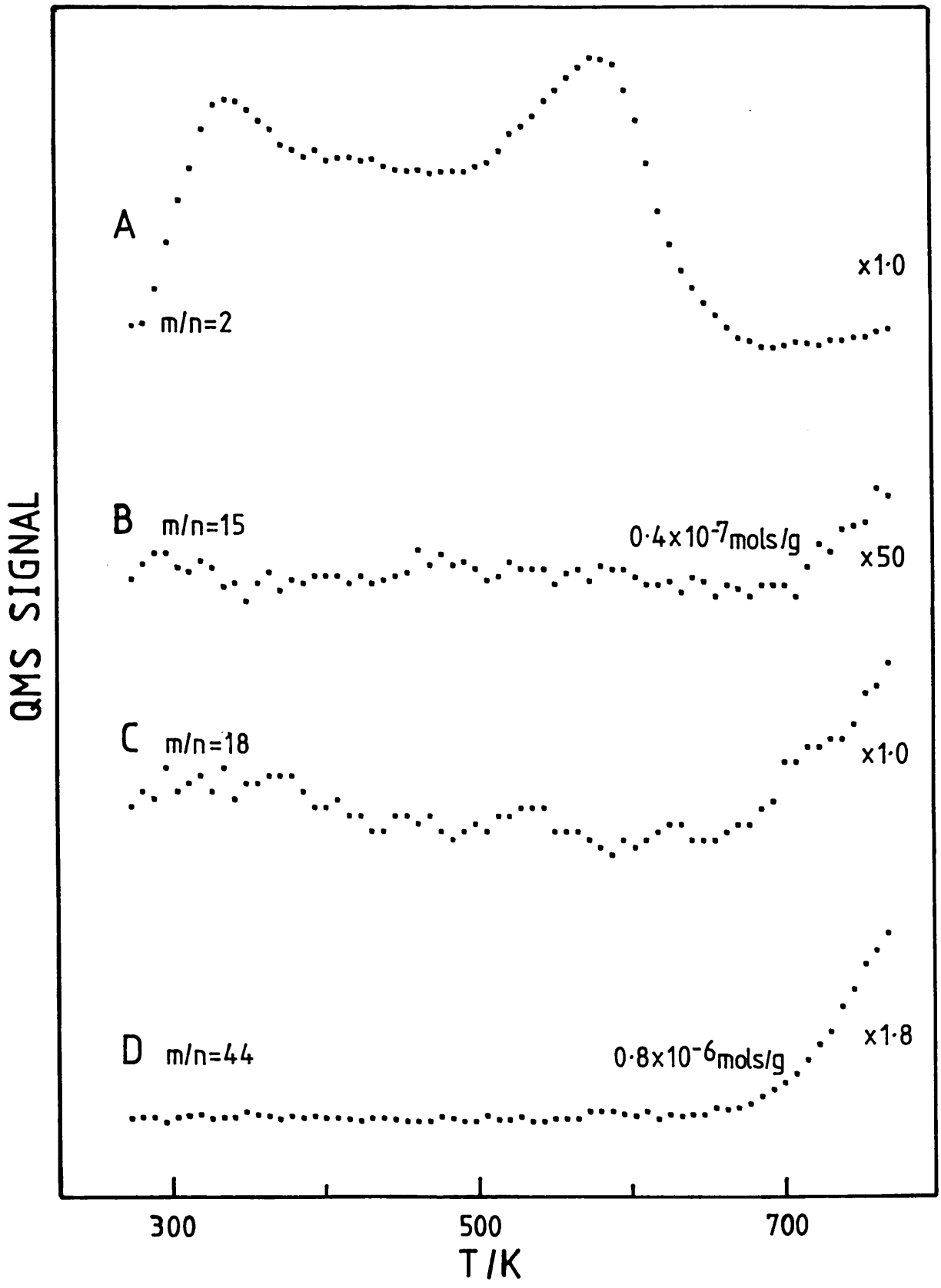

Fig. 5.5: Desorption Profile for Sample Pt100 Subjected to Pretreatment R610 D740 R610

b) Samples Reduced at 740K

Fig. 5.6 shows the hydrogen desorption profiles for samples Ir100 (curve A), Pt100 (curve B), and PtIr43 (curve C) subjected to reduction at 740K (coded R740). In all cases hydrogen desorption extends to higher temperatures than those found for pretreatment R610.

The middle peak in the profile for the Pt100 sample (curve B) is now much less intense and has shifted to 461K. Hydrogen desorption also extends up to 750K at which temperature the desorption experiment was ended. Changes in the position and intensity of the second desorption peak may arise from structural changes in the clusters, resulting in a decrease in the quantity of low coordination number platinum atoms. Thus the amount desorbed from such sites will decrease, whilst the temperature for desorption will increase since the relative fraction of lower coordinated atoms is greater.

The profiles shown for the iridium-containing samples are quite different from those obtained for pretreatment R610. For the Ir100 sample (curve A) the previously large 420K peak is now absent. A high temperature peak now reaches its maximum at 676K, but it is approximately a third less intense than the 600K peak formed following the R610 pretreatment. The low temperature peak around 340K has also reduced in size. Overall these differences result in a decrease in the H/M ratio to 0.38.

The bimetallic sample also shows a large reduction in the sizes of the low temperature desorption peaks and a decrease in the H/M ratio to 0.49. Graham and Wanke (1981), using a conventional hydrogen adsorption apparatus, have obtained a H/M value of 0.4 for similar samples reduced at 770K. Bimetallic interactions are clearly evident for this sample since the hydrogen desorption profile is not the sum of the monometallic profiles. The entire desorption profile for the PtIr43 sample is shown in Fig. 5.7. Clearly no impurity desorption can be detected below 700K. Similar impurity profiles were obtained for the Pt100 and Ir100 samples.

In order to help elucidate the effect of the high temperature reduction treatment, fresh samples were subjected to temperature-programmed reduction to 740K. On reaching this temperature the

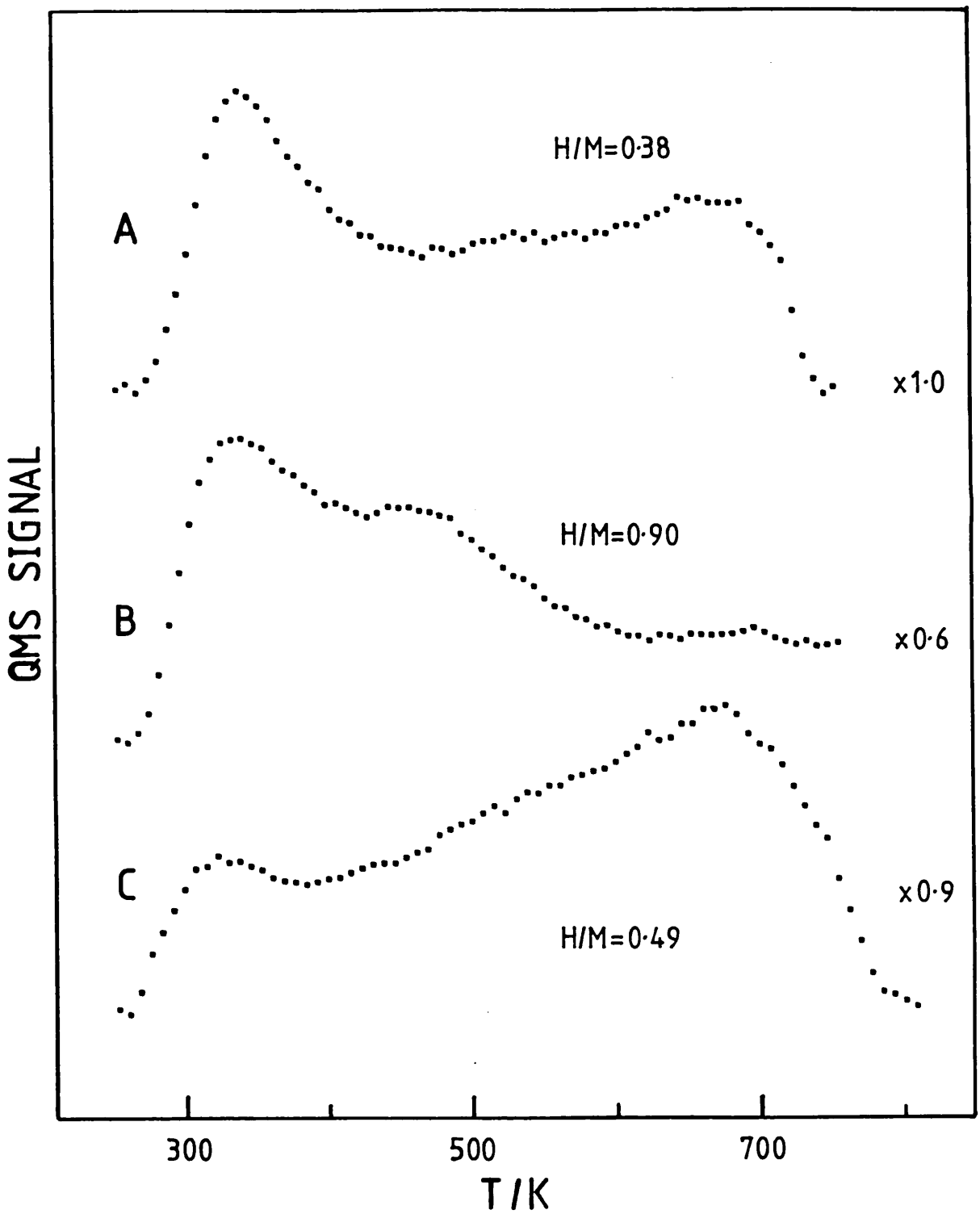

Fig. 5.6: Hydrogen Desorption Profiles for Samples Ir100 (curve A), Pt100 (curve B) and PtIr43 (curve C) Subjected to Pretreatment R740.

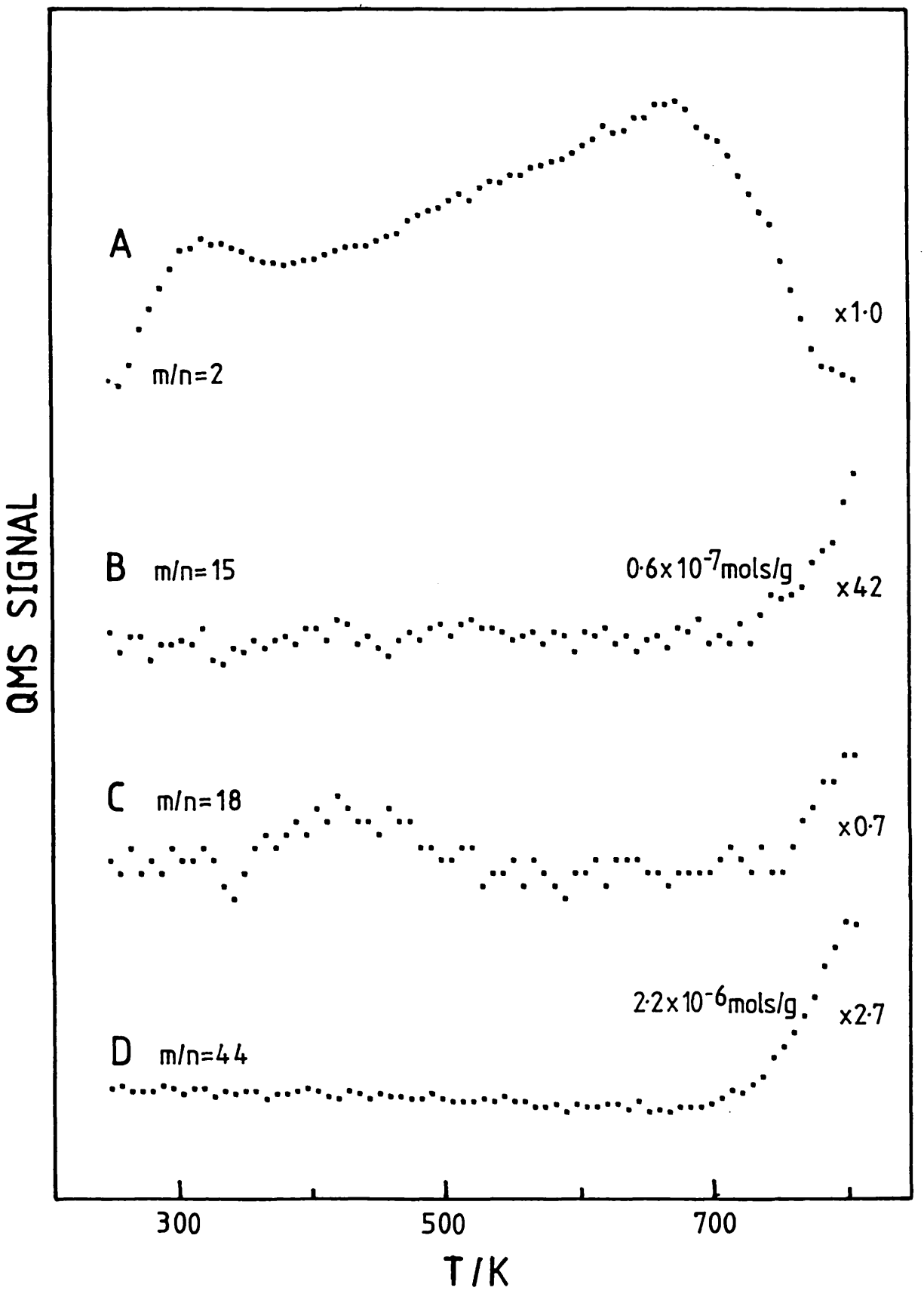

Fig. 5.7: Desorption Profile for Sample PtIr43 Subjected to Pretreatment R740.

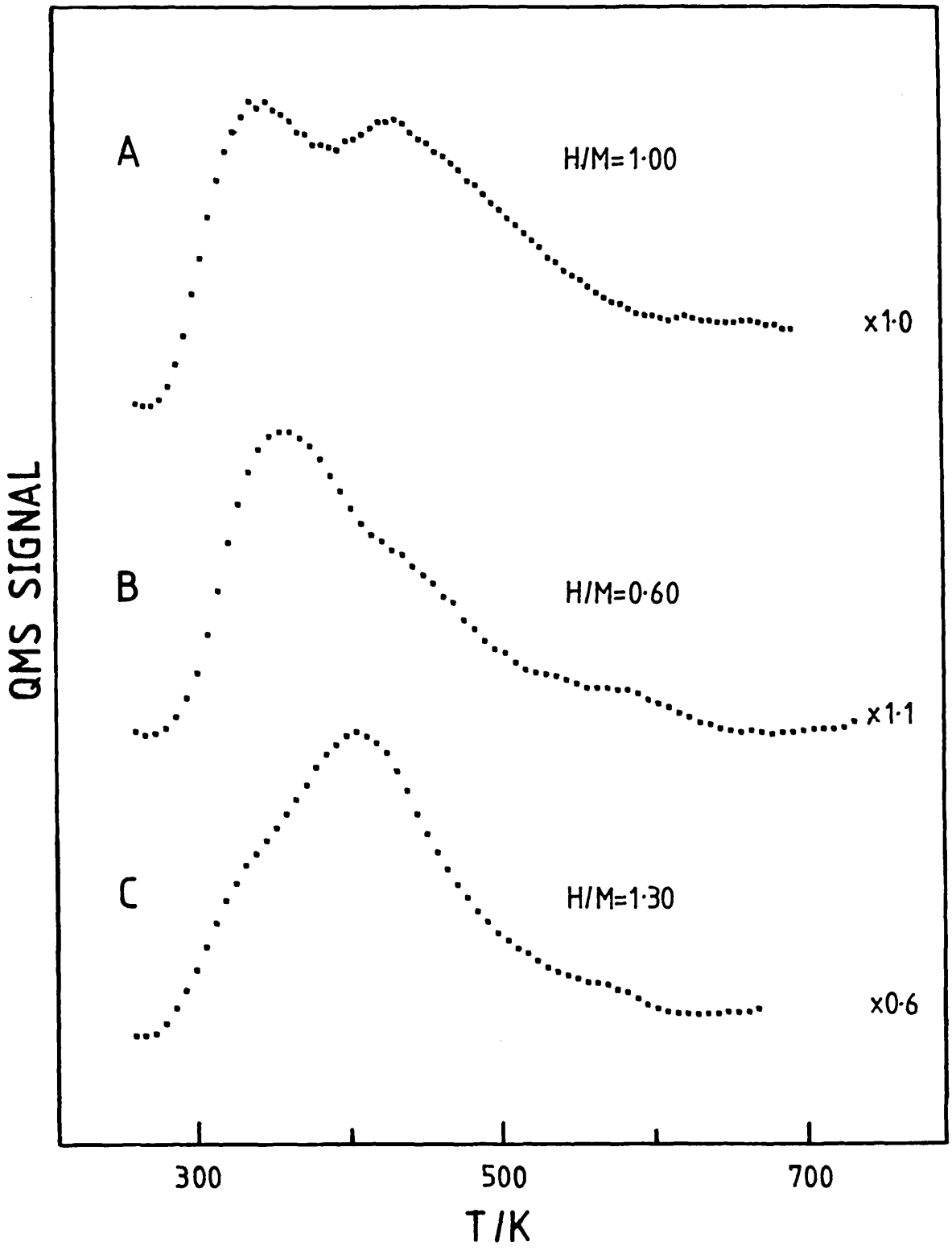

Fig. 5.8: Hydrogen Profiles for Samples Pt100 (curve A), Ir100 (curve B) and PtIr43 (curve C) Subjected to Pretreatment TPR740.

samples were immediately allowed to cool to room temperature (code TPR740). Hence no isothermal reduction was carried out. Fig. 5.8 shows the hydrogen desorption profiles for samples Pt100 (curve A), Ir100 (curve B) and PtIr43 (curve C) subjected to pretreatment TPR740. Water, methane and carbon dioxide production was not detected for any of the samples during the desorption experiment.

The Pt100 profile is similar to that shown in Fig. 5.6 with the exception that the 461K peak is now more intense and occurs at 423K. Hydrogen desorption still extends up to 700K, which was not observed following pretreatment R610. The Ir100 sample gives a single peak at 353K with a slight shoulder at 439K, but in contrast to Fig. 5.6 this peak is much larger. Furthermore, the sample shows little desorption occurring as the temperature approaches 700K. This sample still shows a small feature maximising at 583K though this is smaller than on the profile obtained following pretreatment R610.

The profile for the PtIr43 sample shows the most dramatic change from that in Fig. 5.6. It resembles Fig. 5.3 i.e. the profile for the sample subjected to pretreatment R610. The 600K peak is also smaller for this sample following pretreatment TPR740. Alloy interactions are again evident in the bimetallic sample, since its desorption profile is not the sum of the profiles for the monometallic systems.

The results shown in Fig. 5.4 and 5.6 indicate that a greater reduction in the hydrogen adsorption capacity for the iridium-containing samples can be produced by heating in hydrogen than by heating under an inert atmosphere. However, the opposite was true for the Pt100 sample. This indicates that the effect may be related, in some way, to the formation of an H-Ir-H species. Also, the results shown in Fig. 5.8 show that the presence of iridium causes a reduction in the size of the highest temperature desorption feature. This can be produced in these samples only by an isothermal high temperature reduction pretreatment.

In the forthcoming discussion of the results presented in Fig. 5.6 and 5.8, hydrogen desorption peaks occurring below approximately 500K will be described as the low temperature peaks, whilst peaks above this temperature will be referred to as the high temperature desorption peaks.

The diminution in the size of the low temperature hydrogen desorption peaks for the iridium-containing samples may be due to any of the following:

1) Sintering of the metal into large crystallites.
2) Poisoning caused by extensive contamination of the metal surface at elevated temperatures.
3) Formation of an unreactive SMSI state between the metal and the support caused by the high temperature reduction pretreatment.

The high temperature desorption peak at 680K may arise from the same type of process which produced the 580K peak observed after pretreatment R610. Accordingly, this process would be activated and heating to the higher reduction temperatures will populate the more inaccessible sites resulting in desorption extending to temperatures beyond 580K. Alternatively, the peaks around 680K and 580K may be due to different processes. It may be significant that in the Pt100 profile shown in Fig. 5.6 hydrogen is still desorbing at the highest temperatures whereas the hydrogen signal drops sharply for the iridium-containing samples. Hence the high temperature desorption process shown for the Pt100 sample may be due to a different or additional process to that for the iridium-containing samples. An alternative explanation for the high temperature desorption feature is that reduction at elevated temperatures produces new sites which strongly readsorb hydrogen desorbing from the metal surface. This readsorption effect would result in a shift of the desorption peaks from low to higher temperatures. However, the desorption profiles, shown in Fig. 5.6, were obtained following cooling from 740K under hydrogen. Therefore, it would be expected that if any new sites had been produced they would have been already populated before the TPD experiment began. Hence this possibility is discounted.

i) The Low Temperature Peaks

The various possibilities for the cause of the reduction in size of the low temperature peaks are discussed separately below. However, these processes are not necessarily mutually exclusive and a combination of them may operate.

1) Sintering

If a metal sintering effect is dominant then the results for the Ir100 sample, shown in Fig. 5.8, can be explained by proposing that exposure to hydrogen at high temperatures results in the incorporation of low coordination number iridium atoms into clusters and/or growth of the iridium clusters into larger crystallites containing the more closely packed surfaces. Thus the 420K peak is smaller and the amount of hydrogen desorbed is lower than unity. Crystallite growth continues during the isothermal period of pretreatment R740 resulting in a decrease in size of the low temperature peak.

The results for the Pt100 sample could then be explained by suggesting that it is more stable than iridium in a reducing atmosphere. For the bimetallic sample, the presence of the platinum in the alloy clusters would then be sufficient to prevent sintering during the TPR740 pretreatment. However, prolonged isothermal reduction at this temperature results in greater sintering than is found for the monometallic samples. Presumably, this would be caused by an activated process in which the alloy clusters aggregate faster than the monometallic samples during the isothermal reduction period.

2) Poisoning

The results contained in Chapter Four showed that reduction of samples not subjected to an initial oxidation at 740K resulted in the production of methane above approximately 500K. This methane resulted from the reaction of formate or carbonate species which were originally bound to the support. It was further concluded that hydrogenation only removed a fraction of these carbon-containing species from the samples. Therefore, a reasonable explanation for the reduction in the size of the low temperature peaks is that the high temperature reduction pretreatment, R740, result in extensive carbon deposition on the iridium-containing samples which reduces their capacity to chemisorb hydrogen.

The results for the Ir100 sample, shown in Fig. 5.8, could then be explained by proposing that carbon deposition occurs preferentially on the low coordinated iridium metal, whilst the Pt100 and PtIr43 samples are able to resist this deposition following pretreatment TPR740. The profile for the Pt100 sample, shown in

Fig. 5.6, would then indicate that this resistance was maintained during the isothermal reduction period. However, changes in the profile for the bimetallic sample could now be interpreted as arising from an activated poisoning process which has had sufficient time to occur.

As mentioned above, the carbon deposition could result from exposure of the metal clusters to methane at high temperatures during the reduction step. However, the fact that methane production had significantly reduced by 740K for all samples (see Section 4.3.1) may indicate that the source of the contamination was carbon remaining on the support. Indeed, the earlier TPR and TPO studies revealed that carbon-containing species remained on the support following reaction in hydrogen. Hence the activated poisoning process proposed for the bimetallic sample could result from the support-bound carbon requiring sufficient time to diffuse onto and, perhaps, into the metal at elevated temperatures. The Pt100 sample does not seem to be as readily affected. This could result from the absence of carbon deposition. Alternatively, the hydrogen chemisorption properties of the platinum sample could be unaffected by the presence of carbonaceous material.

At this point it is important to re-emphasize that possible carbon deposition and sintering effects are not mutually exclusive processes. Hence one possibility is that rapid diminution of the 420K peak for the Ir100 sample, shown in Fig. 5.8, results from a sintering effect. However, further reduction in this peak intensity and the entire reduction in the size of the low temperature peaks for the bimetallic sample, observed during the isothermal reduction period, could then result from the activated carbon deposition process.

3) SMSI

Several workers have observed that high temperature reduction of alumina-supported platinum results in a reduction in the ability of the metal to chemisorb hydrogen at room temperature, which could not simply be attributed to sintering of the metal. Den Otter and Dautzenberg (1978) suggested that this was caused by the formation of fully, or partially, reduced alumina species that combine with the platinum to produce an alloy which does not chemisorb hydrogen.

Several other possibilities have been suggested and these have been outlined in Section 4.4.1. For the purposes of this discussion no particular theory will be preferred for the nature of newly formed species which will be referred to as an SMSI state.

The results for the Ir100 sample, shown in Fig. 5.8 could be explained by proposing that the SMSI state readily forms with the more coordinatively unsaturated iridium atoms. The results for the platinum-containing samples would then show that the presence of platinum inhibits the formation of the SMSI state. However, following the isothermal pretreatment the resistance of the bimetallic sample is apparently overcome and the SMSI state forms. The Pt100 sample would remain resistant to the formation of the SMSI state following pretreatment R740.

In order to elucidate further the nature of the possible formation of the SMSI state, a desorption experiment was performed in the presence of hydrogen on a PtIr43 sample previously subjected to pretreatment R610. The results obtained are shown in Fig. 5.9. The hydrogen profile (curve A) shows a peak at 320K which is now slightly more intense than the corresponding feature observed in Fig. 5.3. This state probably represents the weak, reversible form of hydrogen observed by Sinfelt and Via (1979). Additionally the 405K peak, observed in Fig. 5.3, has now shifted to 430K and the high temperature tail appears to be more populated. The previously observed peak around 600K may be absent, although it is difficult to be certain since the desorption profile was measured on a high background of hydrogen. The total amount of hydrogen desorbed over the whole of this region, shown enlarged in the figure, gave a H/M ratio of 2.0.

At temperatures corresponding to the initial reduction temperature a hydrogen uptake starts to occur, which maximises around 715K. As expected, similar uptakes were observed in the TPR profiles shown in Section 4.3.1. Point A indicates the point where the temperature was held constant, at 790K, whilst the reactor was allowed to cool at point B.

Since the hydrogen uptake does not coincide with any particular hydrocarbon formation reaction, it is tempting to assign this uptake to the metal catalysed reduction of the support which may result in the formation of the SMSI state. Since this state would be

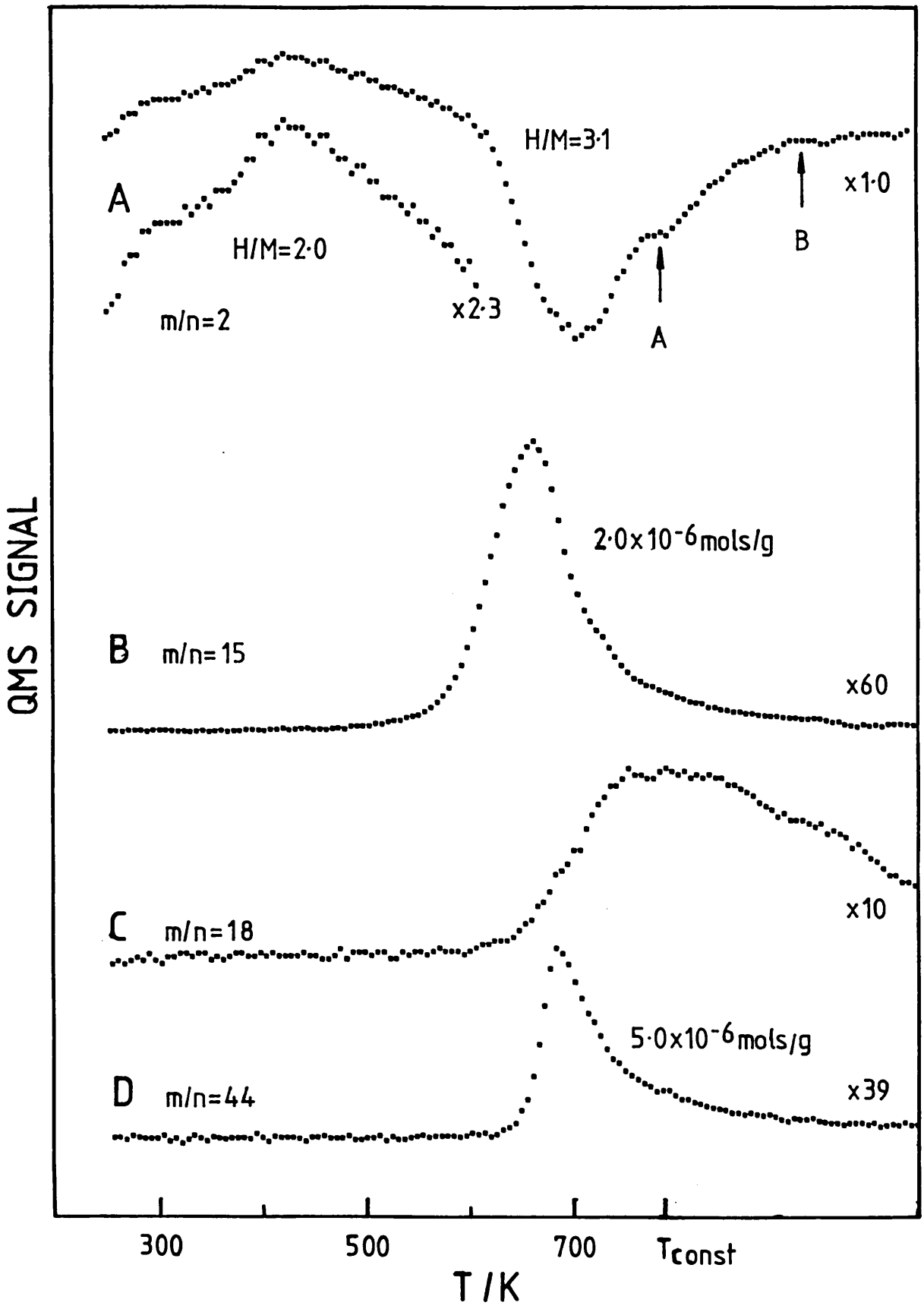

Fig. 5.9: Desorption Profile Obtained in the Presence of Hydrogen for Sample PtIr43 Subjected to Pretreatment R610.

expected to be inactive towards carbon dioxide hydrogenation, the appearance of this gas above 650K could signify the onset of the metal-support interaction. However, if the sample is immediately allowed to cool down at point A, a subsequent hydrogen desorption experiment produces a profile similar to that shown in Fig. 5.8, indicating that the SMSI state has not formed. Therefore, the previous explanation given in Chapter Four for the observed carbon dioxide peak still stands and the results are consistent with the observation that a high temperature hydrogen uptake in a TPR profile cannot necessarily be used as firm evidence for the formation of an SMSI state.

However as discussed in Section 4.4.1, the hydrogen uptake may be significant since the Pt100 sample did not exhibit a mismatch between methane formation and hydrogen uptake during TPR. Moreover, this is the only sample for which a possible SMSI state does not form following pretreatment R740. Thus it can be argued that this additional uptake represents a reduction of the support, which occurs more readily for the iridium-containing samples. However, the SMSI state is formed by an activated process requiring time for the combination of the metal with the partially, or fully reduced alumina species. Hence, the PtIr43 sample would only exhibit SMSI type behaviour following the isothermal reduction step.

The Ir100 desorption profile shown in Fig. 5.6 might then be explained in a similar manner. However, the increased height of the 338K peak would indicate that the iridium does not form the SMSI state as readily as the PtIr43 sample. This could arise if the rapid decrease in the size of the 420K peak, shown in Fig. 5.8, was primarily due to a sintering effect. This produces larger iridium crystallites which do not form the SMSI state as readily as the highly dispersed bimetallic sample during the isothermal reduction pretreatment.

The lack of an SMSI state for the Pt100 sample would then explain the absence of the extended high temperature uptake in the TPR profile of this sample, shown in Fig. 4.1. As explained in Section 4.4.1 this may be related to the presence of carbonaceous material in this sample, possibly located at the metal-support interface. Rasser (1977) has observed, using AES, that the presence

of iridium in platinum-Kuliphay powders reduced the carbon contamination on such samples. Hence, in the iridium-containing samples there may be less carbonaceous material remaining after reduction than with the Pt100 sample. The absence of the carbon barrier may then enable these samples to undergo formation of an SMSI state possibly by allowing a closer, epitaxial relationship between the metal and the oxide support during the isothermal reduction period.

Similar results to those shown for the iridium containing samples in Fig. 5.6, have been obtained by Menon and Froment (1979) for alumina-supported platinum catalysts which were oxidised at 770K prior to the reduction step. However, these workers found that the total amount of hydrogen desorbed from such samples stayed constant and shifted to higher temperatures. In a later paper Menon and Froment (1981) rejected the SMSI alloy model in favour of a mechanism in which occluded hydrogen most probably inhibited the adsorption of hydrogen on the metal surface. However, the results shown in Fig. 5.6 show that the total amount of hydrogen decreases. Therefore, such an 'inhibition' model does not seem to readily account for the reduction in the low temperature hydrogen desorption peaks for the iridium-containing samples.

ii) The High Temperature Peaks

As previously mentioned, the high temperature hydrogen peaks, shown in Fig. 5.6, may be due to the same process that caused the 580K peak following pretreatment R610. The absence of this state for the iridium-containing samples shown in Fig. 5.8 could then signify that the presence of this metal slowed down the population of this state. However, if the 580K peak results from the decomposition of carbonaceous material then the reduced intensity of this peak for the iridium-containing samples shown in Fig. 5.8 could indicate that pretreatment TPR740 removes most of these species from these samples. The desorption of hydrogen at temperatures up to 700K for the Pt100 sample could be due to the presence of carbonaceous material of a highly heterogeneous nature which dissociates to give hydrogen in this temperature range.

Alternatively, separate processes may be operative in the formation of the 580K and 680K peaks. For instance, the 580K peak may be due to the metal-support combination proposed by Frennet and

Wells (1985), or due to the decomposition of carbonaceous material, whilst the 680K may arise from a different process such as desorption of spillover hydrogen. Furthermore, if pretreatment R740 resulted in the formation of an SMSI state for the iridium-containing samples, then the 680K peak may be due to desorption of hydrogen strongly bound to the SMSI state. The smaller size of this peak for the Ir100 sample compared to the PtIr43 sample, shown in Fig. 5.6, could then arise from the reduced formation of this state for the Ir100 sample, possibly as a result of a rapid sintering of the iridium.

To summarise, reduction of iridium-containing samples at 740K results in the diminution in size of the hydrogen desorption peaks previously associated with desorption from the metal surfaces. In addition, hydrogen desorption extends to temperatures above 700K, following the high temperature isothermal reduction pretreatment. The high temperature feature may arise from a similar process to that which caused the 580K peak observed after pretreatment R610, or alternatively different processes may be active. At this present stage it is not possible to distinguish between the alternatives. The Pt100 sample also exhibited a high temperature desorption feature, but peaks due to desorption from the metal surface were still present. The reduction in size of the low temperature peaks for the iridium-containing samples can be explained by processes involving sintering, poisoning or metal-support interactions. These processes are not mutually exclusive and at this stage it is impossible to determine their relative importance. However, the influence of carbon contamination may be determined from the results of samples oxidised at 740K prior to reduction which are discussed in the next section.

5.3.2 Samples Subjected to Oxidation Prior to Reduction

a) Samples Subjected to Pretreatment O740 R610

Fig. 5.10 shows the hydrogen desorption profiles for samples Ir100 (curve A), Pt100 (curve B) and PtIr43 (curve C) subjected to an initial oxidation at 740K before reduction at 610K (coded O740 R610). All three samples show that the desorption of hydrogen occurs in three regions around 340K, 410K and 540K. The peak previously obtained around 600K, following pretreatment R610 is absent.

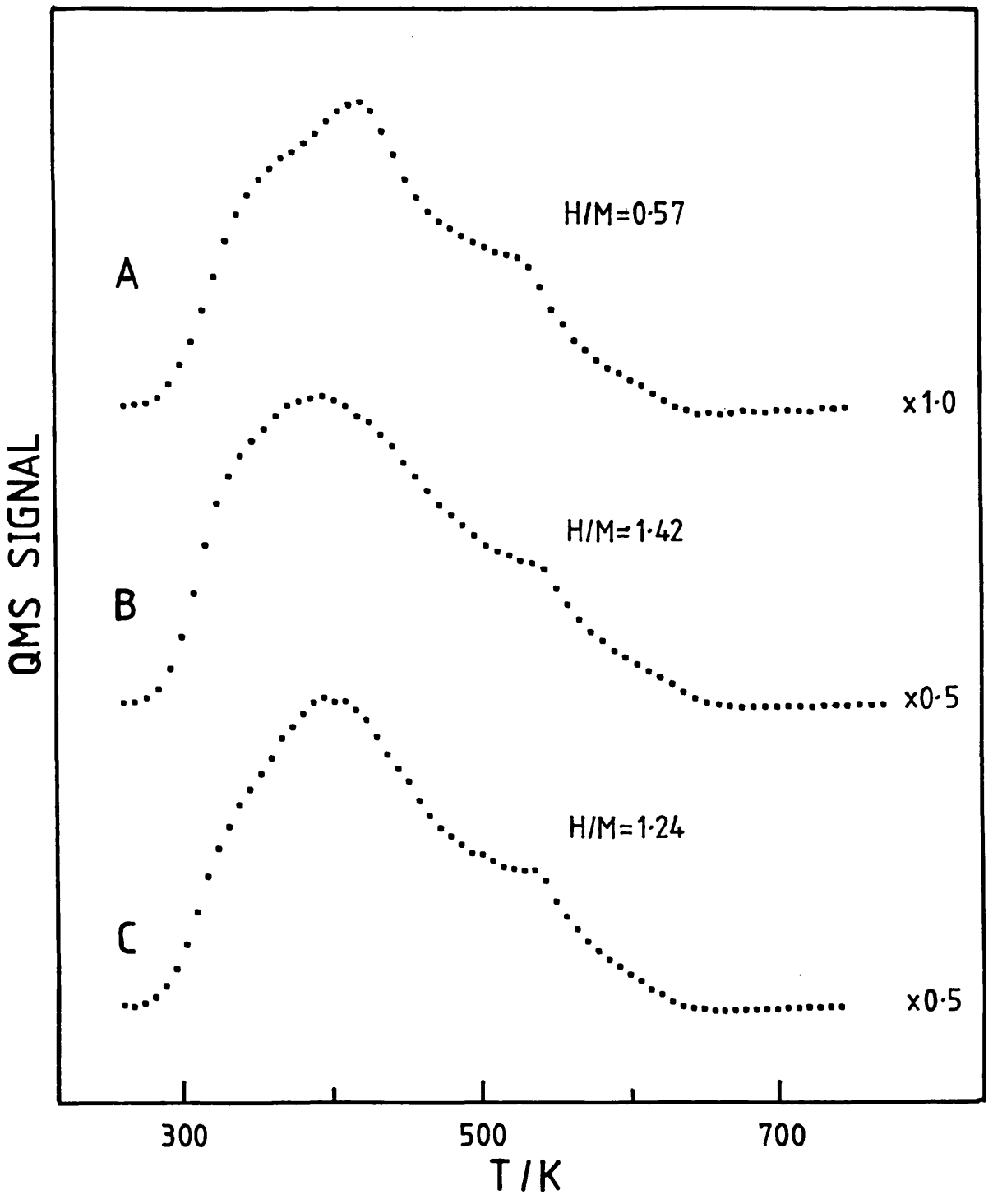

Fig. 5.10: Hydrogen Desorption Profiles for Samples Ir100 (curve A), Pt100 (curve B) and PtIr43 (curve C) Subjected to Pretreatment O740 R610.

The 416K peak in the Ir100 sample is much reduced compared to the peak shown in Fig. 5.2. This result is consistent with the results found using TPR in Section 4.3.1 in which oxidation at 740K resulted in the formation of large IrO_2 crystallites and some remaining highly dispersed species. The H/M ratio of 0.57 for this sample shows that agglomeration of the metal had occurred during the oxidation step. The presence of the 416K peak also shows that more highly dispersed species of a lower coordination number exist following the reduction step.

The results for the Pt100 sample show a broad peak centred around 390K. Closer inspection reveals that this feature consists of two components situated around 340K and 410K. However, the 410K peak is more intense than the corresponding peak shown in Fig. 5.1. This gives rise to the increase in the H/M ratio to 1.42. Therefore it may be that platinum atoms of low coordination number, like iridium, can form H-M-H complexes. The O740 R610 pretreatment may produce relatively more of these species when compared to pretreatment R610. Alternatively, the presence of carbonaceous impurities on the platinum following the latter pretreatment may inhibit the formation of such complexes.

The results for the bimetallic sample show that the presence of platinum reduces the sintering tendency of the iridium component. This may be due to reduced agglomeration of the iridium component during oxidation or to a redispersion of the large iridium-rich crystallites during the reduction step. However, the total amount of hydrogen desorbed by this sample is lower than the total for the Pt100 sample which indicates that some agglomeration of the iridium does occur.

Fig. 5.11 shows the entire desorption profile for the Pt100 sample. Similar impurity profiles were obtained for the Ir100 and PtIr43 samples. No carbon-containing species were apparent during the desorption run; this is consistent with the oxidation behaviour observed in Section 4.3.2. Desorption of water did occur at temperatures in excess of 600K. This may be due to desorption of water produced during the reduction of the oxidised metal species at temperatures in excess of the reduction temperature.

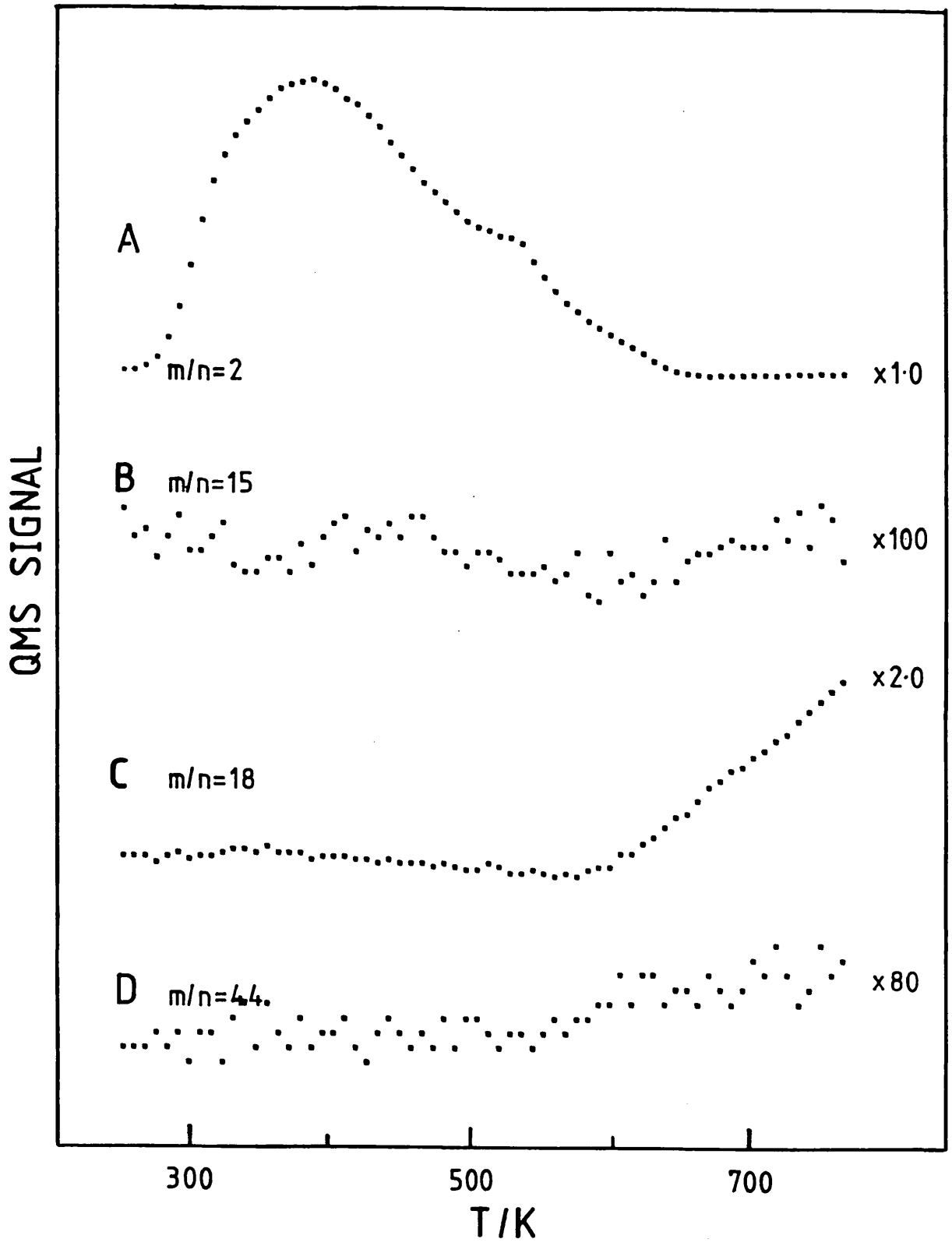

Fig. 5.11: Desorption Profile for Sample Pt100 Subjected to Pretreatment O740 R610.

The absence of a peak at around 600K supports the proposal that the peak arises from the dehydrogenation of carbonaceous material, since the high temperature oxidation removes most of the carbon-containing impurities (see Section 4.3.2). However, the profiles of all samples do show an additional feature at temperatures around 540K. Initially, this was thought to arise from a small peak superimposed on the sloping tail of the 410K peak. However, when temperature-programmed desorption was performed in the presence of hydrogen this feature was no longer clearly observed and a hydrogen uptake may begin at these temperatures. It is difficult to be certain since the hydrogen profiles were measured on a high background of hydrogen. The results for the PtIr43 sample are shown in Fig. 5.12. The desorption profile shows that formation of water occurs at the temperature at which the feature was observed in Fig. 5.11. Hence the features observed around 540K in Fig. 5.10 may represent cut-offs in the hydrogen signal. It seems possible that at temperatures in excess of 540K adsorbed spillover-hydrogen reacts with the alumina to form water. However, why this should occur so suddenly below the previous reduction temperature of 610K is unclear.

A further explanation for the cut-off behaviour observed when desorption is performed in the argon carrier, is that a rapid phase change takes place in the alumina which stops hydrogen desorption occurring from the support. Alternatively, desorption of hydrogen from the support may occur by the removal of hydrogen from separate 'island' phases to the metal centres where recombination and desorption can take place. Initially, as the temperature increases the rate of removal of hydrogen from the 'island' phases, and rate of desorption from the metal centres increases. However, at a certain temperature (~540K) the island concentration may become exhausted and the rate of desorption rapidly drops. Whatever the cause of the cut-off behaviour, the oxidation pretreatment must have produced some change in the catalyst sample which enabled the process to occur following the reduction step, since similar features were not observed following pretreatment R610.

b) Samples Subjected to Pretreatment O740 R740.

Fig. 5.13 shows the hydrogen desorption profiles for samples Ir100 (curve A), Pt100 (curve B) and PtIr43 (curve C) subjected to an initial oxidation at 740K followed by reduction at 740K.

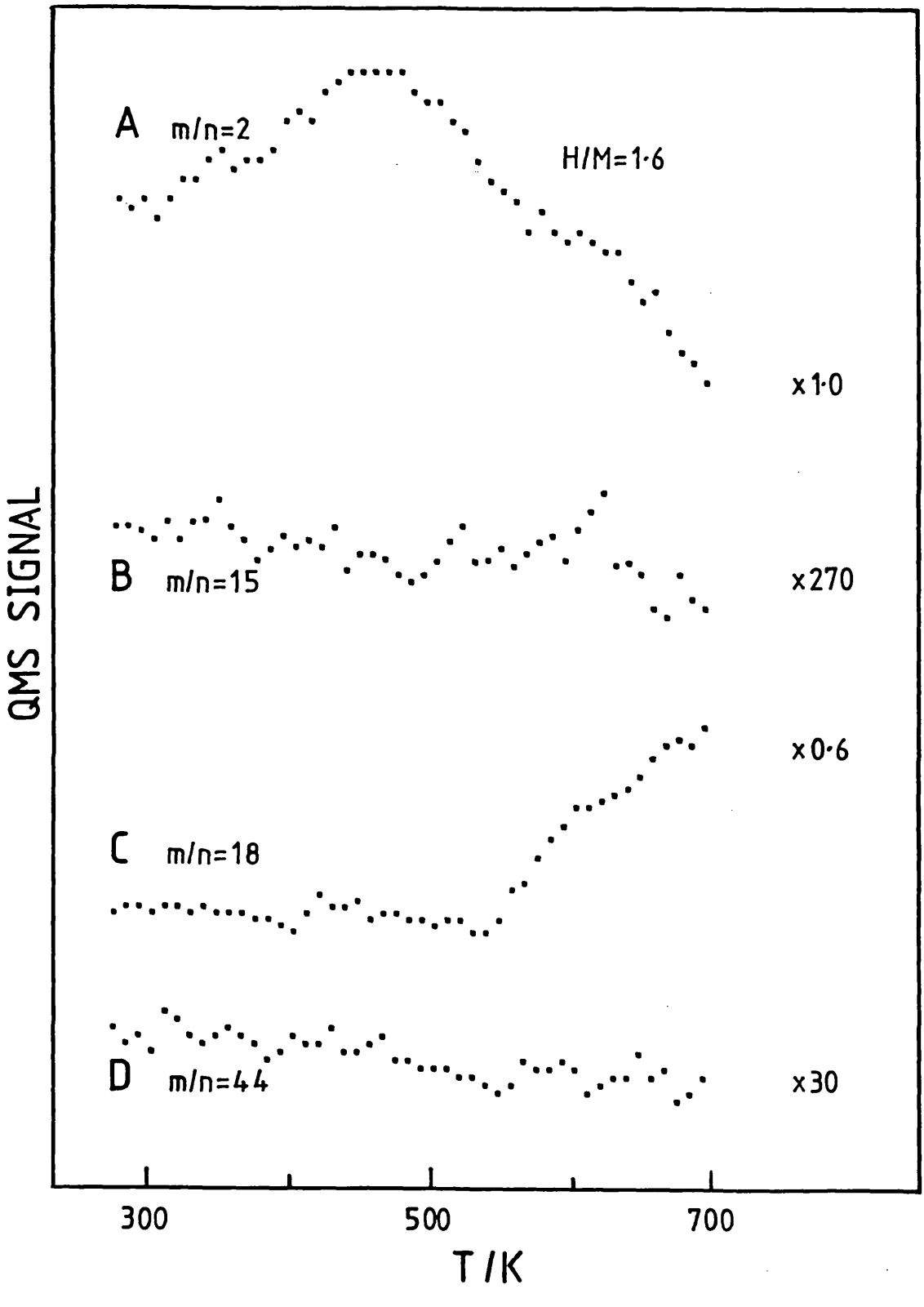

Fig. 5.12: Desorption Profile Obtained in the Presence of Hydrogen for Sample PtIr43 Subjected to Pretreatment O740 R610.

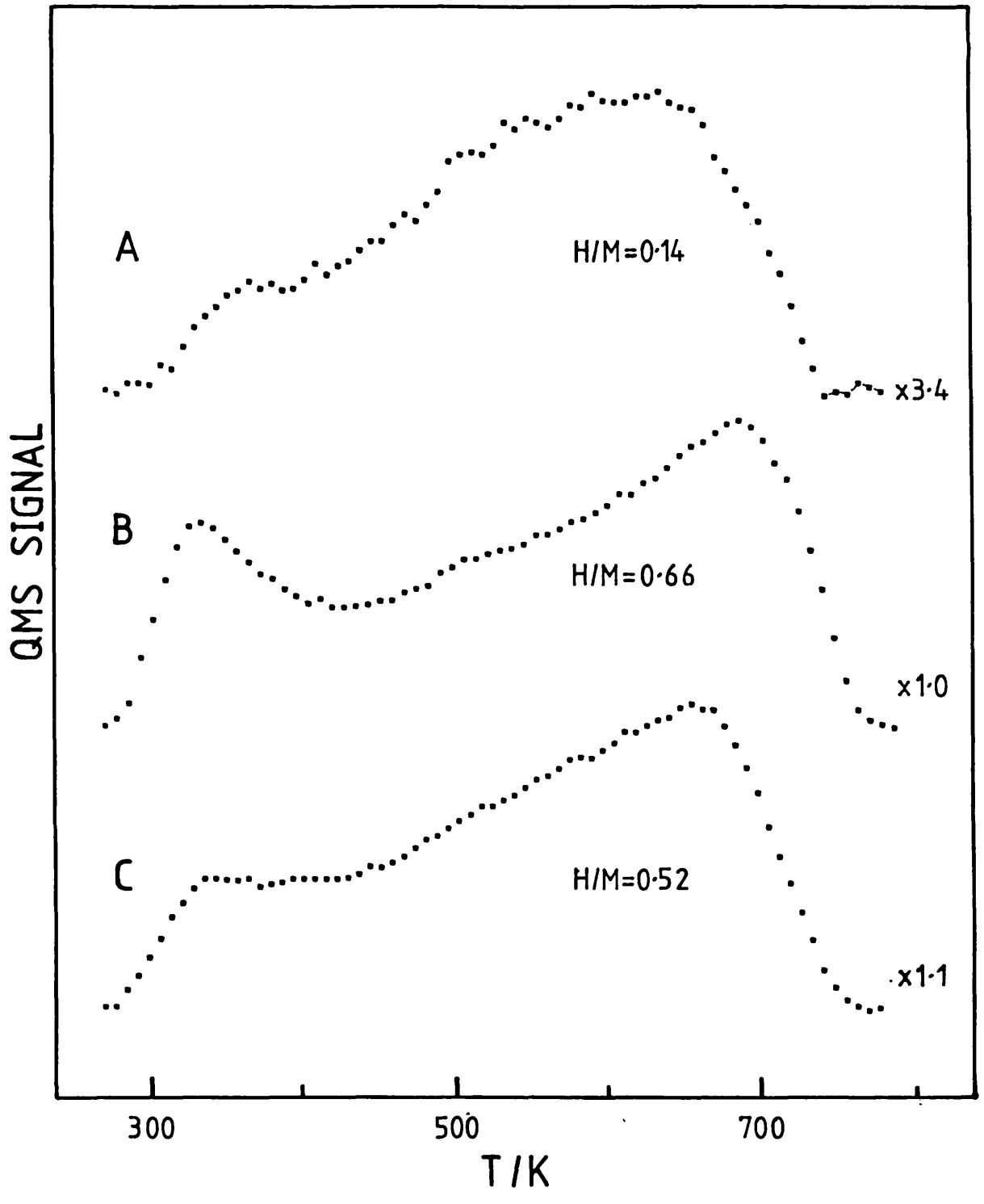

Fig. 5.13: Hydrogen Desorption Profiles for Samples Ir100 (curve A), Pt100 (curve B) and PtIr43 (curve C) Subjected to Pretreatment O740 R740.

The hydrogen desorption profile for the PtIr43 sample closely resembles that shown in Fig. 5.6 for a sample subjected to pretreatment R740. For the latter pretreatment the diminution in size for the low temperature desorption peaks were explained by processes involving sintering, poisoning or metal-support interactions. However, the oxidation pretreatment O740 has been shown to remove most of the carbon contamination (see Section 4.3.2). Hence, poisoning by carbon deposition now seems to be a less likely cause. The hydrogen desorption profile for the Ir100 sample is also similar to the profile shown in Fig. 5.6. The reduction in height of the 361K desorption peak shown in Fig. 5.13, compared to Fig. 5.6, can be attributed to the production of larger iridium crystallites during the O740 R740 pretreatment. The formation of larger metal particles may reduce the amount of hydrogen spiltover onto the support, and hence the high temperature peak at temperatures around 630K is smaller than that shown in Fig. 5.6. Alternatively, if this peak represents desorption from an SMSI state then the reduced peak intensity could result from the larger iridium crystallites not forming such an SMSI state. Fig. 5.14 shows the full desorption profile for the Ir100 sample. Similar impurity profiles were obtained for the Pt100 and PtIr43 samples.

The hydrogen desorption profile for the Pt100 sample, shown in Fig. 5.13, is similar to the profiles for the iridium-containing samples. This is in contrast to the results shown in Fig. 5.6 for a Pt100 sample subjected to pretreatment R740. Hence, when subjected to pretreatment O740 R740 the Pt100 sample shows the same behaviour as iridium-containing samples subjected to pretreatment R740. To clarify the processes involved, hydrogen desorption experiments were performed on samples subjected to oxidation at 740K followed by temperature-programmed reduction to 740K. On reaching this temperature the samples were immediately allowed to cool to room temperature under hydrogen (code O740 TPR740). The results for samples Ir100 (curve A), Pt100 (curve B) and PtIr43 (curve C) are shown in Fig. 5.15.

The hydrogen cut-off behaviour, previously observed following pretreatment O740 R610, is particularly evident in the profiles for the iridium-containing samples. The hydrogen desorption profile for the Ir100 sample indicates that the hydrogen desorption involved in

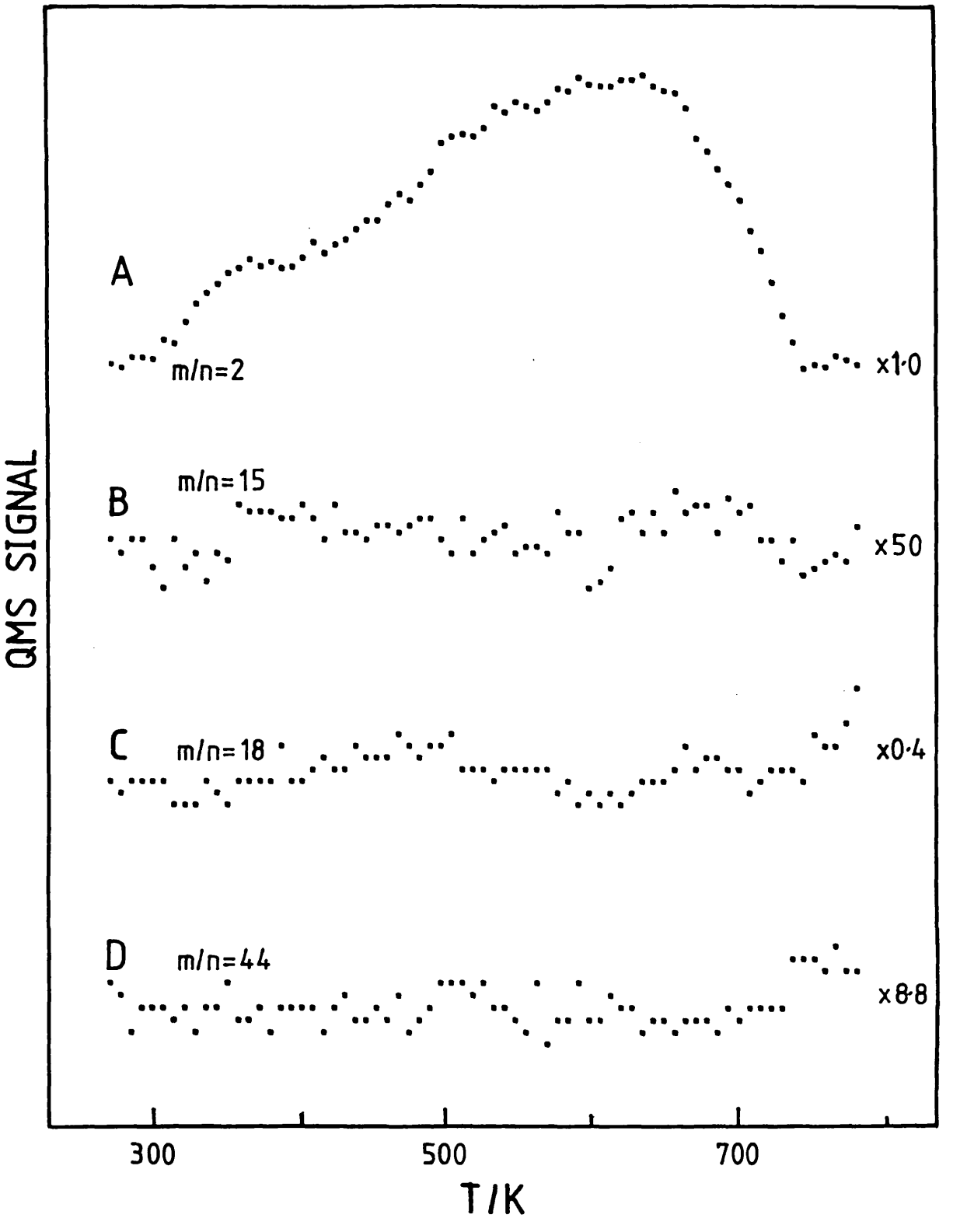

Fig. 5.14: Desorption Profile for Sample Ir100 Subjected to Pretreatment O740 R740.

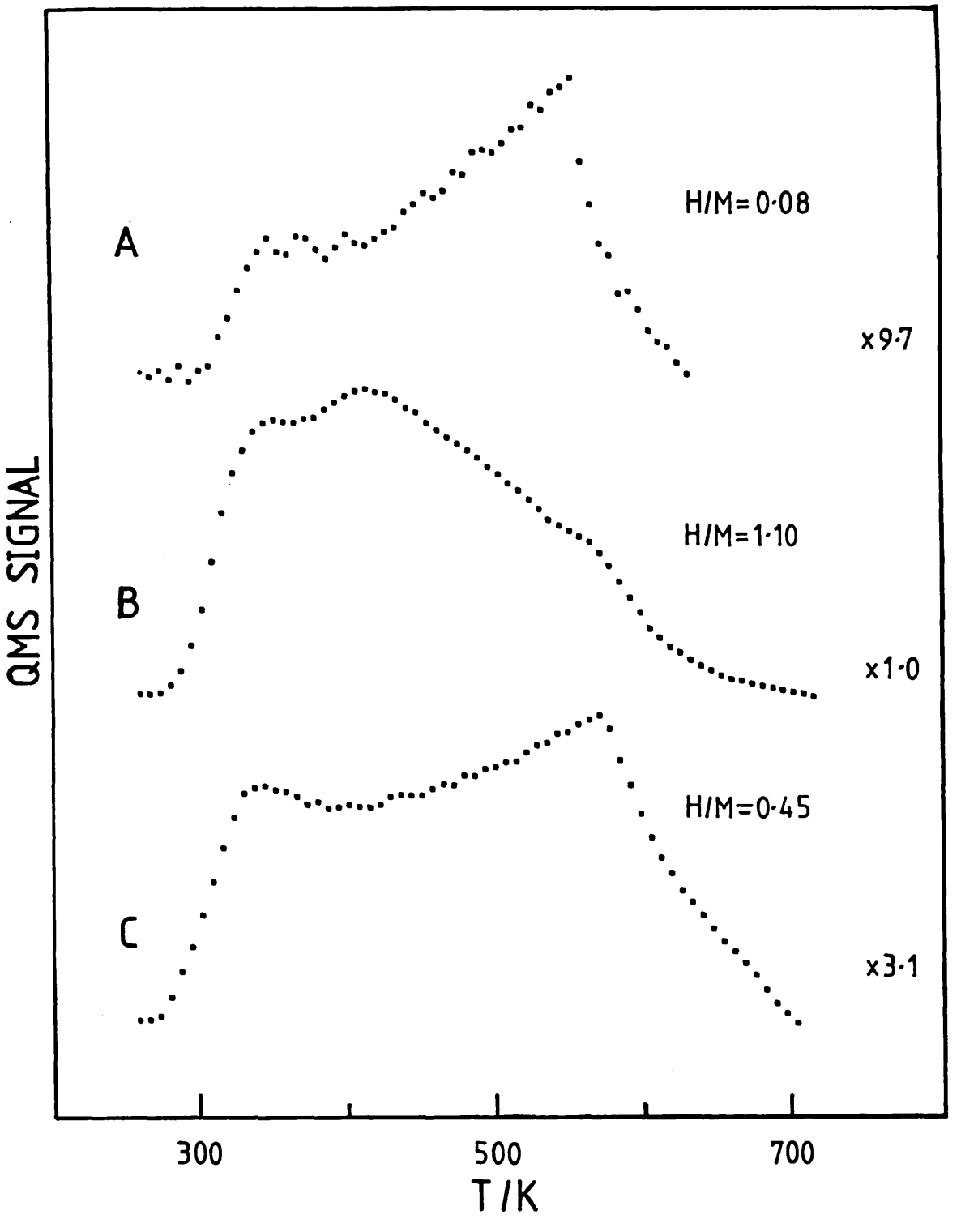

Fig. 5.15: Hydrogen Desorption Profiles for Samples Ir100 (curve A), Pt100 (curve B) and PtIr43 (curve C) Subjected to Pretreatment O740 TPR740.

this process begins at quite low temperatures. The almost linear rise of pressure is a clear indication that the desorption is from a highly heterogeneous state or results from a diffusion controlled process. The low temperature hydrogen desorption peaks shown in Fig. 5.10 may be superimposed on a similarly rising hydrogen signal. Therefore, the dispersion of the supported metals, shown in Fig. 5.10, could be somewhat lower than the H/M ratios for these samples suggest. In addition, the profiles show that an activated process causes the reduction in size of the low temperature hydrogen desorption peaks for the platinum-containing samples.

The reduction in size of the low temperature hydrogen desorption peaks for the Pt100 sample subjected to pretreatment O740 R740 may be due to:

i) Sintering during the oxidation step.
ii) Poisoning caused by carbon deposition.
iii) Sintering during the reduction step.
iv) Formation of an SMSI state.

Explanation (i) can be dismissed since the results shown in Figs. 5.10 and 5.15 show that highly dispersed platinum species can be obtained following this oxidation pretreatment. To support this, the TPR results of Section 4.3.1 indicated that highly dispersed oxidised platinum species existed following this pretreatment.

Explanation (ii) also seems unlikely since the oxidation pretreatment would be expected to remove most of the carbon-containing species. Furthermore, the results illustrated in Fig. 5.6 showed that when such species were present the platinum sample was resistant to the effects of the high temperature pretreatment. Introduction of a new contaminent during the oxidation step can also be excluded since impurities were not detected in the oxygen gas stream. Also a Pt100 sample subjected to pretreatment O570 R740 produced a desorption profile similar to the profile obtained following pretreatment R740.

Explanation (iii) cannot readily be discounted although it is difficult to understand why the oxidation step would enable the sintering to take place. This could be due to the removal of the carbon-containing species which would otherwise inhibit the sintering

of the platinum. Alternatively, the high temperature oxidation could cause a change in the support (e.g. sintering) which enables the platinum to agglomerate more readily when reduction is performed at temperatures around 740K. The formation of platinum oxychloride surface species and changes in the overall chlorine content of the samples may also be important.

Explanation (iv) could also account for the desorption behaviour of the Pt100 sample. In Section 5.3.1b it was proposed that the SMSI state did not form after pretreatment R740, probably because of carbonaceous impurity in the sample. The high temperature oxidation pretreatment removes most of this impurity which would allow the SMSI state to form. However, the low temperature desorption peak for the Pt100 sample is relatively larger than the corresponding peak, (shown in Fig. 5.6), obtained for the PtIr43 sample. This could be explained by proposing that a small fraction of the platinum clusters still had sufficient carbonaceous material associated with them to prevent the formation of the SMSI state. Indeed, the Pt100 sample was the only sample for which a small amount of methane was detected during the TPR experiment following the O740 pretreatment (Section 4.3.1).

Subjecting the Pt100 sample to reoxidation at 700K followed by a mild reduction at 610K (code O740 R740 O700 R610) caused the sample to exhibit desorption behaviour similar to that shown in Fig. 5.11. Carbon dioxide and methane were not detected during the regenerative procedure. This confirms that explanation (ii) cannot be the prime cause of the reduction in size of the low temperature desorption peaks. These results could be interpreted as arising from an oxidative redispersion effect or, alternatively, the oxidation may cause the SMSI state to break down.

The high temperature peaks observed at temperatures above 600K for all samples could be due to the processes previously outlined for similar peaks observed following pretreatment R740. However, explanations involving the dehydrogenation of carbonaceous species seem less plausible since the oxidation pretreatment removes most of the carbon-containing material.

To summarise, oxidation of a Pt100 sample at a temperature of 740K followed by reduction at 610K results in the formation of highly

dispersed metal clusters. An Ir100 sample subjected to the same pretreatment contains metal particles with a wide range of sizes. The majority of the iridium seems to be located in large crystallites but with a significant fraction still remaining in the lower coordination state. The platinum component in the bimetallic sample reduces the amount of the larger iridium-rich crystallites. This may be due to a redispersion effect during the reduction step.

Reduction of samples at 740K following oxidation at 740K results in a diminution in the size of the hydrogen desorption peaks previously associated with desorption from the metal surfaces. An explanation attributing this to a carbon poisoning effect is difficult to maintain since the oxidation pretreatment removes most of the carbon-containing species. The diminution most probably results from a sintering or metal-support effect or a combination of both. All desorption profiles are dominated by a high temperature desorption feature which may be due to processes such as desorption of spillover hydrogen or desorption of hydrogen bound to the entities formed by the metal-support interaction.

5.4 **Discussion**

The hydrogen desorption results presented in Section 5.3 clearly show that the choice of reduction temperature is important in determining the state of the metal particles in alumina-supported platinum-iridium catalysts.

For all the non-oxidised samples that had been reduced at a temperature of 610K, the amounts of hydrogen desorbed indicated that the metal consisted mainly of highly dispersed metal particles in which most of the metal atoms were surface atoms. Surprisingly the monometallic iridium catalyst was capable of binding two hydrogen atoms per metal atom. Whilst this could represent hydrogen bound to isolated metal atoms, as suggested by McVicker et al. (1980), it is more likely that surface iridium atoms in small metal particles are capable of binding more than one hydrogen atom. In fact, Kip et al. (1986b) using EXAFS, have recently reached a similar conclusion and suggested that small metal particles with a diameter less than 15Å should be considered as transition metal polyhydride species of the type examined theoretically by Minot et al. (1986).

The broader significance of these results is that a simple hydrogen-metal adsorption stoichiometry cannot be assumed for the analysis of conventional hydrogen chemisorption results. It would appear from the desorption profiles presented in this chapter that a hydrogen-metal adsorption stoichiometry of around two is obtained for hydrogen adsorption upon metal atoms of low coordination number such as those in a (100)-type environment, whereas, a stoichiometry of around one is found for adsorption upon metal in a more densely packed environment (e.g. (111)-type). Apparently, metal atoms in highly dispersed iridium clusters tend to favour a more open bonding arrangement than do platinum particles of similar metal content. It follows that conventional hydrogen adsorption experiments cannot be used to determine metal particle dimensions with any degree of confidence since the relative amounts of the above types of adsorption site are unknown. At best the adsorption technique gives only an indication of metal dispersion, assuming a particular site distribution and adsorption stoichiometry.

The desorption spectra for the bimetallic sample subjected to pretreatment R610 were more or less the sum of the spectra for the individual metals and there was little evidence of alloy formation. Three explanations can be advanced for this result, namely:

i) Separate monometallic particles are present.

ii) The metals are highly dispersed as isolated atoms.

iii) An alloy is formed but the metal-hydrogen interactions are insensitive to platinum-iridium interactions in highly dispersed mixed-metal clusters. Although it would be expected that desorption of two hydrogen atoms adsorbed on adjacent Pt and Ir atoms would not result in a desorption spectrum which is the sum of the individual metal spectra.

However it should be noted that the TPD spectrum for the unoxidised bimetallic sample subjected to the higher reduction temperature at 740K is not the sum of the individual metal spectra showing that Pt-Ir interactions are present. This evidence, although indirect, strongly suggests that bimetallic alloy particles are formed during pretreatment R610 and that explanation (iii) holds.

The TPR results of the preceeding chapter suggested that a high temperature reduction would cause an alteration in the sorption properties of the supported metal particles and carbon 'impurities' were thought to be involved in this process. Indeed, the results presented in this chapter for the iridium-containing samples show that pretreatment R740 causes a large decrease in the amount of desorbed hydrogen. However, of the various possibilities considered in Section 5.3 for the cause of this effect, the explanation involving carbon deposition seems least plausible, especially in the light of the desorption results for the samples initially oxidised at 740K. However, the carbon may perform a more subtle role, i.e. its presence may prevent particle sintering or the formation of an SMSI state for the monometallic platinum sample.

If sintering causes the change in gas chemisorption on the iridium-containing samples then particle growth could occur at 740K by any of the processes previously proposed in Section 4.4 for oxidative agglomeration; namely, atomic migration, crystallite migration or a combination of both. On this basis, the presence of carbon in the Pt100 sample would prevent the platinum particles from coalescing. However, if the formation of an SMSI state is responsible then the carbon in the Pt100 sample may act as a barrier between the metal and the oxide which prevents the interaction from occurring. At the present state of knowledge it is unclear which, if any, of the sintering or SMSI state formation explanations are valid.

The TPR results of Section 4.3.1b for the Ir100 and PtIr43 samples oxidised at 740K showed that the proportion of the iridium tht had agglomerated into a bulk-type oxide was 80% and 65% respectively. Such behaviour is in agreement with previous studies of iridium catalysts described in Section 4.4. Furthermore, the TPR results provide evidence that some redispersion of the agglomerated iridium occurs during a subsequent reduction. The hydrogen desorption results confirm this proposal. If it is assumed that two hydrogen atoms desorb per surface metal atom and that the large crystallites have a negligible surface area, then the H/M ratio of 0.57 found for the Ir100 sample indicates that around 70% of the metal remains in the large crystallites. However, for the bimetallic sample, assuming that desorption from the platinum component is

independent of the iridium component (cf. pretreatment R610), the desorption results indicate that the amount of iridium contained in the large crystallites has dropped to around 40% of the total iridium content. Therefore, whilst redispersion occurs for both iridium-containing samples, the degree of redispersion is greater for the bimetallic sample.

Metal particle redispersion, as described by Ruchenstein and Dadyburjor (1983), can proceed by mechanisms which are related to sintering processes. Large crystallities are thought to 'dissolve' by the removal of atomic and/or multiatomic entities which then become trapped on the oxide surface before recombination can occur. On this basis the increased degree of iridium redispersion for the bimetallic sample could be explained by the presence of the dispersed platinum-rich phase which could trap out the above iridium species. If this is the case then the dispersed clusters produced during redispersion would be expected to have an iridium-rich exterior. In addition, the redispersion process could be promoted by the presence of platinum metal in the large iridium-rich particles which may destabilise the large crystallites.

5.5 **Summary**

The hydrogen thermal desorption profile for the alumina-supported platinum-iridium sample subjected to pretreatment R610 shows that highly dispersed metal particles are present in which the majority of the metal atoms are surface atoms. The low temperature portion of the profiles contained two desorption features which were identified as representing the desorption of hydrogen from metal atoms in different site symmetries. The higher temperature region of the profiles contained features which may be caused by several processes including desorption from carbonaceous material or from sites formed by a metal-support combination. The exact cause of this behaviour remains unclear. None of the thermal desorption profiles following reduction at 610K gave any evidence of alloy formation; this became apparent only for samples reduced at higher temperatures. The desorption results show that hydrogen-metal adsorption stoichiometries are difficult to estimate, since they are largely dependent upon the nature of the bonding environment around each surface metal atom. Thus, the use of the conventional hydrogen

adsorption technique to measure metal particle size is of limited service.

For bimetallic samples oxidised at a temperature of 740K prior to reduction at 610K some redispersion of the agglomerated iridium-rich phase occurs, probably as a result of the interaction of the dispersed platinum phase with the iridium species emanating from the large crystallites.

Finally, the desorption profile for the PtIr43 sample subjected to pretreatment R740 could be interpreted in terms of sintering, SMSI state formation, or poisoning by carbon deposition. However, the results for a sample initially oxidised at 740K prior to reduction at 740K largely eliminates the final possibility. The next Chapter aims to clarify whether metal-sintering or the formation of an SMSI state occurs as a result of the high temperature reduction pretreatment.

CHAPTER SIX

Transmission Electron Microscopy and X-ray Photoelectron Spectroscopy Studies

6.1 Introduction

6.1.1 Aim

The aim of this Chapter is to establish in more detail the effect that the pretreatments used in the preparation of Pt-Ir/alumina catalysts have on catalyst structure. Transmission Electron Microscopy (TEM) has been employed to observe directly the oxidation-induced iridium agglomeration identified in Chapters Four and Five. The technique has also been used to determine whether a metal-sintering or SMSI-type phenomenon is the cause of the change in chemisorption characteristics observed following high temperature reduction. A second technique that has been utilised to provide a characterization of the surface of the catalyst is X-ray Photoelectron Spectroscopy (XPS). This technique has been used to examine the effects of oxidative iridium agglomeration and to investigate the distribution of the metals in the catalysts. An attempt has also been made to probe the electronic structure and composition of samples which, according to the results presented in previous Chapters contain bimetallic alloy clusters.

Before the TEM and XPS results are presented the two techniques will be briefly described. The description used is largely qualitative and serves to introduce the reader to the general features and limitations of the techniques. The Section on the XPS technique is concerned mainly with the photoemission properties of supported metal clusters, in particular the way in which photoemission peak intensity can be used to obtain information on the dispersion and distribution of the supported metal. This is followed by a discussion of sample charging and initial and final state effects which complicate the analysis of the results. The final part contains a summary of the results of previous studies which have employed XPS to characterise a variety of supported bimetallic catalysts.

6.1.2 Transmission Electron Microscopy

TEM is a standard technique used for the characterization of catalyst systems. By examination of suitably thin regions of a supported metal catalyst, differences in the electron scattering properties of the support and the metal enables the metal particles to be directly imaged by TEM. Thus, in principle the technique allows metal particle size distributions and particle morphology to be determined. However, because the region under investigation depicts only a small portion of the sample, several areas have to be investigated before the data for the observed metal can be judged to be representative of the entire sample. In addition, as discussed by Flynn et al. (1974), it is difficult to differentiate between small contrast areas arising from the structure of the support and those due to sub-nanometer metal clusters. Hence, support interference seriously limits the reliability of conventional TEM for the determination of cluster size distributions in supported metal catalysts with high metal dispersions.

Nevertheless, TEM can provide valuable insights into the structure of supported metal catalysts especially when larger metal particles are present. Hence, in this study the technique has been used to observe the crystallites produced following high temperature oxidation and, most importantly, to determine whether high temperature reduction causes a sintering of the highly dispersed metal clusters.

6.1.3 X-ray Photoelectron Spectroscopy

The use of XPS in surface analysis has been reviewed recently by Bowling et al. (1985), Turner et al. (1984) and earlier by Briggs and Seah (1983). The following description of the technique, and its application in catalyst studies, is confined to a qualitative presentation which will establish the underlying principles necessary for the interpretation of the XPS results.

a) General Principles

In an XPS experiment soft X-rays (1-1.5keV) are used to eject core-level electrons from the sample material and the emitted photoelectrons are energy analysed. For a conducting bulk sample, in which the Fermi level is coupled to that of the spectrometer, the

measured kinetic energy of the photoelectron, E_{ke}, is given by the following relationship:

$$E_{ke} = h\nu - \phi_{sp} - E_B \qquad (6.1)$$

where $h\nu$ is the energy of the exciting radiation, ϕ_{sp} is the spectrometer work function and E_B is the binding energy of the core-level electron relative to the sample Fermi level. Thus, equation (6.1) enables the binding energies of the core-level electrons to be determined from measurement of the kinetic energy of electrons ejected from these levels. Since core-level binding energies are elementally specific the XPS technique can be used to obtain a chemical analysis of the sample.

The most important feature of the technique is its surface sensitivity. This is not due to a lack of penetration of the exciting radiation into the sample, but to the low escape depth of the ejected photoelectrons due to inelastic scattering or adsorption processes which occur before the electron reaches the sample surface. Electron escape depths, calculated by Penn (1976) show that, in general, the XPS technique only samples the top 2-5 atomic layers of a specimen.

XPS data are normally presented as a plot of electron count against the electron kinetic or core-level binding energy. The XPS spectrum, or profile, therefore consists of peaks centered at the characteristic elemental electron energies. For a given element the relative intensity of such peaks depends on the core-level photoionisation cross-section. Scofield (1976) has calculated values for the core-level orbitals of most elements. In addition, the intensities of the photoemission peaks are dependent on the exciting radiation used and instrumental sensitivity parameters. Knowledge of such factors enables the relative surface composition of bulk samples containing more than one element to be obtained. Hence the technique has been widely used to determine bulk alloy surface compositions. However, for supported metal particles the peak intensities are also dependent on factors such as the dispersion of the metal, particle shape and the porosity of the support. Such effects are discussed in the following Section.

The core-level electron binding energies of an element in a conducting sample are modified to some extent by its chemical state, physical form and general environment. Changes in the peak positions are generally dependent on both initial state and final state effects. The former arise from differences in the electrostatic potential in which the core-electrons move and are generally referred to as chemical shifts. These would include changes in sample oxidation state, or electronic interactions in alloy systems. Final state effects are related to the interaction of the ejected photoelectron with the charge remaining on the atom. These effects may be due to changes in the shape and size (dispersion) of the sample, for example.

However, initial state effects can also result in changes in the core-level binding energies when the sample dispersion is altered. Consequently, much disagreement exists concerning the relative importance of initial state and final state effects in causing binding energy shifts in supported metal clusters. The significance of these effects for catalyst studies and the complications arising from the use of non-conducting catalyst supports are discussed in the following Section.

The photoemisson peaks in the XPS spectra can also be structured. For electrons arising from non s-orbitals the peaks are usually observed as doublets. This is due to spin-orbit coupling of the orbital ($\boldsymbol{l}$) and spin ($\mathbf{s}$) angular momentum vectors of the core-level electrons. Two possible states arise when $l > 0$ which are given by the quantum number j, with $\mathbf{j} = \boldsymbol{l} + \mathbf{s}$. The difference between the energy of the two states arises from the parallel or anti-parallel nature of the spin and orbital angular momentum vectors. This difference is dependent on the size of the spin-orbit coupling constant which varies with the size of the core-level orbital. The relative intensity of the two peaks depends on the degeneracy $(2j + 1)$ of the states. Hence the metal 4d peaks observed in this study were split into a $4d_{5/2}$ and $4d_{3/2}$ doublet with intensities in the ratio of approximately 3 to 2, respectively.

In addition, secondary features are often present in the XPS spectrum. Extra peaks can arise from shake-up or shake-off processes. In the former the core hole created by the photoemission

process causes a reorganisation of the valence electrons. This relaxation can result in the transition of a valence electron to a higher unfilled level. This reduces the energy of the emergent photoelectron and results in discrete structure on the low kinetic energy side of the photoemission peak. For the shake-off process similar processes occur, although the valence electron is completely removed from the atom leaving an ion with vacancies in both the core-level and valence level.

So-called satellite peaks can arise from the presence of achromatic exciting radiation. This radiation results primarily from less probable electronic transitions occurring in the magnesium or aluminium X-ray source targets. The presence of such peaks can be problematic, for instance the Al2p* peak satellite coincides in binding energy with the Ir4f core level doublet. Hence, for alumina-supported samples containing low loadings of iridium, the Ir4f photoemission peaks cannot be used to examine the nature of the metal.

Finally, peaks in the XPS spectra can result from electronic transitions in which Auger electrons are produced subsequent to the filling of the core-holes. These transitions can also result in overlap problems for certain peaks.

In brief, XPS is a surface sensitive technique which provides information on:

i) Sample surface composition

ii) Sample electronic properties

The following sections consider some of the problems and applications of XPS in catalyst studies.

b) Metal Dispersion

Since XPS is a surface sensitive technique it may be expected that information concerning the dispersion of the metal can be extracted from a quantitative analysis of the metal photoemission peak intensities. Indeed, Scharpen (1974) observed a correlation between the dispersion of a metal, obtained by gas chemisorption, and the metal/support XPS signal ratio. This author concluded that such a correlation strongly supported the use of XPS for the measurement of metal particle size in supported catalysts.

*Note: The Al2p peak consists of a $2p_{3/2,1/2}$ doublet, however, for brevity this will be simply referred to as the Al2p peak.

Following this, Fung (1979) and Kerkof and Moulijn (1979) produced models which enabled metal crystallite sizes to be obtained from the XPS signal intensity ratio. However, such models required that the distribution of the metal, both on and in the support, did not change with dispersion and that a stable particle shape was maintained. Moreover, the models can only be applied to metal crystallites in which the characteristic particle dimension, d, is at least an order of magnitude greater than the electron escape depth, λ_e. For highly dispersed clusters in which $d \sim \lambda_e$, or for any thin raft-like crystallite, the XPS signal intensity is in fact independent of cluster size.

Therefore, for the highly dispersed samples used in this study little change will be observed in the XPS signal intensity as a result of differences in particle shape or size. However, changes in the signal intensity following oxidation at 740K should provide an indication of the extent of iridium agglomeration, bearing in mind factors such as metal redistribution into the support pore structure.

c) Sample Charging

One problem experienced in the interpretation of XPS data for catalysts is that of sample charging which causes the core-level binding energies to be shifted from their true values. The problem of binding energy referencing has been reviewed by Madey et al. (1977), Lewis and Kelley (1980) and Barr (1983).

Sample charging is observed when the supports used for catalysts are non-conductive. Hence following the photoemission process the positive charge remains on the sample since it is not neutralised by a flow of electrons from the spectrometer. This residual charge produces a retarding field in front of the sample which causes the photoelectron kinetic energy to be reduced. It could be envisaged that such a process would cause an increasing charge build-up eventually resulting in the total suppression of photoemission. However, the charge on the sample rapidly reaches a steady-state equilibrium value since background low-energy electrons partially neutralise the charge. These electrons are produced by the bremsstrahlung X-rays, emitted by the X-ray source, striking the X-ray gun window and other internal parts of the apparatus. There-

fore, for any one particular catalyst sample the observed binding energies are shifted by a constant amount to higher values than are predicted by equation 6.1.

An additional complication for the determination of the true core-level binding energies has been identified by Lewis and Kelley (1980). This arises from the lack of Fermi edge coupling between the spectrometer and the insulating sample. Hence binding energies are not only shifted by sample charging but they can also be shifted due to the floating Fermi edge.

The method generally used to obtain the true binding energies is to set the binding energy for photoemisson peaks for the elements comprising the support to a certain fixed value. This assumes that such support binding energies are independent of pretreatment and the presence of the supported metal. The remaining binding energies are then corrected by assuming that each has shifted by the same amount. Differential charging for a heterogeneously distributed metal can cause peak broadening and is difficult to correct for.

An alternative approach is to use an electron flood gun to reduce the build up of charge on the sample. However, it can never be assumed that this method is entirely effective and therefore the referencing described above still needs to be performed. For this reason, a flood gun was not used in the present study and the core-level binding energies were calibrated by setting the Al2p binding energy to 74.40 eV as suggested by Huizinga et al. (1983).

d) Metal-Support Interactions - Initial and Final State Effects

XPS is frequently used to obtain information concerning changes in the electronic structure of metals when highly dispersed on a support. Anderson (1985) has recently discussed particle size effects in metal catalysts. In general, particles larger than about 2nm have electronic properties similar to bulk metal. However, MO calculations for small clusters, containing around 20 atoms, show that the electronic properties of the clusters differ substantially from bulk metal properties, with the clusters being electropositive. Hence, small metal clusters, when dispersed on certain supports, could be electron deficient with some electron transfer occurring from the metal to the support.

Indeed, supported metal clusters usually have core-level binding energies which are higher than those found for the bulk metals and the peaks are broader. Consequently, the results of early XPS studies, such as those of Escard (1973, 1975) for alumina-supported iridium, were interpreted as showing that an electronic interaction existed between the support and the heterogeneous metal.

However, this was soon realised to be an oversimplification since the observed deviation from the binding energies for the bulk metal could reflect changes in both the initial and final states of the system. Mason (1983), and Dicenzo and Wertheim (1985) have described the physical basis for binding energy shifts in supported metal clusters. Mason (1983) concluded that initial state effects were dominant for metals held on weakly interacting supports such as carbon and silica. He argued that the small size of the clusters reduced the s-d hybridisation of the valence levels, which would cause a flow of charge from the s band into the d band. The d electrons, having a smaller radial extent than the s electrons, were proposed to interact strongly with the core electrons producing a change in their binding energy. However, Dicenzo and Wertheim (1985) pointed out that this interaction would result in a decrease in the core-level binding energies, whilst in fact, supported metals show an increase in binding energy with increased dispersion.

These workers concluded that, although rehybridisation may occur, core-level photoemission from supported metal clusters is dominated by the effects of final state charging. Therefore, it is thought that in small metal clusters there are insufficient metal atoms in the particle to completely screen the core-holes created by photoemission and it is this incomplete screening which gives rise to the positive shift. These workers further conclude that the peak broadening, as cluster size decreased, reflected a broad particle-size distribution producing a photoemission peak which consisted of overlapping, shifted spectra from inequivalent clusters. Fritsch and Legare (1984) reached similar conclusions for the interpretation of photoemission peak widths of iridium particles supported on pyrographite.

Thus, final state effects are extremely significant for the use of XPS to characterise supported metals, since it is difficult

to separate such effects from true metal-support interactions. This is illustrated below for studies performed to examine the nature of the SMSI interaction for titania-supported metals.

Fung (1982) observed that platinum core-level binding energies were lower for titania-supported catalysts than for silica-supported samples following a high temperature reduction. This worker concluded that electron transfer from reduced titania centres to platinum particles probably caused the SMSI state. However, it was recognised that the higher binding energy for the silica-supported platinum may be due to a decrease in the extra atomic relaxation energy associated with smaller particles on this support compared to titania. Significantly, the binding energies reported for the titania-supported samples were actually greater than values found for bulk metal samples.

Sexton et al. (1982) obtained similar results for rhodium or platinum supported on several Group IIIa-Va oxides. These workers observed a large initial binding energy difference between the low and high temperature reduced samples. However, following several oxidation/reduction cycles it was concluded that the initial difference was mostly due to a large relaxation energy difference. After the oxidation/reduction annealing treatments a small reversible shift of -0.2eV was observed which was attributed to the SMSI shift. However, as the authors pointed out, this too could have arisen from reversible changes in metal particle size during the pretreatment cycles.

Huizinga et al. (1983) attempted to separate SMSI effects from metal particle size effects by comparing the effect of high temperature reduction on alumina- and titania-supported metals of wide ranging dispersions. No difference in binding energies were observed between the Rh/TiO_2 and Rh/Al_2O_3 samples of similar dispersion, for the range of dispersion used. Similar results were obtained for the platinum containing catalysts although the titania-supported metal usually had a higher binding energy. It was concluded that final state effects caused an increase in core-level binding energies with dispersion and that the SMSI state cannot be due to negatively charged metal. However, this conclusion was based on the assumption that alumina-supported metals do not form an SMSI state.

To conclude, metal particle size-dependent final state (or initial state) effects impose limitations on the use of XPS to determine electronic modifications of supported metal particles. This is particularly evident from the results of studies investigating metal-support interactions produced following high temperature reduction pretreatments.

In view of this it was concluded that the XPS technique would provide little, or no additional information concerning the cause of the change in the hydrogen chemisorption characteristics described in Chapter 5. In addition, such an investigation would have been difficult experimentally since the insitu sample heater could not raise the temperature of the sample to a sufficiently high value to perform such an examination.

e) Supported Bimetallic Catalysts

The XPS technique has been widely used to investigate the properties of bulk alloys for reasons mentioned earlier. Similarly, the technique has been employed to examine the properties of supported bimetallic catalysts. In general, such studies have attempted to determine if the metals exist as bimetallic entities or as separate monometallic particles, although some work has been done to determine the nature of any bimetallic clusters formed.

Table 6.1 summarises the conclusions reached following XPS examination of a wide range of supported bimetallic catalysts. In several of the investigations XPS was used in conjunction with techniques such as gas chemisorption and hydrocarbon conversion measurements.

In many studies surface enrichment of the metal particles with one of the metal components was identified. However, for highly dispersed metal clusters the notion of surface segregation may be inapplicable. Furthermore, for low dispersion metal the enrichment interpretation must be viewed with caution since several authors have observed that the two metals distribute differently in the alumina support.

Electronic interactions between the metals can be deduced from binding energy shifts in the bimetallic samples compared to the monometallic systems. Although care should be used because of

Table 6.1: XPS Studies of Supported Bimetallic Catalysts

CATALYST SYSTEM	CONCLUSIONS	REFERENCE
$Pt-Sn/Al_2O_3$	Sn(II) present as an aluminate over alumina surface. Pt exists as islands on aluminate - no alloy formed.	Adkins and Davis (1984)
$Pt-Sn/Al_2O_3$	Sn(II) present after reduction. Strongly adsorbed on outer surface of alumina - no alloy formed with Pt.	Sexton et al. (1984)
$Pt-Re/SiO_2$	Pt-Re alloy formed - electronic interaction between metals.	Biloen et al. (1980)
$Pt-Re/Al_2O_3$	No Pt-Re alloy formed. Pt metal surrounded by Re(IV).	Onuferko et al. (1984)
$Pt-Cu/Al_2O_3$	Both separate metals and combined Pt-Cu entities exist. Bimetallic clusters surface enriched in Cu.	Liao et al. (1982)
$Pt-Mo/Al_2O_3$	Pt promoted reduction of Mo oxides but Mo not present as metal.	De Vries et al. (1983)
$Pt-Au/SiO_2$	Both separate metals and combined Pt-Au clusters exist. For 50/50 sample bimetallic surface enriched in Au	Galvagno and Parravano (1979)
$Pt-Ge/Al_2O_3$	Pt-Ge alloy formed - also Ge(II) present	Bouwman and Biloen (1977)

Table 6.1 (continued): XPS Studies of Supported Bimetallic Catalysts

CATALYST SYSTEM	CONCLUSIONS	REFERENCE
M-Fe/SiO_2 (M=Ru,Rh,Ir,Pt)	~80% Fe present as Fe(III) - Fe(O) present as alloy with M.	Niemantsverdriet et al. (1985)
Pt-Rh/SiO_2	Alloys formed. Oxidation enriches surface in Re	Wang and Schmidt (1981)
Ir-Rh/SiO_2	Alloys formed - surface enriched in Rh (?)	Wong et al. (1981)
Ru-Cu/SiO_2	Small amount of Cu with Ru - electronic interactions between metals.	Rouco et al. (1983)
Ru-Ag/SiO_2	Ag islands on top of Ru crystallites. Also some Ag not associated with Ru.	Rouco et al. (1983)
Ru-Au/MgO	Alloy clusters - surface enriched in Ru.	Bassi et al. (1980)
Ru-Au/SiO_2	Alloy clusters (?) - no surface enrichment in Ru observed.	Galvagno et al. (1981)
Pd-Ni/SiO_2	Alloy clusters - surface enriched in Pd	Mintsa-Eya et al. (1982)

particle size-dependent final state or initial state effects which can produce shifts in the photoemission peak binding energies.

Whilst Table 6.1 shows that platinum based bimetallic catalysts have been extensively studied no XPS examination has been reported in the open literature for the Pt-Ir/alumina combination. However, Hilaire et al. (1984) have performed a photoemission study of the oxidation behaviour of the bulk Pt-Ir alloy system. These workers found that the entire surface of alloys containing more than approximately 15% iridium could be oxidised. This behaviour was interpreted in terms of an electronic effect. However, these workers did not examine whether the core-level binding energies or photoemission peak shapes were altered in the alloy.

In this present study XPS has been used to determine whether an electronic modification of the metals occurs when, according to the TPR and hydrogen desorption results, bimetallic clusters are present. In addition experiments have been performed on samples subjected to a high temperature oxidation step to examine the nature of the agglomerated iridium component.

6.2 Experimental

6.2.1 TEM

TEM examinations were carried out using a JEOL JEM-2000FX transmission electron microscope. Catalysts were prepared for examination by placing a small amount of lightly ground sample onto a 400 mesh copper grid coated with a 6nm carbon film. Images were recorded using a 200kV accelerating voltage at instrumental magnifications of 100 000 to 250 000. Metal crystallite sizes were measured from photographic prints. The largest dimension of the particle was recorded. Several regions of each catalyst were examined in an attempt to obtain an analysis as representative as possible of the entire specimen. This was especially important since the alumina support was found to consist of particles with sizes approximately ranging from 20 to 400nm.

The PtIr43 sample, prepared by the method described in Chapter Three, was examined in this study. Portions of this sample (50mg) were subjected to an ex-situ pretreatment in the micro-reactor system. The pretreatments used are summarised in Table 5.1 (see

Section 5.2). Hence samples were studied which had received either no oxidation treatment, or oxidation at a temperature of 740K, prior to reduction at either 610K or 740K. The catalysts were examined in the microscope after transport through the air.

6.2.2 XPS

XPS measurements were carried out using the VG ESCALAB-MKII instrument manufactured by Vacuum Generators Limited and previously described in Chapter Two. The catalysts used in this study were prepared by the methods outlined in Chapter Three and consisted of the two monometallic samples Pt100 and Ir100 and the bimetallic sample PtIr43. XPS spectra were first recorded for the unreduced samples and subsequently for the same samples subjected to two different, consecutive insitu reduction pretreatments. In order to examine oxidation effects fresh samples were subjected to oxidation at a temperature of 740K in the micro-reactor system (pretreatment coded O740) prior to insitu reduction in the ESCALAB system. Although these pretreatments are not identical to those used in the micro-reactor-based work they do simulate the micro-reactor conditions fairly well and it will be assumed that direct comparisons can be made between the results obtained using the different systems.

To prevent spillage during sample manipulation the powder catalyst sample was contained in a specially constructed tantalum box which has been described in Chapter Two. A small quantity (~10mg) of sample was placed in the container. This was sufficient to evenly cover the bottom of the box but produced a layer which was thin enough to ensure that sample reduction was homogeneous.

Following the first XPS experiment, insitu sample reduction was performed in the prepchamber by heating the sample container using the P8 probe. Hydrogen (BOC HP grade), was used to fill the isolated prepchamber to a pressure of around 30 Torr by expansion of the gas previously stored at a pressure of 760 Torr in the gas handling section. The final hydrogen pressure was not directly measured but was approximately evaluated from the estimated ratio of the prepchamber and gas handling section volumes. Earlier experiments performed using a low hydrogen pressure of around 0.05 Torr were found to produce incomplete sample reduction for all temperatures used.

The temperature of the sample was measured during the reduction pretreatment using a 0.125mm diameter chromel/alumel thermocouple mounted vertically on a z-shift above the catalyst. The sample box lid was left open during heating and the junction of the thermocouple was placed in contact with the side walls just above the sample. No difference in temperature was observed when the thermocouple junction was placed in contact with the catalyst powder. However, a large temperature gradient of around 150K was found to exist between the catalyst sample and the region surrounding the thermocouple encapsulated in the P8 probe body, even following isothermal reduction periods of around 20 minutes.

The temperature of the sample was allowed to rise at a rate similar to that used in the micro-reactor work. Samples were first reduced at a temperature of around 450K for 20 minutes after which the catalyst was allowed to cool to room temperature before the hydrogen was pumped from the prepchamber. The sample was then transferred to the analysis chamber and positioned in front of the analyser and X-ray source in a position previously established to produce the greatest signal. The pressure in the analysis chamber was routinely maintained in the 10^{-10} Torr region. Following the XPS experiment the sample was returned to the prepchamber and subjected to reduction at a temperature around 610K before the third, and final, XPS experiment was performed.

XPS measurements were carried out using achromatic X-rays produced from either the Al ($h\nu$ = 1486.6eV) or Mg ($h\nu$ = 1253.6eV) anode. The photoelectrons were energy analysed at normal emission angles using the concentric hemispherical analyser (CHA) operated in the constant analyser energy (CAE) mode. This enabled a constant absolute peak resolution to be obtained. A 50eV pass energy was chosen since this value produced an optimum compromise between the peak resolution and the signal-to-noise ratio. Table 6.2 summarises the core-level binding energy regions examined and the number of scans, N_S, performed over the regions during a typical experiment controlled by an Apple IIe microcomputer. The low level of catalyst metal loadings used in this study required that XPS data from a large number of scans had to be collected and accumulated until a reasonable signal-to-noise ratio was achieved.

Table 6.2: Summary of Core-level Binding Energy Regions Scanned During the XPS Experiments

Region/eV	Elemental Peak(s)	N_s [a]
65- 90	Al2p3/2,1/2	40
280-305	C1s	50
190-215	Cl2p3/2,1/2	50
295-345 [b]	Ir4d5/2,3/2	300
305-355	Pt4d5/2,3/2	300
520-545	O1s	30

Notes: a) Time for each scan = 30s; step size = 0.05eV

b) Scan range for the PtIr43 sample (both the Pt and Ir4d peaks)

The scan region for the metal core-level binding energies enabled both the 4d5/2 and 4d3/2 peaks to be observed. The 4f peaks could not be used for analysis since the Ir4f peaks coincided with an Al2p satellite peak whilst the Pt4f peaks were masked by the parent Al2p peak. Besides the standard scans through particular elements in Table 6.2 both a wide scan (50-1000eV) and additional narrow range scans were performed to determine if impurities such as iron or sulphur were present in the catalyst samples or the alumina support. No such impurities were detected.

The Fermi level referenced binding energies were corrected for sample charging effects by setting the Al2p peak position at 74.40eV, as suggested by Huizinga et al. (1983). In addition, the instrument binding energy scale was checked by examining the Cls peak position arising from the box material. Due to sample charging this peak was well separated from the Cls signal from carbon on the catalyst.

An Apple IIe micro-computer equipped with data analysis software supplied by Vacuum Generators Limited, was used to determine binding energies and measure peak areas. The software enabled peak expansion to be performed thus permitting the peak position to be identified more accurately than inspection of the wide scan allowed. No data smoothing was performed since in certain cases this was found to alter the peak envelop shape. The XPS data was stored on flexible disks.

6.3 Results and Interpretation

This section has been divided into two major parts. The first part describes the results of the TEM examination which was performed to observe the effects of pretreatment on metal particle size. This investigation will establish if the primary cause of the decrease in hydrogen chemisorption capacity, observed in Chapter Five, was a result of a reduction induced particle growth process. The second part describes the results of the XPS investigation which was used to probe the electronic properties and surface composition of the Pt-Ir/alumina catalysts. This includes an investigation of the effect of pretreatment on the chlorine and carbon contained in the samples.

6.3.1 TEM Examination

a) Samples that had received no oxidation pretreatment

Fig. 6.1(A) shows a typical micrograph for the PtIr43 sample subjected to reduction at 740K (coded R740). No metal particles can be observed in this region of the sample and examination of portions of the specimen containing larger alumina particles produced similar results. Micrographs of a PtIr43 sample subjected to reduction at 610K (coded R610) also showed an apparent absence of metal particles.

These results show that the metal clusters, presumably formed during either reduction pretreatment, must be smaller than approximately 2nm in size.

For the sample subjected to pretreatment R610, this finding is consistent with the hydrogen thermal desorption results described in Section 5.3.1 where it was concluded that such samples contained monoatomically dispersed metal or , more probably, clusters containing approximately 20 metal atoms. More problematic is the lack of large crystallites following reduction at 740K. Changes in the hydrogen thermal desorption profiles of samples subjected to this pretreatment were explained by metal sintering or SMSI effects. However, it is hard to understand how sintering can occur on a scale sufficient to reduce the amount of hydrogen desorbed from the metal sites in the PtIr43 sample to virtually nothing without producing metal crystallites large enough to be detected using TEM. Therefore, it appears that metal particle sintering is unlikely to be a cause of the reduction in hydrogen chemisorption capacity observed following the high temperature reduction pretreatment.

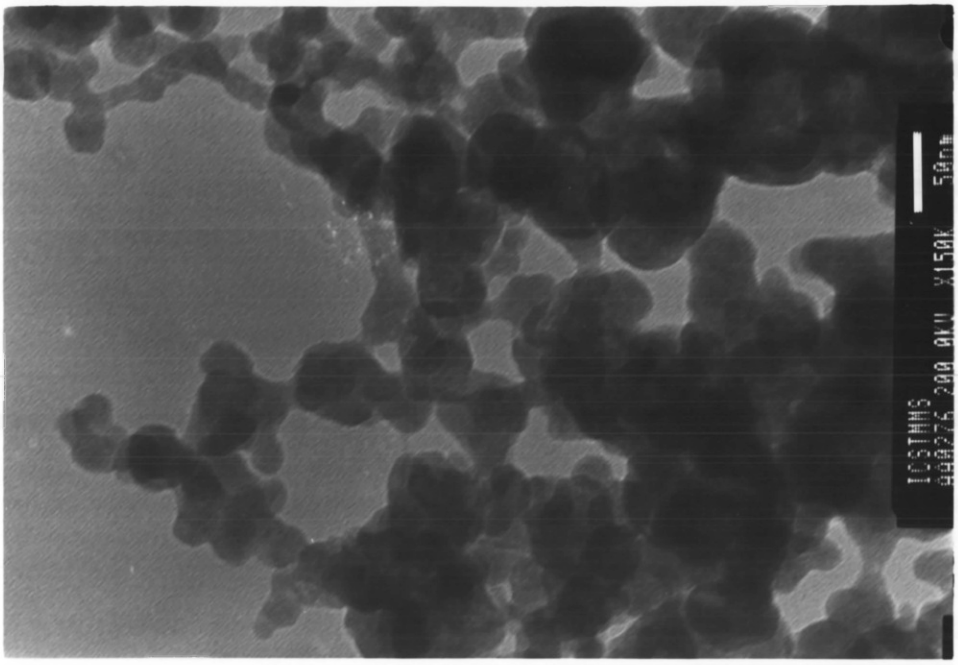

Fig. 6.1(A): TEM Micrograph for Sample PtIr43 Subjected to Pretreatment R740

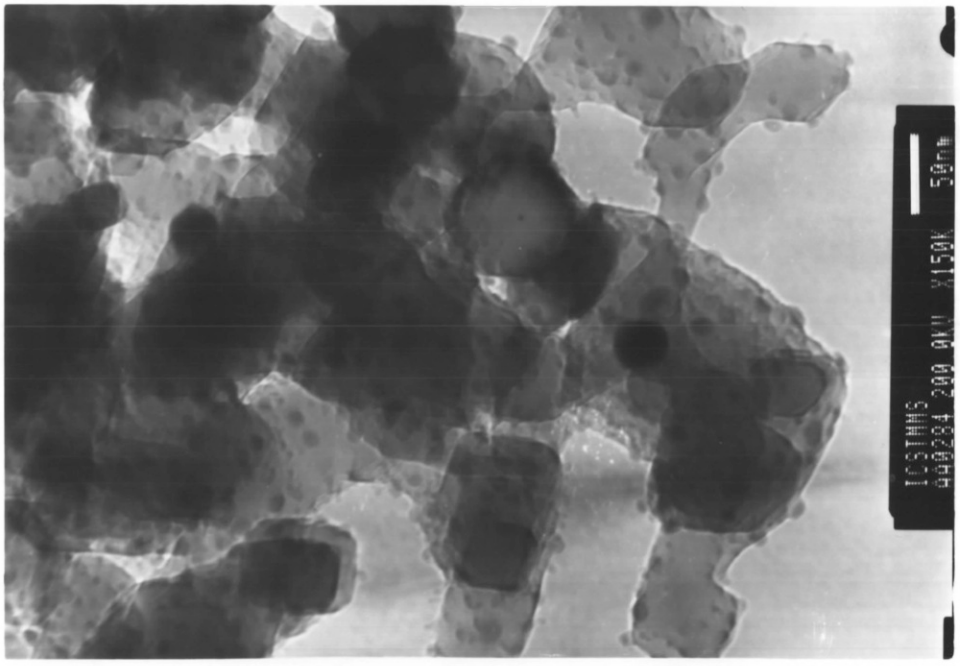

Fig. 6.1(B): TEM Micrograph for Sample PtIr43 Subjected to Pretreatment 0740 R610

b) Samples subjected to oxidation prior to reduction

Fig. 6.1(B) shows a micrograph for sample PtIr43 subjected to an initial oxidation at 740K before reduction at 610K (coded O740 R610). Hemispherical metal crystallites can be clearly seen with a diameter of around 9nm as well as smaller metal particles with a size of around 4nm. The metal particle size distribution (PSD) for this micrograph is shown in Fig. 6.2 where the bimodal nature of the distribution is immediately apparent. Pick et al. (1983) have also observed bimodal PSDs in TEM micrographs for Pt-Ir/alumina catalysts subjected to a pretreatment involving oxidation at temperatures around 773K. The observed crystallites are probably enriched in iridium. The TPR results described in Chapter Four showed that an iridium-rich phase with bulk reduction characteristics was formed following the O740 pretreatment. These results are consistent with the known oxidation-induced agglomeration properties for iridium in supported Pt-Ir bimetallic catalysts, first recognised by Sinfelt and Via (1979).

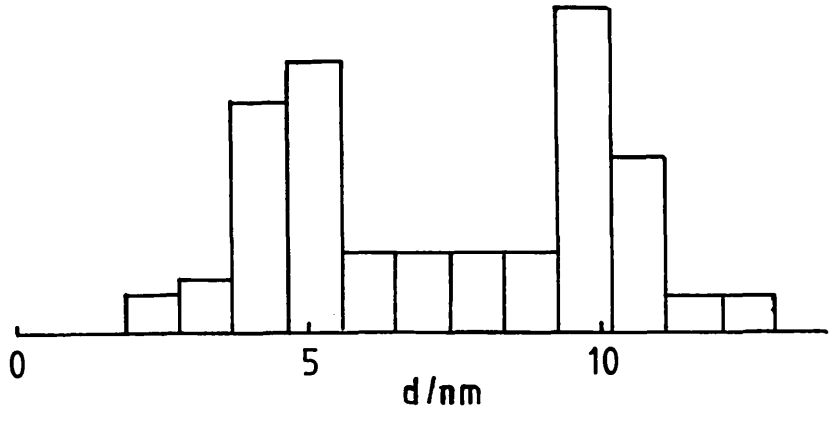

Fig. 6.2: Particle Size Distribution for Sample PtIr43 Subjected to Pretreatment O740 R610

However, the hydrogen thermal desorption results for the PtIr43 sample, shown in Fig. 5.10, indicate that a large fraction of the metal remains highly dispersed following pretreatment O740 R610. Thus, in addition to the large crystallites, small metal clusters must also be present which are below the detection limit (<2nm) of the technique.

Fig. 6.3(B) shows a micrograph of a different region of the same sample. The bimodal nature of the observed metal PSD is not so apparent for this region, perhaps because the thick alumina particles reduced the contrast, thereby obscuring the smaller metal crystallites. Fig. 6.4(B) shows another micrograph for this sample in which the larger metal crystallites are not evident. Thus, whilst Figs. 6.1(B) and 6.3(B) indicate that the observed metal is present with a bimodal PSD following pretreatment O740 R610, the results should be interpreted with caution since some regions appear to contain smaller quantities of the larger crystallites. However, the results generally confirm that catalyst pretreatments which include an oxidation step at 740K, followed by reduction at 610K, result in the formation of iridium-rich crystallites which are of sufficient size to be readily detected using TEM.

Fig. 6.3(A) shows the micrograph for a PtIr43 sample subjected to an initial oxidation at 740K followed by reduction at 740K (coded O740 R740). This micrograph is of a region which contained large alumina particles. Regions containing smaller alumina particles were also examined and similar results were observed. Fig. 6.4(A) shows a region of the specimen containing slightly smaller support particles. (Unfortunately, this particular micrograph is partially darkened due to the thickness of the support in this region). Interestingly, several metal particles appear to be present at the end of 'stalks' attaching them to the alumina. An example of such behaviour is indicated by the arrow in Fig. 6.4(A). Similar behaviour was found in samples subjected to pretreatment O740 R610.

The metal particle size distribution obtained from Fig. 6.3(A) is shown in Fig. 6.5 where a bimodal distribution is once again observed. However, the modal sizes at around 4 and 7nm suggest that the O740 R740 pretreatment produces detectable metal crystallites which are generally smaller than those obtained

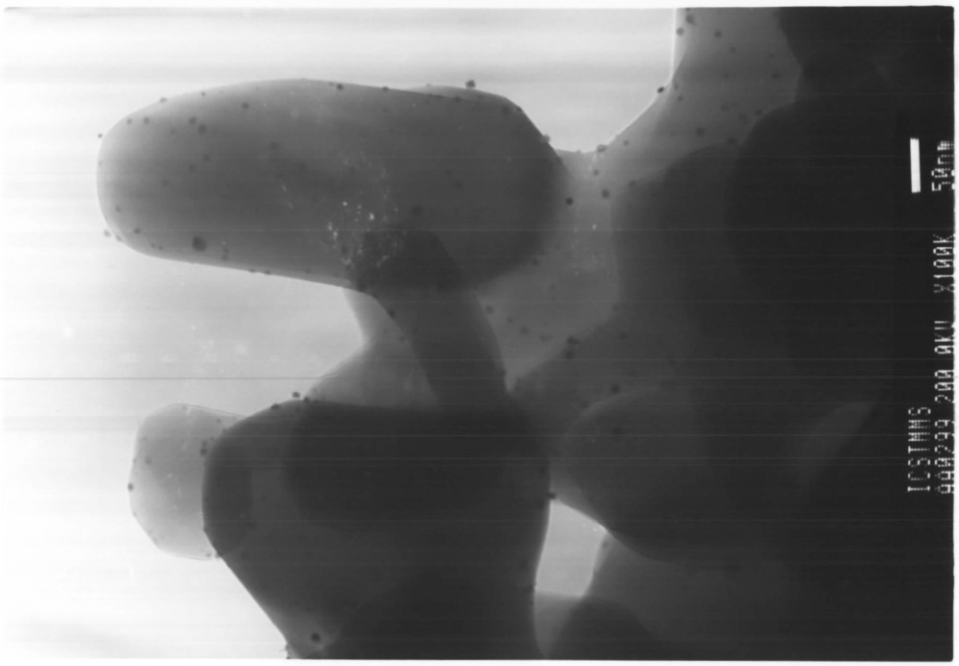

Fig. 6.3(A): TEM Micrograph for Sample PtIr43 Subjected to Pretreatment 0740 R740

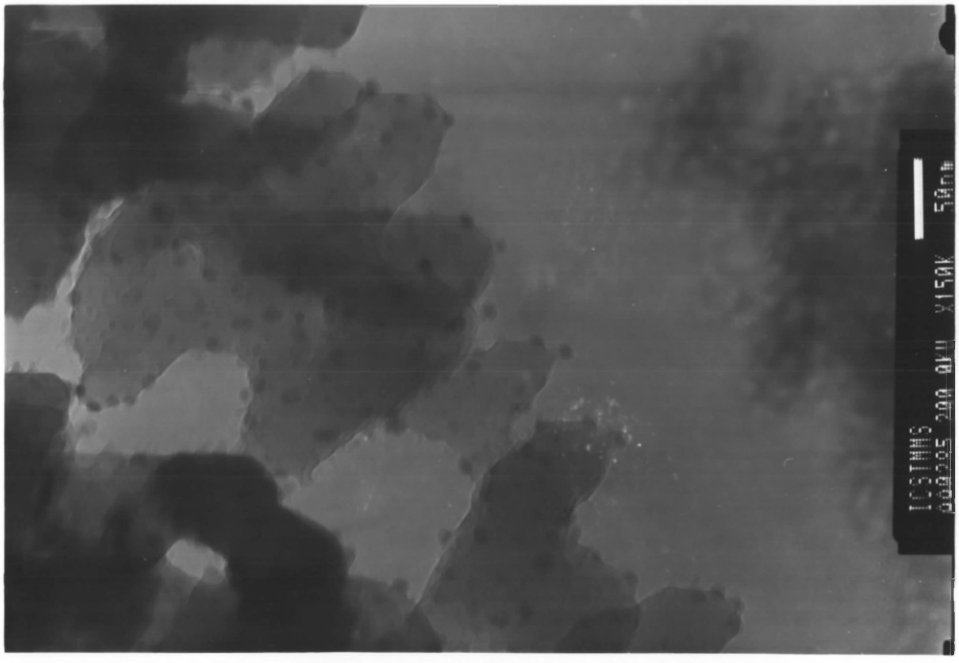

Fig. 6.3(B): TEM Micrograph for Sample PtIr43 Subjected to Pretreatment 0740 R610 (region 2)

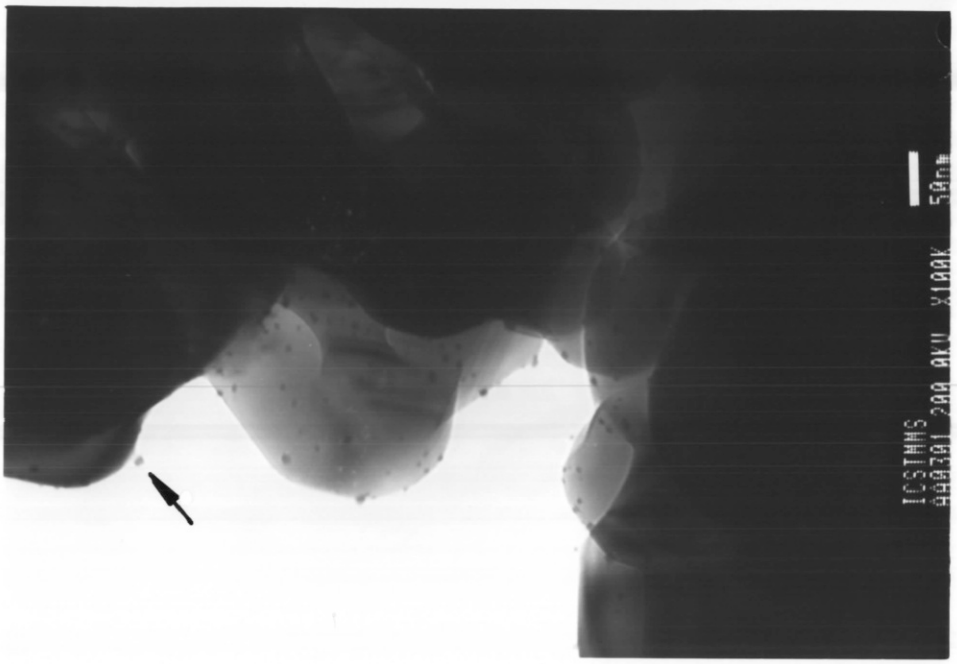

Fig. 6.4(A): TEM Micrograph for Sample PtIr43 Subjected to Pretreatment 0740 R740 (region 2)

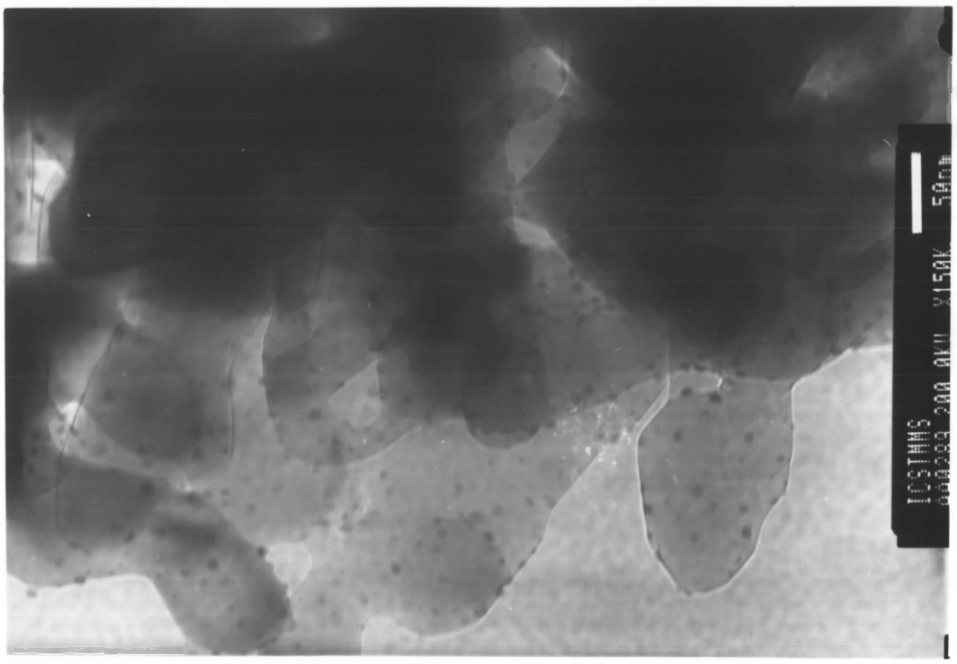

Fig. 6.4(B): TEM Micrograph for Sample PtIr43 Subjected to Pretreatment 0740 R610 (region 3)

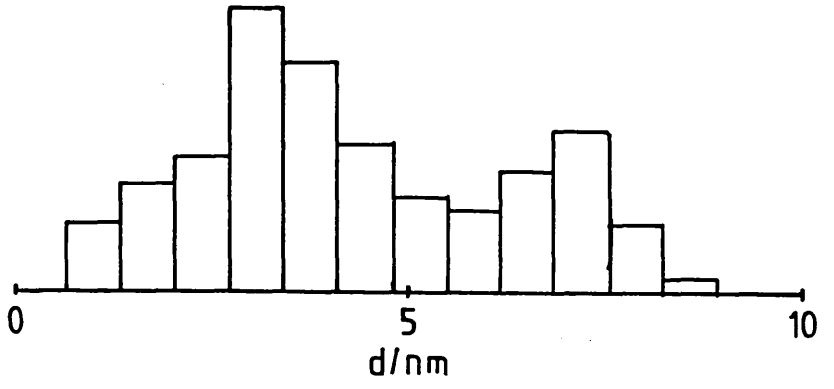

Fig. 6.5: Particle Size Distribution for Sample PtIr43 Subjected to Pretreatment O740 R740

following pretreatment O740 R610. On the basis of these results, it is tempting to conclude that high temperature reduction results in a limited redispersion of the larger crystallites. However, the finer details of a metal particle size analysis can always be open to a degree of question due to unrepresentative regional examination. Despite these reservations the results presented here do at least show that high temperature reduction does not cause further sintering of the larger observable metal particles.

Since such particles are absent from the micrograph shown in Fig. 6.1(A), the almost indentical hydrogen desorption profiles obtained for samples subjected to pretreatment R740 and O740 R740 respectively (see Figs. 5.7 and 5.13) indicate that the metal crystallites observed in Figs. 6.3(A) and 6.4(A), do not significantly contribute to the desorption profile.

It can be concluded from these results that the suppression of hydrogen chemisorption capacity of samples oxidised and reduced at 740K, must arise from changes in the nature of the highly dispersed sub-nanometer particles which cannot be observed using the TEM technique.

To summarise, the TEM examination has shown that reduction of an unoxidised PtIr43 sample produces only highly dispersed metal clusters, less than ~2nm in size. However, oxidation at 740K prior to reduction at 610K leads to the additional formation of large crystallites possibly with a bimodal PSD. These particles have modal sizes of around 4 and 9nm and on the basis of the results given in Chapters Four and Five, they are expected to be iridium-rich. Samples subjected to pretreatment O740 R740 also seem to maintain an observed metal bimodal PSD. However, for the regions examined the higher reduction temperature appears to have caused a decrease in the overall size and number of the observed metal crystallites. Taken as a whole, this examination suggests that the decrease in chemisorption capacity reported in Chapter Five is not primarily a result of metal particle growth induced by the high temperature reduction.

6.3.2 XPS Measurements

In this section photoemission from the metal 4d core-levels will be discussed first, followed by data for the Cl2p and Cls core levels. Although the pretreatments used in this XPS examination differ in some respects from those used in the preceding micro-reactor based studies they are very similar and for ease of discussion the same pretreatment coding system is used. For instance, the pretreatment consisting of an exsitu oxidation at 740K followed by a final reduction at 610K is coded O740 R610.

a) Metal XPS

i) Samples that have not been oxidised

Table 6.3 contains the results for samples Pt100, Ir100 and PtIr43 (i) prior to any reduction (coded O0), (ii) following reduction at 450K (R450) and (iii) following a second reduction at 610K (R610). All reductions were carried out in the ESCALAB prep-chamber.

As a representative example of the XPS data Fig. 6.6 shows the unsmoothed XPS profiles for the metal 4d regions of samples that had received the full reduction treatment (R610). Expansion of the spectra enabled peak binding energies to be determined to within ±0.05eV. However, because of the broadness of the peaks, the error in the peak position binding energies quoted in Table 6.3 are around

Table 6.3: Metal XPS Data for Samples Subjected to No Oxidation Pretreatment Prior to Reduction

Sample	Pretreat-ment	Binding Energy/eV		Peak[b] Width/eV		I_M	
		$4d_{5/2}$	$4d_{3/2}$	$4d_{5/2}$	$4d_{3/2}$	$4d_{5/2}$	$4d_{3/2}$
Pt100	O0	316.15	333.25	5.5	5.5	5.5	6.7
Pt100	R450	315.45	332.85	6.1	6.6	5.3	7.2
Pt100	R610	315.05	332.45	5.8	7.5	4.9	6.5
Ir100	O0	297.60	313.35	4.5	5.0	18.8	19.3
Ir100	R450	297.35	313.00	4.7	5.4	18.4	17.4
Ir100	R610	296.40	312.00	5.3	5.8	18.2	16.2
PtIr43[a]	O0	297.60	332.85	4.6	5.7	10.3	3.0
PtIr43[a]	R450	296.30	332.70	5.3	7.0	9.7	2.7
PtIr43[a]	R610	296.05	332.75	5.7	7.0	9.2	2.6

Notes: a) For sample PtIr43 the $4d_{5/2}$ peak is the Ir$4d_{5/2}$ peak and the $4d_{3/2}$ peak is the Pt$4d_{3/2}$ peak.

b) FWHM values.

± 0.10eV. Since the Ir$4d_{3/2}$ and Pt$4d_{5/2}$ peaks overlap, only the Ir$4d_{5/2}$ and the Pt$4d_{3/2}$ binding energies can be measured for the ItIr43 sample. Thus the values listed in the table for the PtIr43 sample refer to these peaks. The peak widths recorded were the widths of the peak at half the peak maximum height.

Table 6.3 contains the normalised intensity ratio, I_M, for the $4d_{3/2}$ and $4d_{5/2}$ photoemission peaks. This was calculated from the expression:

$$I_M = \frac{A_M/N_M}{\alpha A_S/N_S} \cdot 10^3 \qquad (6.2)$$

where A_M and A_S are the measured peak areas of the metal 4d and

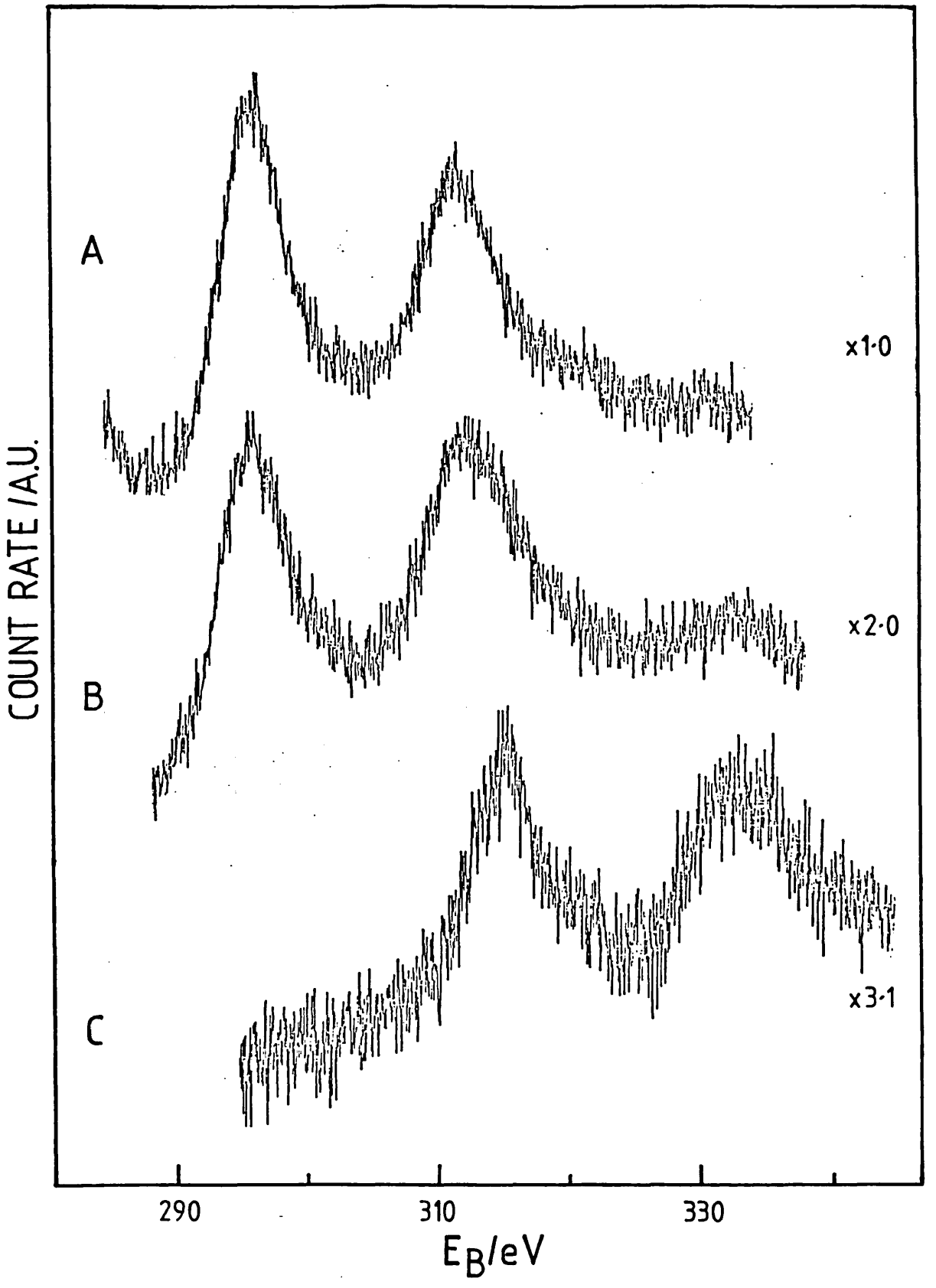

Fig. 6.6: Metal 4d Photoemission Spectra for Samples Ir100 (curve A), PtIr43 (curve B) and Pt100 (curve C) Subjected to Pretreatment R610

aluminium 2p peaks respectively. N_M and N_S are the number of scans performed over these respective peaks and α is the transition metal core-level photoemission cross section as calculated by Scofield (1976). This term is included so that a direct comparison of the normalised peak intensities of the two different metals (Pt or Ir) can be made. The uncertainty in the value of I_M amounts to around $\pm$5% which is due to the error in the measurement of the peak area. This arises mainly from the choice of the peak start and end positions and the use of a linear interpolation between these two points. The errors may be especially significant for the $4d_{5/2}$ peaks since these are placed on a sloping background of unknown shape arising from inelastic photoelectron scattering processes. This could explain why in several cases the value of I_M for the $4d_{5/2}$ peak is smaller than the value for the $4d_{3/2}$ peak, whereas if peak areas were strictly in the ratio of the corresponding degeneracies then the values of I_M for these peaks should be equal. For sake of brevity in all further discussion the normalised intensity ratio will be referred to simply by an expression such as the 4d peak intensity.

The peak intensity and binding energy results will be discussed separately since they relate to different aspects of catalyst structure.

Peak Intensities

For all samples the 4d peak intensities showed a general decrease as the reduction temperature was increased. This may be due to the formation of metal clusters from the more highly dispersed impregnating complex. However, the hydrogen desorption results showed that the metal clusters were still very highly dispersed even after reduction at the highest temperatures (R610) and it is therefore unlikely that sintering can account for the reduced peak intensity. An alternative explanation is that the small decrease arises from a limited redistribution of the metal from the surface of the support into the pore structure where it would be less visible to examination by XPS. Brinen and Schmidt (1976), have found that for carbon-supported rhodium catalysts the metal XPS peak intensities are dependent on the porosity of the carrier used.

It is significant that the 4d peak intensities for the Pt100 sample are always much lower than the corresponding values for the Ir100 sample irrespective of the pretreatment conditions. This may be for one or more of the following reasons:

i) A difference in the level of metal loading in the samples.

ii) Differences in the metal dispersion or cluster morphology at all stages of catalyst preparation.

iii) Differences in the distribution of the metal in the samples.

Explanation (i) above is most easily dismissed since the results of the spectrophotometric analysis presented in Chapter Three showed that the loading of platinum and iridium in the monometallic samples was almost the same at around 7.6×10^{-5} and 8.4×10^{-5} mol g^{-1} catalyst respectively. Explanation (ii) is less easily discounted. Indeed the hydrogen desorption results described in Chapter Five could be interpreted as showing that the Ir100 sample had a metal dispersion twice that of the Pt100 sample. However, the Pt100 sample was still very highly dispersed (H/M ~1) and at such levels of metal dispersion the XPS signal intensity should be fairly independent of cluster size. Furthermore the unreduced samples show the same relative difference in their peak intensities. Therefore, explanation (ii) appears to be unlikely.

This leaves explanation (iii) as the most probable one. Thus, more metal appears to be located on the surface of the alumina with iridium than with platinum. Similarly, Ragaini and Cattania-Sabbadini (1985) have concluded, using XPS that iridium appears to be found mainly on the surface of alumina. This leads to two possibilities; either the platinum is evenly distributed throughout the alumina particles whilst the iridium is relatively more concentrated on the surface of the alumina or the iridium is evenly distributed whilst the platinum is located preferentially within the pore network. Whatever the exact nature of the metal distribution, the results show that relatively more metal is located on the surface of the alumina in the Ir100 sample compared to the Pt100 sample. Furthermore, this cannot be a result of mobility differences occurr-

ing during the reduction step since the unreduced samples have a similar metal distribution.

The ratio of the Ir4d$_{5/2}$ peak intensities for the unreduced PtIr43 and Ir100 samples is around 55%. This value agrees quite closely with the relative amount of iridium present in the bimetallic sample. A comparison of the Pt4d$_{3/2}$ peak intensities allows a similar conclusion to be drawn from the relative amount of platinum present. Therefore, the presence of the additional metal during the co-adsorption procedure causes no change in the distribution of the second metal. Thus the difference in metal distribution observed for the monometallic samples is maintained in the bimetallic sample. It follows that the PtIr43 sample has an enrichment of iridium relative to platinum in the alumina surface which is largely preserved following the reduction pretreatments. Such differences in metal distribution are not unknown for bimetallic catalysts. For instance, Adkins and Davis (1984), using XPS, have found that excess tin is present on the surface of the support in Pt-Sn/alumina catalysts.

Binding Energies

Table 6.3 shows that the metal core-level electron binding energies tend to decrease as the reduction temperature is increased. The only exception is the Pt4d$_{3/2}$ state in the PtIr43 sample. However, this anomalous behaviour for the latter could result from the large error involved with the measurement of the small 4d$_{3/2}$ peak position.

The general decrease in binding energies could be due to an increased degree of reduction of the oxidised metal species as the temperature is increased. However, the TPR results of Chapter Four indicate that by 450K the majority of the metal should be in the zero-valent state. If this is the case then the core-level binding energies following the R450 or R610 pretreatments would be comparable. This leaves two possibilities; either the static pretreatment at 450K used in the prepchamber is not equivalent to the flow system pretreatment and reduction is incomplete, or an interaction may exist between the zero-valent metal formed following the R450 pretreatment and the support, or nearby chloride ions, producing metal with a lower valence-level electron density which results in

an increase in the 4d core-level binding energies. The general increase in peak width following the R450 pretreatment might be an indication that partial reduction had occurred. Alternatively, this may reflect a heterogeneous distribution of metal or it could arise from the presence of nearby chloride ions, as suggested by Bozon-Verduraz et al. (1976). In either case the effect is small since comparison of the peak envelopes revealed little change in peak shape following the reduction pretreatments.

Following the R610 pretreatment the peak widths are generally broader than for the preceding pretreatments. This probably results from a particle size dependent final state broadening effect of the kind outlined earlier or it may be due to differential charging effects. Interestingly, the platinum-containing samples have peak widths which are greater than those found for the Ir100 sample following comparable pretreatments.

For the Pt100 sample subjected to pretreatment R610 the 4d binding energies are in excess of those found by Fuggle and Martensson (1980) for bulk platinum (314.6, 331.6eV). This could be due to incomplete reduction, but the $4d_{5/2}$ peak showed no particular structure that might indicate the presence of more than one oxidation state. Another possibility is that the high binding energy results from the suppression of core-hole relaxation arising from the highly dispersed nature of the supported metal.

For the Ir100 sample, following reduction at 610K, the 4d binding energies are much closer to the values for the bulk metal (296.3, 311.9eV) obtained by the above workers. Whilst it might be tempting to suggest that the iridium is present as large crystallites in which relaxation during photoemission occurs easily it must be remembered that the hydrogen desorption results described in Chapter Five showed that the iridium was very highly dispersed and could even be present as monoatomic entities.

It is possible that the close agreement between the bulk and Ir100 4d binding energies is coincidental and that two opposing effects are at work. For example, it could be that for the Ir100 sample the final state relaxation shift is largely offset by an initial state shift, which results in 4d binding energies of approximately the same value as the bulk metal.

However, it must be remembered that bulk metal 4d binding energies were not measured in the instrument. Furthermore, all the core-level binding energies are referenced to an Al2p binding energy set at 74.40eV. Several values for this binding energy have been reported in the literature and the metal 4d binding energies calculated are clearly dependent on the value chosen. However, the difference in behaviour between the Pt100 and Ir100 samples would remain, i.e. the 4d binding energies for the latter would still be closer to the bulk metal values.

For the unreduced PtIr43 sample (coded O0) the $Ir4d_{5/2}$ binding energy is the same as that for the Ir100 sample. However, the value for the $Pt4d_{3/2}$ peak is lower in the bimetallic sample. These results suggest that in the untreated bimetallic samples the platinum is partially reduced compared to the monometallic system. Significantly, the samples were not stored in a desiccator before being inserted into the UHV system and all the iridium-containing samples were pale in colour. Therefore, it appears that the adsorbed metal precursor complexes in the Ir100 and PtIr43 samples, are more susceptible to partial reduction when exposed to moist air. Presumably, the partially reduced iridium promotes the reduction of the platinum. Storage in a desiccator would appear to suppress the reduction process for the Ir100 sample whilst the presence of platinum in the bimetallic sample further abates the reduction process.

Fig. 6.7(A) shows the unsmoothed $Ir4d_{5/2}$ photoelectron peaks for the Ir100 sample (curve A) and the PtIr43 sample (curve B) following pretreatment R610. The binding energy peak positions recorded in Table 6.3 are shown arrowed in the figure. The profile for the bimetallic sample appears to have an additional feature on the low binding energy side of the peak which is not observed with the Ir100 sample. This is seen in the increased peak width for the bimetallic catalyst. The effect is only slight but, if real, this could indicate that at least some of the iridium in the bimetallic catalyst is present in a more reduced state. Alternatively, the effect could result from a different particle size distribution for the bimetallic, the binding energy shift arising from differences in initial or final state effects. However, no particular difference in metal dispersion was evident in the hydrogen desorption profile

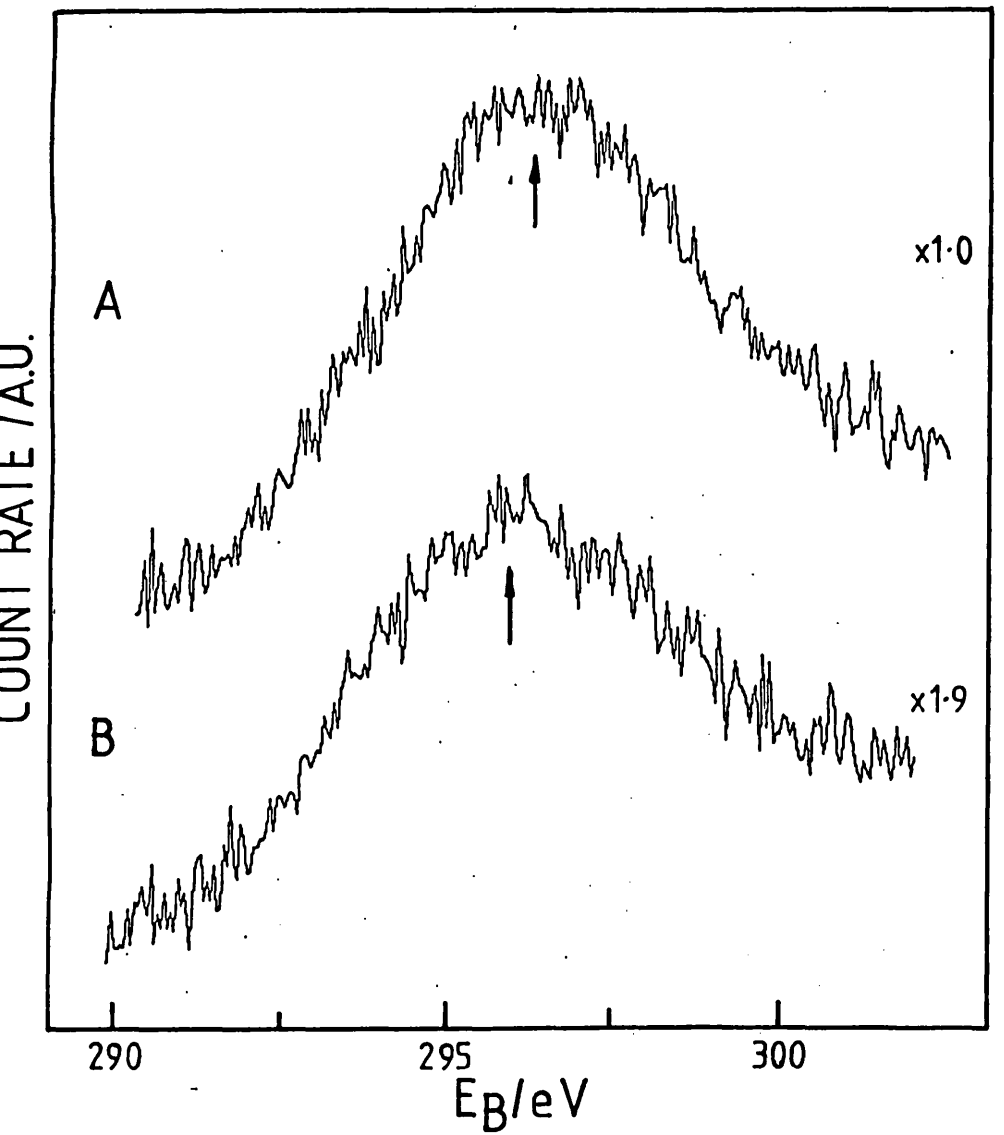

Fig. 6.7(A): Ir4d5/2 Photoemission Spectra for Samples Ir100 (curve A) and PtIr43 (curve B) Subjected to Pretreatment R610

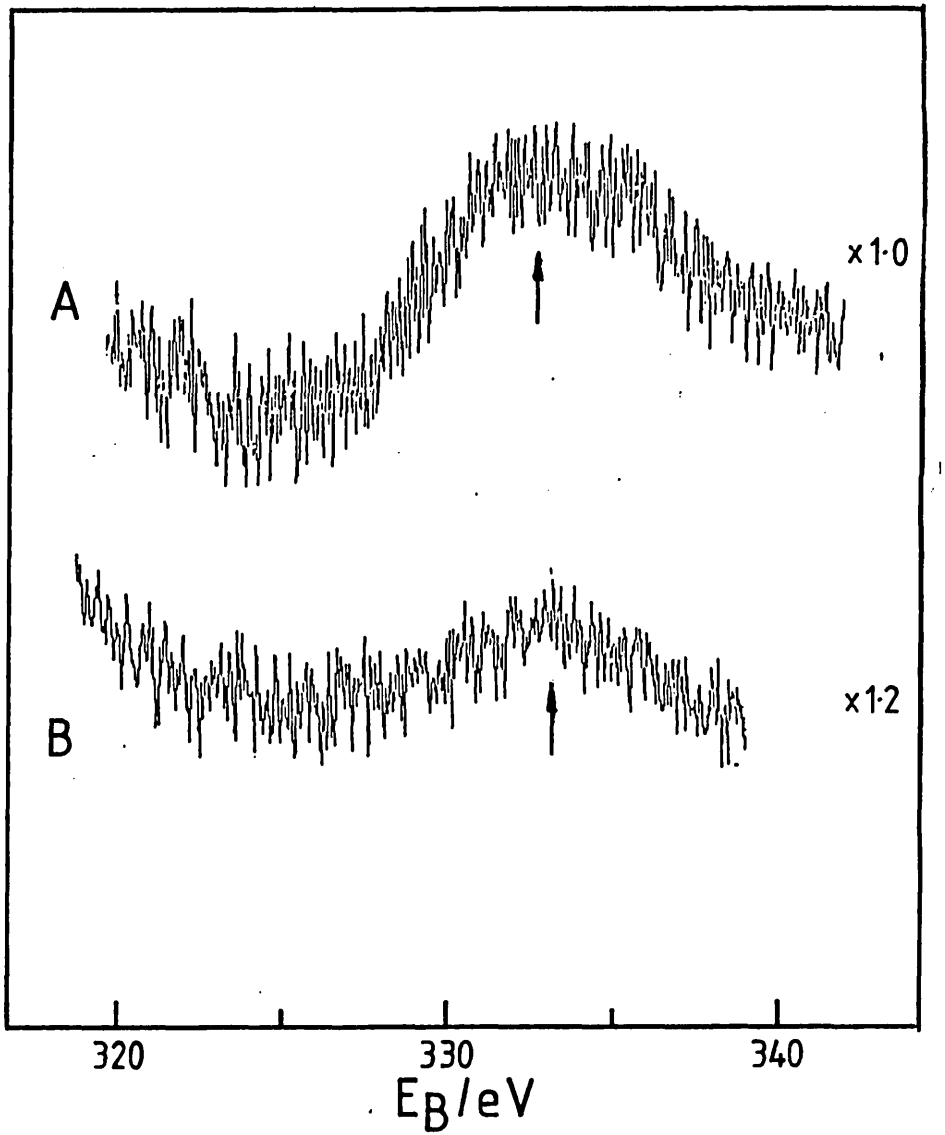

Fig. 6.7(B): Pt4d3/2 Photoemission Spectra for Samples Pt100 (curve A) and PtIr43 (curve B) Subjected to Pretreatment R610

for the bimetallic (see Section 5.3.1) which was the average for the monometallic samples.

Fig. 6.7(B) shows the $Pt4d_{3/2}$ photoelectron peaks for the Pt100 sample (curve A) and the PtIr43 sample (curve B). The binding energy peak positions given in Table 6.3 are marked in the figure. The $Ir4d_{3/2}$ and $Pt4d_{5/2}$ peaks were not used for analysis because of the overlap problem mentioned earlier.

Because of the broadness of the $Pt4d_{3/2}$ peaks and the small size of the $Pt4d_{3/2}$ peak, in the PtIr43 sample, it is difficult to be certain whether the peak positions and shapes are truly different. If the peak positions are in fact those recorded in Table 6.3 then this would suggest that some of the platinum was in a more oxidised state than platinum in the monometallic sample.

Generally it can be stated that the bimetallic catalyst subjected to pretreatment R610 appears to contain at least some iridium which is more reduced and platinum which could be more oxidised than is found in the corresponding monometallic catalysts. It is reasonable to suggest that such metal exists in bimetallic alloy clusters on the support. Indeed such an electronic modification of the metals in the alloy clusters is to be expected since platinum is one place to the right of iridium in the periodic table. Hilaire et al. (1984) in their study of Pt-Ir bulk alloys have suggested that an electronic interaction occurs between the two metals which would alter the core-level peak shapes. However, it must be stressed that the observed effect is only very slight. This may be due to a broad composition range for the bimetallic clusters with the detected metal existing as separate monometallic and as combined bimetallic clusters. The XPS technique has not been able to probe the nature of the metal entities present in the pore network although the hydrogen desorption profiles shown in Fig. 5.8 indicate that alloy formation following a similar pretreatment is extensive throughout the catalyst.

To summarise, the XPS technique has shown that the distribution of platinum and iridium in the catalysts is different. The platinum may be evenly distributed between the surface and the pores of the alumina whilst relatively more iridium can be found on the surface of the support. This difference is also shown by the

bimetallic sample and is maintained for all samples following reduction. Following pretreatment R610 the measured 4d core-levels shift to lower binding energies. For the Pt100 sample the resulting values are still higher than those found for the bulk metal. This probably arises from the dominance of final state relaxation effects. However, for the iridium sample the 4d binding energies are much closer to the bulk values despite the metal being highly dispersed. Initial state effects may be significant for this sample.

Finally, following reduction of the bimetallic sample at 610K, the binding energies of the core-level peaks may provide evidence that bimetallic clusters are formed in which there is an effective electron transfer from one metal to the other. The results suggest that, compared to the monometallic samples, the iridium is more reduced whilst the platinum is partially oxidised. However, the effect on the photoelectron peaks is only very slight and difficult to evaluate. This is especially true of the $Pt4d_{3/2}$ peak since this peak is broad and may well be structured. Further work is required with longer scan times and lower pass energies to firmly establish whether such a modification truly exists.

ii) Samples submitted to an initial oxidation at 740K

Table 6.4 contains the results for samples Pt100, Ir100 and PtIr43 which had been oxidised at 740K prior to the insitu reduction pretreatments. Fig. 6.8 shows the unsmoothed XPS profiles for the metal 4d regions for samples subjected to pretreatment O740 R610. Since the iridium 4d photoelectron peaks are largely absent for the PtIr43 sample the binding energies and peak intensities recorded in Table 6.4 refer to the $Pt4d_{5/2}$ and $Pt4d_{3/2}$ photoelectron peaks.

For the Pt100 sample subjected to pretreatment O740 the 4d binding energies are slightly lower, and the peaks broader, than those obtained for the sample prior to any pretreatment. These differences may be due to the presence of various oxychloride platinum surface complexes in the former sample which cause the peaks to broaden. The TPR results for the Pt100 sample also showed that pretreatment O740 increased the heterogeneity of the oxidised platinum. In addition, the 4d peak intensities for this sample are slightly lower than those obtained prior to the oxidation pretreatment. It seems likely that the oxidation step causes a slight redistribution

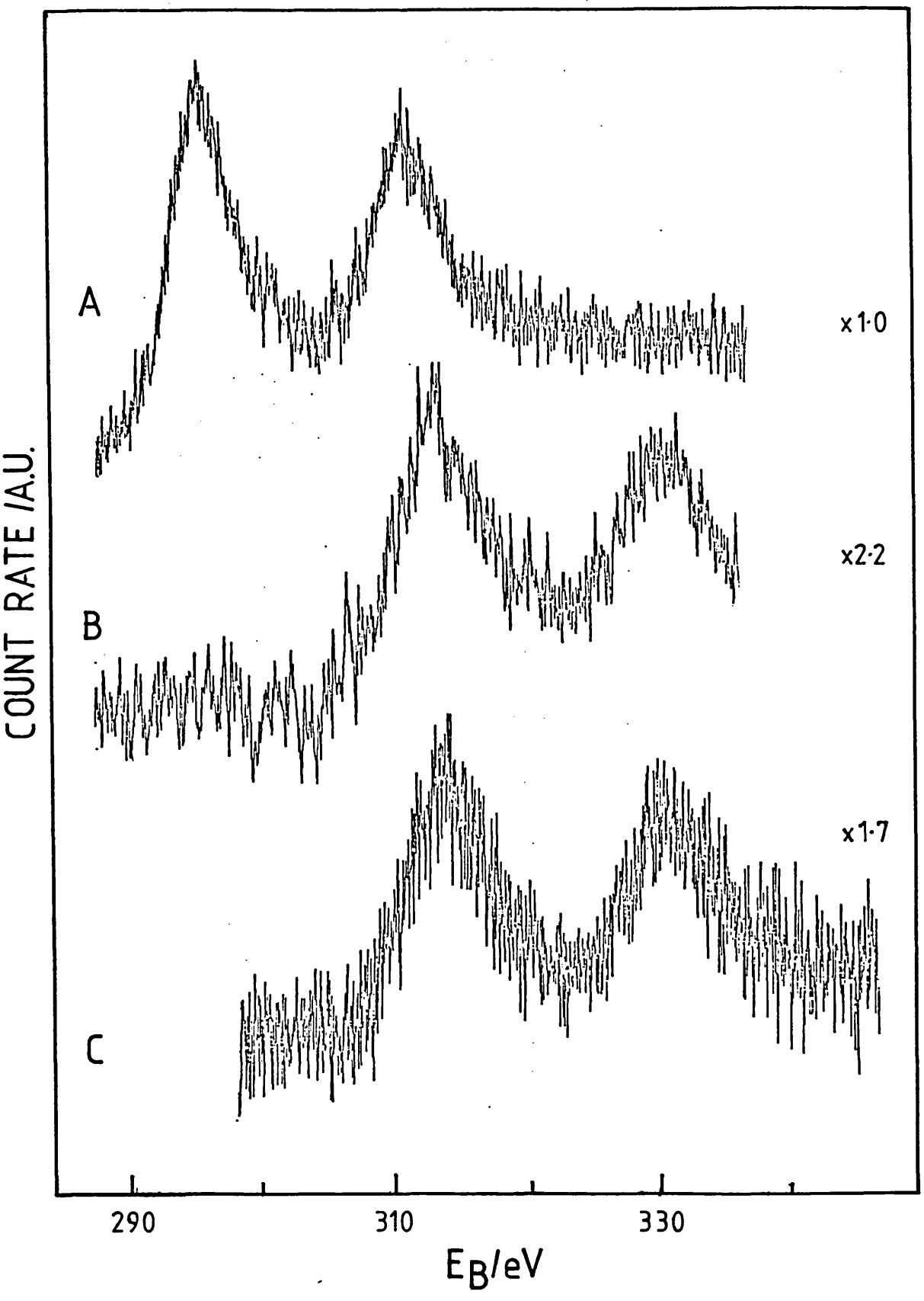

Fig. 6.8: Metal 4d Photoemission Spectra for Samples Ir100 (curve A), PtIr43 (curve B) and Pt100 (curve C) Subjected to Pretreatment O740 R610.

Table 6.4: Metal XPS Data for Samples Subjected to Oxidation at 740K Prior to Reduction

Sample	Pretreatment	Binding Energy/eV		Peak[b] Width/eV		I_M	
		$4d_{5/2}$	$4d_{3/2}$	$4d_{5/2}$	$4d_{3/2}$	$4d_{5/2}$	$4d_{3/2}$
Pt100	O740	315.90	332.80	6.8	6.8	4.7	5.5
Pt100	O740 R450	315.05	332.15	6.4	7.1	4.4	5.1
Pt100	O740 R610	314.85	331.90	6.2	7.4	3.8	4.5
Ir100	O740	298.60	314.20	5.7	6.5	6.7	5.1
Ir100	O740 R450	298.15	313.45	6.3	6.7	6.9	5.2
Ir100	O740 R610	296.80	312.55	5.3	5.8	6.8	5.2
PtIr43[a]	O740	315.50	332.80	6.8	7.1	3.1	2.6
PtIr43[a]	O740 R450	314.90	332.10	6.4	6.8	2.9	2.6
PtIr43[a]	O740 R610	314.80	331.85	6.2	7.3	3.0	2.3

Notes: a) For sample PtIr43, Ir peaks very small therefore $Pt4d_{5/2}$ and $Pt4d_{3/2}$ peaks recorded.

b) FWHM values.

of the platinum into the support structure. Similar calcination-induced motion has been reported by Edmonds and Mitchell (1980) for MoO_3/alumina catalysts.

Following each reduction step the peak intensities of the Pt100 sample decrease in a manner similar to that observed previously (see Table 6.3). It is therefore reasonable to assume that the same processes are operative. The 4d binding energies also decrease as the catalyst is subjected to higher reduction temperatures, showing an increased degree of reduction of the oxidised platinum species as the temperature is increased. Although for this sample the majority of the metal should be reduced by 450K.

The 4d peak widths appear to show anomalous behaviour. Whilst, the $4d_{3/2}$ peak width shows a gradual increase, the $4d_{5/2}$ peak width decreases as the reduction temperature is raised. The cause of such behaviour remains unclear. However, the 4d peaks are generally broader than those obtained for the unoxidised Pt100 sample and the 4d binding energies are lower. For example, the

Pt100 sample subjected to pretreatment O740 R610 has a $4d_{3/2}$ binding energy of 331.90eV compared to 332.45eV for the R610 sample. These results indicate that oxidation prior to reduction causes the formation of different forms of highly dispersed platinum clusters. Indeed, the hydrogen desorption profiles described in Section 5.3.2 for the corresponding samples exhibited differences which could be interpreted as arising from differences in the nature of the metal particles.

For the oxidised Ir100 sample the peak intensities are much reduced compared to those shown in Table 6.3. This could be due to any one of the following:

i) Removal of iridium from the sample due to the formation of volatile IrO_3.
ii) Redistribution of iridium into the pore network during oxidation.
iii) Oxidative agglomeration of the iridium into large oxide crystallites.

Explanation (i) above can be easily discounted since a quantitative analysis of the TPR results showed that no iridium was removed. Whilst explanation (ii) cannot be entirely dismissed there is little evidence to support it and the major cause of the decrease is most probably oxidative agglomeration (explanation (iii)). This would be consistent with previously reported oxidative agglomeration of supported iridium and the TPR results of Section 4.3.1b in which bulk-like reduction properties of the metal were observed. However, the TPR results also showed that some of the oxidised iridium was present in a more dispersed state and at present it is not clear how much this phase contributes to the observed 4d peak intensities. For instance, if the dispersed phase is predominantly in the support pore structure the Ir4d peak intensity would mostly arise from the large crystallites. The increased peak width of this sample compared to those for the sample prior to any pretreatment could be due to the presence of these two phases. Alternatively, the larger peak width could reflect the presence of more than one form of bulk-like oxide. Interestingly, the TPR profile for this sample contained a twinned bulk-oxide reduction peak.

Significantly, the 4d binding energies for the O740 Ir100 sample are greater than those obtained for the O0 sample showing that the former sample is in a higher oxidation state. Furthermore, despite exposure to moist air, the O740 sample retained its colour unlike the O0 sample. Hence the high temperature oxidation produces species which are less easily reduced by moist air than those which are initially present in the O0 sample.

Following pretreatment O740 R450 the Ir4d binding energies fall slightly whilst the width of the peaks increase. The TPR results suggest that such a pretreatment would have caused reduction of the more dispersed oxide whilst some of the bulk-like phase would remain oxidised. Pretreatment O740 R610 causes a larger decrease in the 4d binding energies and thus these results are consistent with the findings of the TPR study which showed that reduction above 500K leads to complete reduction of the bulk-like oxide.

There is also an interesting difference in binding energy between samples that have been oxidised prior to reduction and those that have not. The 4d binding energies for the Ir100 sample subjected to pretreatment O740 R610 are higher than those shown for the sample following pretreatment R610. This could be due to final state effects. A possible explanation would be that the 4d peak intensity arose mainly from photoemission from the larger iridium crystallites in which final state effects predominate over the initial state rehybridisation effect, previously observed for the dispersed iridium particles. This would mean that the highly dispersed iridium species existed only inside the pore network.

If this is assumed to be the case the decrease in the Ir4d peak intensity can be used to obtain an approximate size for the crystallites formed. The details of this calculation and further assumptions used are given in Appendix A1. Assuming a hemispherical crystallite geometry the calculation yields a particle diameter of the order of 20nm. Interestingly, the results of the TEM investigation (See Section 6.3.1) of the PtIr43 sample showed that hemispherical crystallites around 10nm in diameter were formed following pretreatment O740 R610.

The XPS results for the PtIr43 sample subjected to pretreatment O740 show large changes when compared to the results for the

untreated sample. Comparison of Fig. 6.6 and 6.8 shows that peaks due to the iridium component are largely absent and only a small feature is observed where the Ir4d$_{5/2}$ peak should be. For this reason the results given in Table 6.4 for the PtIr43 sample are those for the observed Pt4d photoelectron peaks.

The Pt4d$_{5/2}$ binding energy for this sample is lower than that observed for the corresponding Pt100 sample. This might be thought to indicate that the platinum is present in a different oxidised form. However the Pt4d$_{3/2}$ binding energies are the same. Hence the 4d$_{5/2}$ peak may be slightly offset due to the presence of a small Ir4d$_{3/2}$ component. In accordance with such an interpretation the Pt4d$_{5/2}$ peak intensity is larger than would be expected, whilst the Pt4d$_{3/2}$ is closer to that expected from the known composition of the bimetallic sample. However, some doubt still exists about the validity of this interpretation since the 4d$_{5/2}$ peak width is the same as that for the corresponding peak in the Pt100 sample.

Following the reduction steps, the Pt4d binding energies are quite similar to those obtained for the Pt100 sample. Thus the XPS results, taken as a whole are consistent with the previous findings obtained using TPR, TPD and TEM in which oxidation caused the iridium component to agglomerate into large iridium-rich crystallites leaving a dispersed platinum-rich phase. If it is assumed that the majority of the Ir4d peak intensity observed in the monometallic sample is due to photoemission from iridium in the large crystallites then the near absence of this peak for the PtIr43 sample could be due to one of the following:

i) Removal of iridium from the catalyst.
ii) Redistribution of the iridium into the pore structure.
iii) Increased degree of iridium agglomeration in the bimetallic sample.
iv) Suppression of the Ir4d peaks.

Explanation (i) above can be dismissed on the same grounds as those previously described for the Ir100 sample. Explanation (ii) seems unlikely since large, iridium-rich crystallites were observed in the alumina surface using TEM. Explanation (iii) can also be dismissed since the hydrogen thermal desorption results showed no evidence for

increased iridium agglomeration. The most plausible explanation is that the large iridium-rich oxide crystallites are covered by a shell of platinum-rich oxide which suppresses the iridium XPS signal. The presence of this platinum could account for the difference in the Pt4d5/2 binding energies described earlier. Electron escape depths, calculated by Penn (1976), indicate that this layer must be at least 1nm thick to cause a sizable decrease in the iridium signal. In agreement with this interpretation, the TPR profile for the PtIr43 sample following oxidation at 740K showed an increase in the temperature for reduction of the bulk iridium-rich component over that found for the Ir100 sample. This was attributed to a stabilising effect of platinum in the bulk-like oxide.

On the basis of the TPR results it was also suggested that some iridium redispersion may occur in the bimetallic sample following reduction. However, the intensity of the Ir4d peaks do not increase following reduction and any redispersed iridium must be preferentially present in the alumina pore structure. It also follows that the platinum coating must still be present on the outside of the large crystallites. This is in agreement with alloy surface enrichment predictions using surface segregation models based on differences in the heats of vapourisation of the alloy components, as discussed by Sachtler and Van Santen (1977). However, the similarity of the Pt4d peaks with those for the Pt100 sample shows that either the relative amount of platinum on the iridium is small or that the Pt4d binding energies for the two forms of platinum are comparable.

The hydrogen desorption results did show that a large fraction of the iridium in the bimetallic sample remained highly dispersed whilst the TEM study showed that large (~10nm) crystallites were present. To account for this and the absence of XPS 'visible' iridium it has to be proposed that iridium on the surface of the alumina agglomerates easily to form the larger crystallites whilst iridium present in the pore structure (and hence 'invisible' to XPS) remains more highly dispersed. The higher relative concentration of platinum inside the pore structure could stabilise the iridium towards agglomeration. Alternatively, the iridium may interact differently with the support inside the pores which could account for the difference.

To summarise, the XPS results for a Pt100 sample oxidised at 740K prior to reduction indicate that the heterogeneity of the platinum increases following the oxidation step. This may be due to the formation of various oxychloride-type complexes. Furthermore, core-level binding energy differences between the Pt100 samples subjected to pretreatements O740 R610 and R610, show that differences exist in the nature of the metal particles formed. This has also been observed previously using hydrogen thermal desorption.

The results for the Ir100 sample are most easily interpreted as showing that oxidation at 740K causes the formation of large iridium oxide crystallites with diameters of approximately 20nm. However, the technique does not probe the pore regions of the support in which some highly dispersed iridium could be present. The platinum component in the bimetallic sample gives XPS peaks similar to those obtained with the Pt100 sample thereby indicating the presence of a platinum-rich dispersed phase. However, the decrease in Ir4d peak intensity is much larger than would be found for an iridium agglomeration similar to that observed for the monometallic sample. The results may therefore indicate that the iridium-rich crystallites are covered by a platinum-rich shell. If some of the iridium is highly dispersed, which is indicated by the chemisorption results, then this metal must be present inside the pore structure, since it is not observed by XPS.

b) Chlorine

Table 6.5 contains the results for samples Pt100, Ir100 and PtIr43 subjected to the entire range of pretreatments used. Chlorine impurity was not detected in the untreated alumina used for the catalyst support. Fig. 6.9 shows the unsmoothed XPS profiles for the $Cl2p_{3/2,1/2}$ doublet for samples that have received no pretreatment. For simplicity this doublet will henceforth be referred to as the Cl2p peak. The Cl2p peak intensity, I_{Cl}, was calculated using the following expression:

$$I_{Cl} = 10^3 \frac{A_{Cl}/N_{Cl}}{A_{Al}/N_{Al}} \qquad (6.3)$$

where A_{Cl} and A_{Al} are the measured areas of the Cl2p peak and the Al2p peak respectively and N_{Cl}, N_{Al} are the number of scans per-

Table 6.5: Chlorine XPS Data

Sample	Pretreatment	Binding Energy/eV	Peak Width/eV	I_{Cl}
		$2p_{3/2,1/2}$		
Pt100	O0	199.30	3.8	212
Pt100	R450	199.35	3.7	127
Pt100	R610	199.40	3.6	66
Pt100	O740	199.50	3.7	119
Pt100	O740 R450	199.30	3.7	90
Pt100	O740 R610	199.05	3.9	78
Ir100	O0	199.15	3.5	685
Ir100	R450	199.30	3.4	655
Ir100	R610	199.20	3.5	85
Ir100	O740	199.05	3.5	95
Ir100	O740 R450	199.30	3.9	91
Ir100	O740 R610	199.40	3.9	92
PtIr43	O0	199.20	3.7	348
PtIr43	R610	199.15	3.8	81
PtIr43	O740	199.45	3.9	61
PtIr43	O740 R450	199.30	3.7	59
PtIr43	O740 R610	199.10	3.7	54

formed over the two peaks. A photoemission cross section term was not included since only comparisons between the Cl2p photoelectron peaks were made.

Because of the broadness of the peaks the error in the Cl2p binding energies recorded in Table 6.5 is around $\pm$ 0.10eV. Since the largest change in binding energy for any one sample was only around 0.45eV this shows that only a limited degree of information concerning the nature of the chlorine can be extracted from the XPS data. However, some general trends can be observed and these are outlined in the following discussion.

For every sample the Cl2p binding energies are lower than the value (201.0eV) for chlorine tabulated by Cardona and Ley (1978).

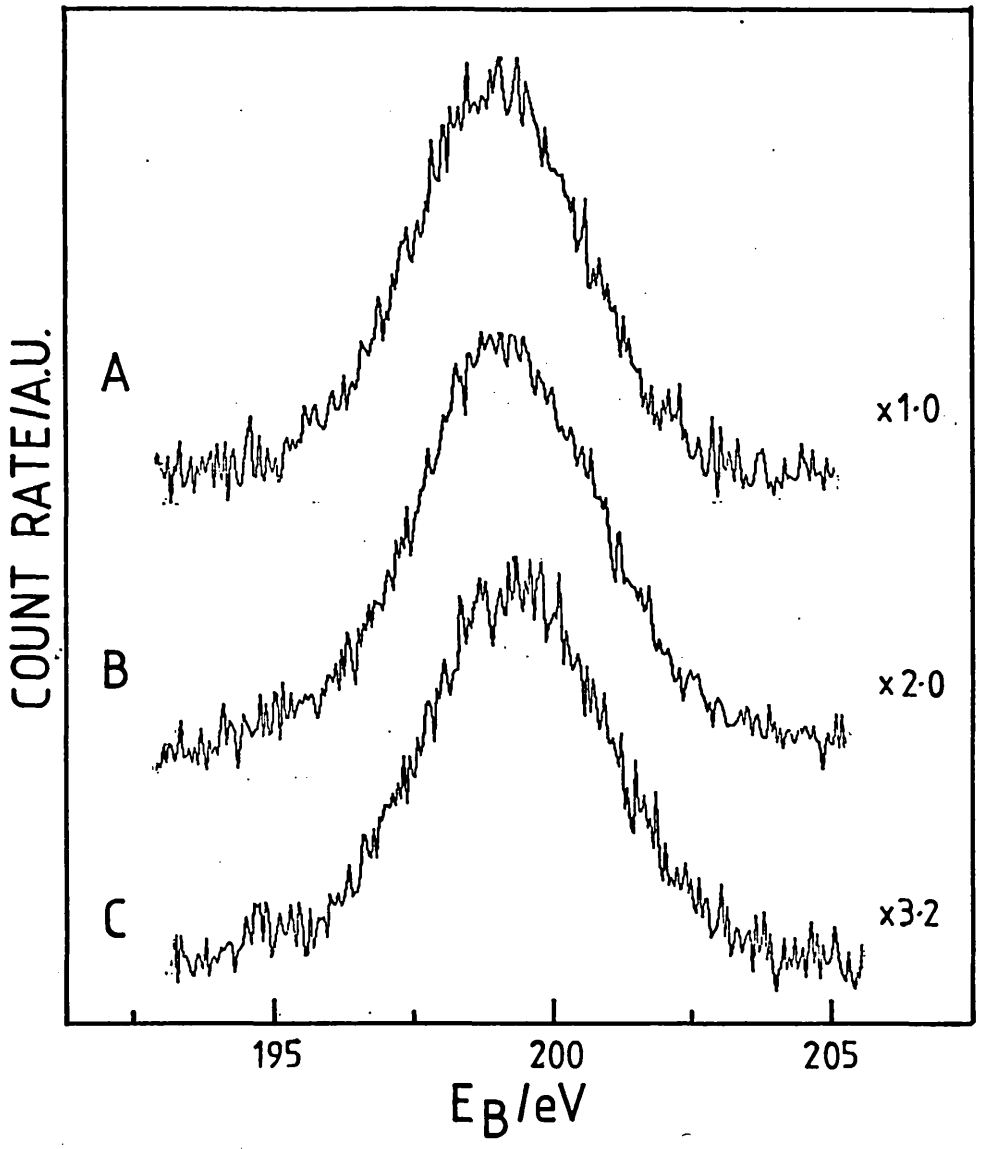

Fig. 6.9: Chlorine 2p3/2,1/2 Photoemission Spectra for Samples Ir100 (curve A), PtIr43 (curve B) and Pt100 (curve C) Subjected to Pretreatment O0.

This indicates that on the whole the chlorine remains negatively charged following all pretreatments. Since the level of charging varies, depending on the sample and pretreatment, the species will be referred to as chlorine in the following discussion and not chloride.

For the unoxidised Pt100 sample, the Cl2p binding energies remain unchanged following each reduction step showing that little

alteration occurs in the electronic structure of the chlorine following reduction of the metal.

However, reduction does produce a decrease in the Cl2p peak intensity. This could be due to the removal of chlorine from the sample but no evidence for chlorine removal was found in the TPR study described in Section 4.3.1 for this or any other sample. Thus the majority of the chlorine liberated during reduction of the metal complex must redistribute into the support pore structure of the alumina. Adkins and Davis (1984) have observed a similar redistribution phenomenon for chlorine during reduction of Pt-Sn/alumina catalysts.

Oxidation of the Pt100 sample also reduces the Cl2p peak intensity. Whilst this may also be due to redistribution of the chlorine the TPO results of Section 4.3.2 showed that some chlorine could be removed from the samples during oxidation. At present it remains unclear as to which, if any, of the above processes is dominant. The Cl2p binding energy for this sample is greater than the value obtained for the sample subjected to pretreatment O0 perhaps indicating that a different complex is formed. Taken as a whole, these results confirm that various oxychloride-type species are present following the O740 pretreatment. Escard et al. (1976), using XPS, reached similar conclusions for Pt/alumina catalysts calcined at 820K.

With iridium extensive hydroxylation and polymerisation of the impregnated complex, coupled with partial reduction of the metal, may be expected to cause an alteration in the Cl2p peak profile. Indeed, the Cl2p binding energy is quite low for the fresh Ir100 sample, although the peak width is not particularly indicative of chlorine in a heterogenous state. The fact that the Cl2p peak intensity is very much greater for this sample than it is for the corresponding Pt100 sample indicates that the iridium impregnating complex is found predominantly on the outer surface of the alumina whereas the platinum prefers to go into the pores.

Following the first reduction of the Ir100 sample the Cl2p peak intensity decreases only slightly although a sharp drop to a value similar to that obtained for the Pt100 sample occurs following the final reduction. Hence for the Ir100 sample the surface

chlorine appears to be stabilised towards redistribution at the low reduction temperature. This may be due to an interaction with the metal or with sites on the support which are possibly modified by the nearby metal. The difference in behaviour between the monometallic samples could be related to the different metal distributions. However, the high temperature reduction is sufficient to cause the stabilising interaction to break down and redistribution of the chlorine occurs.

Furthermore, the fact that, following reduction at 610K, the two monometallic samples have similar surface chlorine levels, despite having different surface metal loadings, suggests that the chlorine remaining on the surface is largely unassociated with the metal. In other words discrete chloride complexes, such as MCl_2, are not present following the final reduction.

The Cl2p peak intensity of the Ir100 sample is similar in size for both freshly reduced samples (R610) and oxidised samples (O740). This suggests that the surface chlorine is largely associated with the support in the oxidised sample, which is to be expected if large iridium oxide crystallites are present. It remains unclear whether the total chlorine contents for the two samples are equivalent. The small difference in the Cl2p binding energies and peak widths, between the samples subjected to pretreatment O740 R610 and R610, suggest that the interaction of the chlorine with the support is modified by the inclusion of the oxidation step.

For the PtIr43 sample prior to any pretreatment the Cl2p binding energy is intermediate between the values for the monometallic samples. Although the peak intensity lies between those for the Pt100 and Ir100 samples the value is less than would be expected from the known surface composition of the bimetallic catalyst. The reason for this difference is not readily apparent. Data for the PtIr43 sample subjected to the first reduction pretreatment were not collected. However, following the final reduction the peak intensity decreases to a value similar to that found for the monometallic samples showing that chlorine redistribution also occurs for this sample.

For the PtIr43 sample subjected to pretreatment O740 the Cl2p peak intensity is below the values obtained for the monometallic samples. This may reflect the lower than expected chlorine level initially present in the untreated sample. Following reduction the Cl2p binding energies alter in the same manner as found for the Pt100 sample. This indicates that the behaviour of the chlorine is primarily influenced by the presence of the dispersed platinum-rich phase.

To summarise, the XPS results show that chlorine, liberated during reduction of the supported metal complexes, does not entirely stay on the alumina surface but redistributes into the pore network. From the amount of chlorine remaining on the support surface it appears that discrete metal-chloride entities do not form on the surface following reduction. The results for the Pt100 sample oxidised at 740K suggest that platinum oxychloride-type complexes are formed. In addition, decreases in the Cl2p peak intensities for all oxidised samples are consistent with removal of chlorine as observed during the TPO experiments. However, all samples still contain surface chlorine and it is unclear how much of the decrease results from a possible oxidation induced redistribution of the chlorine.

c) Carbon

Details of the C1s photoelectron peaks observed for both pure and impregnated alumina are summarised in Table 6.6. Fig. 6.10 shows the C1s peaks for pure alumina and the Pt100 catalyst subjected to pretreatment R610. The C1s signal from the sample holder has been subtracted from the spectra. The C1s peak intensities, I_C, given in Table 6.6 were evaluated in a similar manner to that used for the Cl2p peak intensities.

The C1s peak intensities for all metal impregnated samples are much greater than the value obtained for the pure alumina sample. This is consistent with the TPR/TPO results of Chapter Four where it was shown that impregnation of alumina with metal chloride complexes resulted in the adsorption of atmospheric carbon dioxide which formed additional carbon-containing species in the sample.

Table 6.6: Carbon XPS Data

Sample	Pretreatment	Binding Energy/eV 1s	Peak Width/eV	I_C
Pt100	O0	284.55	3.3	72
Pt100	R450	285.05	3.0	60
Pt100	R610	284.60	3.2	55
Pt100	O740 R450	285.15	3.7	26
Pt100	O740 R610	284.64	3.7	30
Ir100	O0	284.90	2.5	220
Ir100	R450	284.75	2.6	102
Ir100	R610	285.15	2.8	57
Ir100	O740	285.10	3.1	89
Ir100	O740 R610	285.00	2.8	33
PtIr43	O0	285.00	2.7	73
PtIr43	R610	284.45	3.0	48
PtIr43	O740	285.05	2.7	37
PtIr43	O740 R450	284.90	3.3	36
PtIr43	O740 R610	285.20	3.3	27
Al_2O_3 a)	O0	285.15	3.3	15

Note: a) Pure alumina support material

For the Pt100 sample reduction at 450K or 610K causes the C1s peak intensity to decrease. However, following the final reduction the peak intensity is still in excess of the value for the support material.

The amount of carbon observed with the freshly prepared Ir100 sample is much greater than the amount observed with the comparable Pt100 sample. Since the previously described XPS results have shown that relatively more iridium is present on the alumina surface these results confirm that the amount of carbon-containing species formed is directly related to the amount of metal complex present. However, the C1s intensity of the Ir100 sample falls following each reduction step and finally attains the same value found for the Pt100 sample following pretreatment R610. This could indicate that

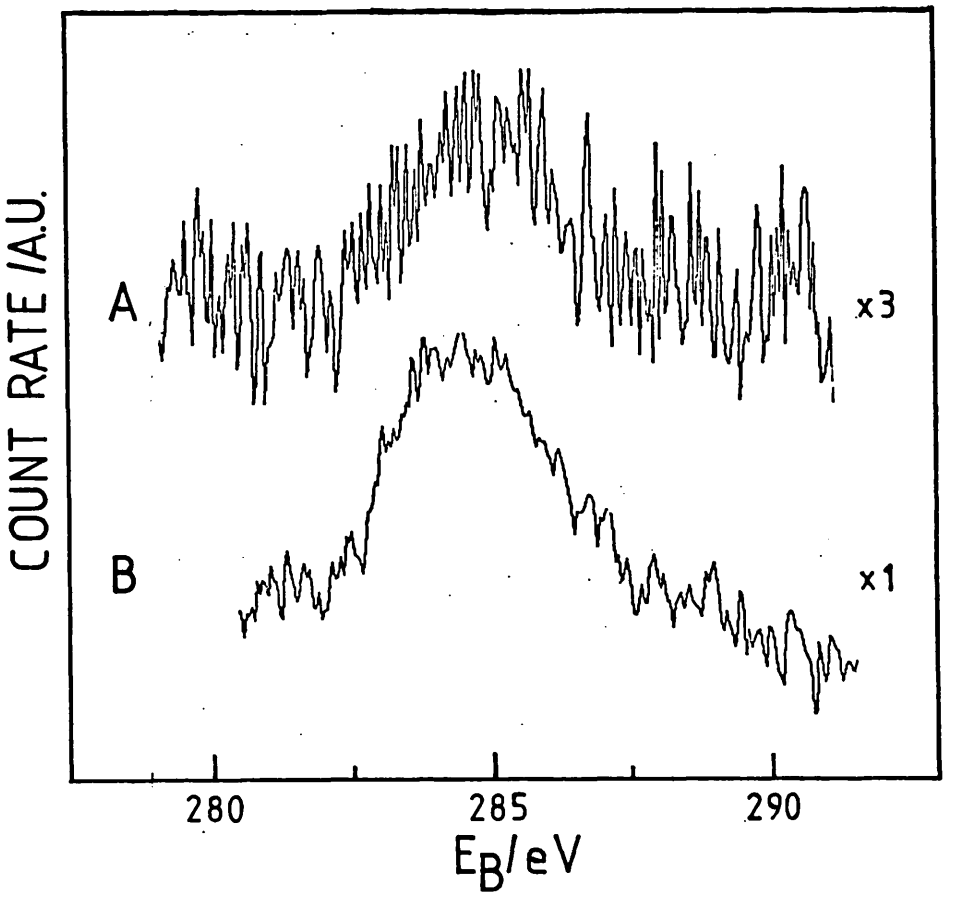

Fig. 6.10: Carbon 1s Photoemission Spectra for the Untreated Alumina Sample (curve A) and the Pt100 sample (curve B) Subjected to Pretreatment R610.

reduction of the iridium sample removed a large fraction of the carbon possibly as methane. However, the TPR/TPO study showed that most (~90%) of the carbon remained on the catalyst following reduction at temperatures up to 740K. This apparent inconsistency can be resolved in one of two ways.

i) The observed carbon may only represent a minor fraction of the total carbon in the catalyst. Therefore large changes in the C1s peak intensity may represent the removal of only small amounts of total carbon.

or

ii) The observed carbon may represent a sizable fraction of the total and the decrease could arise from this carbon becoming invisible to XPS.

Whilst the first explanation cannot be entirely discounted the finding that the C1s peak intensity of the Pt100 sample decreased only comparatively slightly whilst the amount of methane formed was comparable to that found for the Ir100 sample (see Section 4.3.1) suggests that this explanation is less likely.

Thus hydrogen treatment may result in the formation of carbon which diffuses into the alumina lattice or alternatively, to more stable sites in the pore network. Such carbon is extremely stable since the TPO results showed that it could not be removed below temperatures of approximately 800K. For the PtIr43 sample subjected to pretreatment O0 the C1s peak intensity is lower than would be expected, with the amount being equal to that found for the Pt100 sample. Following reduction the amount of carbon observed decreased still further.

The presence of several carbon-containing species (i.e. bicarbonates, formates and carbonates) may be expected to produce differences in C1s binding energies and peak widths. However, no systematic variation, indicative of such species, can be discerned from the data presented in Table 6.6. This may be due to the broadness of the C1s peaks or to the surface species being unstable in a UHV or X-ray irradated environment. Alternatively, different species may be present in different regions of the catalysts. In addition, pump oil contamination may be a complication. Although in no sample does the C1s intensity increase following the second reduction which would be expected for such a time dependent contamination process. The peak widths for the Ir100 sample are less than those for the platinum-containing samples which could be due to the predominance of one particular species for this sample. Interestingly, all the C1s binding energies observed with these catalysts are much lower than the value characteristic of carbonate anions (289.3eV) tabulated by Wagner et al. (1979). Either carbonate anions are not formed or, if they do form, there must be extensive electron donation from the support to the complex.

For all samples previously subjected to oxidation at 740K, the C1s peak intensity is less than that observed for the corresponding unoxidised samples. However, the amount is still in excess of that found for the alumina sample. These results show that air exposure of the oxidised samples leads to the readsorption of carbon dioxide into the samples. However, the oxidation step does cause a reduction in the amount which can be adsorbed, perhaps because of changes in the metal complex or changes in the nature of the support close to the metal. In general, the C1s binding energies for the samples previously oxidised before reduction are comparable to those found for the unoxidised samples. Although the PtIr43 sample subjected to pretreatment O740 R610 appears to be an exception to this rule, having a C1s binding energy similar to the corresponding Ir100 sample.

To summarise, the C1s peak shapes and binding energies do not provide clear evidence for the presence of several forms of carbon-containing species. However, the amounts of carbon detected on the catalysts are greater than those found on the alumina support. The decrease in size of the C1s peak intensity following reduction suggests that the highly stable carbon, proposed in the TPR/TPO study, is probably located inside the alumina lattice structure or the pore network in a form which is stable to oxidation at 800K. For samples previously oxidised at 740K the C1s peak intensity is decreased but is still in excess of that found for the alumina control. This exposure to air following oxidation results in renewed, although suppressed, carbon deposition presumably from atmospheric carbon dioxide.

6.4 Discussion

This section is divided into two parts. The first discusses the possibility that an SMSI state is formed during the high temperature reduction pretreatment, whilst the second is concerned with alloying and electronic interactions in the bimetallic Pt-Ir catalyst system.

6.4.1 Strong Metal-Support Interactions

The TEM results obtained for the bimetallic PtIr43 sample provide evidence for the formation of a so-called SMSI state

following a high temperature reduction at 740K. Explanations involving simply particle sintering or carbon poisoning seem less plausible when all the experimental evidence contained in this and preceeding chapters is viewed as a whole. However, it should be noted that the presence of carbon may be relevant since it could actually inhibit the onset of the SMSI effect for the monometallic platinum sample.

Much research effort has been expended in an attempt to determine the nature of the SMSI state since the expression was first used by Tauster et al. (1978) as an explanation for the anomalous properties of platinum supported on titania following high temperature reduction. Similar SMSI states have been postulated for a wide range of transition metals supported on many metal oxide supports (excluding silica). In general, it has been found that reduction of these materials at temperatures in excess of approximately 650K has a significant influence on catalyst properties which cannot be ascribed simply to metal particle growth. In particular, hydrogen and carbon monoxide chemisorption tend to decrease substantially and the activity of structure sensitive reactions such as hydrocarbon hydrogenolysis are markedly reduced. However, so-called structure insensitive reactions, such as the hydrogenation of unsaturated hydrocarbons, are little effected.

Bond and Burch (1983) have discussed the possible nature of the SMSI state. From the general body of evidence it would appear that several explanations can account satisfactorily for the change in catalyst properties. The most likely causes of a genuine metal-support effect at high reduction temperatures are:

i) Diffusion of the metal into the oxide.

ii) Encapsulation of the highly dispersed metal particles by a layer of partially reduced oxide; a mechanism recently favoured by Anderson et al. (1986) for the Pt/TiO_2 system.

iii) Electron transfer between the metal and the support (possibly partially reduced).

iv) Alloy formation between the metal and the partially reduced support producing an inactive surface; a process suggested by Den

Otter and Dautzenberg (1978) for the Pt/Al_2O_3 system.

v) Support-induced changes in metal particle morphology (not involving particle growth); e.g. the transformation of particle surfaces into (111) planes as suggested by Burch and Garla (1982) for alumina-supported platinum.

For the iridium-containing samples explanation (v) above seems to be ruled out since the nature of the hydrogen desorption profiles points to a reduction in low index-type planes rather than an increase (see Section 5.3). Explanation (i) also seems unlikely since the TPR results showed that some reduction of the oxide could take place at high temperatures. Unfortunately, it is impossible with our present knowledge to determine which, if any, of the remaining explanations are operative in the Pt-Ir/alumina system. However, all of the remaining explanations would probably require a close interaction between the highly dispersed metal particles and the support. It may be that an epitaxial relationship between the metal and the oxide surface may be required, which could easily be disrupted by the presence of carbon, as outline above for the Pt100 sample. For the iridium-containing samples such carbon might not be present at the metal-metal oxide interface or the relationship between the oxide and metal may be more tolerant to the presence of carbon. Further effects relating to high temperature reduction will be found in the next Chapter where the effect of SMSI state formation on the conversion of hydrocarbons over alumina- supported platinum-iridium catalysts is described.

6.4.2 Bimetallic Alloying and Electronic Interactions

The TPR, TPD and XPS results taken together show that alumina-supported Pt-Ir catalysts subjected to an initial oxidation at 560K, or to no oxidation at all, reduce to form samples containing bimetallic metal particles. As outlined in Chapter Four this behaviour is in agreement with previous studies on bimetallic Pt-Ir systems employing techniques such as XRD (Sinfelt and Via (1979)), Mossbauer Spectroscopy (Garten and Sinfelt (1980)) and EXAFS (Sinfelt et al. (1982)). However, Yacamen et al. (1980), using high resolution defocused weak electron beam imaging, could find no

particular evidence for alloy formation in this system despite the technique being sensitive to the state of metal clusters of around 5Å in diameter.

Nevertheless, the majority of evidence now available indicates that alloy particles are indeed present following the above catalyst pretreatment and the following discussion outlines the properties of bulk alloy systems to provide an insight into the nature of the supported Pt-Ir particles.

The surface composition of unsupported binary alloy systems has received widespread attention since the performance of an alloy catalyst is largely determined by the catalytic properties of the surface atoms. In general techniques such as AES, LEIS‡, XPS and selective gas chemisorption have shown that the surface regions of binary alloys are enriched in one component. A theory of surface enrichment in alloys has been produced by Williams and Nason (1974) and the subject has been reviewed by Sachtler and van Santen (1977, 1979).

On the basis of the broken bond approximation for the surface of a solid, it can be shown that an alloy surface should be enriched with the component of lowest heat of atomisation, ΔH_a, especially at crystallite edges, corners or high index faces. This will occur because the surface free energy of the system can be minimised by preferentially filling the surface with atoms of the constituent which has the lowest binding energy (i.e. lowest ΔH_a). In addition, the surface composition can be governed by the gaseous atmosphere in contact with the alloy and by constituent atom size effects. However, the latter is not significant for the Pt-Ir system since the lattice constant, x, for the two metals are very similar (x(Pt) = 0.3916nm; x(Ir) = 0.3831nm).*

There have been several reported investigations of the bulk Pt-Ir alloy system and the results of these are briefly outlined below. Raube and Plate (1956) showed that a miscibility gap existed at temperatures lower than about 1248K and at 700K the gap was found to extend over the composition range 7 to 99% iridium. The cause of this behaviour for such similar metals remains unclear although

‡ Low Energy Ion Scattering
* source: Raube and Plate (1956)

Raube (1959) later proposed that the gap was related to the difference between the melting points of the two metals (Pt mpt = 2042K; Ir mpt = 2716K).† These results are significant since, as outlined by Sachtler and van Santen (1979), the miscibility gap could result in the formation of large metal particles which consist of an alloy kernel surrounded by a flesh consisting of a different alloy. The relative amounts of kernel and flesh and their composition would be derived from the bulk phase diagram using the lever rule. The surface free energy would determine which phase formed the outer shell, whilst the skin of this layer would be enriched in the component of lowest ΔH_a, namely Pt (ΔH_a(Pt) = 565 kJ mol^{-1}; ΔH_a(Ir) = 665 kJ mol^{-1}).† Significantly, this arrangement results in a surface composition which remains constant over the full range of immiscibility since changes in the overall composition mostly affect the relative sizes of kernel and flesh.

Kuijers and Ponec (1978), using AES, have examined the surface composition of Pt-Ir bulk alloys and as expected from the above argument, observed a surface enrichment in the platinum component. Furthermore, their results showed that very little iridium (< 10%) was present in the surface of alloys whose overall composition was less than 60% iridium. These workers concluded that the small amount of iridium present in the surface of such catalysts is likely to exist as isolated atoms and would not react in the same way as a monometallic iridium sample. A similar surface enrichment phenomenum has been observed by Hilaire et al. (1984) with XPS.

In agreement with this behaviour the XPS results obtained in the present study for alumina-supported samples initially oxidised at 740K indicate that the surfaces of the large (~10nm) iridium-rich particles are enriched in platinum. However, and not altogether surprisingly, surface enrichment was not observed for the highly dispersed clusters (< 2nm). Indeed, Burton et al. (1975) pointed out that surface enrichment in small particles is restricted by the limited availability of the atoms in which the surface is expected to be enriched. In addition, the notion of surface enrichment becomes inappropriate for alloy particles in which most of the metal atoms are surface atoms. An exception to this would be for raft-

† source: "Selected values of Chemical Thermodynamic Properties", National Bureau of Standards, Washington (1969)

like particles with platinum atoms located around the particle perimeter. However, no evidence for such entities was found with TEM.

The XPS results for the bimetallic sample also indicated a general difference between the location of the two metals on the alumina. Iridium appears to prefer the outer surfaces of the support whilst the platinum component is more evenly distributed between the oxide pore network and the surface. Hence an overall picture of the highly dispersed particles begins to emerge in which clusters are present having a wide Pt-Ir composition range. On average, particles on the outer surfaces of the alumina will contain more iridium than those inside the pore network. It should be noted that this interpretation does not preclude the presence of small iridium-rich particles inside the pores, although the relative amount of these would be less compared to the surface region of the oxide.

Although not entirely conclusive, the XPS results also indicated that an electron transfer occurred from the platinum to the iridium in the dispersed bimetallic clusters. This result is significant, since it suggests that the catalytic properties of such alloy particles may not be governed solely by so-called ensemble effects but may also depend upon ligand effects. In the former, individual surface atoms retain their identity and changes in catalytic properties caused by alloying are ascribed to geometric effects such as the dilution of an active component. For the latter situation, the new properties of alloys are attributed to changes in collective electronic parameters such as alterations to the Fermi-level and electron density. Rasser (1977) has considered the electronic interaction between alloyed platinum and iridium at compositions of around 25% Ir and proposed that a strong interaction between the metals should take place in which s-charge transfer towards the more electronegative platinum is compensated for by d-electron shift to the iridium. Such a proposal does not run counter to the XPS results obtained in this study. The following Chapter examines such effects on the catalytic properties of alumina-supported platinum-iridium catalysts.

6.5 Summary

The TEM examination confirmed that the iridium component agglomerates to form large iridium-rich particles after oxidation of the PtIr43 sample at temperatures of around 740K. Following reduction the sintered particles appear to have a bimodal particle size distribution with modal sizes of around 4 and 9nm. Furthermore, the TEM investigation has shown that metal particle sintering cannot account for the alteration in the hydrogen chemisorption properties of the PtIr43 sample following reduction at 740K. The most likely cause of this effect is the formation of an SMSI state for which an epitaxial relationship between the oxide and the metal particles may be required.

The XPS results for the agglomerated PtIr43 sample show that the large iridium-rich crystallites are most likely covered by a layer of platinum, which is consistent with alloy surface enrichment predictions. However, as expected no evidence for surface enrichment was found for the highly dispersed bimetallic samples. Furthermore, the XPS results show that the iridium component appears to favour the surface region of the support whilst the platinum component may be more evenly distributed between the surface and the pore network. Hence, the dispersed bimetallic clusters formed are expected to have a broad composition range with, on average, a higher iridium content on the surface of the support. However, for the agglomerated samples the redispersed iridium component appears to favour the pore locations.

Finally, the XPS results for the highly dispersed alloy particles indicate that an electron transfer occurs from the platinum to iridium. The consequences of such a ligand effect and/or possible geometric effects on the catalyst reactivity are investigated in the following Chapter.

CHAPTER SEVEN

Hydrocarbon Thermal Desorption Studies

7.1 Introduction

7.1.1 Aim

The aim of this Chapter is to determine the way in which pretreatment conditions affect the conversion reactions of hydrocarbons on alumina-supported platinum-iridium catalysts. This has been assessed by performing Temperature-Programmed Desorption (TPD) of adsorbed hexane from the catalyst surface. It is anticipated that the hydrocarbon thermal desorption technique will probe the nature of the supported metal clusters, provide information on hydrocarbon reaction mechanism and elucidate the reasons for the improved performance of bimetallic catalysts.

Before the desorption results are presented the hydrocarbon desorption technique will be briefly described. This is followed by an introduction to metal-catalysed hydrocarbon reactions, including a review of papers on hydrocarbon conversion over bimetallic platinum-iridium catalysts. The purpose of this Section is to establish the mechanisms of hydrocarbon reactions and the typical conversion properties of bimetallic catalysts observed under isothermal conditions. As a further aid to the interpretation of the results the final Section includes a review of the hydrocarbon desorption studies performed on platinum and iridium single crystal surfaces and supported metal catalysts.

7.1.2 Hydrocarbon Thermal Desorption

The hydrocarbon thermal desorption technique is similar in principle to the hydrogen thermal desorption technique described in Section 5.1. Following catalyst pretreatment the hydrocarbon under investigation is adsorbed on the sample at room temperature. The sample is then heated and adsorbate desorption followed as outlined in Section 5.1. In addition, the adsorption of the hydrocarbon and subsequent heating can cause the hydrocarbon to react on the catalyst surface resulting in the formation of new hydrocarbon species. Some products may desorb whilst others remain on the surface to undergo further conversion. Furthermore, desorbed products can

readsorb on the support where further reaction may occur. The new products can also desorb and react further over the metal sites. As outlined by Falconer and Schwartz (1983), such processes may also occur under practical catalyst conditions and the technique may therefore be a good mimic of isothermal catalytic reactions. Sklyarov et al. (1978) have concluded that under appropriate experimental conditions isothermal reaction intermediates can appear in the desorption profile. Thus the technique can provide information on the mechanism of reactions observed under isotherm conditions.

The complexity of the reaction processes is the most likely reason why this powerful technique has received relatively little attention in the literature. In this study the use of a computer interfaced mass spectrometer has enabled simultaneous desorption of multiple reaction products to be followed.

Provided readsorption effects are not too significant the kinetics of the reaction process can be evaluated from an analysis of the desorption profiles, using the procedures outlined in Section 5.1. Komers et al. (1969) carried out such an analysis for the hydrogenolysis of ethylene on silica-supported platinum. However, the evaluation of kinetic parameters has not been attempted in this study. Instead the emphasis has been placed on a comparison of the desorption profiles obtained for catalysts of different composition and subjected to different pretreatments. This has enabled the catalyst samples to be characterised and information to be obtained about the hydrocarbon reaction mechanism. Moreover, such experiments can identify the factors responsible for the improved performance of bimetallic platinum-iridium catalysts compared to their monometallic counterparts.

7.1.3 Metal Catalysed Hydrocarbon Conversions

a) General Survey

The reaction of hydrocarbons over metal and supported metal catalysts has been intensively studied primarily because of the commercial importance of the reforming process used for the conversion of petroleum naptha into high octane fuel. This process is usually carried out at temperatures of 750K and pressures around 10 atm. using a hydrogen-hydrocarbon feed ratio of around 6:1. Excess hydrogen is necessary to prolong catalyst life. Under these

operating conditions the main reactions observed in the process are:

- Isomerisation of alkanes.
- Dehydroisomerisation of alkylcyclopentanes to aromatics.
- Dehydrogenation of napthenes to aromatics.
- Dehydrocyclisation of alkanes to aromatics.
- Hydrogenolysis of parent hydrocarbons to lower molecular weight species.

Aromatic compounds and branched isomers are desirable products of the reforming process, whilst excessive hydrogenolysis is an undesirable reaction since it leads to production of fuels of excessive volatility.

The conversion of hydrocarbons over alumina-supported platinum catalysts was originally explained by Mills et al. (1953) in terms of a mechanism which recognised the bifunctional character of these catalysts. The metal centres were thought to act as hydrogenation/dehydrogenation sites whilst acidic centres on the alumina support promoted C-C bond rearrangements via the formation of carbonium ion species. Gas phase transport of the various intermediates between the two catalytic centres was thought to result in a series of reactions which eventually leads to the isomerisation and aromatisation of alkanes. More recently bifunctional behaviour during catalytic reforming has been discussed by Ciapetta and Wallace (1972).

However, it was eventually realised that hydrocarbon skeletal rearrangements could also occur on the surface of the metal without the participation of the support. Reviews on the topic have been published by Anderson (1973), Clarke (1975), Clarke and Rooney (1976), Paal (1980), Gault (1981) and Ponec (1983). The relative importance of the two routes is generally dependent on the reaction conditions used. Christoffel and Paal (1982) concluded that at temperatures below ~620K platinum catalysed reactions are dominant, whilst above this temperature the bifunctional mechanism becomes more important. Earlier Silvestri et al. (1969) observed that pretreatments involving sulphurisation (included to reduce the hydrogenolysis activity of the catalysts) reduced the metal cyclisation route under reforming conditions.

With the sulphur-free catalysts used in this study and at the low temperatures used during thermal desorption experiments, metal catalysed reactions are expected to be important. Therefore in order to aid the interpretation of the thermal desorption experiments this Section includes a brief introduction to three important metal catalysed hydrocarbon processes namely isomerisation, dehydrocyclisation (aromatisation) and hydrogenolysis. For more detailed accounts of these processes the reader should refer to the reviews previously mentioned.

b) Isomerisation

The skeletal isomerisation of hydrocarbons over platinum metals can occur by two alternative mechanisms as shown in scheme 7.S1

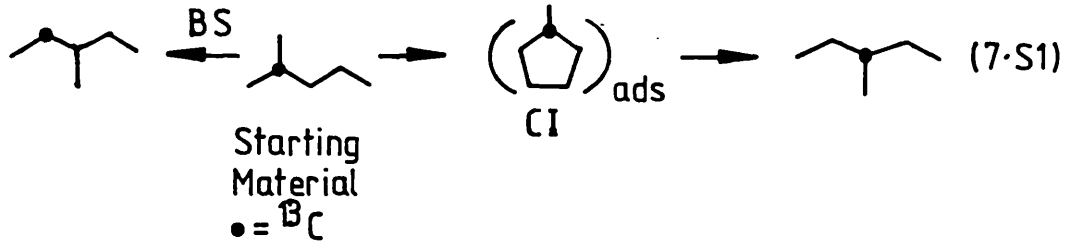

(7·S1)

Anderson and Avery (1966) proposed the Bond Shift (BS) mechanism for the isomerisation of light alkanes (e.g. propane) which involves a simple C-C bond displacement. The second route requires the formation of a cyclopentane Cyclic Intermediate (CI) and was proposed by Barron et al. (1966). This pathway is restricted to hydrocarbons containing a sufficient number of carbon atoms to form the ring.

The results of experiments performed by Corolleur et al. (1972a, 1972b) using ^{13}C labelled molecules showed that the BS mechanism predominates on supported catalysts of low dispersion, whilst the CI mechanism was more predominant on catalysts with a smaller metal particle size. In addition, the CI mechanism was categorised according to the way in which the intermediate underwent ring opening; non-selective ring opening (NSCI) took place on highly dispersed samples, whilst selective rupture of bisecondary C-C bonds (SCI) occurred on less dispersed catalysts. However, the relative importance of the two pathways is also dependant upon the metal used, for instance with iridium, Weisang and Gault (1979)

observed that the major isomerisation process was via the SCI pathway irrespective of the degree of dispersion of the metal. Another important factor is the amount of carbonaceous material present on the metal surface. Van Senden et al. (1984) have proposed that the CI mechanism becomes less selective in the presence of carbon.

Despite a widespread consensus about the existence of two distinct isomerisation pathways there is very little agreement about the mechanistic details for such conversions. Anderson and Avery (1966) proposed that the BS mechanism involves an unsaturated intermediate polyadsorbed at position 1,3. However, McKery et al. (1973) argued that it involves a σ-adsorbed alkyl species bound to a single metal atom. Gault et al. (1979a) also favoured a single metal atom site but insisted that metallocycloalkanes are intermediates in this isomerisation. Finally, Garin et al. (1982), using hydrocarbon isomerisation over stepped single crystal surfaces, concluded that BS isomerisation requires the participation of two metal atoms possibly located at step positions.

Disagreement also exists over the nature of the two CI processes. Gault et al. (1979b) have suggested the formation of a 1,5 dicarbyne intermediate bound to two metal atom sites for the SCI pathway, whilst the NSCI processes were supposed to involve a 1,5 dicarbyne bound to a single metal atom. However, Finlayson et al. (1984) rejected these models in favour of SCI isomerisation involving a 1,5 di-σ-adsorbed cyclic intermediate bound at a single metal atom. The NSCI route was attributed to interconversion on a single metal atom of a π-allyl to pentadienyl or σ-alkyl to π-alkene species. Paal (1980) has suggested a multiplet mechanism whereby adsorption occurs on a small cluster of metal atoms; planar adsorption results in an NSCI process whilst edge adsorption produces the SCI products.

Many workers have attempted to link changes in the mode of isomerisation to the presence of different catalytically active sites on large and small metal particles. Such particle size effects have been reviewed recently by Anderson (1985) and Burch (1985). Atoms at corner, edge, kink or B_5 positions have often been identified as the sites responsible for the NSCI process, whilst BS and SCI pathways are thought to be confined to sites occurring on

low index planes. However, Gault (1981) dismissed such interpretations since products of the CI process did not vary with metal dispersion in the manner expected for a statistical distribution of such sites on metal particles of various size. Instead it was proposed that the electronic properties of the metal particles primarily determine the nature of the isomerisation process, with BS and CI reactions occurring on topographically similar sites. It was proposed that the change from SCI to NSCI products arose from a geometric effect although the results of van Senden et al. (1984) indicate that the formation of carbonaceous deposits may also be important.

c) Dehydrocyclisation (Aromatisation)

In this discussion the term dehydrocyclisation is used to describe the formation of aromatic products from acyclic alkanes. A recent review of dehydrocyclisation processes has been published by Sharan (1984).

Davis and Venuto (1969) have proposed that dehydrocyclisation occurs via a 1,6 ring closure step in which hexane directly cyclises to cyclohexane over the metal before being dehydrogenated to benzene. However, Lester (1969) concluded that the formation of a C_5 ring intermediate by a 1,5 cyclisation step was the likely route for the dehydrocyclisation of methyl substituted pentanes. This intermediate would subsequently undergo ring expansion to form a C_6 ring. One way in which this might occur would be by isomerisation of the methyl pentanes via the CI mechanism, as outlined in the previous section, to form a C_6 species which could then undergo direct 1,6 cyclisation. Alternatively the 1,5 ring closure might be followed by ring opening and 1,6 ring closure, all occurring during a single residence on the metal site. Amir-Ebrahimi et al. (1980) have suggested such a mechanism in which the ring expansion occurs by a carbene-alkene addition reaction.

Dautzenberg and Plateeuw (1970) suggested a cyclisation step involving a thermally activated 1,6 ring closure of hexatriene to cyclohexadiene as an alternative to the metal catalysed ring closure mechanism. Paal and Tetenyi (1973) have also proposed such a mechanism but maintained that the metal catalysed the 1,6 cyclisation of the hexatriene. The formation of hexatriene species is

likely to be more prevalent under conditions of low hydrogen partial pressure and hence will not be significant during reforming. However, the thermal desorption work described in this chapter were performed in the absence of a hydrogen-containing carrier gas and hence such a process may be important in these experiments.

Somorjai and coworkers have carried out extensive investigations of alkane dehydrocyclisation over single crystal metal surfaces. A particularly lucid account of their work has been published by Davis and Somorjai (1982). These workers have found that dehydrocyclisation occurs most readily on platinum surfaces containing steps rather than just flat planes, and this is true at both high and low reaction pressures. Optimum conversion was obtained with terraces of intermediate width (4-7 atoms) which were just large enough to accomodate chemisorbed reactants and products. It was proposed that dehydrocyclisation occurred preferentially over platinum catalysts at low coordination step sites because the unique stereochemistry and electronic properties of such sites facilitated the formation of C_5 and C_6 metallocyclic ring species. On platinum single crystal surfaces and at low reaction pressures the reaction was further promoted by the presence of an ordered (9 x 9) carbon overlayer. This was attributed to a 'template' effect whereby the ordered carbon created sites with the specific size or orientational requirements necessary for high cyclisation activity.

Dehydrocyclisation also occurs over iridium metal. Karpinski and Clarke (1975) observed that both the 1,5 and 1,6 ring closure routes were possible for iridium. In contrast to platinum Nieuwenhuys and Somorjai (1977) found no significant differences in dehydrocyclisation activity between stepped and flat Ir(111) surfaces or Ir(111) precovered with a (9 x 9) carbon overlayer. Further discussion of the dehydrocyclisation activity of supported iridium catalysts will be deferred to Section 7.1.3e).

d) Hydrogenolysis

Only the formation of lower molecular weight hydrocarbons from a parent molecule as a result of C-C bond breaking will be discussed in this Section. Ring opening of cyclic species has already been described in Section 7.1.3b.

Hydrogenolysis of C-C σ bonds has been widely investigated and the work has been reviewed by Sinfelt (1973) and Paal and Tetenyi (1982). The sequence of steps generally postulated for the reaction mechanism includes:

i) Chemisorption of a hydrocarbon reactant with dissociation of C-H bonds to form an unsaturated residue.

ii) Rupture of the C-C bonds in the surface residue.

iii) Hydrogenation of the species formed in step (ii) to form the products of the reaction. Alternatively, some of the adsorbed hydrocarbon fragments may remain on the catalyst surface and eventually result in catalyst deactivation. This situation is usually favoured by the use of low hydrogen partial pressures during the reaction.

Thus, hydrogenolysis reactions usually require an ensemble of metal atom sites and are found to be structure sensitive. Hydrogenolysis activity is usually dependent on such factors as the reaction conditions, the metal and its degree of dispersion and the pretreatment used during catalyst preparation. Low hydrogen partial pressure and high temperatures favour hydrogenolysis reactions, as identified by Cimino et al. (1954). Of particular significance was the observation of Carter et al. (1971) that the hydrogenolysis activity of iridium was approximately five orders of magnitude greater than that of platinum. These authors correlated hydrogenolysis activity with the percentage d character of the metal and suggested that the reaction mechanism involved the formation of 1,3 diadsorbed intermediates. Gault (1981) has proposed that the high hydrogenolysis activity of iridium is related to its ability to easily form metallocarbene species.

Barbier and Marecot (1981) and Brunelle et al. (1976) have observed that the hydrogenolysis activity of iridium decreases as the dispersion of the supported metal increases. Similar results were found by Anderson and Shimoyana (1973) for hydrogenolysis of hexane over platinum films. This behaviour may be attributed to a

decrease in the concentration of the active low coordination number sites, that are responsible for C-C bond breaking. Blakely and Somorjai (1976) have observed that kink sites on Pt single crystals are especially important for C-C bond breaking at low reaction pressures. However, the picture is unclear since Foger and Anderson (1979) found that iridium hydrogenolysis activity was independent of particle size over the range 1-7nm.

Catalyst pretreatment can also markedly affect the hydrogenolysis activity of supported metals. Den Otter and Dautzenberg (1978) were among the first to observe that a reduction pretreatment in the temperature range 680-800K reduced the hydrogenolysis activity of alumina-supported platinum, without causing an apparent growth in metal particle size. Several explanations have been offered to account for this phenomenon but they will not be discussed at this stage. The effect is important since it provides an alternative method to sulphurisation for reducing the hydrogenolysis activity of catalysts used in the reforming process. Similar hydrogenolysis passivation for the bimetallic Pt-Re/alumina system has been reported by Parera et al. (1984). However, such a phenomenon has not been previously reported for the Pt-Ir/alumina system. The hydrocarbon desorption results presented in Section 7.3 will show the extent and nature of hydrogenolysis passivation for this system following high temperature reduction pretreatments.

To conclude, hydrocarbon conversions over metal surfaces are extremely complex processes. Even after the extensive research effort that has been undertaken over the past fifty years many aspects of the interactions of hydrocarbons with supported metal catalysts remain incompletely understood. Factors which can be important for many of these reactions include metal particle size, morphology and composition, reaction conditions, hydrocarbon structure, metal-support interactions (both chemical and electronic) and the presence of poisons and promoters (e.g. carbon and sulphur).

e) Hydrocarbon Conversion over Pt-Ir Catalysts

Sinfelt (1983) has discussed the industrial use of bimetallic Pt-Ir/alumina catalysts in the reforming process. Such catalysts replaced their original monometallic platinum counterparts because of their improved reformate yield and increased resistance to

deactivation. Several studies have been published in the open literature which try to identify the reasons for this improved performance.

Ramaswamy et al. (1976) in a study of heptane conversion over a Pt(90 at%)-Ir(10 at%)/alumina catalyst observed that the presence of iridium leads to the increased formation of hydrogenolysis products, a lowering of coke formation and a decrease in dehydrogenation activity relative to a monometallic platinum sample. The high rate of coke formation with platinum was attributed to the dehydrogenation activity of platinum which would result in the production of olefinic intermediates and cause catalyst fouling. However, it was argued that the incorporation of an element of lower dehydrogenation activity such as iridium causes a dilution effect which results in a lower concentration of coke precursors.

Rasser et al. (1979) studied the reactions of hexane and heptane at 650K over Pt-Ir alloy Kuliphay powders and alumina-supported samples. These workers prepared their catalysts by oxidation at 820K followed by reduction at 650K. By the use of AES it was observed that alloy powders exhibited a surface enrichment in platinum and that iridium-containing samples were much more easily freed from carbon by treatment in hydrogen. The catalytic reactivity of these powders and the supported samples were very similar to those of the monometallic platinum catalysts and no observed improvement in aromatisation (dehydrocyclisation) selectivity was observed. However, a lower rate of catalyst fouling was reported. The improved activity maintenance of the bimetallic samples was attributed to a mechanism in which carbon atoms deposited on platinum sites migrated to iridium sites where hydrogenation to gas phase methane occurred.

Charcosset et al. (1979b) carried out heptane conversion over alumina-supported platinum-iridium catalysts containing metal particles in the size range 100-200Å. Catalyst reduction was carried out up to temperatures of 1200K and XRD measurements showed that the presence of iridium prevented alloy formation between the platinum and the support. The hydrogenolysis activity of the iridium-containing samples was generally higher than that of the monometallic platinum sample but the latter sample exhibited a

higher isomerisation and cyclisation activity. Surface enrichment in platinum was not apparent from the hydrocarbon conversion results.

Rice and Lu (1982) further examined the role of iridium in an alumina-supported platinum-rich catalyst. The conversion of heptane was studied over the monometallic and bimetallic systems at temperatures of 755K and pressures of 135 and 790 kPa. Catalyst pretreatment involved oxidation at 615K, followed by reduction at 755K and finally sulphurisation at 615K. The iridium sample was observed to have a higher activity for dehydrocyclisation and hydrogenolysis than the platinum sample. In the bimetallic catalyst the iridium component imparted superior dehydrocyclisation activity and deactivation resistance relative to the platinum sample when reaction was carried out under the high pressures typical of those used in reforming. At low pressures the iridium sample was vulnerable to coking, which was attributed to a high dehydrocyclisation activity resulting in a higher surface concentration of olefinic precursors. However, the coke formation was suppressed in the bimetallic sample probably because of a cooperative interaction between the two metals resulting in an increased ability to hydrogenate off the coke precursors. Unfortunately, the bimetallic sample, even when sulphided, exhibited an undesirably high hydrogenolysis activity. Apesteguia and Barbier (1982) also investigated the effect of catalyst presulphurisation and observed that addition of iridium to platinum-containing samples increases the sulphur resistance of the platinum.

McVicker et al. (1982) carried out model compound reforming studies over alumina-supported platinum and iridium catalysts. The platinum catalyst was subjected to a pretreatment involving oxidation at 773K followed by reduction at the same temperature, whilst the iridium sample was oxidised at 543K prior to reduction at 773K. The platinum catalyst was found to be more active and selective than the iridium catalyst for the aromatisation of cyclohexane and methyl cyclopentane. On the other hand the iridium sample was observed to be a more active and selective heptane dehydrocyclisation catalyst. However, the hydrogenolysis activity of the iridium was greater. Feed sulphur levels of 0.1 to 10ppm had little effect on the heptane conversion pattern of platinum samples but significantly lowered the hydrogenolysis activity of the iridium catalyst.

Carter et al. (1982) have reported similar results to those obtained by McVicker et al. (1982) for hydrocarbon conversions over Ir/alumina catalysts. The former workers also examined conversions over Pt-Ir/alumina catalysts and found that rates of dehydrocyclisation of heptane for iridium-containing samples were more than twice the rate for the monometallic platinum catalyst. However, the iridium-containing catalysts exhibited a higher hydrogenolysis activity than the platinum sample. The improved activity maintenance of the bimetallic samples was attributed to the higher hydrogenolysis activity of the iridium component which resulted in the hydrogenation of coke precursors from the sample surface.

McVicker and Ziemiack (1985) have examined the effect of iridium agglomeration on the performance of alumina-supported platinum-iridium catalysts. Iridium agglomeration was produced by oxidation at temperatures above 773K prior to reduction at 773K and sulphurisation at 640K. The conversion of heptane over the bimetallic catalyst was found to become like that over platinum as the extent of iridium agglomeration was increased. An inverse correlation was found between the rate of heptane dehydrocyclisation and the degree of iridium agglomeration.

To summarise, alumina-supported iridium catalysts have a higher dehydrocyclisation activity than their monometallic platinum counterparts. However, the high hydrogenolysis activity of the former precludes their use in the reforming process. The importance of iridium is related to its anti-coking properties. Thus under reforming conditions when a high partial pressure of hydrogen is present, the surface of the Ir/alumina catalysts is kept clean of coke most probably as a result of the high hydrogenolysis activity of these samples. However, this activity can lead to opposite results, namely rapid coking, under conditions of low hydrogen partial pressure. The improved activity maintenance of bimetallic platinum-iridium catalysts, compared to their platinum counterpart, may result from a lower rate of formation of carbonaceous residues on the catalyst. This is most likely due to the increased hydrogenolysis activity produced by the presence of iridium which is sufficient to hydrogenate coke precursors from the catalyst surface without substantially affecting the yield of C_{6+} hydrocarbons. One

of the reasons for performing the hydrocarbon desorption experiments described in Section 7.3 was to provide further information on the hydrogenolysis activity of the bimetallic catalyst.

7.1.4 Hydrocarbon Thermal Desorption Studies

The first part of this Section contains a selective review of hydrocarbon desorption studies performed on platinum and iridium single crystal surfaces. No attempt has been made to provide a comprehensive and critical survey of all the work performed with metal single crystals. Results obtained with other techniques (e.g. EELS and LEED) are also included where these help to establish the nature of the processes observed during the desorption experiments. The aim of this review is to establish a firm basis for the interpretation of the desorption profiles presented in Section 7.3. This is especially necessary since similar experiments performed with supported metal catalysts have not been widely reported. The final part of this Section contains a brief review of the work published by a Soviet group which has made the most extensive use of the technique when applied to supported metal systems.

a) Platinum Surfaces

Demuth (1979) studied the thermal desorption of ethylene and acetylene following room temperature adsorption of these hydrocarbons on a Pt(111) surface. The only desorption products obtained were the parent hydrocarbon and hydrogen. Ethylene desorbed between 350 and 450K whilst hydrogen produced peaks at around 370, 490 and 590K. Similar behaviour was observed for acetylene although the 370K hydrogen peak was absent. It was proposed that ethylene dehydrogenated at room temperature to form a C_2H_3 species, with the removed hydrogen bound to the metal surface. The 370K hydrogen peak was attributed to the desorption of the latter. A vinyl species ($H_2C{=}CH$) was suggested for the dehydrogenated ethylene complex whilst the acetylene was thought to form a $H_2C{=}C$ type complex. The hydrogen peaks at 490K and 590K were considered to arise from the decomposition of these species.

There has been much controversy concerning the nature of the adsorbed hydrocarbon species and the views of Demuth are not now generally accepted. The matter appears to have been resolved by

Kesmodel et al. (1979) whose model is based on a LEED intensity analysis and a re-interpretation of the EELS results published by Ibach and Lehwald (1978). It was shown that ethylene and acetylene chemisorbed associatively below 300K on Pt(111) forming (2 x 2) structures in which the C-C bond was orientated parallel to the surface. These species were metastable and could be transormed by heating to 310K into a stable phase which maintained the (2 x 2) structure. Addition of hydrogen was required for acetylene to complete this transformation. It was proposed that this new phase was an ethylidyne molecule with the C-C bond axis perpendicular to the metal surface and the α-carbon bound to three metal atoms. Koestner et al. (1982) have observed the formation of similar alkylidyne species for a number of C_3 and C_4 unsaturated hydrocarbons.

Salmeron and Somorjai (1982) studied the desorption of ethylene, propylene and butenes from Pt(111) and interpreted their results as arising from the formation and decomposition of alkylidyne species. The desorption of undissociated olefin was observed around 280K but no other hydrocarbon products were formed. Hydrogen desorption peaks were found in three temperature regions. The lowest temperature peak at 295K was attributed to the production of hydrogen arising from the formation of alkylidyne species. Experiments performed using acetylene did not produce this peak and it was concluded that acetylene converts to vinylidene species under hydrogen deficient conditions. Further hydrogen desorption occurred in the temperature range 380-490K and this was associated with the decomposition of the alkylidyne species. The highest temperature hydrogen desorption feature was broad and contained three peaks at temperatures of around 550, 640 and 710K which were thought to result from the complete dehydrogenation of disordered surface hydrocarbon residues.

Avery and Sheppard (1986a, 1986b) have also observed the formation of alkylidyne species following the adsorption of unsaturated hydrocarbons on Pt(111). These species decomposed above 300K and it was estimated that at temperatures around 450K adsorbed hydrocarbon fragments had compositions of approximately C_3H_2 for the species derived from propene, C_4H_2 from but-1-ene and C_4H_4 from isobutenes. Previously, Steininger et al. (1982), using EELS, had observed that ethylidyne species decomposed to CH or CH_2 residues at temperatures of around 415-510K on Pt(111).

Wang et al. (1985) have used NMR to determine the structure of ethylene adsorbed at room temperature on small platinum clusters supported on alumina. It was concluded that ethylidyne species were formed which underwent C-C bond rupture in the temperature range 390-480K. However, in contrast to single crystal studies the decomposition was found to result in the formation of single carbon atoms, with no attached hydrogen, and a small amount of adsorbed methyl species.

The decomposition of hydrocarbons on platinum single crystal surfaces at elevated temperatures has been studied by Baron et al. (1974). These workers found that hydrocarbons adsorbed on a Pt(111) surface (at temperatures of 770K) were entirely decomposed to carbon and formed a rotationally disordered graphitic structure. A similar effect was observed for the Pt(S)-[9(111)x(100)] stepped surface. However, on a Pt(S)-[6(111)x(100)] surface high temperature heat treatment resulted in the formation of an ordered carbonaceous overlayer. This was attributed to the dehydrogenation activity of the stepped sites which promoted the nucleation and growth of the ordered structure. On the Pt(S)-[7(111)x(310)] kinked surface the rate of hydrocarbon decomposition was found to be very rapid and no ordered carbonaceous layer was produced.

Whilst the thermal desorption of unsaturated hydrocarbons from Pt surfaces has been fairly extensively investigated similar experiments using acyclic saturated hydrocarbons (e.g. hexane) have received scant attention. However, such compounds may also form alkylidyne species and hence similar desorption behaviour could be expected. From an investigation into the structure sensitivity of hexane skeletal rearrangement reactions on platinum single crystal surfaces, Davis et al. (1984) have proposed that one route for the hydrogenolysis of hexane involves the formation of alkylidyne species.

The desorption of cyclic hydrocarbon from platinum surfaces has also received widespread attention and the results of several studies are summarised below. Avery (1984), using EELS and thermal desorption techniques, has observed that cyclopentane is di σ-bonded at temperatures below 250K. Thermal desorption results in the production of hydrogen with peaks at temperatures around 305, 570, 620

and 720K. The only hydrocarbon desorbed was cyclopentene at around 285K. However, at 250-300K the adsorbed hydrocarbon did not form an alkylidyne species but partially dehydrogenated to form an adsorbed cyclopentadienyl species which subsequently decomposed producing hydrogen at temperatures above 480K. The formation of this species is significant since it has been proposed that hydrocarbon isomerisation over supported catalysts occurs by a C_5 ring mechanism (see Section 7.1.3b). Similar results have been reported by Avery (1985) for cyclopentane adsorption on Pt(111).

Tsai and coworkers (1982a, 1982b, 1982c) have made an extensive investigation of the thermal desorption of cyclohexane, cyclohexene, cyclohexadiene, benzene and toluene on Pt(111), Pt(100) and Pt(S)-[6(111)x(111)] surfaces. Experiments performed using benzene (1982a) produced several high temperature hydrogen desorption peaks in the temperature range 443-653K which were associated with the decomposition of the irreversibly held hydrocarbon. In addition, reversibly held benzene desorbed at temperatures below ~500K. Similar results were obtained for toluene although on the stepped surface all the adsorbed toluene underwent decomposition. Cyclohexane adsorption (1982b) on the (111) plane was nearly reversible at 273K, although some hydrogen desorption was observed which gave peaks similar to those found for benzene desorption. This was attributed to the formation and decomposition of benzene on the metal surface. Cyclohexane interacted more strongly with the stepped surface and more intense hydrogen peaks were obtained. For both the flat and stepped single crystals the desorption profiles for cyclohexene and cyclohexadiene were similar. These compounds also produced the high temperature hydrogen desorption peaks although no parent hydrocarbon desorption was observed. Significantly, benzene production was observed at temperatures around 393K, this being the only desorption experiment in which products other than the parent hydrocarbon and hydrogen have been detected. This probably reflects the facile conversion required for the production of benzene from such starting materials. Similar results were found when the Pt(110) surface (1982c), was used although the use of deuterated compounds showed that C-H bond breaking was largely reversible on this surface in contrast to the irreversible scission observed for the (111) surface.

To summarise, hydrocarbon adsorption on most platinum surfaces results in the formation of ordered hydrocarbon surface structures. Adsorption of acyclic, unsaturated (and possibly saturated) hydrocarbons leads to the formation of alkylidyne species at temperatures slightly above room temperature. Upon further heating these species decompose releasing hydrogen and leaving hydrocarbon fragments in a disordered state on the metal surface. No hydrocarbon product other than the parent species is detected during any stage of the heating process. On the other hand adsorbed cyclic hydrocarbons usually retain their cyclic structure at low temperatures but decomposition and fragmentation finally ensues as the temperature is raised. Benzene formation can result following the adsorption of C_6 ring hydrocarbons although desorption of benzene is only detected with cycloolefin adsorbates.

As the temperature is raised even higher any remaining hydrocarbon fragments break down, liberating more hydrogen, and at temperatures around 800K disordered graphitic structures are frequently observed. However, this is dependent on the platinum surface structure since some stepped surfaces can produce an ordered graphitic structure.

b) Iridium Surfaces

Nieuwenhuys et al. (1976) have used LEED to study the interaction of ethylene, acetylene, cyclohexane and benzene with the Ir(111) and Ir(S)-[6(111)x(100)] surfaces. The formation of poorly ordered structures was observed with all adsorbates on both surfaces at 300K. Heating the (111) surface above 1073K, in the presence of hydrocarbon, resulted in the formation of an ordered carbonaceous overlayer with a (9 x 9) surface structure. With the stepped surface the (100) steps prevented the formation of such an ordered overlayer. Thermal desorption experiments showed that benzene was the only adsorbate that could be desorbed in large quantities; a desorption peak occurring at a temperature around 430K. Ethylene remained largely on the metal, whilst acetylene and cyclohexane could not be desorbed at all. The main product of the thermal desorption experiment was hydrogen, which desorbed in two peaks at temperatures around 473K and 620K for both surfaces. The hydrogen desorption behaviour was only slightly dependent on the hydrocarbon

used, although cyclohexane produced a smaller low temperature peak. Adsorption at 573K resulted in the production of the high temperature hydrogen peak only. This peak was more intense during desorption experiments performed on the stepped surface.

It was concluded that the low temperature hydrogen peak resulted from desorption from the metal whilst the high temperature peak was due to hydrogen production arising from the decomposition of adsorbed hydrocarbon fragments. Furthermore, it was suggested that the lower degree of adsorbate ordering, observed at 300K, with the iridium surfaces as compared to the platimum surfaces was due to easier adsorbate fragmentation occurring on the iridium. This was attributed to an electronic effect whereby iridium with one less d-electron, permitted greater electron donation from the adsorbate resulting in a weakening of bonds within the hydrocarbon molecule.

Nieuwenhuys and Somorjai (1978) extended this study by examining the adsorption of ethylene and benzene on the reconstructed Ir(110) surface. These workers also found that these hydrocarbons did not form ordered structures on this surface at 300K. However, heating to 1000K in the presence of the hydrocarbon resulted in the formation of a carbonaceous overlayer with a perfect (1 x 1) periodicity. It was concluded that this overlayer was in direct registry with the iridium substrate, thereby showing that the M-C bond is stronger than the C-C bond with iridium. This is in direct contrast with the graphitic overlayer on platinum surfaces which are independent of the substrate periodicity.

Weinberg and coworkers have studied the chemisorption and thermal desorption of several hydrocarbons on the reconstructed Ir(110) surface. Wittrig et al. (1982a, 1982b, 1982c) have examined the interaction of ethane, propane, cyclopropane, isobutane and neopentane, whilst Szuromi et al. (1984) have investigated adsorption and reaction of propylene, propyne and allene. Szuromi and Weinberg (1985) have extended these studies by performing similar experiments using butane, pentane, hexane and heptane.

In general, it was found that ordered carbonaceous overlayers were not formed. The parent hydrocarbon was found to desorb at temperatures around 150K but no other peaks attributable to hydrocarbons were observed. The main product observed in all experiments

was hydrogen which desorbed with peaks at temperatures around 300, 410 and 520K. The only exception was ethane which had a single peak at 410K. In all cases the 410K peak was attributed to desorption from the metal surface (β_2 sites), whilst the peaks at 300K and 520K were assigned to hydrogen produced, from the breakdown of hydrocarbon fragments. The average composition of the more stable fragments were estimated to be C_2H_0 (ethane), C_3H_2 (propene, propane, cyclopropane allene and propyne), C_4H_1 (butane), C_4H_4 (isobutane), C_5H_4 (neopentane and pentane), C_6H_2 (hexane) and C_7H_6 (heptane). Similar hydrocarbon fragments have been found by Avery and Sheppard (1986a) for the species derived from propene and isobutane on Pt(111).

The desorption behaviour was explained by proposing that hydrocarbon chemisorption was dissociative at temperatures around 130K, the released hydrogen occupied the β_2 sites whilst the presence of the adsorbed hydrocarbon blocked the filling of the hydrogen β_1 sites (Tm ~200K). Once the β_2 sites were saturated further hydrocarbon adsorption could occur in a non-dissociative form. Preadsorbed hydrogen was found to impede the dissociative adsorption process. It was suggested that C_3 hydrocarbons dissociated to form metallocyclic rings containing three carbon atoms, two of which were completely dehydrogenated and bonded to the metal. The 520K peak was thought to arise from the removal of hydrogen from the CH_2 group in the ring. The formation of extended ring structures was proposed for hydrocarbons containing an odd number of carbon atoms but the low hydrogen content of the fragments found for even-number hydrocarbons required that such species were more extensively decomposed. The reason for this difference in behaviour is unclear. The extent of hydrocarbon decomposition was found to be dependent upon the availability of vacant β_2 sites. Where these sites were not available the hydrocarbon fragments were thought to be less stable, decomposition occurring at around 300K and giving rise to the hydrogen peak observed at this temperature.

In brief, hydrocarbon adsorption on iridium surfaces at around room temperature results in the formation of poorly ordered adsorbate surface structures. This indicates that alkylidyne species are not formed on the iridium surface, the metal causing a more extensive breakdown of the hydrocarbon adsorbate as compared to

platinum. The thermal desorption profiles for iridium and platinum surfaces have some features in common and it appears that similar fragments can form and decompose on both metals. However, the structure of the carbonaceous overlayers formed following excessive heat treatment is dependent on the metal used. The underlying periodicity of the iridium surface structure (when steps are absent) dictates the structure of the overlayer. This is in contrast to the corresponding platinum surfaces on which rotationally disordered graphitic overlayers are formed. Small differences between the electronic structures of the two metals is the most likely cause of the above.

To conclude, the hydrocarbon desorption profiles for platinum and iridium single crystal surfaces generally show that only parent hydrocarbon and hydrogen are liberated during the desorption experiment. Hydrogen desorption occurs from the metal surface and is also produced from the decomposition of surface hydrocarbon residues. The majority of the carbon remains on the surface.

To determine the effect of hydrocarbon residues on the desorption spectra from supported metals a sequence of adsorption-desorption experiments have been performed on the same sample and the results will be discussed in Section 7.3.

c) Supported Metal Studies

The thermal desorption of higher hydrocarbons from supported metal catalyst surfaces has received little attention. Indeed only Sklyarov and his coworkers have made an extensive use of the technique using a vacuum flow system with a mass spectrometer for product analysis. This Section will describe the published results of this group.

Walkov et al. (1977) examined the reactions of benzene, cyclohexane and heptane during thermal desorption from alumina-supported Pt, Pt-Pb and Pt-Sn catalysts which had previously been reduced at 753K. Unfortunately these workers did not monitor the hydrogen signal during the desorption experiments. The desorption spectrum for samples exposed to benzene at room temperature contained a benzene peak at around 380K and an ethylene peak at temperatures around 523K. Experiments performed using cyclohexane

produced mainly benzene as a hydrocarbon product and this desorbed in two peaks at temperatures of 440K and 540K. It was found that incorporation of Sn or Pb into the catalysts reduced the amount of benzene formed. With heptane, desorption peaks appeared at 340K (heptane), 480K (benzene) and 540K (ethylene). In addition, a second dehydrocyclisation was observed which produced toluene and benzene at 590K and 630K respectively. It was concluded that benzene formation occurred via the cyclisation of a hexatriene intermediate which could also undergo hydrogenolysis to ethylene. Surprisingly carbon monoxide, carbon dioxide and water were produced at temperatures above 570K, during experiments involving all hydrocarbon starting materials. This was attributed to a reaction of hydrocarbon fragments wiht the hydroxyl groups on the support.

In a separate study Sklyarov et al. (1977) examined the reactions of heptane, toluene and benzene on a Pt/alumina catalyst. Results for heptane and benzene were similar to those obtained by Walkov et al. (1977). With toluene, desorption of benzene was observed at 623K and this process was identified with the similar desorption of benzene observed when heptane was the adsorbate. Since benzene itself produced a desorption peak at a much lower temperature it was concluded that benzene could form either directly from heptane or via a secondary conversion of toluene to benzene. Hence it was proposed that one possible pathway for the formation of benzene from heptane involves toluene as an intermediate. No methane was detected during any experiment and signals due to carbon monoxide, carbon dioxide, hydrogen and ethylene were not reported.

Rozanov et al. (1979) also investigated the dehydrocyclisation of heptane and observed that benzene and methane were desorbed simultaneously at a temperature of 593K. It was proposed that the methane signal was evidence for the demethylation of toluene to benzene.

Rozanov and Sklyarov (1978) used the TPD technique to examine the stepwise mechanism of hexane dehydrocyclisation on a Pt/alumina catalyst. Experiments were also performed with benzene and with possible reaction intermediates such as methyl cyclopentane (MCP) and hexatriene in an attempt to resolve the cyclisation mechanism. It was found that only the starting materials and benzene were

observed in the desorption spectrum. The former desorbed below 370K and this was attributed to desorption from the support. Benzene was observed as a dehydrocyclisation product with all starting materials, except MCP, and was produced in a peak around 490K. Experiments performed with MCP produced a benzene peak at 573K. By a further analysis of the desorption profiles produced using unsaturated cyclic and acyclic C_6 compounds it was concluded that hexane dehydrocyclisation does not occur via the C_5 ring pathway under the hydrogen deficient conditions used in their study. It was proposed that this conversion occurred by a stepwise mechanism possibly involving the cyclisation of hexatriene to cyclohexadiene. However, other possibilities such as cyclisation of hexadiene to cyclohexene were also thought to be possible. These workers did not observe the formation of oxygenated products. However, carbon monoxide and carbon dioxide were observed by Rozanov et al. (1982) in the hexane desorption profile when a pulsed laser was used to heat the sample. In this case it was thought that the laser pulse had initiated a reaction between hydrocarbon fragments and the support which resulted in CO and CO_2 formation.

Zimmer et al. (1982) have also carried out desorption experiments using n-C_6 hydrocarbons of various degrees of unsaturation from Pt/alumina and Pt black catalysts. The former were prepared by oxidation at 873K followed by reduction at 373K. The results were similar to those of Rozanov and Sklyarov (1978) and consequently similar conclusions concerning the dehydrocyclisation mechanism were made. However an important additional feature was the observation of hydrogen desorption peaks at temperatures of around 400K and 520K with an additional desorption process occurring above 575K. Benzene desorption at temperatures around 500K was observed for both catalysts and for all hydrocarbons used. This peak was structured and consisted of three overlapping peaks centred around 483, 503 and 527K. These peaks were attributed to the presence of a variety of dehydrogenated surface intermediates (benzene?) the decomposition of which required hydrogen. It was proposed that higher temperature benzene peaks represented the reaction of intermediate species in which C-H bond dissociation was more extensive. A small mass 15 peak was detected at temperatures around 530K, however no comment was made concerning the origin of this peak. Carbon monoxide and carbon dioxide production were not reported.

To conclude, the thermal desorption of higher hydrocarbons (C_6, C_7) has been used primarily to obtain information concerning the mechanism of dehydrocyclisation reactions over supported metal catalysts under hydrogen deficient conditions. The results obtained are consistent with the hexatriene cyclisation model proposed by Paal and Tetenyi (1973). In contrast to desorption experiments performed on single crystal surfaces, hydrocarbon reaction products are frequently observed to desorb from the catalyst. However, the above overview shows that many contradictions exist concerning the finer details of the desorption profiles. For example, within the same research group, there is disagreement over the temperatures at which products such as hydrogen, methane, ethylene, carbon monoxide and carbon dioxide desorb or, in some cases, whether they desorb at all. This may arise from differences in catalyst composition and the pretreatments used. In the present study, hexane thermal desorption experiments have been performed on catalyst samples subjected to a variety of pretreatments. It is envisaged that the desorption behaviour will probe the nature of the supported metal clusters and will also provide further information on the reactions of hydrocarbons over supported metal catalysts.

7.2 Experimental

Hexane thermal desorption experiments were performed in the micro-reactor system described in Chapter Two. During thermal desorption an argon carrier gas was passed over the catalyst at a flow rate of 12 $mlmin^{-1}$ and a pressure of 1-1.1 atm. Approximately linear temperature ramps of 12K min^{-1} were used for all temperature-programmed experiments.

The catalysts used in this study were prepared as outlined in Chapter Three and consisted of the two monometallic samples Pt100 and Ir100 and the bimetallic sample PtIr43. Fresh portions (50mg) of the samples were loaded into the reactor and subjected to one of the insitu preteatments outlined in Table 5.1.

Following the isothermal reduction stage of the pretreatment the sample was allowed to cool to 298K under hydrogen. Once this temperature was reached the hydrogen was removed from the carrier gas and the system was left (~40 mins.) to allow the non-adsorbed hydrogen to flush away. Spectroscopically pure hexane, supplied by

BDH Limited, was further purified in the gas handling system by pumping on the frozen material. The purified hexane was then pulsed over the catalyst using the reactant inject valve. A pulse containing approximately $5x10^{-7}$ mols of hexane was used and pulsing was continued until the catalyst was saturated with hydrocarbon. The amount of hexane from each dose that was not adsorbed was monitored by the mass spectrometer and hence the total quantity of hexane adsorbed could be calculated. Blank experiments, performed by bypassing the reactor, or using a pure alumina sample, showed that adsorption of adsorbate on the walls of the apparatus was negligible. Before the desorption experiment was started the system was left for approximately 10 mins to allow unadsorbed hexane to pump away from the mass spectrometer vacuum chamber. The mass spectrometer was used to detect the desorbed products as the catalyst temperature was slowly raised to a temperature of around 700K, after which the reactor was allowed to cool to 298K. Further doses of hexane were then admitted to the catalyst at this temperature and the desorption process was repeated.

To determine the nature of any hydrocarbon products formed during desorption the mass numbers shown in Table 7.1 were monitored in addition to those contained in Table 4.1. Repeat experiments were performed in order to cover the entire range of mass numbers given in both Tables. The amount of each corresponding product formed was determined in the manner described in Section 4.2.

Table 7.1: Additional* Species Monitored During Hexane Thermal Desorption Experiments

Hydrocarbon Species	Mass Numbers
Hexane	86,57
Benzene	78
Cyclohexane	56,84,41
Methylcyclopentane	56,84,69
Hexadienes	67,41,82
Hexenes	55,84
Hexatriene	79,80,39
Cyclohexadiene	79,80,27
Cyclohexene	67,54,82
Butane	43,58
Dimethylbenzenes	106
Toluene	91

* see also Table 4.1

7.3 Results and Interpretation

As in Section 5.3 the term hydrogen desorption profile, or more simply hydrogen profile, will be used to describe the variation of the mass 2 signal with temperature. The variation of the mass signals corresponding to other gases will be similarly expressed. The methane profile has been obtained from the mass 15 signal, for the reason outlined in Section 4.2. However, this was checked by inspecting the mass 16 profile, also recorded, to verify that the mass 15 signal did not arise from the production of other hydrocarbons. The entire collection of all the mass profiles will be referred to as the hexane thermal desorption profile. For purposes of comparison, the results of consecutive desorption experiments, performed on the same sample, are contained offset in the same figure. The upper portion of each figure contains the results for the first experiment, whilst the lower half contains the results for the second experiment, these thereafter being referred to as runs 1 and 2 respectively. For clarity the individual profiles are always presented in the same order and have been further designated by the subscript 1 or 2 to emphasise the run number for the profile. For example, the hydrogen profile for run 2 is labelled A_2 for all samples.

7.3.1 Samples Subjected to Pretreatment R610

The hexane thermal desorption profiles for samples Pt100, Ir100 and PtIr43 subjected to pretreatment R610 are shown in Figs. 7.1-7.3 respectively. Profiles are shown for the following species, with their profile labels in parenthesis; hydrogen ($A_{1,2}$), carbon dioxide ($B_{1,2}$), hexane ($C_{1,2}$), methane ($D_{1,2}$) and benzene ($E_{1,2}$). Included in the figures are the amounts of each desorption product with respect to a 50 mg sample. Thus to convert to mol gm^{-1} cat. all values should be multiplied by a factor of 20. Furthermore all quantities of hydrogen are given in moles of hydrogen atoms in the following description, whilst desorbed quantities are expressed as hydrogen to metal ratios in the figures. No signal was observed at the mass numbers corresponding to the species listed below following this, or any other, pretreatment; cyclohexane, methylcyclopentane, hexenes, hexadienes, hexatrienes, cyclohexane, cyclohexadiene, toluene, C_5 to C_2 species and water. Hence for reasons of clarity these desorption profiles are not included in the figures.

Table 7.2 contains the results of mass balance calculations performed for each of these desorption experiments. Appendix A2 gives further details concerning the various quantities listed in this Table and the method of their calculation. Also included in the Table are the amounts of metal present, M/mol; the quantity of hexane adsorbed, Hx_{ads}/mol; and the number of hydrogen atoms liberated, H_{lib}/mol, during the adsorption experiments carried out at 298K. In general, Hx_{ads} is around one tenth the value of M and this represents the amount of hydrocarbon initially present on the surface since no hydrocarbon species desorbed during the adsorption process. Because of the complexity of the results obtained, the results for the Pt100 sample are described in detail below before attention is given to the iridium-containing samples.

a) Pt100

In run 1 with the Pt100 sample a small amount of hexane is observed to desorb at a temperature of around 320K. Because of the small amount desorbing no conclusions concerning reactant isomerisation can be made. Similar results were obtained for all samples irrespective of the pretreatment conditions. Rozanov and Skylarov (1978) observed a similar process and attributed this to hydrocarbon desorption from the support. However, in the present work it was

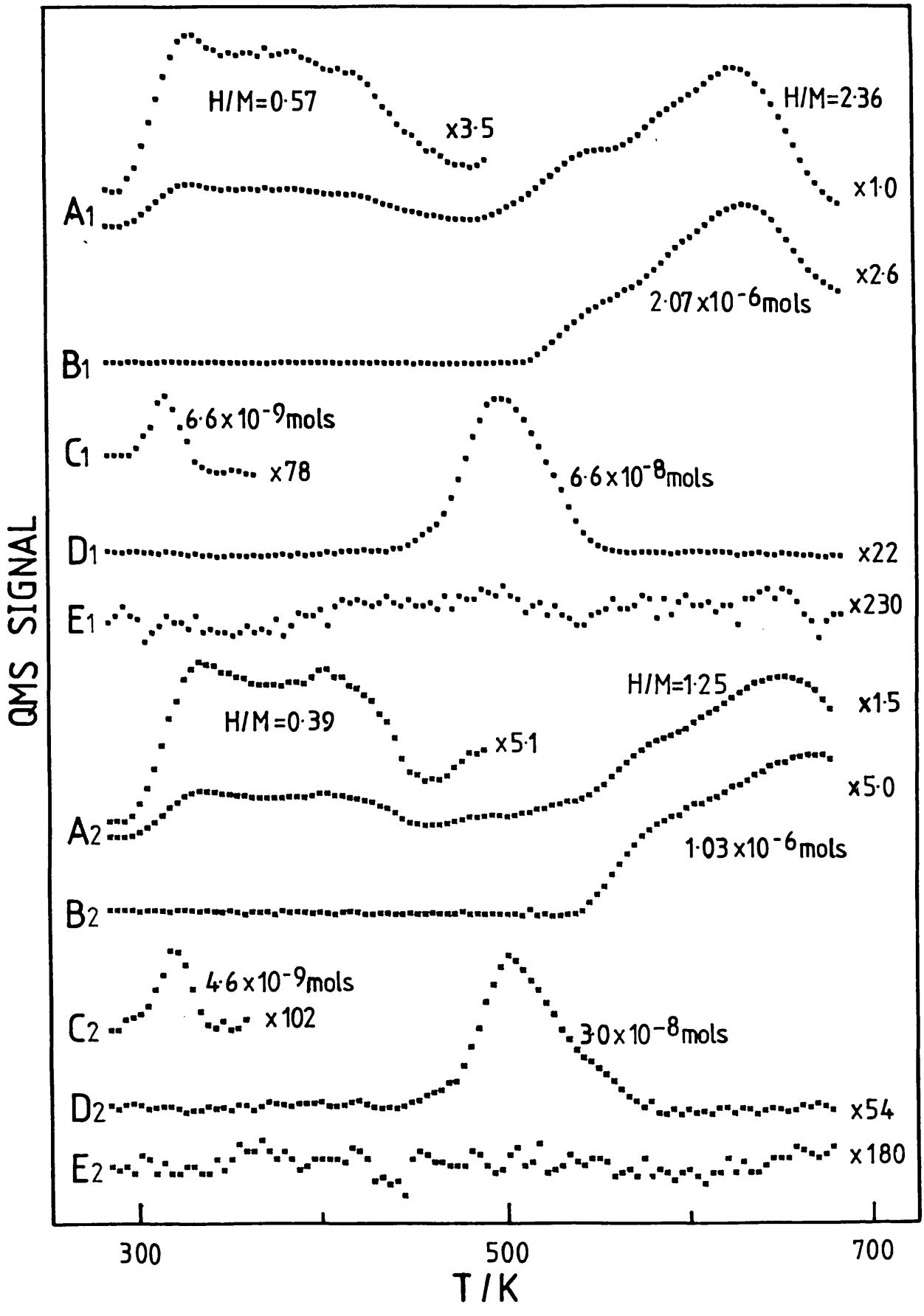

Fig. 7.1: Hexane Thermal Desorption Profiles for Sample Pt100 Subjected to Pretreatment R610 (See text for details)

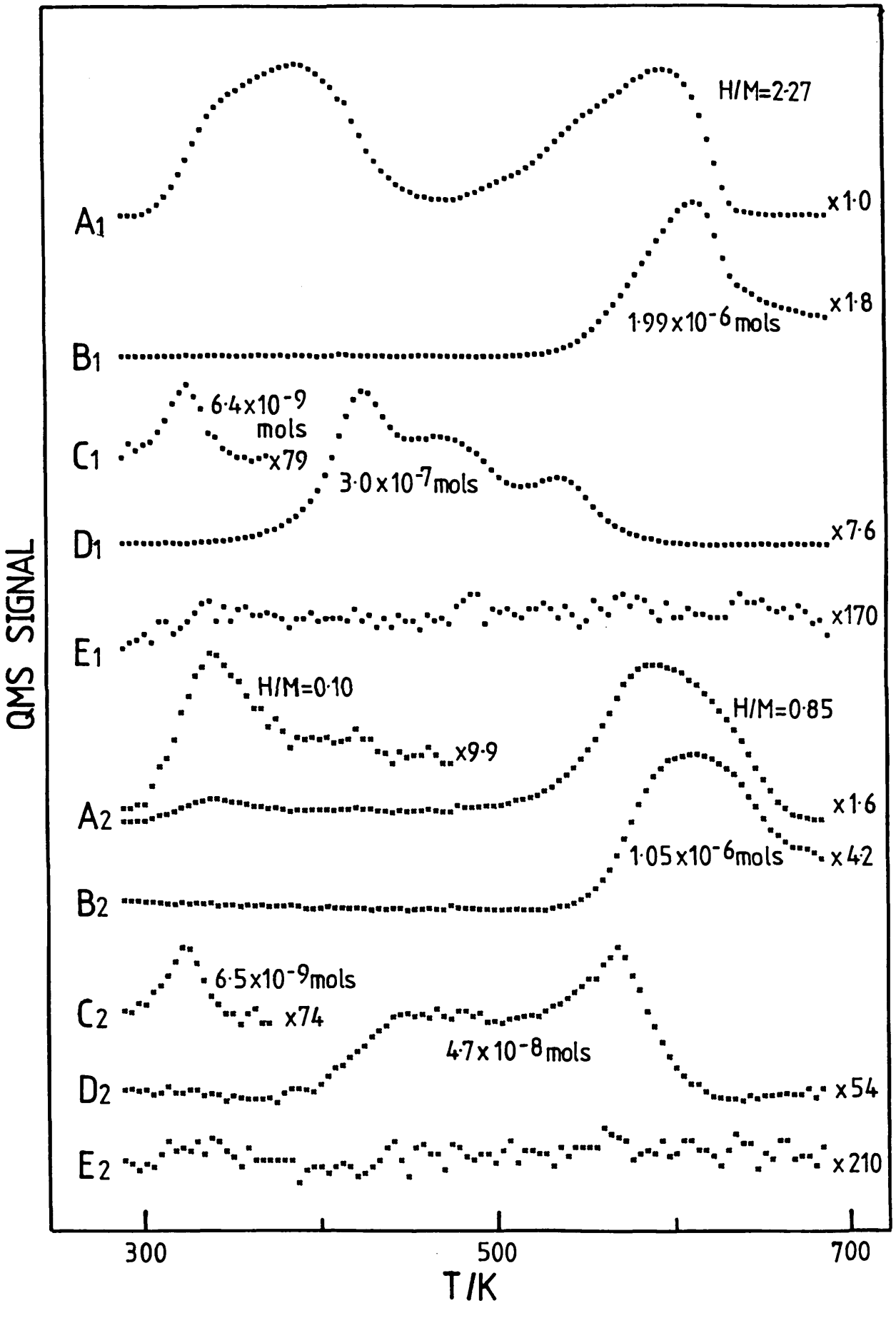

Fig. 7.2: Hexane Thermal Desorption Profiles for Sample Ir100 Subjected to Pretreatment R610 (See text for details)

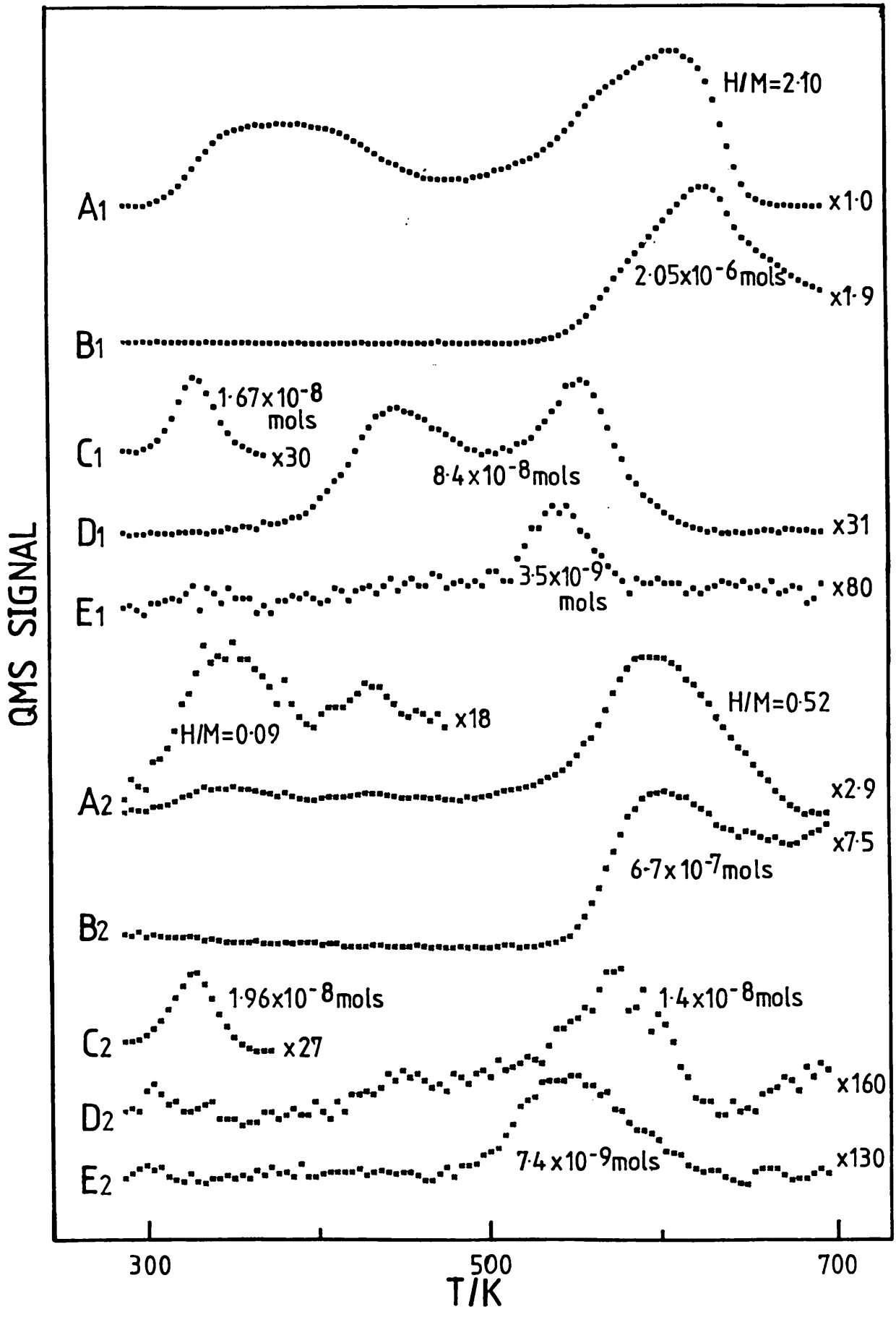

Fig. 7.3: Hexane Thermal Desorption Profiles for Sample PtIr43 Subjected to Pretreatment R610 (See text for details)

found that hexane could not be adsorbed on the pure alumina support nor on a Pt100 sample prior to reduction. Similarly a sample that had been oxidised at 740K (O740) was inactive. Therefore, the hexane desorption must occur from metal sites present on the sample.

Table 7.2: Hexane Desorption Mass Balance Results for Samples Subjected to Pretreatment R610

	Pt100		Ir100		PtIr43	
	Run 1	Run 2	Run 1	Run 2	Run 1	Run 2
10^6M/mol	3.8	-	4.2	-	4.0	-
10^7 Hx_{ads}/mol	2.9	3.6	4.2	4.1	3.1	3.4
10^7 H_{lib} /mol	9.5	9.9	4.6	1.7	5.6	0.8
10^7 H_{rem}^{M}/mol	9.1	-	26.0	-	20.0	-
10^6 H_{hT} /mol	6.8	3.3	4.7	3.2	5.2	1.7
10^6 H_{left}/mol	3.7	2.3	6.7	4.8	5.2	3.9
10^6 C_{left}/mol	1.6	2.1	2.2	2.4	1.7	1.9
H_{left}/C_{left}	2.3	1.1	3.1	2.0	3.1	2.1
10^6 C_c /mol	1.6	1.0	1.4	1.1	1.3	0.7
10^6 H_R /mol	6.9	3.1	7.1	4.4	6.6	2.9
10^7 C_{end} /mol	0.2	10.5	7.7	13.0	3.8	11.9
H_{end}/C_{end}	0.0	0.2	3.1	0.9	3.7	1.0
$(H_{end}/C_{end})_{NR}$	-155.0	-1.0	2.6	1.2	0.0	1.9
$(H/C)_R$	2.3	1.3	1.4	0.9	2.0	0.4
$(H_{end}/C_{end})_{UR}$	5.0	1.0	6.2	2.9	6.8	3.0

N.B. Run 2 data is not cumulative, for instance the total amount of carbon remaining after run 2 for Ir100 = 20.7 x 10^{-6} mols.

At temperatures below 500K the hydrogen profile has features similar to those obtained for hydrogen desorption from a pure hydrogen adlayer (see Fig. 5.1). The profile obtained in this region from hexane is shown enlarged in Fig. 7.1. The two peaks occurring at around 332K and 388K correspond to the two low temperature peaks shown in Fig. 5.1. Therefore, it is reasonable to infer that hydrogen desorption in this temperature region represents desorption from the metal surface. This is not entirely surprising since the sample was cooled in hydrogen before being exposed to hydrocarbon. The shift in temperature between the two sets of results most probably

arises from the lower heating rate used in the hydrocarbon work. Alternatively, the presence of adsorbed hydrocarbon species could modify the hydrogen desorption characteristics of the sample. However, the hydrogen peak at around 420K cannot readily be observed in the profile shown in Fig. 5.1. This may indicate that this feature is due to the decomposition of adsorbed hydrocarbon species. Alternatively, the 420K peak may be present in Fig. 5.1 but is obscured by the larger low temperature peaks. If hexane adsorption has the effect of reducing these peaks it would make the 420K peak appear more prominent.

At temperatures in excess of 480K the Pt100 sample shows a much changed hydrogen profile compared to that shown in Fig. 5.1. Hydrogen desorption now occurs with a large structured peak at around 626K. A peak at a similar temperature was observed following hydrogen adsorption on to the metal surface but it was much smaller. It was suggested that a probable cause of this peak was the decomposition of hydrocarbon impurity fragments on the presumed clean surface. Clearly, hydrogen peaks in this temperature range are related to the presence of such fragments.

Hydrocarbon desorption experiments from single crystal metal surfaces produce similar hydrogen desorption behaviour over this temperature range. Such features have been assigned to the decomposition of hydrocarbon fragments usually originating from alkylidyne species. Thus, it is tempting to interpret the profile shown in Fig. 7.1 in the same manner. However, the mass 44 profile has the same form indicating that, for this sample, the two processes are linked.

Initially, the mass 44 profile was thought to arise from the formation of propane during hydrocarbon decomposition. Indeed, small peaks for the mass 41 and 43 profiles expected with propane were obtained. However, the mass 29 signal (also a characteristic propane cracking fragment) was too small to account for this hydrocarbon. Similarly the small size of the mass 41 peak eliminated propene. Thus, the mass 44 signal must be largely due to the production of carbon dioxide. This surprising observation was in fact first made by Walkov et al. (1977) who observed the production of carbon monoxide with carbon dioxide at such temperatures. They

attributed the formation of these species to a reaction of absorbed hydrocarbon fragments with support hydroxyl groups. No evidence for the formation of carbon monoxide was found in this study. A small increase in the mass 28 profile was entirely attributable to a carbon dioxide cracking fragment. Importantly, no change in the oxygen signal was observed which shows that CO_2 was not produced by the reaction of oxygen with carbon-containing species. Thus, the oxygen must already have been present in some form on the catalyst surface. At this stage it is necessary to examine the mass balance results, collected in Table 7.2, in order to further elucidate the nature of the processes observed in the desorption profiles. Thus, the mass balance analysis for the hexane adsorption process is used to determine the nature of the hydrocarbon species initially present at 298K. This is followed by an assessment of the cause of the high temperature hydrogen/carbon dioxide desorption processes occurring above 500K.

The method of calculation of the quantities listed in Table 7.2 is given in Appendix A2. The errors in the amounts of gas adsorbed/desorbed are around $\pm$ 10% leading to errors in derived quantities such as H_{left}/C_{left} of at least $\pm$ 20%. Thus, whilst it is unwise to try to extract precise information concerning the specific nature of the adsorbed species the analysis does allow overall trends to be identified.

For the first adsorption experiment 2.9×10^{-7} mols of hexane adsorb on to the sample and liberate 9.5×10^{-7} mols of hydrogen atoms. In addition, the amount of hydrogen desorbed from the metal drops by 9.1×10^{-7} mols. It should be noted that the H_{rem}^{M} values listed in the Table are the difference between the amount of hydrogen desorbed in the low temperature region below 500K from the hydrogen saturated surface and from a surface that has subsequently been exposed to hexane. This quantity represents the amount of hydrogen removed from the metal hydrogen profile when hydrocarbon is present.

Hence, for each hexane molecule adsorbed approximately three hydrogen atoms are liberated and three hydrogen atoms are removed from the metal sites. Therefore, it appears that hydrogen missing from the metal profile in fact desorbs as the hexane adsorbs.

Possible adsorption reaction processes which might account for these quantities are the following:

i) Hexane breakdown forming C2 species:

$$C_6H_{14} + 3M\text{-}H \rightarrow 2(M\text{-}CH_2\text{-}CH_3) + H_2C\underset{M}{-}CH_2 + \tfrac{3}{2}H_2 \qquad (7.1)$$

where M represents a surface metal site, although adsorbed ethylene normally requires two sites.

ii) Adsorbed hexane does not fragment but forms a multiplet complex of the type suggested by Paal (1980):

$$C_6H_{14} + 3M\text{-}H \rightarrow M_3\text{-}C_6H_{14} + \tfrac{3}{2}H_2 \qquad (7.2)$$

where the multiplet species is represented by $M_3\text{-}C_6H_{14}$, in which partial dissociation of C-C and C-H bonds occurs.

iii) Formation of an alkylidyne species, frequently observed with single crystal metal surfaces:

$$C_6H_{14} + 3M\text{-}H \rightarrow (H\text{-}M)_3C\text{-}C_5H_{11} + \tfrac{3}{2}H_2 \qquad (7.3)$$

This mechanism would require the alkylidyne species to interact strongly with the three adjacent hydrogen adatoms since they do not appear in the hydrogen profile below ~500K. However, because of steric effects, the existence of strongly bound hydrogen on metal atoms to which an alkylidyne complex is bonded is unlikely.

If routes (7.2) and (7.3) were predominant then the production of a range of hydrocarbon fragments would be expected during the desorption run. However, the only hydrocarbon fragment desorbed during run 1 was methane, which appeared in a structured peak at around 500K. The amount formed corresponded to ~1 mol of methane for every 4 mols of hexane adsorbed. Zimmer et al. (1982) have observed a mass 15 peak at similar temperatures to those found in this study. Thus it appears that the extensive formation of higher alkylidynes or multiplet species is unlikely. However, the presence of small quantities of either species could account for the small hexane peak at around 320K. Furthermore, if reaction (7.1) represents the major adsorption process then the absence of lower hydrocarbons in the desorption spectra suggests that the metal clusters are of sufficient size to accommodate the whole of the fragmented adsorbate.

Significantly, Wang et al. (1985) have found that ethylidyne species undergo C-C bond rupture at temperatures below 480K on small platinum particles. Thus, the methane peak may be due to the conversion and subsequent breakdown of C2 hydrocarbon species formed by reaction (7.1) according to the following type of process:

$$M\text{-}CH_2\text{-}CH_3 \rightarrow M{\equiv}CH + CH_4 \qquad (7.4)$$

possibly via formation of an ethylidyne intermediate. If this is so, the small quantity of methane produced must be explained in one of the following ways:

i) The amount of the C2 species is small.
ii) C2 decomposition at around 500K requires the presence of special catalyst sites.
iii) C2 decomposition is widespread but liberation of methane is restricted.

Alternatively, the small amount of methane desorbed may be due to a limited breakdown of hexane into adsorbed C1 species.

Whatever the exact nature of the adsorbed species and the origins of the methane peak, the findings of the mass balance analysis are significant since they establish that adsorption of hexane at single metal atom sites of the type originally proposed by McKery et al. (1973) is not important under the adsorption conditions used. In fact it appears that at least 3 metal sites on the same cluster are used to adsorb each mole of hexane. However, adsorption at single atom sites might account for the hexane desorption at 316K.

Turning now to the nature of the high temperature H_2/CO_2 desorption process, the amount of hydrogen apparently available for this process is given by H_{left} in Table 7.2. Also included is the amount of carbon, C_{left}/mol, available for CO_2 formation. The ratio of these quantities can be used to give an indication of the average composition of the adsorbed hydrocarbon fragments before the high temperature process occurs. However, this carbon and hydrogen need not necessarily be in an associated form and thus the actual composition of the hydrocarbon fragments may be lower than the H_{left}/C_{left} value.

It is immediately apparent that during run 1, for the Pt100 sample, the amount of hydrogen liberated in the high temperature region, H_{hT}/mol, is in excess of the amount actually present (H_{left}). Thus, some of this hydrogen must come from a source other than the adsorbed hydrocarbon and hydrogen, originally present on the metal surface.

Reactions which could account both for the excess hydrogen production and the related CO_2 formation are:

$$\text{i)}\quad 2H_2O + M\text{-}CH_x \rightarrow CO_2 + 2\left(1 + \frac{x}{2}\right) H_2 + M \qquad (7.5)$$

$$\text{ii)}\quad S\text{-}OH + H_2O + M\text{-}CH_x \rightarrow CO_2 + \left(\frac{3 + x}{2}\right) H_2 + MS \qquad (7.6)$$

$$\text{iii)}\quad 2S\text{-}OH + M\text{-}CH_x \rightarrow CO_2 + \left(1 + \frac{x}{2}\right) H_2 + S_2M \qquad (7.7)$$

In these equations S-OH represents a surface hydroxyl group and S_2M and MS are metal-support complexes caused by the elimination of the hydroxyl groups. A possible alternative to reaction (7.7) would be the following:

$$(S\text{-}O\rightarrow)_2M\text{-}CH_x + 2H_{sp} \rightarrow CO_2 + \left(1 + \frac{x}{2}\right) H_2 + S_2M \qquad (7.8)$$

where H_{sp} is spillover hydrogen and $(S\text{-}O\rightarrow)_2M$ represents a support-metal interaction of the type proposed by Joyner and Meehan (1983).

Intermediate steps in the above reactions may include the formation of CO. For instance, reaction (7.6) coud proceed as follows:

$$S\text{-}OH + M\text{-}CH_x \rightarrow S\text{-}M + CO + \left(\frac{1+ x}{2}\right) H_2 \qquad (7.6a)$$

$$H_2O + CO \rightarrow CO_2 + H_2 \qquad (7.6b)$$

where the final reaction is the well known Water-Gas Shift reaction.

Thus the number of moles of hydrogen atoms produced, H_R/mol, can be predicted from the value of x, the amount of CO_2 produced, C_C/mol, and the stoichiometry of the reaction chosen. Hence, by comparison with the actual amount of hydrogen liberated (H_{hT}) the reaction which is actually occurring can be deduced.

On the assumption that the H_{left}/C_{left} value is a realistic estimate of x, reactions (7.5), (7.6), (7.7) or (7.8), are calculated to produce 13.8×10^{-6}, 8.5×10^{-6} and 6.9×10^{-6} mols H atoms respectively. The experimental result is very close to the last figure showing that reaction (7.7), or one involving a similar

stoichiometry, is responsible for the H_2/CO_2 profiles during run 1 for the Pt100 sample. Table 7.2 also contains the quantity $(H/C)_R$. This is the average composition of the reactive hydrocarbon fragments, calculated from the amount of CO_2 produced with the assumption that all hydrogen desorbed in the high temperature region arises from reaction (7.7). Thus, for the Pt100 sample the $(H/C)_R$ and H_{left}/C_{left} values are the same. However, for the iridium-containing samples the two values are different for reasons that will be discussed in further detail in a following section. Structure in the H_2/CO_2 profiles may arise from differences in the reactivities of surface hydroxyl groups and/or fragments bound to different catalyst sites. Alternatively, different reactions with the same stoichiometry may occur.

An indication of the composition of the carbon-containing species left at the end of run 1 can be obtained in a variety of ways. The H_{end}/C_{end} ratio is calculated on the assumption that reaction (7.7) has been operative and the zero value obtained for the Pt100 catalyst shows that there is no hydrogen associated with the carbonaceous deposit. The $(H_{end}/C_{end})_{UR}$ ratio is obtained from the $(H/C)_R$ value (see Appendix A2) and gives the composition of the unreactive hydrocarbon fragments also assuming reaction (7.7) to be occurring. Finally, if it is assumed that CO_2 is formed by a process which did not abstract hydrogen from some additional source, then the composition of the remaining fragments is given by $(H_{end}/C_{end})_{NR}$. The very small amount of carbon remaining, C_{end}/mol, on the Pt100 sample indicates that most of the metal surface was clean following run 1.

Run 2 differs from run 1 in that the catalyst starts with a virtually clean surface, whereas for run 1 the surface was initially saturated with hydrogen. It can be seen from the Table that Hx_{ads} is greater than during the first run, whilst H_{lib} is similar. It would appear that preadsorbed hydrogen suppresses adsorption of hexane. However, the amount of hydrogen desorbed from the metal surfaces is now lower (see Fig. 7.1). Significantly, the total amount of carbon and hydrogen atoms adsorbed on the metal at 298K is equivalent to an adsorbate atom (carbon and hydrogen) to metal ratio of 0.96. This value is very close to the H/M ratio for this sample obtained using hydrogen desorption (see Section 5.3). Hence,

whatever the exact nature of the adsorption process it appears that hexane adsorption, on to the hydrogen-free metal surface, results in a greater breakdown of the hexane adsorbate than was obtained for a hydrogen covered surface.

The Hx_{ads}, H_{lib}, H_m and H_{left}/C_{left} values suggest the following type of adsorption process occurs:

$$C_6H_{14} + 10M \rightarrow (M\text{-}CH_2) + 5(M\text{-}CH) + 4M\text{-}H + \tfrac{3}{2}H_2 \qquad (7.9)$$

This would produce 3 mols of hydrogen atoms for each hexane molecule adsorbed and would result in the formation of two H-M complexes for every three $M\text{-}CH_x$ species formed. The smaller amount of methane produced could also indicate greater fragmentation than for run 1, since this peak was assigned to the breakdown of C_2 species.

The carbon dioxide and high temperature hydrogen profiles still behave in a similar manner although the C_C value is lower than was obtained for run 1. This suggests that a process such as reaction (7.7) is still operative. Therefore, although the number of reactive surface hydroxyl groups decreases following run 1, sufficient remain to take part in the reaction. However, the larger value of C_{end} for run 2 indicates that carbon is no longer easily removed from the sample.

b) Ir100 and PtIr43

For the two iridium-containing samples the hydrogen profiles for run 1 again show hydrogen desorption occurring in two temperature regions; the lower one corresponding to desorption from metal sites ($T_{des} \lesssim 500K$) and the higher one being associated with CO_2 desorption.

For the Ir100 sample $H_{rem}{}^M$ is much greater than H_{lib}, indicating that hydrogen initially adsorbed on the metal interacts strongly with the adsorbed hydrocarbon fragments. A possible reaction scheme which accounts for this behaviour is the following:

$$C_6H_{14} + 5(H\text{-}M\text{-}H) + M\text{-}H \rightarrow 6(H\text{-}M\text{-}CH_3) + \tfrac{1}{2}H_2 \qquad (7.10)$$

The H/M ratio obtained in Section 5.3 indicated that approximately one metal atom in six bound only one hydrogen atom. The higher degree of hydrocarbon breakdown on the Ir100 sample compared to the Pt100 sample is consistent with the higher hydrogenolysis activity

of iridium catalysts. The large H_{rem}^{M} value for the PtIr43 sample indicates that a similar adsorption process occurs with this sample.

The absence of lower hydrocarbon fragments in the gas phase during the hexane adsorption shows that the active metal entities for adsorption are of sufficient size to adsorb the hydrocarbon in its entirety. This suggests that the highly dispersed iridium is not present in a monoatomic form, as proposed by McVicker et al. (1980), but is present as small clusters of sufficient size (> 6 atoms) to adsorb the entire hydrocarbon. Furthermore, if a hexane molecule adsorbed entirely on a single metal atom site of the type suggested by Findlayson et al. (1984) this would be expected to produce smaller hydrocarbon fragments during the desorption run, whilst the H_{rem}^{M} and H_{lib} values would be similar. In fact no $C_2 \rightarrow C_5$ hydrocarbons were desorbed from any sample and, therefore, the participation of such sites under the conditions used is questionable.

For both iridium-containing samples the H_{left}/C_{left} values indicate that methyl species are on the catalyst prior to the commencement of the high temperature hydrogen desorption process. This shows that the fragments are, on average, of higher hydrogen content than those found on the Pt100 sample.

Unlike the Pt100 sample the CO_2 profiles for the Ir100 and PtIr43 catalysts are not in step with the hydrogen profiles. No CO or other oxygenated carbon products were observed. Furthermore, H_{left} is now greater than H_{hT} for the Ir100 catalyst and is equal to H_{hT} for the bimetallic catalyst. Thus it is now unnecessary to propose hydrogen abstraction according to a process such a reaction (7.7). In this case the hydrogen signals may be due to decomposition of adsorbed hydrocarbon fragments, in agreement with single crystal studies, with CO_2 production occurring by some hitherto unknown route. Alternatively, the similarity of the hydrogen profiles for all samples suggests that a reaction such as (7.7) occurs but the CO_2 formation/desorption is suppressed/delayed in some manner which results in the non-alignment of the profiles. However, the value of H_R is greater than H_{hT} for both iridium-containing samples. Thus, either the assumption that H_{left}/C_{left} is a true estimate of x is no longer valid or the hydrogen is generated

by a different reaction from (7.7). As mentioned earlier, the $(H/C)_R$ values have been calculated assuming rection (7.7) occurs and that all the hydrogen is produced by this reaction. These values are much lower than the H_{left}/C_{left} values showing that the reactive fragments contain lower amounts of hydrogen than is indicated by the latter.

A further possible explanation for the different high temperature desorption behaviour of the platinum and iridium-containing samples is as follows. With the Pt100 sample there are three types of hydrocarbon fragments which react according to reaction (7.7) to give a CO_2 peak with three components. However, in the case of the iridium-containing samples there may exist an alternative reaction which produces methane (see below) instead of carbon dioxide, namely:

$$M\text{-}CH_3 + S\text{-}OH \rightarrow CH_4 + S\text{-}O\text{-}M \qquad (7.11)$$

This may also generate hydrogen by a mechanism which is not clear. Hence, for these samples only the most stable hydrocarbon fragment follows reaction (7.7) whilst the remainder produce methane instead of carbon dioxide. In reality, the high temperature desorption process for the Ir100 and PtIr43 samples most probably results from a combination of the above alternatives.

Following run 1 both iridium-containing samples contain more carbon than the Pt100 sample which suggests a greater M-C bond strength for the former. In addition, irrespective of the method of calculation, the remaining fragments generally have a larger amount of hydrogen present. However, this should be viewed with caution since not all the hydrogen may be directly associated with the carbon. For instance, the $(H_{end}/C_{end})_{UR}$ values would lead to the existence of CH_6 units which is clearly impossible. One way of avoiding this difficulty is to postulate that the excess hydrogen is associated with the support. However, as previously discussed in Chapter Five other forms of strongly adsorbed hydrogen have been proposed which might account for the excess hydrogen.

The most significant differences between the behaviour of the samples occurs for the methane profiles.

For the Ir100 sample three large methane peaks were observed at temperatures of around 424, 472 and 537K. Interestingly, the ratio of the amounts contained in each peak are respectively 1:0.67:0.44 (i.e. $1:{}^{2}/_{3}:({}^{2}/_{3})^{2}$). The total amount of methane produced is much greater than that obtained with the Pt100 sample, which produced methane in a single peak at around 500K. This difference in behaviour must reflect the higher hydrogenolysis activity of iridium catalysts first demonstrated by Carter et al. (1971).

The production of three methane peaks may be due to a three step sequential decomposition of a single species on the same site or decomposition of species adsorbed at three different sites. Alternatively, a combination of the two may occur. Since the metals are all highly dispersed, the presence of low coordination number metal atoms (equivalent to the kink position atoms on single crystals) would be expected to occur with a high frequency and these are the type of site which might produce methane peaks. The hydrocarbon adsorption data indicated that a high degree of hydrocarbon fragmentation occurred at 298K. Hence, the former explanation seems unlikely since this requires at least C_3 species to be present.

The two lower temperature peaks could result from a combination of hydrogen and methyl species bound to the same iridium atom. This complex is produced by reaction (7.10) at low coordination sites. Thus:

$$H\text{-}M\text{-}CH_3 \rightarrow M + CH_4 \qquad (7.12)$$

However, hydrogen adsorbed on the metal surface might not be expected to contribute to the methane production since a large fraction of the adsorbed hydrogen desorbs before methane production begins. Indeed, hydrogen in a $H\text{-}M\text{-}CH_3$ complex may be very weakly bound and hence could desorb as hydrogen at low temperatures. Thus, for the Ir100 sample, methane may be produced by a reaction not involving hydrogen bound to the metal surface, such as by reaction (7.11) described earlier (although other sources of strongly bound hydrogen may exist).

The two low temperature methane peaks may arise from reaction on two types of configurationally different metal atom sites. For instance, one peak could arise from desorption from metal atoms with

an open 100-type environment symmetry whilst the other could be due to desorption from more coordinatively saturated metal atoms with a 111-type environment. Alternatively, the desorption may occur from very highly coordinatively unsaturated metal atoms bound to either of the above regions.

The highest temperature peak contained in the triplet occurs at a similar temperature to that found for the Pt100 sample. Therefore, it is possible that this peak arises from a common process. If, however, this peak is due to the decomposition of C_2 species then this shows that the hexane adsorption process is more complicated for iridium than is shown by reaction 7.10.

The methane profile for the bimetallic sample contains two large peaks of roughly equal area centred at temperatures of 446 and 555K. Further inspection reveals the lower temperature peak to be comprised of two components occurring at temperatures equivalent to those found for the two largest peaks for the Ir100 sample. Clearly, the amounts of methane are now much reduced and overall this profile is not the average of the profiles for the two monometallic samples. The decreased quantity of methane liberated cannot be due to the presence of lower amounts of $H\text{-}M\text{-}CH_3$ species since the adsorption results for the Ir100 and the bimetallic sample are similar. In addition, it is not related to a smaller quantity of hydrogen initially present on the sample, since the hydrogen desorption profile shown in Chapter Five for the bimetallic sample was the average of the monometallic profiles. In addition, an interpretation based on bimetallic particles having a lower iridium surface concentration is inconsistent with the highly dispersed nature of the metal.

The most likely explanation is that a Pt-Ir interaction modifies the reactivity of the metal sites responsible for the methane production. Indeed, such an interaction was inferred from the XPS results. The presence of platinum probably suppresses the hydrogenolysis activity of the iridium, although some intrinsic hydrogenolysis activity of the iridium must remain. This may well be the explanation for the improved activity maintenance of these bimetallic catalysts, as outlined in Section 7.1. It is highly significant that benzene desorption was observed only with the PtIr43 sample.

The reason for this could be that the low temperature methanation reactions of the Ir100 sample are largely suppressed in the bimetallic catalyst. An alternative, but less likely explanation, is that the PtIr43 sample possesses a unique configuration of sites at which dehydrocyclisation can occur.

Benzene formation by a simple hexatriene cyclisation step, of the type proposed by Paal and Tetenyi (1973), is not appropriate since the adsorbed hydrocarbon has been proposed to exist largely as methyl fragments. Therefore, the benzene formation sites are probably restricted to sites at which strong lateral C-C interactions exist between the fragments and where the underlying metal structure aids the formation of the C_6H_6 units.

Whilst runs 1 and 2 on the Pt100 sample produced very similar desorption profiles there were large differences between runs 1 and 2 with the iridium-containing samples, the amount of hydrogen desorbed from the metal sites being much reduced. The amount of methane formed was also less. In fact, the Ir100 methane profile resembles the run 1 profile for the PtIr43 sample (although the total amount of methane desorbed is much less). Furthermore, for the second run, the CO_2 profiles follow the high temperature hydrogen profile much more closely. These changes are not due to a change in the amount of hydrocarbon adsorbed, since the Hx_{ads} values are largely unaltered. Similarly, sintering of the metal during the heat treatment cannot be significant since the results shown earlier in Fig. 5.4 show that these samples are moe resistant to sintering than the Pt100 sample under such conditions.

The changes most likely reflect the larger amount of carbon remaining on the sample after run 1 and an increased dependence of adsorbed hydrocarbon reactions on the amount of preadsorbed hydrogen initially present on the catalyst. The H_{left}/C_{left} values for run 2 are lower than those for run 1 showing that there has been a reduction in the hydrogen content, probably due to the absence of initially adsorbed hydrogen.

In run 2 the adsorption of hexane does not produce much adsorbed hydrogen as evidenced by the smallness of the low temperature hydrogen peaks. In fact the lowest temperature peak is the only one that is significantly repopulated. Presumably, hexane

adsorption produces species which retain most of the original hydrogen in a manner such as the following:

$$C_6H_{14} + 6M \rightarrow 2(M\text{-}CH_3) + 4(M\text{-}CH_2) \qquad (7.13)$$

The lack of hydrogen bound directly to the metal could account for the large differences observed in the methane profiles between the two runs. The adsorption process is probably more complex than reaction (7.13) would indicate since the highest temperature peak has been attributed to the decomposition of C_2 species. Alternatively, the carbon remaining from run 1 could prevent the population of the states responsible for the two lower temperature methane peaks.

Significantly, benzene was not produced from the Ir100 sample whilst the amount of benzene produced by the PtIr43 catalyst was greater for run 2. It may be that the M-C bond strength is too great with the Ir100 catalyst to allow significant C-C interactions to occur. The increased amount of benzene in run 2 with the bimetallic could arise from a template effect whereby the carbon remaining, following run 1, aids the formation of benzene in a way proposed for single crystal surfaces by Davis and Somorjai (1982). Zimmer et al. (1982) observed similar structured benzene peaks, albeit for Pt/alumina samples exposed to hexane at 373K. This structure was thought to arise from the presence of adsorbed benzene precursors of varying degrees of C-H bond dissociation.

Finally, the C_{left} values for run 2 are much greater than for run 1, which indicates that carbonaceous overlayer growth increases following the initial carbon deposition during run 1.

In brief, temperature-programmed desorption following adsorption of hexane on samples subjected to pretreatment R610 shows the following:

1) Hydrogen desorbs from hydrocarbon-covered metal surfaces in a manner similar to that observed in Chapter Five, although the amount is reduced and the profile has a slightly different shape.

2) The sites responsible for hexane adsorption and reaction are not isolated metal atoms since lower hydrocarbon species ($C_2 \rightarrow C_5$) were not observed to desorb at any stage.

3) All samples show a much enhanced high temperature hydrogen desorption process compared to the results of Chapter Five. For the Pt100 sample the exact correspondence of the hydrogen and CO_2 profiles indicates that, for this sample, both have a common cause. Quantitative analysis shows that these desorption products are most likely to be produced by the reaction of the alumina hydroxyl groups with the adsorbed hydrocarbon fragments. However, for the iridium-containing samples the lack of correspondence between the hydrogen and carbon dioxide profiles, and the quantities desorbed, suggest that there is some thermal decomposition of hydrocarbon fragments as well as fragment oxidation. Whatever the exact cause, the presence of hydrogen peaks at such temperatures are clearly related to the presence of hydrocarbon species.

4) The methane profiles show that Pt-Ir interactions are present in the bimetallic sample. The results suggest that the high hydrogenolysis activity of iridium is lowered in the bimetallic catalyst. However, sufficient hydrogenolysis activity remains to explain the improved activity maintenance of such bimetallic catalysts prepared under similar conditions. Benzene was only observed for the bimetallic sample.

5) A second experiment on the Pt100 sample largely reproduced the original desorption profile whilst profiles for the iridium-containing catalysts were appreciably altered. This probably resulted from the influence of the larger amount of carbon remaining on the latter following run 1 and/or differences in the influence of preadsorbed hydrogen for subsequent hydrocarbon reaction.

7.3.2 Samples Subjected to Pretreatment O740 R610

The hexane thermal desorption profiles for samples Pt100, Ir100 and PtIr43 subjected to pretreatment O740 R610 are shown in Figs. 7.4-7.6 respectively. The mass balance results are given in Table 7.3. Overall, the profiles show some features which are similar to those obtained following pretreatment R610, but significant differences exist which are discussed in detail below.

For the Pt100 sample the high temperature desorption process in the hydrogen profile now contains a well resolved peak at around 560K. In addition, the CO_2 peak found in the earlier work at around 620K is now missing. However, the most significant difference for this sample compared to the R610 tretment is the production of benzene. The hydrogen desorption results of Section 5.3 showed that platinum atoms of lower coordination number were present in this sample. Thus, it appears that benzene formation on supported platinum is promoted by the presence of such sites. This is in contrast to the results for single crystal work of Somorjai and coworkers, who have generally observed that the more coordinatively saturated sites have the highest dehydrocyclisation activity. Furthermore, the close alignment of the methane and benzene peaks suggest that the two processes are linked, although the detailed mechanism by which this could happen remains unclear.

The second adsorption experiment on the Pt100 sample (run 2) does not repopulate the lower temperature hydrogen states to the same extent as was found with the sample following the R610 treatment. In addition, the amount of benzene liberated is now greater than for run 1. The H_{left}/C_{left} values for runs 1 and 2 are similar and hence this changed behaviour must be due to the presence of carbon remaining from run 1. A similar effect was observed for the PtIr43 sample subjected to pretreatment R610.

In general, the differences occurring between the desorption profiles for the Pt100 catalyst subjected to the O740 R610 and R610 pretreatments are most probably due to the presence of a greater number of lower coordination number metal atoms in the former sample.

For the Ir100 sample the amounts of hydrocarbon adsorbed and hydrogen desorbed during thermal desorption are much lower than were obtained for the sample simply reduced at 610K. These results are generally consistent with the previously observed oxidative agglomeration for this sample produced by such a pretreatment.

The most interesting change between the desorption profiles shown in Figs. 7.5 and 7.2 occurs for the methane desorption. The 537K peak present in Fig. 7.2 has disappeared in Fig. 7.5 whilst the lower temperature doublet remains. The relative amounts contained

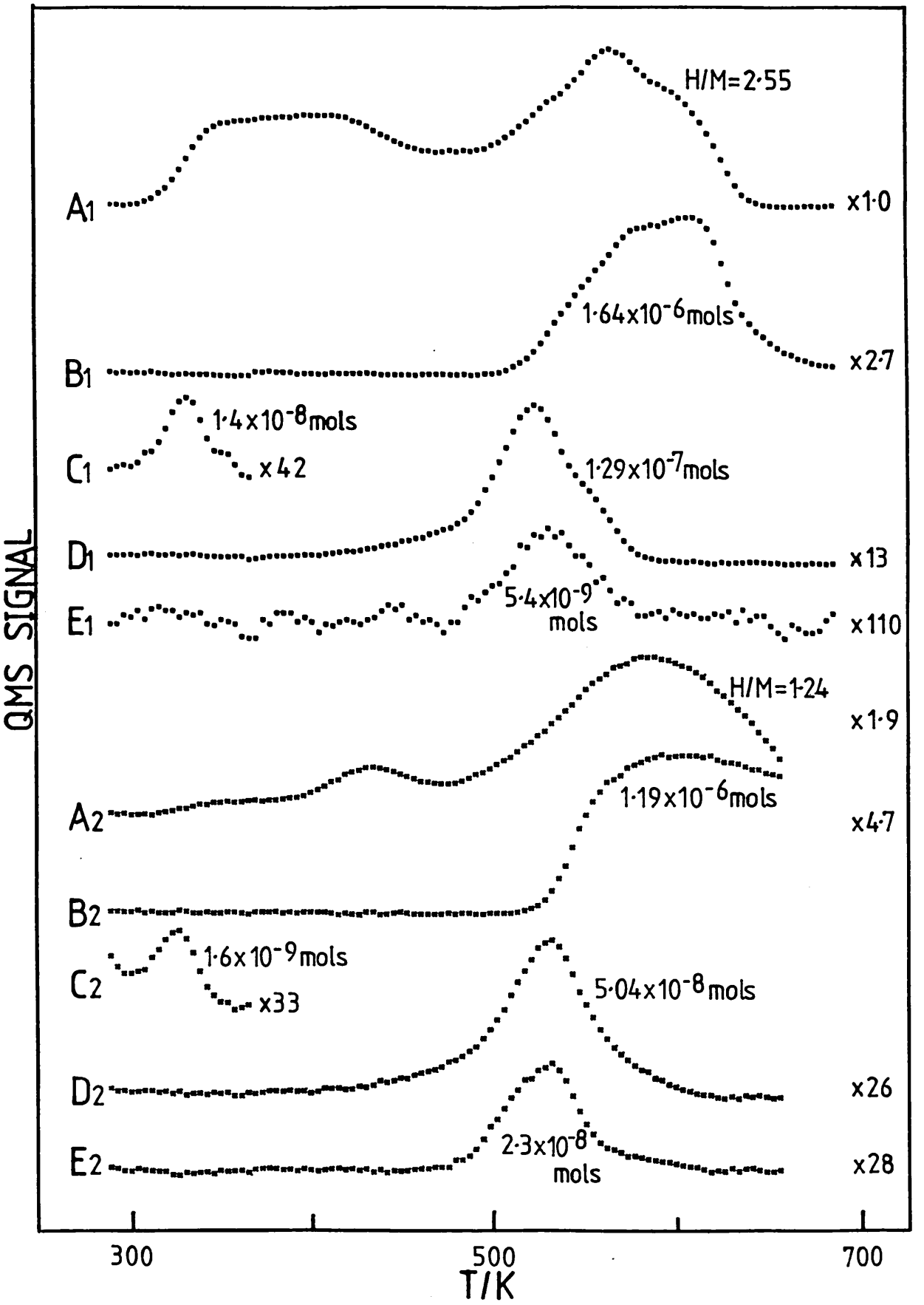

Fig. 7.4: Hexane Thermal Desorption Profiles for Sample Pt100 Subjected to Pretreatment O740 R610 (See text for details)

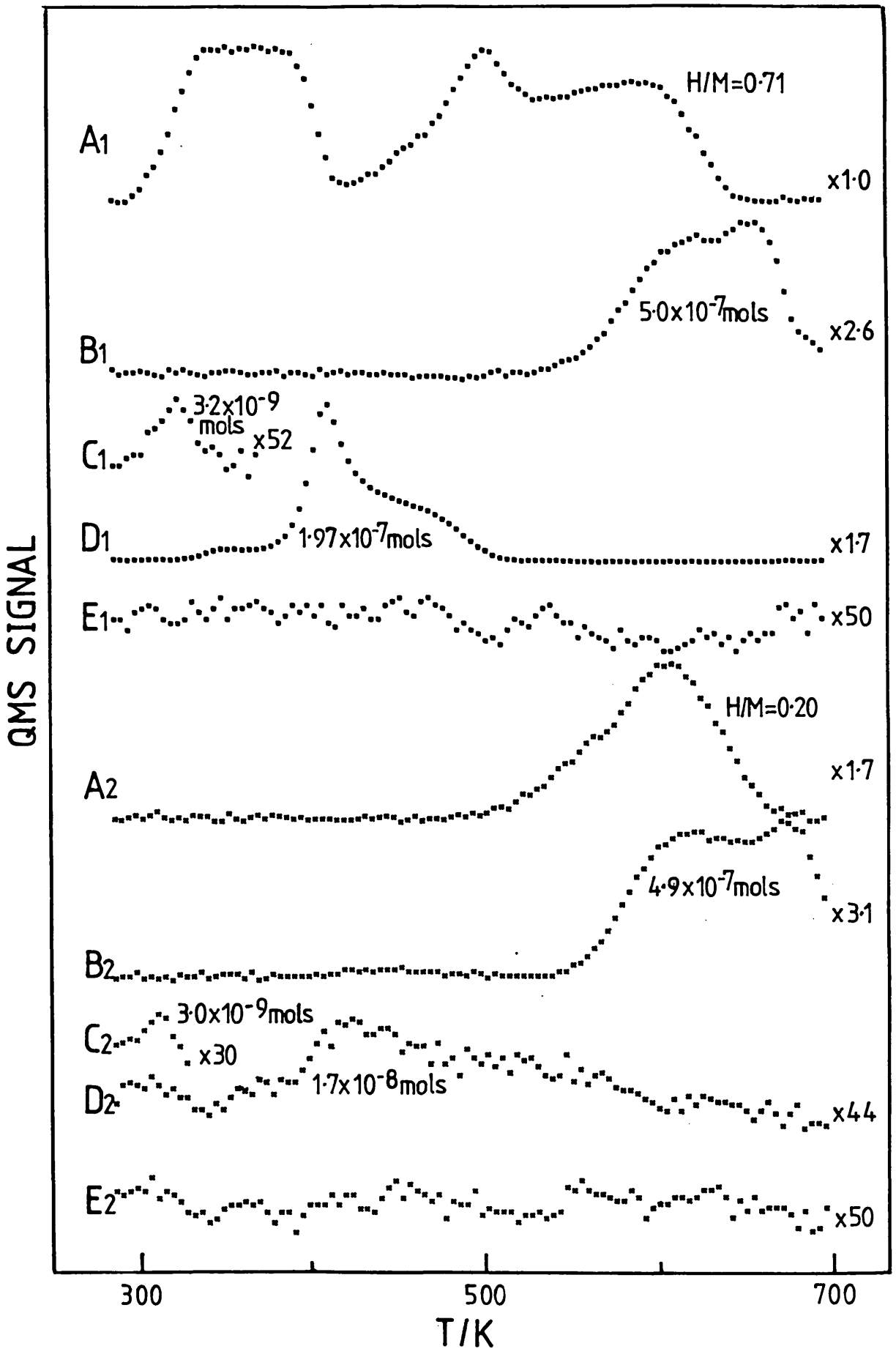

Fig. 7.5: Hexane Thermal Desorption Profiles for Sample Ir100 Subjected to Pretreatment O740 R610 (See text for details)

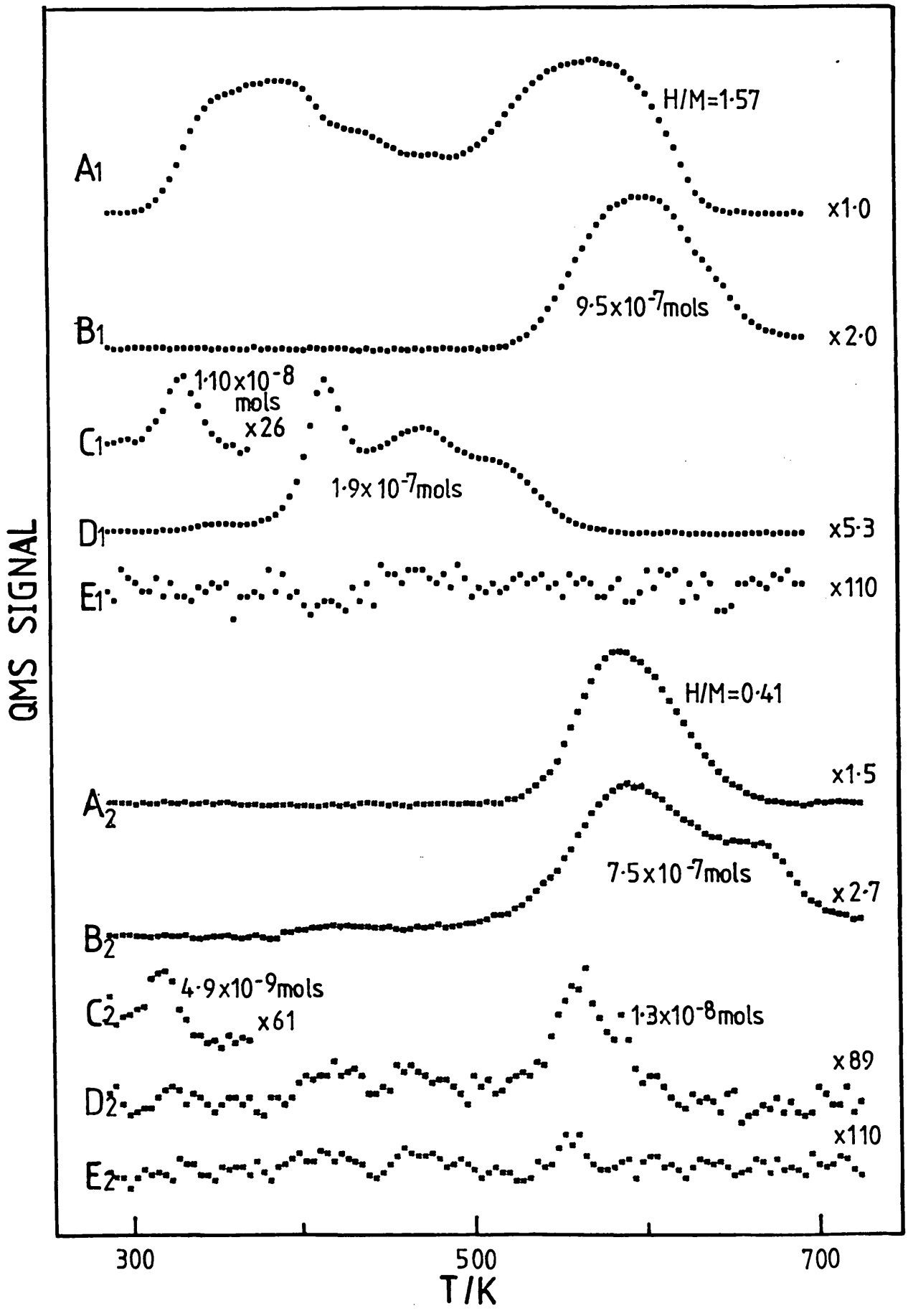

Fig. 7.6: Hexane Thermal Desorption Profiles for Sample PtIr43 Subjected to Pretreatment O740 R610 (See text for details)

Table 7.3: Hexane Desorption Mass Balance Results for Samples Subjected to Pretreatment O740 R610

	Pt100		Ir100		PtIr43	
	Run 1	Run 2	Run 1	Run 2	Run 1	Run 2
10^7 H_{ads}/mol	3.3	3.8	2.2	1.4	2.4	1.8
10^7 H_{lib} /mol	12.2	0.0	5.5	2.9	7.6	0.0
10^7 $H_{rem}{}^{M}$/mol	5.7	-	4.2	-	13.0	-
10^6 H_{hT} /mol	6.0	3.9	1.9	0.8	3.6	1.6
10^6 H_{left}/mol	3.2	4.1	2.1	1.6	3.0	2.3
10^6 C_{left}/mol	1.8	2.1	1.1	0.8	1.2	1.0
H_{left}/C_{left}	1.8	2.0	1.9	2.0	2.5	2.3
10^6 C_c /mol	1.6	1.2	0.5	0.5	1.0	0.8
10^6 H_R /mol	6.1	4.8	2.0	2.0	4.5	3.4
10^7 C_{end} /mol	1.1	8.7	5.7	3.1	2.6	2.5
H_{end}/C_{end}	0.9	1.0	0.2	3.9	3.5	7.2
$(H_{end}/C_{end})_{NR}$	-25.5	0.2	0.4	2.6	-2.3	2.8
$(H/C)_R$	1.8	1.3	1.8	-0.4	1.6	0.0
$(H_{end}/C_{end})_{UR}$	3.6	2.9	2.1	5.8	5.4	9.2

in these two peaks are in the ratio of around 2:1. In addition a new small peak at around 350K is apparent.

The methane peaks at 410 and 462K for the Ir100 sample subjected to pretreatment O740 R610 could be due to:

i) Desorption from sites on any highly dispersed metal that remains.

ii) Desorption from sites on the larger crystallites which have similar characteristics to those found on the highly dispersed phase.

Explanation (i) above seems attractive since Brunelle et al. (1976) and Barbier and Marecot (1981) found that the hydrogenolysis activity of iridium decreases as the size of the metal particles increases. Hence, any methane produced may be expected to originate predominantly from the highly dispersed metal sites. However, the total amount of methane formed (2.0×10^{-7} mols) when compared to that formed following pretreatment R610 (3.0×10^{-7} mols) would suggest that two thirds of the metal remained highly dispersed

following the O740 R610 pretreatment. This is inconsistent with the hydrogen desorption results presented in Chapter Five which showed that a larger fraction of the iridium had agglomerated. This problem together with the absence of a peak at 540K (present for the known highly dispersed sample) makes explanation (i) difficult to accept.

If the individual methane peaks represent desorption from different types of site rather than the reaction of different species, one is forced to the conclusion that the large crystallites possess sites similar to those found on the highly dispersed clusters, this being the only way to explain the similarity of the two largest methane peaks. Since Somorjai and coworkers have found that kink sites on single crystal samples are important for hydrogenolysis activity it is tempting to assign the 410 and 462K peaks to reaction on such sites. Similar metal configurations may be found on both low and high dispersed samples leading to the same degree of coordinative unsaturation. However, the difference in relative intensity of the peaks contained in the doublet shows that the relative number of the sites producing the 460K peak is less on the larger crystallites. Thus this peak may arise from reaction on the less coordinatively saturated metal.

The absence of a methane peak at around 540K for the O740 R610 sample might indicate that this peak represents reaction on sites present only on highly dispersed clusters, which are common to both highly dispersed platinum and iridium. However, it is more likely that this peak represents reaction of C_2 species, formed only on the highly dispersed clusters.

The hydrogen content of the fragments remaining on the Ir100 sample following run 1 is much lower than was found with samples that had not been oxidised. This probably reflects the higher initial hydrogen content of the latter sample.

During run 2 on the Ir100 sample, some changes in the hydrogen and carbon dioxide profiles were observed which were similar to those discussed in the previous section for samples that had received pretreatment R610. Thus, the explanations given previously for the latter pretreatment generally apply. However, the quantities desorbed are now much lower than for run 2 of pretreatment

R610 and no hydrogen desorption from metal sites is observed. Thus, the less dispersed sample appears to be deactivated more readily. Furthermore, the methane peak observed at 569K in Fig. 7.2 is absent from Fig. 7.5. This adds confirmation to the view that this particular peak is unique to desorption from highly dispersed samples.

In general, the differences occurring in the desorption profiles for the Ir100 catalyst following the O740 R610 and R610 pretreatments reflect the larger metal particle size produced by the former pretreatment.

For the bimetallic sample the hydrogen profile may be considered to be the average of the profiles for the monometallic samples. This would be expected if extensive phase separation had occurred, although the hydrogen desorption results of Fig. 5.3 show that hydrogen-metal interactions are fairly insensitive to bimetallic alloy interactions. However, the methane profile shows a considerable change when compared with Fig. 7.3. The highest temperature peak now occurs at around the same temperature as the peak found for the Pt100 sample. Furthermore, the amount of gas in this peak is consistent with the platinum loading in the bimetallic sample. It is also significant that the lowest temperature peaks in Fig. 7.6 are larger than the corresponding ones in Fig. 7.3 and are similar in size to those observed for the Ir100 sample, shown in Fig. 7.2.

Thus it is tempting to assign the 414 and 474K peaks to desorption from large iridium-rich crystallites. However, the XPS results indicated that such crystallites are covered by ~10 Å thick layer of platinum. Such a layer would be expected to alter the reactivity of the crystallites considerably. The hydrogen desorption results of Chapter Five showed that a large fraction of the iridium was redispersed following reduction whilst the XPS examination indicated that this phase was located inside the support pores. Therefore, it seems most likely that the 414K and 474K peaks represent desorption from the redispersed iridium. However, the absence of the 540K peak shows that these species are not identical to those formed following pretreatment R610, which may be related in some way to the pore environment. Confirmation of this view is obtained from the size of the 474K peak, which is much larger than would be expected if the doublet represented desorption from the larger

crystallites (cf. Fig. 7.5 and 7.6). Conceivably, the overlayer of platinum could cause this effect.

Whatever the exact cause of the methane profile for the PtIr43 sample, the results are suggestive of an increased hydrogenolysis activity compared to the sample subjected to pretreatment R610. In accordance with this interpretation the O740 R610 sample did not produce any benzene.

Interestingly the data given in Table 7.3 show that the hydrocarbon fragments formed on this sample during run 1 contain a large amount of hydrogen.

For run 2 the hydrogen and carbon dioxide profiles largely resemble those shown in Fig. 7.3. However, hydrogen desorption from the metal surface is no longer apparent. The methane profile is similar to those shown in Figs. 7.2 (run 2) and 7.3. This is surprising since the platinum-rich dispersed phase would be expected to show similarities to the Pt100 sample, with a methane profile like that in Fig. 7.4. It would appear that incorporation of iridium into the platinum-rich clusters suppresses the methane formation from such entities but only when carbon is also present. This effect may be caused by the greater amount of carbon generally observed to be retained by iridium. In addition, benzene was not observed during run 2 which shows that retained carbon no longer promotes benzene formation.

Finally, following run 2, the total amount of carbon remaining on all samples, except Pt100, was significantly lower than that found following pretreatment R610, although the hydrogen content was generally greater.

To summarise, desorption profiles following adsorption of hexane on samples subjected to pretreatment O740 R610 show some features in common with the profiles obtained for samples reduced at 610K. However, the methane and benzene profiles show significant differences. For the Pt100 sample a benzene peak now appears at approximately the same temperature as that found for the methane peak. The production of the benzene appears to be associated with the larger number of lower coordination number metal atoms present after the oxidation treatment.

For the Ir100 samples large changes in the methane profile occur following insertion of the oxidation step. A quantative analysis of the profiles shows that a low temperature doublet represents reaction from sites common to both large crystallites and highly dispersed clusters. These could be highly coordinatively unsaturated metal atoms at regions of low and high coordination number metal. The methane profile for the bimetallic sample indicates that highly dispersed iridium and large iridium-rich crystallites co-exist in this sample, in addition to highly dispersed platinum-rich entities. The results suggest that the hydrogenolysis activity of alumina-supported platinum-iridium catalysts can be increased by insertion of an oxidation step at 740K prior to reduction at 610K.

7.3.3 Sample Subjected to Pretreatment R740

The hexane thermal desorption profiles for samples Pt100, Ir100 and PtIr43 subjected to reduction at 740K are shown in Figs. 7.7-7.9 respectively. The mass balance results for these samples are given in Table 7.4. For all samples the amount of hexane

Table 7.4: Hexane Desorption Mass Balance Results for Samples Subjected to Pretreatment R740

	Pt100		Ir100		PtIr43	
	Run 1	Run 2	Run 1	Run 2	Run 1	Run 2
10^7 Hx_{ads}/mol	1.2	1.4	1.2	1.3	0.9	1.3
10^7 H_{lib} /mol	0.0	0.0	0.0	0.0	0.0	0.0
10^7 H_{rem}^{T}/mol	9.5	-	-14.3	-	-0.4	-
10^7 C_c /mol	1.7	0.6	1.7	1.3	1.8	1.4
10^7 C_{end} /mol	5.1	7.5	4.8	6.0	3.3	5.8
10^6 H'_{end} /mol	2.9	1.7	0.5	1.5	1.5	1.7
H'_{end}/C_{end}	5.7	2.3	1.0	2.5	4.5	2.9

adsorbed is much lower than that found following either the R610 or O740 R610 pretreatments. In addition, whilst the latter samples liberated hydrogen during hydrocarbon adsorption none of the samples reduced at 740K did so. There seem to be two possible ways of explaining this result; either the site for hydrocarbon adsorption is not covered initially by hydrogen or the hydrogen interacts with

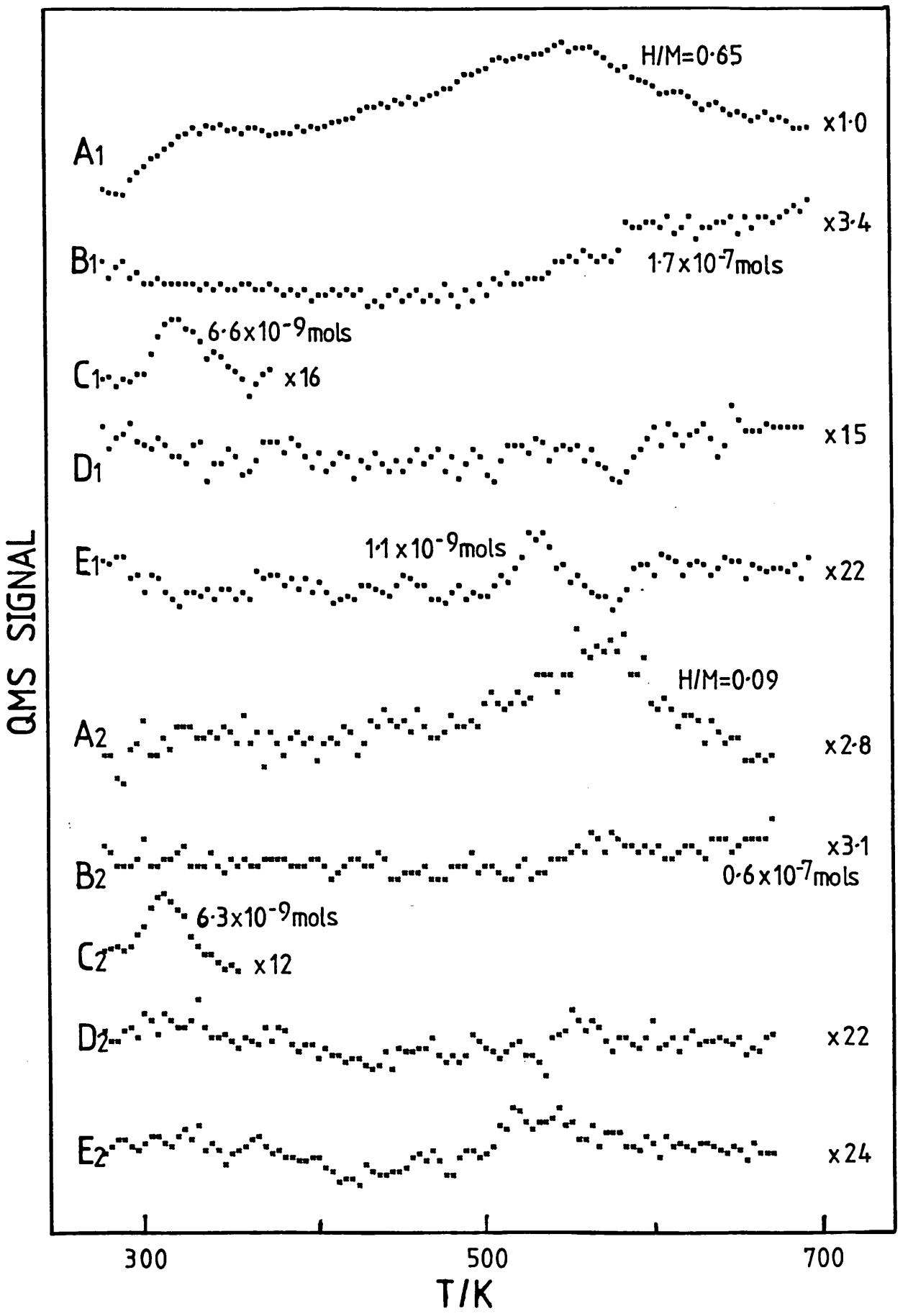

Fig. 7.7: Hexane Thermal Desorption Profiles for Sample Pt100 Subjected to Pretreatment R740. (See text for details)

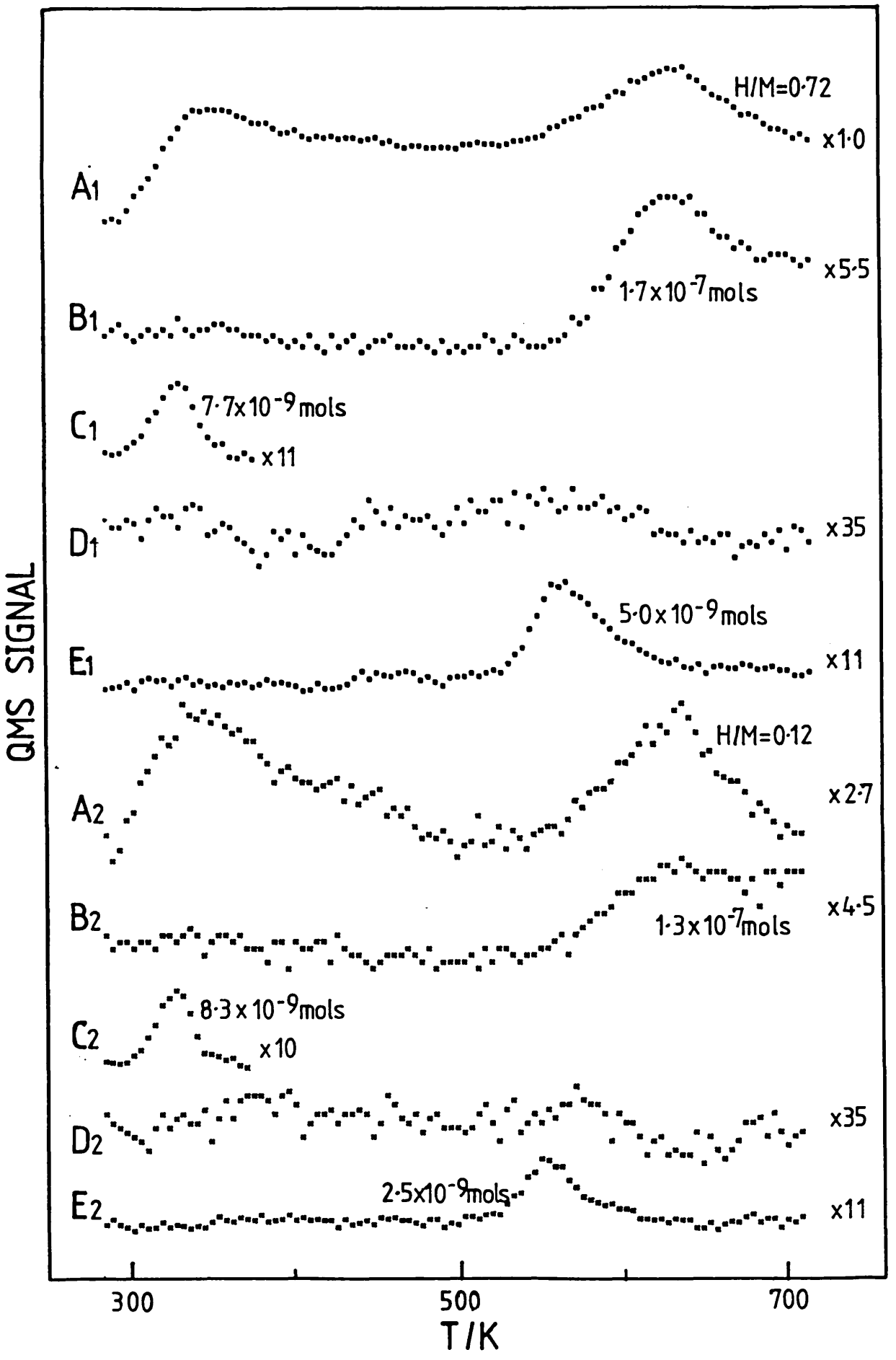

Fig. 7.8: Hexane Thermal Desorption Profiles for Sample Ir100 Subjected to Pretreatment R740. (See text for details)

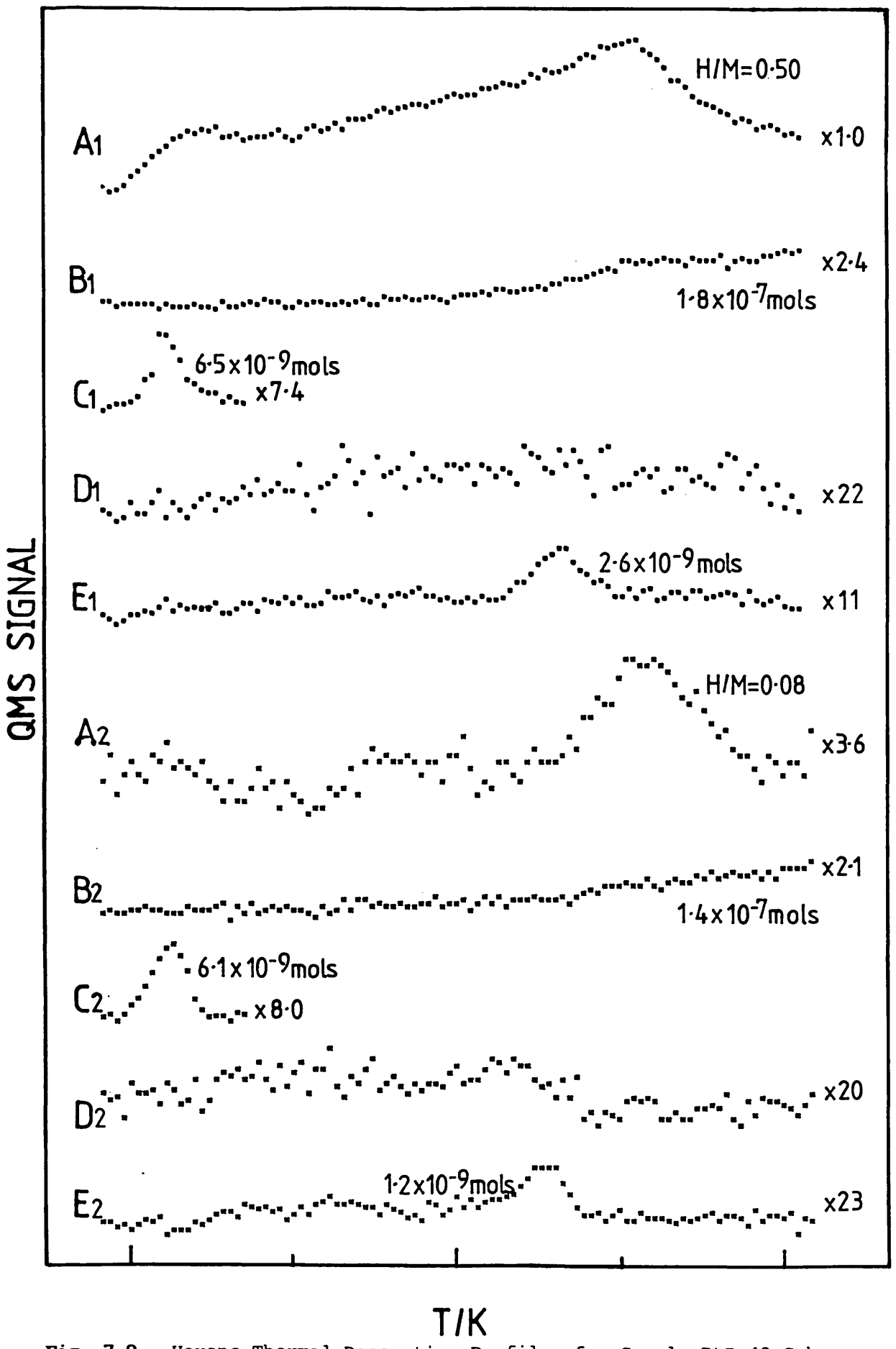

Fig. 7.9: Hexane Thermal Desorption Profiles for Sample PtIr43 Subjected to Pretreatment R740. (See text for details)

the hydrocarbon during the adsorption process. However, since no hydrogen was liberated, further information concerning the nature of the adsorbed hydrocarbon species cannot be obtained.

For run 1, the hydrogen profiles for all samples are similar with peaks at temperatures of around 350K and above 550K. The temperature of the second peak increases with iridium content.

The hydrogen profiles for the iridium-containing samples are generally similar to those shown in Fig. 5.6 for hydrogen desorption in the absence of hydrocarbon. However, for the Ir100 sample, the high temperature peak is now more intense whilst for both the Ir100 and PtIr43 samples this peak now occurs at lower temperatures. Significantly, the value of H_{rem}^{T}/mol for the iridium-containing samples is negative showing that more hydrogen is desorbed from these samples following hexane adsorption than is desorbed in the absence of hexane. The extra hydrogen desorbed from the Ir100 sample is roughly equivalent to the total amount of hydrogen contained in the adsorbed hydrocarbon.

However, for the Pt100 sample H_{rem}^{T} is positive and, therefore, the amount of hydrogen produced is lower than that shown in Fig. 5.6. Furthermore, the hydrogen profile does not resemble that obtained for desorption in the absence of hydrocarbon. In fact the shape of the profile broadly resembles that shown in Fig. 5.13 for hydrogen desorption from a sample subjected to pretreatment O740 R740.

The hydrogen desorption results reported in Section 5.3 for the Pt100 sample, gave no evidence either for sintering during pretreatment R740 or for the formation of an SMSI state. However, insertion of an oxidation step at 740K did produce a sharp reduction in the amount of hydrogen desorbed which could arise from either of these two effects. Furthermore, the TEM results for the bimetallic sample indicated that an SMSI state was formed. Hence, it appears that hydrocarbon adsorption on to the Pt100 sample produces a hydrogen profile indicative of SMSI behaviour. This result is puzzling since it was previously proposed that hydrocarbon impurities could have prevented the platinum entering into the SMSI state during pretreatment R740.

For both platinum-containing samples a linear increase in the CO_2 signal is observed. This is consistent with the pretreatment eliminating a substantial number of the reactive support hydroxyl groups. Alternatively the adsorbed hydrocarbon may be less reactive towards the hydroxyl groups. However, for the Ir100 sample a discrete CO_2 peak is observed which shows that the above considerations no longer apply. The H'_{end} values contained in Table 7.4 have been calculated on the assumption that the CO_2 has been produced by reaction (7.7). Appendix A2 should be consulted for further details.

Perhaps the most significant result is the absence of methane from the desorption profiles of all the samples. This provides strong evidence that the pretreatment reduces or eliminates the activity of the catalytic centres which are responsible for hydrogenolysis reactions. Furthermore, this reduced activity would be expected to allow alternative reactions to occur. Significantly all samples now produce benzene, with the amount increasing with iridium content.

To confirm whether the absence of a methane peak in the desorption profile is indicative of reduced hydrogenolysis activity, hexane pulses were passed over a PtIr43 sample held at 770K in a hydrogen-free carrier. The sample was previously subjected to either pretreatment R740 or R610. The only products formed in significant quantities were hydrogen, methane and benzene, the product distributions of which are shown in Fig. 7.10. Unreacted hexane was not observed. The results show that, compared to the R610 sample, the initial hydrogenolysis activity of the R740 sample was reduced whilst the dehydrocyclisation selectivity was increased under the conditions used. It is important to emphasize that these results were obtained in the absence of hydrogen using reactant pulses and they represent only the initial catalyst activities. Isothermal steady state reactivity experiments (additionally performed in the presence of hydrogen) have not been carried out. Nevertheless, the results confirm that the absence of a methane peak in the desorption profile is an indication of a reduced hydrogenolysis activity.

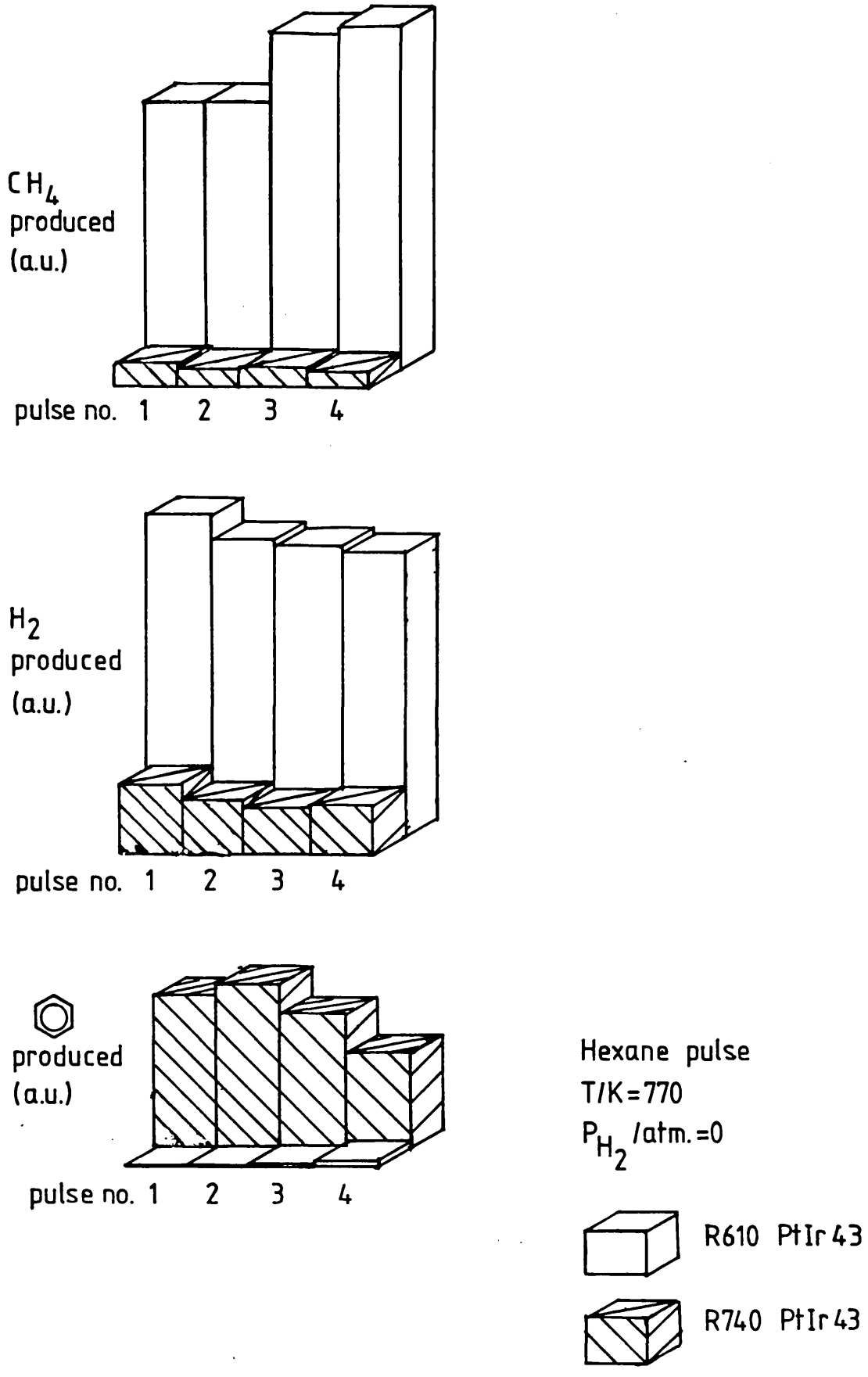

Fig. 7.10: Hexane Pulse Reaction Results for Sample PtIr43 Subjected to Pretreatment R740

Following run 1 the H/C ratio of the residual hydrocarbon fragments remaining on the platinum-containing samples is greater than for the Ir100 sample. In addition, the amount suggests that some of the remaining hydrogen is not associated with the carbon.

The run 1 and run 2 desorption profiles for the platinum-containing samples are very similar with both hydrogen profiles containing a peak at around 600K. Since a discrete CO_2 peak cannot be observed at this temperature it is likely that the hydrogen peak is due to the decomposition of hydrocarbon fragments held on the catalyst.

The hydrogen profile for run 2 on the Ir100 sample contains a prominent peak at lower temperatures which is barely noticeable with the Pt100 sample. The cause of this difference in behaviour is unclear but may be related to a partial sintering of the iridium during reduction at 740K (see Section 5.3). The interaction of the enlarged clusters with the support may be modified which indirectly enables the lower temperature states on the metal to be repopulated during hexane adsorption. This may be directly caused by a difference in the amount of carbon remaining on these particles following run 1. This sample also shows a discrete CC_2 peak which occurs at more or less the same temperature (~630K) as the hydrogen peak, an indication that the two processes are linked.

All samples still exhibit little or no methane production. However, the amounts of benzene formed are now reduced compared to run 1. This is in direct contrast to the samples reduced at the lower temperature for which it was generally found that the amount increased during run 2. Thus the remaining carbon now seems to suppress benzene formation. Significantly, the results of the pulse experiments contained in Fig. 7.10 show that the amount of benzene formed over the bimetallic sample, begins to decrease as the number of pulses increases, whereas for pretreatment R610 the amount increases with pulse number.

To summarise, the absence of methane for all samples suggests that pretreatment R740 reduces the hydrogenolysis activity of platinum and iridium-containing samples. This was confirmed for the bimetallic sample by using pulse conversion measurements. This effect could result from the formation of an unreactive state as a

result of a strong metal-support interaction. However the hydrogen desorption results of Section 5.3 showed that such an interaction did not occur for the Pt100 sample in the absence of adsorbed hydrocarbon. Whilst it is possible that the presence of adsorbed hydrocarbon promotes the formation of this state it is more likely that the high temperature reduction process annealed out metal atoms at sites of uniquely high coordination number which were previously the sites for hydrogenolysis activity.

7.3.4 Samples Subjected to Pretreatment O740 R740

The hexane thermal desorption profiles for samples Pt100, Ir100 and PtIr43 subjected to pretreatment O740 R740 are shown in Figs. 7.11-7.13 respectively. The mass balance results for these samples are given in Table 7.5. For all samples the amount of hexane adsorbed is greater than that following the R740 pretreatment. However, the amounts are still lower than for the R610 and O740 R610 pretreatments. As found for the R740 samples hydrogen was not observed to desorb during the adsorption process.

Broadly speaking, the desorption profiles are similar to those obtained following pretreatment R740. For the Pt100 sample the 450K and 550K peaks in the hydrogen profile are now well resolved. Comparison with the profile shown in Fig. 5.13 shows that the presence of hydrocarbon shifts the highest temperature peak from 685K to 553K. This peak represents either the same process occurring

Table 7.5: Hexane Desorption Mass Balance Results for Samples Subjected to Pretreatment O740 R740

	Pt100		Ir100		PtIr43	
	Run 1	Run 2	Run 1	Run 2	Run 1	Run 2
10^7 Hx_{ads}/mol	2.5	3.3	3.3	2.8	3.0	2.6
10^7 H_{lib} /mol	0.0	0.0	0.0	0.0	0.0	0.0
10^8 $H_{rem}{}^T$/mol	-7.6	-	-8.4	-	8.4	-
10^7 C_c /mol	2.8	2.3	0.0	0.0	1.6	0.0
10^7 C_{end} /mol	10.7	17.7	19.7	16.1	16.5	14.4
10^6 H'_{end} /mol	3.7	4.6	4.5	3.8	5.4	3.4
H'_{end}/C_{end}	3.5	2.6	2.3	2.3	3.3	2.3

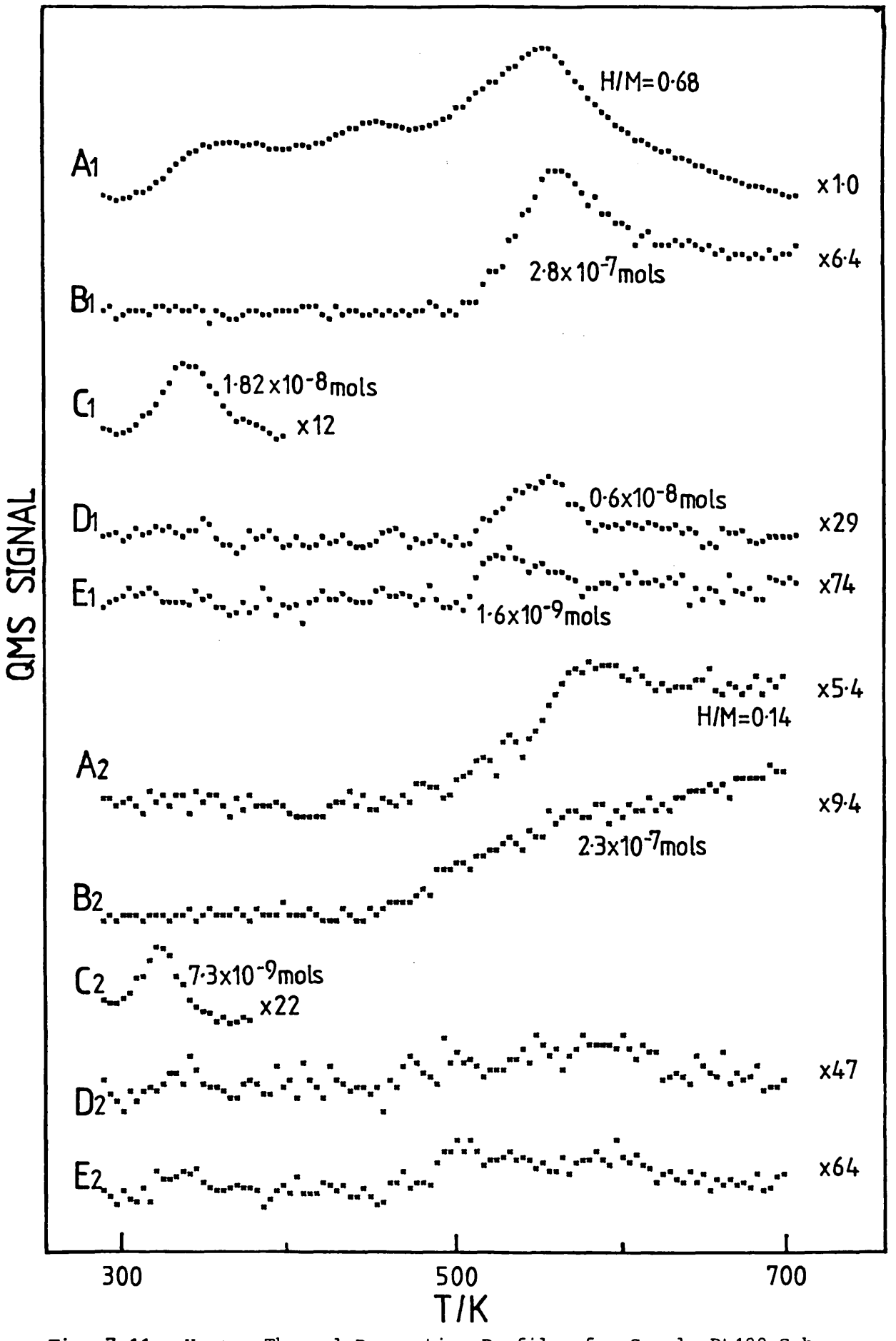

Fig. 7.11: Hexane Thermal Desorption Profiles for Sample Pt100 Subjected to Pretreatment O740 R740. (See text for details)

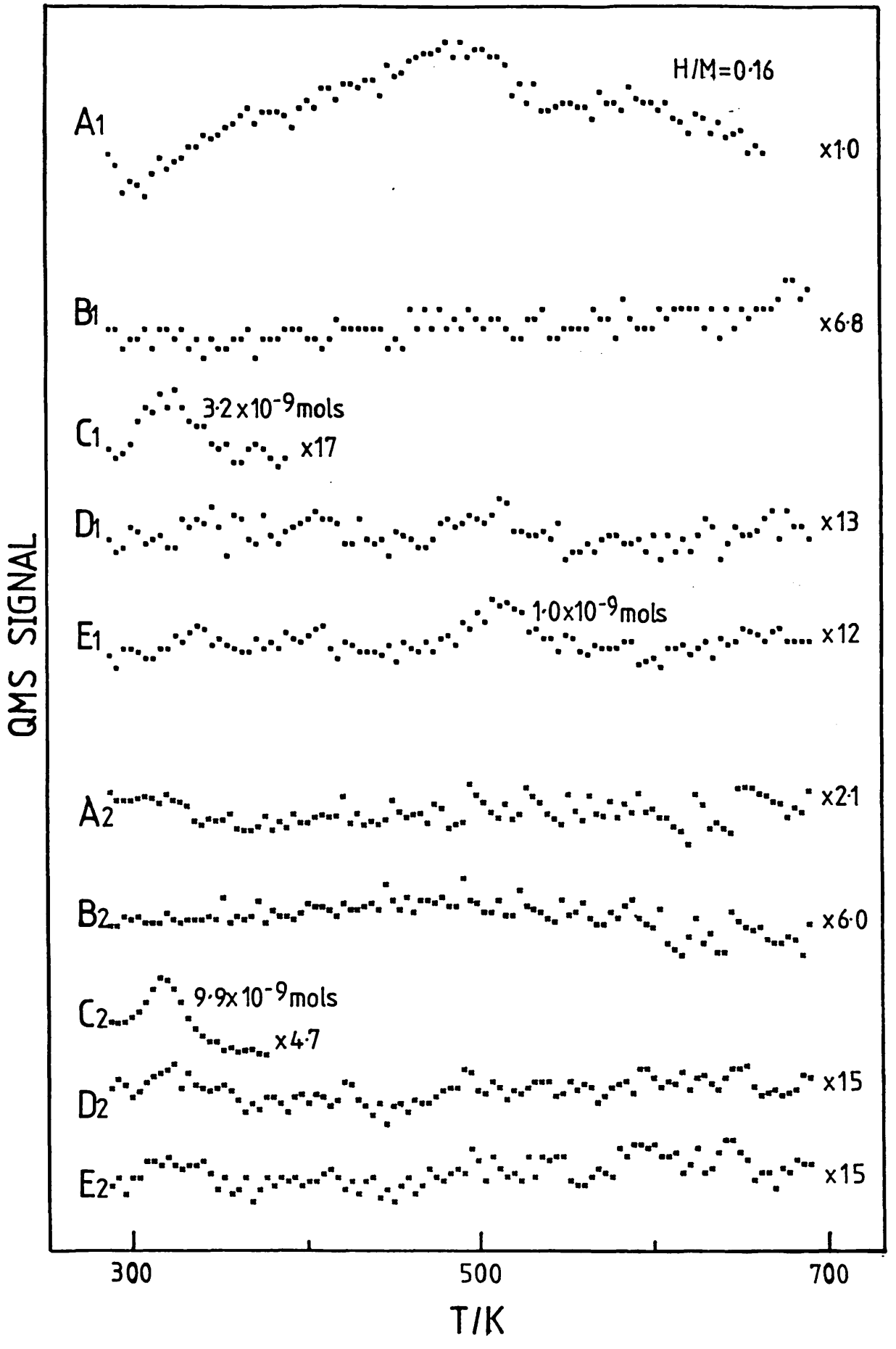

Fig. 7.12: Hexane Thermal Desorption Profiles for Sample Ir100 Subjected to Pretreatment O740 R740. (See text for details)

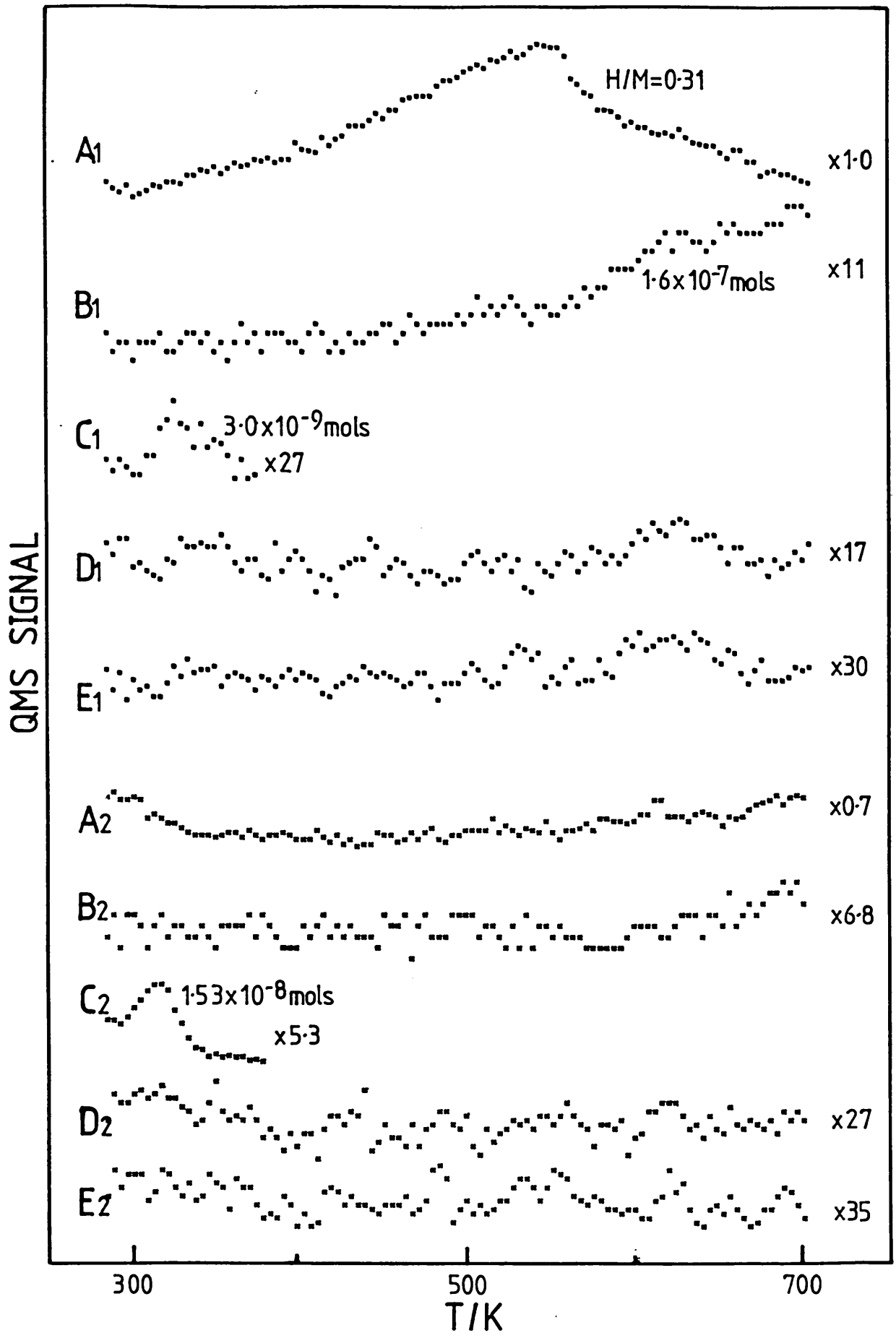

Fig. 7.13: Hexane Thermal Desorption Profiles for Sample PtIr43 Subjected to Pretreatment O740 R740. (See text for details)

at lower temperature, or a new process that consumes the hydrogen which would otherwise desorb at higher temperatures. Interestingly, a discrete CO_2 peak is now observed at these temperatures indicating that the latter process may be the one occurring. For instance reaction (7.8) may be operative which removes spillover hydrogen.

For both iridium-containing samples the hydrogen profiles are also similar to those shown in Fig. 5.13, although like Pt the highest temperature peaks are shifted down in temperature by over 100K. There is also little evidence of methane formation in the methane profiles. Thus the hydrogenolysis activity of the large iridium crystallites must also be reduced by the high temperature reduction. Presumably the size of such particles would preclude the formation of an SMSI state. Thus the reduction treatment must anneal out the metal surface irregularities which are probably the active metal sites for hydrogenolysis reactions.

The profile for the Pt100 sample contains a small methane peak at slightly higher temperatures than the benzene peak. Inspection of Fig. 7.4 shows that this methane peak occurs at the same temperature as a component in the methane peak obtained for the Pt100 sample subjected to pretreatment O740 R610. Therefore, it appears that some of the sites responsible for this peak are resistant to the high temperature reduction. Whatever the exact cause of this peak, overall the results show that samples subjected to the O740 R740 pretreatment have a reduced hydrogenolysis activity compared with the O740 R610 counterparts. It is also significant that the amount of benzene desorbed from the iridium-containing samples has decreased compared to samples subjected to pretreatment R740. This shows that benzene forms on sites predominantly located on the highly dispersed clusters.

Following run 1 the remaining fragments appear to contain less hydrogen than for the R740 pretreatment. However, the figures in Tables 7.4 and 7.5 may be misleading since the hydrogen need not necessarily be associated with the carbon. The amount of carbon remaining does, however, seem to be greater for the O740 R740 samples.

For run 2 of the iridium-containing samples the only product desorbed was hexane (or possibly C_6H_{14} branched isomers) despite

large amounts of hexane being adsorbed. Thus, the hydrocarbon fragments remaining following run 2 would be expected to have an average hydrogen:carbon composition of 14:6 as shown in Table 7.5. The presence of the carbon remaining from run 1, or the absence of adsorbed hydrogen at the start of the experiment, possibly prevents the surface reaction and desorption of these fragments.

For the Pt100 sample run 2 produces some hydrogen as well as CO_2 and C_6H_{14}. The profiles are generally similar to those shown in Fig. 7.7, although the amounts desorbed are now greater. Thus, whilst similar sites remain on both samples, the population is larger for the O740 R740 sample. Hence the two pretreatments are not equivalent as the hydrogen desorption results of Chapter Five show.

To summarise, samples subjected to pretreatment O740 R740 have desorption profiles indicative of reduced hydrogenolysis activity compared to their O740 R610 counterparts. For highly dispersed particles this may result from SMSI state formation. However, for the large crystallites the pretreatment most likely anneals out surface imperfections (atoms of especially low low coordination number) which would otherwise act as active sites for hydrogenolysis reactions.

7.4 **Discussion**

The hexane thermal desorption results presented in Section 7.3 clearly show that the nature and reactivity of Pt-Ir/alumina catalysts are influenced by the choice of pretreatment conditions. For bimetallic samples subjected to a mild reduction (R610) it appears that alloy interactions are significant and the influence of these on catalyst performance will be discussed first. This will be followed by an appraisal of the influence of SMSI phenomena on catalyst reactivity which appear to be important for samples subjected to pretreatments involving reduction at temperatures around 740K.

7.4.1 The Influence of Bimetallic Alloy Interactions

As discussed in Section 7.1 the improved performance of industrial Pt-Ir/alumina catalysts over their monometallic Pt/alumina counterparts has been ascribed to the hydrogenolysis activity of

iridium atoms in the bimetallic particles which enables coke precursors to be hydrogenated from the catalyst surface. Indeed, the hydrogenolysis activity of the bimetallic sample, as judged from the methane desorption profile, is not that expected from a simple average of the two monometallic samples. Furthermore, the methane profile indicates that the hydrogenolysis activity of iridium atoms is reduced when they are incorporated into bimetallic clusters. However, a significant iridium hydrogenolysis activity remains at the sites responsible for the low temperature methane peak (~35% cf. sample Ir100). This component most probably accounts for the 'cleaning' influence of iridium.

It must be emphasized that the conditions used for the desorption experiments and those used for reforming are not entirely comparable, the major difference being the high partial pressure of hydrogen in the reactor feed for reforming. Furthermore, the desorption results were obtained only from the clean (hydrogen-covered) surface or from a partially carbon-covered surface, whereas commercial catalysts operate continuously for several months before being reactivated. Therefore, the initial catalyst performance, as obtained from the desorption profile, may not be particularly relevant to the processes which occur on a catalyst surface after a long time on stream. Nevertheless, the methane desorption profile does show behaviour which is consistent with the above view of the improved performance of alumina-supported platinum-iridium catalysts. The nature of the interaction between the two metal components in the bimetallic clusters and the factors controlling hydrogenolysis activity are discussed in more detail below.

As outlined in Section 6.4 the novel properties of alloy clusters are generally attributed to electronic ligand effects and/or geometric factors. The XPS results contained in Section 6.3 indicated that an electronic effect may be important for Pt-Ir clusters with a possible electron transfer occurring from the platinum to the iridium centres. Indeed, it is possible that such a process accounts for the reduced hydrogenolysis activity of the iridium component in the highly dispersed bimetallic clusters since an increased electron density around the iridium would result in reduced electron donation from an absorbate. Hydrocarbon molecules would therefore be less strongly bound to the iridium atoms and any

weakening of bonds within the hydrocarbon molecule would be reduced. However, the same argument would lead to an increase in the hydrogenolysis activity of the platinum component, a result which was not observed. In addition, the quantification of the desorption results showed that the majority of the hexane molecules fragmented upon adsorption to form C_1 units. Thus hydrogenolysis arguments based on electron donation effects are not valid because the hydrocarbon has already fragmented upon adsorption.

It appears that the observed phenomena cannot be explained entirely in terms of ligand effects and geometric factors must also be taken into account, the extent of hydrogenolysis activity being related in some complex way to the degree of dilution of reactive ensembles of metal atoms. Hence at this stage possible effects due to ligand and geometric factors for the Pt-Ir/alumina system cannot easily be separated. This is most likely due to the wide composition range of the dispersed clusters (see Section 6.4) and also a broad range of cluster sizes.

Recently, Faro and Kemball (1986) and Garden et al. (1986) have examined the reactions of several hydrocarbons over Pt-Ir/alumina catalysts to unravel the importance of electronic factors and ensemble effects for this system. However, in general, these workers could find no particular evidence for alloy interactions, probably because of the catalyst pretreatment, which for both studies consisted of an initial oxidation at 740K followed by reduction at 770K. The effects of an equivalent pretreatment are considered in the following section.

7.4.2 The Influence of SMSI

The results of the catalyst characterisation studies reported in the preceeding Chapters are generally consistent with the formation of a so-called SMSI state between the platinum-iridium metal particles and the oxide support following pretreatment R740. As outlined in Section 7.1 SMSI state formation has been generally found to reduce the hydrogenolysis activity of supported metal catalysts. In agreement with this observation the hexane thermal desorption results for the bimetallic samples subjected to pretreatments R740 and O740 R740 are also indicative of a reduced hydrogenolysis activity for the catalyst. Furthermore, this interpre-

tation was confirmed in experiments in which hexane pulse were passed over the catalyst.

As discussed in Section 7.1 hydrogenolysis reactions usually require an ensemble of metal atom sites and are regarded as 'structure sensitive'. Hence dilution of the active metal component in the surface will generally be expected to produce a marked reduction in catalyst hydrogenolysis activity. On this basis, the reduced hydrogenolysis activity following high temperature reduction could be explained by an interaction of metal particles with the alumina support to produce unreactive areas which dilute the more active metal clusters. Several processes could give rise to such phenomena and these are discussed below.

Den Otter and Dautzenberg (1978) were the first to claim that this dilution effect arose from alloying of some metal atoms with nearby partially reduced regions of the support. A plausible alternative is that high temperature reduction produces an encapsulation of the metal particles by the support (partially reduced?) as recently discussed for the Pt/titania system by Anderson et al. (1986). It should be noted that such coverage/combination effects would be very effective in reducing the hydrogenolysis activity of the very highly dispersed Pt-Ir clusters. However, such phenomena may not be so effective for the larger particles produced during pretreatment O740 R740.

An alternative dilution-type process has been put forward by Menon and Froment (1979, 1981) in which the high temperature reduction process induces the conversion of 'normal' chemisorbed hydrogen into more strongly bound forms (surface states?) that effectively block hydrogenolysis reaction sites. However, the hydrogen desorption results contained in Chapter Five, although showing the presence of strongly bound hydrogen, were not consistent with this interpretation since the total amount of desorbed hydrogen was found to decrease.

Another possibility is that the presence of metal causes a partial reduction of the nearby support with a consequent electron transfer from the partially reduced support to the metal. This is an alternative to the alloy/encapsulation phenomena were geometric effects are important. Indeed, it is expected that increased

electron density on the metal would inhibit hydrogenolysis activity for the reasons given in Section 7.4.1 above.

Finally, Burch and Garla (1982) have suggested that changes in particle morphology other than sintering may contribute to SMSI-type phenomena. In particular, high temperature annealing could result in the formation of particles with densely packed (111)-type faces. The incorporation of coordinatively unsaturated atoms into such faces would result in a decrease in hydrogenolysis activity (see Section 7.1.3). Such an explanation appears especially plausible for samples containing the larger iridium-rich crystallites. However, the hydrogen desorption profiles obtained for the samples containing the highly dispersed platinum-iridium particles do not seem to support this idea since the amount of hydrogen desorbed in the low temperature region, and therefore expected to come mainly from low index faces, actually decreased (see Section 5.3). However, it is possible that this interpretation may be valid for the Pt100 catalyst since the R740 sample possessed a reduced hydrogenolysis activity, whilst the hydrogen desorption profile showed only slight changes.

Thus, an overall picture of the nature of hydrogenolysis suppression processes begins to emerge. For iridium-containing samples subjected to pretreatment R740, the highly dispersed metal particles appear to interact closely with the partially reduced support. The nature of this interaction is uncertain but the change in hydrogenolysis activity is likely to arise from one of the following: (a) a dilution effect caused by encapsulation with the support, (b) a similar effect from alloying or (c) an electronic interaction whereby electrons are transferred from the partially reduced oxide to the metal. Presumably highly coordinatively unsaturated metal atoms will preferentially undergo such interactions. However, for the R740 Pt100 sample a carbon impurity barrier probably prevents this interaction from occurring (see Section 6.4) and a thermal annealing process is probably significant in which highly coordinatively unsaturated atoms are eliminated from the surface of the metal particles. A similar process probably accounts for the decrease in the activity of the larger iridium-rich crystallites produced during pretreatment O740 R740 since these particles would not be expected to interact as closely with the

support. However, the extent to which this annealing process could occur for highly dispersed iridium-containing samples, assuming that SMSI-type processes were not dominant, is unclear. Further examination of the behaviour of such clusters on several support materials is needed to resolve this question.

7.5 Summary

The hexane thermal desorption technique has been shown to be a particularly powerful method of investigating both the nature and the performance of Pt-Ir/alumina catalysts.

For samples subjected to pretreatment R610 the hydrogen desorption profiles show many similarities to hydrogen desorption from hexane-free samples. However, the quantity of strongly bound hydrogen is much greater. This indicates that hydrogen desorbing from the latter samples at temperatures in excess of around 600K may in part be due to the presence of carbonaceous material as well as arising from desorption from the support.

More importantly, methane was formed as a desorption product and the profile for the PtIr43 sample shows that Pt-Ir interactions are present, although it remains unclear whether ligand or ensemble effects are dominant. In addition, the results show that the hydrogenolysis activity of the iridium component is reduced in the bimetallic clusters, although sufficient activity remains to account for the activity maintenance of such bimetallic catalysts under reforming conditions. However, under the hydrogen-free conditions used in this study the hydrogenolysis activity causes an increased coking level for the iridium-containing samples. Oxidation at 740K prior to reduction appears to increase the hydrogenolysis activity of the bimetallic samples, which may be due to the presence of a redispersed iridium-rich phase following the reduction at 610K.

Alloy interactions were not particularly evident for the bimetallic sample subjected to pretreatment R740 although the results contained in previous Chapters show they exist. Furthermore, all samples subjected to this pretreatment and pretreatment O740 R740 exhibit a much reduced hydrogenolysis activity. For the highly dispersed iridium-containing samples this results from the formation of an SMSI state between the clusters and the support.

This probably occurs by an encapsulation or alloying dilution effect although an electron transfer process cannot be eliminated. However, for the monometallic R740 Pt100 sample and the large iridium-rich crystallites a thermal annealing process is the most likely cause of the activity decrease, whereby highly uncoordinatively unsaturated metal atoms are eliminated from the surface of the metal particles.

CHAPTER EIGHT

General Discussion and Summary

The results presented in this thesis show that the state and reactivity of a bimetallic Pt-Ir/alumina catalyst containing approximately equal quantities of the two metals are both very dependent upon the catalyst pretreatment conditions.

For the PtIr43 sample the TPR, TEM, XPS and hexane thermal desorption examinations all show that highly dispersed bimetallic particles are produced when the supported precursor salts are reduced at a temperature of 610K. The alloy clusters formed are less than around 2nm in diameter, and a wide range of cluster sizes probably exists below this dimension. In addition, the quantity of hydrogen produced during thermal desorption indicated that most of the metal atoms were located in the surface of the clusters. Furthermore, metal atoms found in the more coordinatively unsaturated regions of the particles (cf. (100)-type geometry) appear to adsorb two hydrogen atoms each, whilst atoms in the more densely packed zones (cf. (111)-type) bind only one hydrogen atom per surface metal atom. These particles are too highly dispersed to show any surface enrichment phenomena, although there is some evidence that clusters on the surface of the alumina may, on average, contain more iridium compared to particles found on the oxide inside the pore network.

The hexane desorption investigation showed that alloy formation is important in determining the performance of the catalyst. Thus the aromatisation activity of the bimetallic sample following pretreatment R610 was found to be greater than that of either of the two monometallic systems. More importantly, the alloy interaction was found to reduce the hydrogenolysis activity of the iridium component, whilst that of the platinum remained largely unchanged. However, sufficient iridium hydrogenolysis activity remains to reduce the level of coke build-up and this reduced activity is the most likely cause of the improved performance of Pt-Ir/alumina catalysts under reforming conditions. The XPS results provide evidence for an electron transfer from the platinum to the iridium centres and this could be responsible for the reduced iridium hydrogenolysis activity. However, quantification of the

hexane desorption results indicates that geometric factors may also be significant, and at the present stage it remains unclear which of the possibilities, if any, is dominant.

Dramatic changes in the properties of the PtIr43 catalyst take place when the sample is reduced at temperatures around 740K. The hexane thermal desorption investigation has shown that the hydrogenolysis activity of the catalyst is greatly reduced, whilst the initial aromatisation activity is largely unchanged. In principle many explanations can be given to account for this change in behaviour, including particle sintering, changes in cluster morphology, carbon poisoning during the reduction step or the formation of a so-called SMSI state. However, the results of the TEM examination tend to eliminate a sintering effect, whilst the hydrogen desorption examination excludes changes in cluster morphology as the cause of this effect for the iridium-containing samples. The TPR study did show that carbon was present on the samples and, furthermore, the TPO examination gave evidence that this carbon was present in at least three different forms. However, oxidation at 740K was found to remove most of the carbon from the catalyst and for the bimetallic sample subsequently reduced at 740K (pretreatment O740 R740) similar reduced hydrogenolysis activity was produced. Thus, it is unlikely that the change in performance of the R740 PtIr43 sample is due to the presence of carbon and this leaves only one possibility: the formation of an SMSI state.

Several types of metal-support interaction have been considered, the most likely being metal cluster encapsulation or alloy formation with the partially reduced support. However, an electron transfer process from the partially reduced alumina to the metal cannot be entirely ruled out and at the present stage it is unclear which of these possibilities is the cause of this change in catalytic behaviour. In this context, the TPR results for the iridium-containing samples did show that the alumina support was partially reduced at the highest reduction temperatures, whilst no support reduction was apparent for a non-oxidised monometallic platinum sample. Furthermore, the hydrogen desorption study showed that an SMSI state did not form for the latter catalyst, although this state was produced for a Pt100 sample initially oxidised at 740K prior to reduction at 740K. Hence, the presence of carbon in

the Pt100 sample appears to prevent the formation of an SMSI state, presumably by forming a barrier between the support and the metal. However, this leaves unexplained the fact that the hydrogenolysis activity of the R740 Pt100 sample was reduced compared to that of the R610 Pt100 sample despite the apparent absence of an SMSI effect. This result can be explained only by assuming that a change in particle morphology takes place caused by a thermal annealing. Finally, the suppression of the hydrogenolysis activity of the bimetallic sample by the high temperature reduction pretreatment is important since this provides an alternative to sulphurisation as a means of reducing undesirable hydrogenolysis reactions during catalytic reforming.

It is significant that a PtIr43 sample which had been subjected to an initial oxidation at 740K followed by reduction at 610K, showed a reduction in aromatisation activity but an increase in hydrogenolysis activity. Furthermore, there was little evidence of the beneficial action of bimetallic alloy clusters. In fact the TPR/TPO and TEM examinations indicated that around 65% of the iridium had agglomerated to form large iridium-rich crystallites, possibly having a bimodal particle size distribution with modal diameters of around 4nm and 9nm, whilst leaving a dispersed (< 2nm) platinum-rich phase. The formation of the bulk-like oxide crystallites was observed during TPO to occur at temperatures in excess of ~690K. In agreement with this, the TPR study indicated that samples that had been initially oxidised at a lower temperature (around 560K) reduced to form dispersed alloy metal clusters only. Significantly, the XPS results showed that the surface of the large iridium-rich crystallites were probably enriched in platinum, which is consistent with predictions made from alloy enrichment theories. Furthermore, the hydrogen desorption investigation showed that a limited redispersion of the large iridium-rich crystallites occurred during reduction at 610K. This is probably promoted by the presence of platinum both in the large crystallites and in the dispersed phase. The former may destabilise the large crystallites, whilst the latter probably act as redispersion centres by trapping out iridium species emanating from the large crystallites. The latter process most likely results in the formation of dispersed clusters with iridium enriched exteriors, which is a likely explanation for

the increased hydrogenolysis activity of the PtIr43 sample following pretreatment O740 R610.

As mentioned previously, the hydrogenolysis activity of a PtIr43 sample that had undergone an oxidation/reduction cycle depended upon the temperature of the final reduction, being lower for the O740 R740 sample than for the O740 R610 sample. This could partly be explained if the dispersed platinum-rich phase formed an SMSI state with the alumina substrate during high temperature reduction. However, the TEM study showed that the O740 R740 PtIr43 sample still contained large metal crystallites with a bimodal distribution of sizes clustered around 4nm and 7nm. Hence, it appears that hydrogenolysis sites are also removed from the larger iridium-rich crystallites. The latter most probably takes place by the thermal annealing-type process since the interaction is not expected to be as close between the support and the larger metal particles. It should be noted that the O740 R740 sample had a lower aromatisation activity than the R740 sample.

Overall, it has been shown that the inclusion of a high temperature oxidation step is detrimental to the performance of Pt-Ir/alumina reforming catalysts since this generally reduces the aromatisation activity, whilst the catalyst hydrogenolysis activity is increased. However, the latter can be largely offset by a high temperature reduction step following the initial oxidation at 740K. These results are important since 'regenerative' high temperature oxidation treatments are frequently used to burn off coke deposits from supported metal catalysts. Foger et al. (1985), amongst others, have recognised this problem and have proposed that regeneration should involve exposing the sample to Cl_2 and NO/CO gas mixtures to promote the redispersion of the iridium. However, it must be stressed that such regenerative procedures will be most beneficial only if alloy clusters are formed in which bimetallic interactions are maximised. If highly dispersed iridium-rich clusters are formed during regeneration then such entities will result in a catalyst having an undesirably high hydrogenolysis activity for the reforming process, unless the final reduction step is carried out at temperatures close to 740K.

The role of adsorbed chlorine in determining reforming catalyst performance has been discussed by Gates et al. (1979). In general, chlorine tends to increase the acidity of the alumina support which leads to greater hydrocarbon isomerisation under reforming conditions. No particular conclusions regarding the effects of chlorine could be made in this study, especially since no isomerised products could be detected. It is significant that no chlorine-containing species were liberated during reduction pre-treatments and it is therefore concluded that these catalysts have a high chlorine content. To assess the role of this chlorine it would be necessary to prepare bimetallic samples using chlorine-free metal precursor materials, such as carbonyl or acetonato-type complexes.

The main findings of this study can be summarised as follows:

1) TPR and TPO are powerful catalyst characterisation techniques only when the reduction/oxidation processes are followed with a mass spectrometer detector.

2) The conventional isothermal hydrogen chemisorption technique for measuring metal particle sizes should be used with caution since a particular hydrogen-to-metal adsorption stoichiometry cannot be assumed; (111)-type and (100)-type metal regions behave differently, adsorbing one and two hydrogen atoms per surface metal atom respectively.

3) The improved performance of Pt-Ir/alumina catalysts that have been reduced only at temperatures in the region of 610K, is due to the presence of alloy clusters in which the remaining hydrogenolysis activity of the iridium centres reduces catalyst fouling under reforming conditions.

4) The hydrogenolysis activity of the alloy particles is suppressed following reduction at 740K, although the initial aromatisation activity remains largely unaffected.

5) Whilst oxidation at 560K, followed by reduction, results in the formation of dispersed alloy clusters, oxidation at a temperature of 740K, followed by reduction, causes the formation of large (~10nm) iridium-rich crystallites, which are surface enriched in platinum. There also appears to be a highly dispersed platinum-rich phase. The high hydrogenolysis activity of the latter

sample probably results mainly from a limited redispersion of the large crystallites during the reduction step, which produces dispersed metal clusters with an iridium-rich exterior.

6) The undesirably high hydrogenolysis activity of Pt-Ir/alumina catalysts that have been subjected to oxidation at 740K, can be diminished by performing the reduction stage at a similarly high temperature. This probably results from the onset of an SMSI state for the highly dispersed particles as well as a thermal annealing of the large crystallites.

In conclusion, the results described in this thesis have shown that the performance of alumina-supported platinum-iridium catalysts is determined just as much by the method of activation as it is by the composition of the sample. This behaviour can be explained in terms of the way in which various metal species react under different types of pretreatment, resulting under certain conditions in the formation of a strong interaction between the metal particles and the alumina support. This variability of catalyst properties is also found with most other supported metal systems and it is a prime cause of many of the apparent inconsistencies and anomalies that exit in the field of catalytic research. This has to some extent hindered the comprehension of heterogeneous catalyst systems. However, such variability has the potential to allow the properties of a supported metal catalyst to be finely tuned to meet the requirements of industry and the environment. Furthermore, it is only through a complete understanding of the origins of such behaviour that new improved catalysts and catalytic processes can be produced by design rather than by trial and error. This thesis has sought to rationalise the catalytic behaviour of one particular supported metal system under various pretreatment conditions and in this respect it serves to bring this ultimate goal a little closer.

APPENDIX A1

Iridium Crystallite Size Calculation

If the agglomerated iridium crystallites formed during pre-treatment 0740 R610 are assumed to be hemispherical particles, the value of the crystallite radius, R, can be calculated from the formula:

$$V_{Tot} = \frac{2 \pi R^3}{3} \qquad (A1.1)$$

where V_{Tot} is the volume of the hemisphere. If the particles are of constant density and assuming that metal atoms lying deeper than the photoelectron escape depth, λ_e, do not contribute to the observed XPS signal and that all the metal atoms above these contribute equally, then the ratio of the outer shell volume of thickness λ_e to the total particle volume, V_{Tot}, is given by the ratio of the observed XPS $4d_{5/2}$ peak intensitites for the oxidised and unoxidised samples, viz:

$$(V_{Tot} - V_{in})/V_{Tot} = 6.7/18.8 \qquad (A1.2)$$

where V_{in} is the volume of the central core of the crystallites whose atoms do not contribute to the XPS signal. The crystallite radius can be calculated assuming that λ_e is 15Å (a value calculated by Penn (1976) to be appropriate for iridium under the experimental conditions encountered in this study) by combination of equations (A1.1) and (A1.2) to give the following expression:

$$12.1\ R^3 = 18.8(R - 15)^3 \qquad (A1.3)$$

The only real root of which occurs when $R \simeq 110$Å.

APPENDIX A2

Hydrocarbon Mass Balance Calculations

The following sections give details of the mass balance calculations for the hexane thermal desorption experiments, the results of which are summarised in Tables 7.2-7.5. Various examples are given to illustrate the calculations. It should be noted that all quantities are calculated with respect to a 50 mg sample and that all quantities of hydrogen are in moles of hydrogen atoms.

A.1 Carbon Mass Balance

Prior to carbon dioxide production the amount of carbon on the sample, C_{left}, is given by:

$$C_{left} = 6(Hx_{ads} - Hx_{des}) - C_M - 6C_B \qquad (A2.1)$$

where Hx_{ads} and Hx_{des} represent the amount of hexane adsorbed and desorbed respectively, and C_M and C_B are the amounts of methane and benzene produced respectively. Hence for sample R610 PtIr43 equation (A2.1) gives:

$$C_{left} = 6(3.1 \times 10^{-7} - 1.7 \times 10^{-8}) - 8.4 \times 10^{-8} - 6(3.5 \times 10^{-9})$$

Thus, $C_{left} = 1.7 \times 10^{-6}$ mols

The carbon remaining at the end of the desorption experiment, C_{end} is given by:

$$C_{end} = C_{left} - C_C \qquad (A2.2)$$

where C_C/mol is the amount of carbon dioxide produced, corrected for the carbon dioxide which would have desorbed without adsorbing any hexane, C_X/mol (see Figs. 5.1-5.3), hence:

$$C_C = C_T - C_X \qquad (A2.3)$$

where C_T/mol is the total amount of carbon dioxide produced. Therefore, for the above sample, equations (A2.2) and (A2.3) give:

$$C_{end} = 1.7 \times 10^{-6} - (2.05 \times 10^{-6} - 7.3 \times 10^{-7})$$

Thus, $C_{end} = 3.8 \times 10^{-7}$ mols

For run 2, the amounts of carbon remaining have been calculated in the same manner. The values of C_{end} contained in Tables 7.2-7.5 for

run 2 refer to that particular experiment and ignore carbon deposition resulting from run 1. Thus, the total amount of carbon remaining on sample R610 PtIr43 after run 2 is equal to (3.8 + 11.9) x 10^{-6} mols.

A.2 Hydrogen Mass Balance

A.2.1 Samples Subjected to Low Temperature Reduction

a) Run 1. Following hexane adsorption the number of moles of hydrogen atoms missing from the metal profile, H_{rem}^{M} is given by

$$H_{rem}^{M} = H_M - H_C \qquad (A2.4)$$

where H_M and H_C are the numbers of moles of hydrogen atoms desorbed below ~500K in the absence and presence of hexane respectively. Evaluation of equation (A2.4) for sample R610 Pt100 gives:

$$H_{rem}^{M} = (0.81 - 0.57) \times 3.8 \times 10^{-6} = 9.1 \times 10^{-7} \text{ mols}$$

Prior to carbon dioxide production the number of moles of hydrogen atoms remaining on the catalyst, H_{left} is given by:

$$H_{left} = H_{rem}^{M} - H_{lib} + 14(Hx_{ads} - Hx_{des}) - 4\,C_M - 6C_B \qquad (A2.5)$$

where H_{lib} is the number of moles of hydrogen atoms liberated from the sample during hexane adsorption. Evaluation of equation (A2.5) for the above sample gives:

$$H_{left}/\text{mol} = 9.1 \times 10^{-7} - 9.5 \times 10^{-7} + 14(2.9 \times 10^{-7} - 6.6 \times 10^{-9}) - 4\,(6.6 \times 10^{-8}) - 6(0)$$

$$H_{left} = 3.66 \times 10^{-6} \text{ mols}$$

Now the number of moles of H atoms actually desorbed during CO_2 production, H_{hT}, is given by

$$H_{hT} = H_T - H_C \qquad (A2.6)$$

where H_T is the number of moles of H atoms desorbed over the whole profile. Hence for the above sample:

$$H_{hT} = (2.36 - 0.57) \times 3.8 \times 10^{-6} = 6.8 \times 10^{-6} \text{ mols}$$

Thus for the R610 Pt100 sample $H_{hT} > H_{left}$. Assuming that reaction (7.7) causes this inequality, the number of moles of H atoms which would be desorbed during this reaction, H_R, can be calculated from the value of C_C and the composition x of the reactive hydrocarbon

fragments. One estimate of x is given by the following:

$$x = H_{left}/C_{left} \qquad (A2.7)$$

From the stoichiometry of reaction (7.7)

$$H_R = C_C \times 2(1 + x/2) \qquad (A2.8)$$

Evaluation of equation (A2.8) for the above sample gives

$$H_R = 6.9 \times 10^{-6} \text{ mols}$$

and therefore $H_{hT} \sim H_R$. If equation (A2.7) is valid then the amount of H atoms left at the end of the desorption run, H_{end} is given by:

$$H_{end} = H_R - H_{hT} \qquad (A2.9)$$

Thus, the composition of the remaining fragments, assuming that all the hydrogen is associated with carbon, is given by:

$$x_{end} = H_{end}/C_{end} \qquad (A2.10)$$

Alternatively, the composition of the reactive fragments can be back calculated using the value of C_C, assuming that reaction (7.7) occurs and H_{hT} arises predominantly from this reaction. Hence, rearrangement of equation (A2.8) allows the fragment composition, $(H/C)_R$ to be obtained from:

$$(H/C)_R = (H_{hT}/C_C) - 2 \qquad (A2.11)$$

Evaluation of this enables the composition of the unreactive fragments, $(H_{end}/C_{end})_{UR}$, to be determined from:

$$(H_{end}/C_{end})_{UR} = (H_{left} - (H/C)_R \times C_C)/C_{end} \qquad (A2.12)$$

However, if it is assumed that CO_2 is formed by a process which does not abstract hydrogen from some source then the composition of the remaining fragments, $(H_{end}/C_{end})_{NR}$, is given by:

$$(H_{end}/C_{end})_{NR} = (H_{left} - H_{hT})/C_{end} \qquad (A2.13)$$

b) Run 2. For run 2 it has been assumed that any hydrogen or carbon remaining from run 1 is unreactive and for this reason it has not been included in the run 2 mass balance analysis. Thus, the results for run 2 do not represent the total amounts present, but only the additional amounts formed during the second experiment. Hence for run 2:

$$H_{left} = 14(Hx_{ads} - Hx_{des}) - H_{lib} - H_C - 4C_M - 6C_B \quad (A2.14)$$

The calculation of the fragment compositions were carried out as for run 1 with the above assumptions operative.

A.2.2 Samples Subjected to High Temperature Reduction

For these samples the peaks in the hydrogen profile are not well separated and therefore H_C and H_{hT} cannot be evaluated accurately. Since the H_{left}/C_{left} ratios cannot be calculated the mass balance analysis is restricted to finding the amounts of hydrogen and carbon remaining following the desorption run.

a) Run 1. The number of moles of H atoms removed from the entire profile by the adsorbed hydrocarbon, H_{rem}^T, is given by:

$$H_{rem}^T = H_M^T - H_T \quad (A2.15)$$

where H_M^T is the number of moles of H atoms desorbed over the entire profile in the absence of hydrocarbon. Therefore the number of moles of H atoms left at the end of the desorption run, H'_{end}, assuming that all CO_2 produced is formed by reaction (7.7), is given by:

$$H'_{end} = H_{rem}^T + 14(Hx_{ads} - Hx_{des}) - H_{lib} - 4C_M - 6C_B + 2C_C \quad (A2.16)$$

The C_C term is included since reaction (7.7) abstracts 2 mols of hydrogen atoms from the support for every mole of CO_2 produced. This hydrogen contributes to H_T and since it did not originate from the hydrocarbon fragments it must be added to H_{end}. In other words H_T is larger than it would be if all the hydrogen came from the hydrocarbon fragments and hence subtraction of all of this amount from H'_{end} 'removes' too much hydrogen from the hydrocarbon species. This analysis is equivalent to finding H_{end} using equations A2.11 and A2.12.

The composition of the remaining fragments after the desorption run, x'_{end} is then given by

$$x'_{end} = H'_{end}/C_{end} \quad (A2.17)$$

b) Run 2. For run 2 it has again been assumed that any hydrogen or carbon left following run 1 is inactive. Hence, for run 2:

$$H'_{end} = 14(Hx_{ads} - Hx_{des}) - H_{lib} - H_T - 4C_M - 6C_B + 2C_C \quad (A2.18)$$

from which the fragment compositions can be evaluated.

REFERENCES

ACRES, G.J.K., BIRD, A.J., JENKINS, J.W. and KING, F. (1981), Catalysis (London), 4, 1.

ADKINS, S.R. and DAVIS, B.H. (1984), J. Catal., 89, 371.

AMBS, W.J. and MITCHELL, M.M.Jr. (1983), J. Catal., 82, 226.

AMENOMIYA, Y. (1971), J Catal., 22, 109.

AMENOMIYA, Y., MORIKAWA, Y. and PLEIZIE, G. (1977), J. Catal., 46, 431.

AMIR-EBRAHIMI, V., CHOPLIN, A., PARAYRE, P. and GAULT, F.G. (1980), Nouv. J. Chim., 4, 431.

ANDERSON, J.B.F., BURCH, R. and CAIRNS, J.A. (1986), Appl. Catal., 25, 173.

ANDERSON, J.R. (1973), Adv. Catal., 23, 1.

ANDERSON, J.R. (1985), Sci. Prog., 69(276), 461.

ANDERSON, J.R. and AVERY, N.R. (1966), J. Catal., 5, 446.

ANDERSON, J.R., FOGER, K. and BREAKESPEARE, R.J. (1979), J. Catal., 57, 458.

ANDERSON, J.R. and SHIMOYANA, Y. (1973), Proc. 5th Int. Congr. Catal., Vienna, p.695.

D'ANIELLO, M.J. (1981), J. Catal., 69, 9.

APESTEGUIA, C.R. and BARBIER, J. (1982), J. Catal., 78, 352.

AVERY, N.R. (1984), Surf. Sci., 137, 109.

AVERY, N.R. (1985), Surf. Sci., 163, 357.

AVERY, N.R. and SHEPPARD, N. (1986a), Proc. Roy. Soc. London, A, 405, 1.

AVERY, N.R. and SHEPPARD, N. (1986b), Proc. Roy. Soc. London, A, 405, 27.

BALDWIN, V.H. and HUDSON, J.B. (1971), J. Vac. Sci. Tech., 8, 49.

BARBIER, J. and MARECOT, P. (1981), Nouv. J. Chim., 5, 393.

BARO, A.M. and IBACH, H. (1980), Surf. Sci., 92, 237.

BARO, A.M., IBACH, H. and BRUCHMANN, H.D. (1979), Surf. Sci., 88, 384.

BARON, K., BLAKELY, D.W. and SOMORJAI, G.A. (1974), Surf. Sci., 41, 45.

BARR, T.L. (1983), "Practical Surface Analysis by Auger and X.P.S.", ed. Briggs, D. and Seah, M.P., p.283, Wiley, N. York.

BARRON, Y., MAIRE, G., MULLER, J.M. and GAULT, P.G. (1966), J. Catal, 5, 428.

BASSI, I.W., GARBASSI, F., VLAIC, G., MARZI, A., TAUSZIK, G.R., COCCO, G., GALVAGNO, S. and PARRAVANO, G. (1980), J. Catal., 64, 405.

BECK, D.D. and WHITE, J.M. (1984a), J. Phys. Chem., 88, 174.

BECK, D.D. and WHITE, J.M. (1984b), J. Phys. Chem., 88, 2764.

BILOEN, P., HELLE, J.N., VERBEEK, H., DAUTZENBERG, F.M. and SACHTLER, W.M. (1980), J. Catal., 63, 112.

BIRKE, P., BOHM, D. and ENGELS, S. (1985), Z. Chem., 25, 74.

BLAKELY, D.W. and SOMORJAI, G.A. (1976), J. Catal., 42, 181.

VAN'T BLIK, H.F.J. and PRINS, R. (1986a), J. Catal., 97, 188.

VAN'T BLIK, H.F.J., MARTENS, J.H.A. and PRINS, R. (1986b), J. Catal., 97, 200.

VAN'T BLIK, H.F.J., KONINGSBERGER, D.C. and PRINS, R. (1986c), J Catal., 97, 210.

BOER, H., BOERSMA, W.J. and WAGSTAFF, N. (1982), Rev. Sci. Instrum., 53, 349.

BOLIVAR, C., CHARCOSSET, H., FRETY, K., PRIMET, M., TOURNAYAN, L., BETIZEAU, C., LECLERQ, G. and MAUREL, R. (1975), J. Catal., 39, 249.

BOND, G.C. and BURCH, R. (1983), Catalysis (London), 6, 27.

BOUWMAN, R. and BILOEN, P. (1977), J. Catal., 48, 209.

BOWLING, R.A., SHAFFNER, T.J. and LARRABEE, G.B. (1985), Anal. Chem., 57, 130R.

BOZON-VERDURAZ, F. (1970), J. Catal., 18, 12.

BOZON-VERDURAZ, F., OMAR, A., ESCARD, J. and PONTVIANNE, B. (1976), J. Catal., 53, 126.

BRIGGS, D. and SEAH, M.P. (1983) (Eds) "Practical Surface Analysis by Auger and X.P.S.", Wiley, N. York.

BRINEN, J.S. and SCHMIDT, J.L. (1976), J. Catal., 45, 274.

BRUNELLE, J.P. (1978), Pure and Applied Chem., 50, 1211.

BRUNELLE, J.P., MONTARNEL, R.E. and SUGIER, A.A. (1976), Proc. 6th Int. Congr. Cat., London. p.844.

BURCH, R. (1981), J. Catal., 71, 348.

BURCH, R. (1985), Catalysis (London), 7, 149.

BURCH, R. and GARLA, L.C. (1982), J. Catal., 73, 20.

BUREAU-TARDY, M., PEDERSEN, E.P. and DJEGA-MARIADASSOU, G. (1978), C.R. Acad. Sci. Paris, 286, 601.

BURTON, J.J., HYMAN, F. and FEDAL, D. (1975), J. Catal., 37, 106.

CANDY, J.P., FOUILLOUX, P. and RENOUPREZ, A.J. (1980), J. Chem. Soc. Faraday Trans. 1, 76, 616.

CARDONA, M. and LEY, L. (Eds) (1978), "Photoemission in Solids 1: General Principles", Springer-Verlag, Berlin.

CARTER, J.L., CUSUMANO, J.A. and SINFELT, J.H. (1971), J. Catal., 20, 223.

CARTER, J.L., MCVICKER, G.B., WEISMAN, W., KEMAK, W.S. and SINFELT, J.H. (1982), Appl. Catal., 3, 327.

CHARCOSSET, J., FRETY, R., LECLERQ, G., NEFF, B. and TARDY, B. (1976), C.R. Acad. Sci. Paris, 283, 331.

CHARCOSSET, J., BARBIER, J., BLANCHARD, G. FRETY, R., NEFF, B., PERICHOV, V., TARDY, B. and VARLOUD, J. (1979a), Thermochim. Acta, 28, 85.

CHARCOSSET, J., FRETY, R., LECLERQ, G., MORAWECK, B., TOURNAYAN, L. and VARLOUD, J. (1979b), React. Kinet. Catal. Lett., 10, 301.

CHASTON, J.C. (1965), Plat. Met. Rev., 9, 51.

CHEN, H.W. and WHITE, J.M. (1986), J. Mol. Catal., 35, 355.

CHERNGAEV, I.I. and NOVOZHENYUK, Z.M. (1966), Russ. J. Inorg. Chem., 11, 1004.

CHRISTMANN, K. and ERTL, G. (1976), Surf. Sci., 60, 365.

CHRISTMANN, K., ERTL. G. and PIGNET, T. (1976), Surf Sci., 54, 365.

CHRISTOFFEL, E.G. and PAAL, Z. (1982), J. Catal., 73, 30.

CIAPETTA, F.G. and WALLACE, D.N. (1972), Cat. Rev., 5, 67.

CIMINO, A., BOUDART, M. and TAYLOR, H.S. (1954), J. Phys. Chem., 58, 796.

CLARKE, J.K.A. (1975), Chem. Rev., 75, 291.

CLARKE, J.K.A. and ROONEY, J.J.(1976), Adv. Catal., 25, 125.

COLLINS, D.M. and SPICER, W.E. (1977), Surf. Sci., 69, 85.

GAULT, F.G., AMIR-EBRAHIMI, V., GARIN, F., PARAYRE, P. and WEISANG, F. (1979a), Bull. Soc. Chim. Belg., 88, 475.

GAULT, F.G., AMIR-EBRAHIMI, V., GARIN, F. and WEISANG, F. (1979b), Nouv. J. Chim., 3, 529.

GEUS, J.W. (1983), Stud. Surf. Sci. Catal., 16, 1.

GONZALEZ-TEJUCA, L., ALKA, K., NAMBA, S. and TURKEVICH, J. (1977), J. Phys. Chem., 81, 5399.

GRAHAM, A.G. and WANKE, S.E. (1981), J. Catal., 68, 1.

GREGG, S.J. and RAMSAY, J.D.F. (1969), J. Phys. Chem., 73, 1243.

VAN HARDEVELD, R. and HARTOG, F. (1969), Surf. Sci., 15, 189.

HILAIRE, L., GUERRERO, G.D., LEGARE, P., MAIRE, G. and KRILL, G. (1984), Surf. Sci., 146, 569.

HOYLE, N.D., NEWBLATT, P.H., ROLLINS, K., SERMON, P.A. and WURIE, A.T. (1985), J. Chem. Soc. Faraday Trans.1, 81, 2605.

HUIZINGA, T., VAN'T BLIK, H.F.J., VIS, J.C. and PRINS, R. (1983), Surf. Sci., 135, 580.

HUIZINGA, T., VAN GRONDELLE, J. and PRINS, R. (1984), Appl. Catal., 10, 199.

HURST, N.W., GENTRY, S.J., JONES, A. and MCNICOL, B.D. (1982), Catal. Rev. Sci. Eng., 24, 233.

IBACH, J. and LEHWALD, S. (1978), J. Vac. Sci. Technol., 15, 407.

IBBOTSON, D.E., WITTRIG, T.S. and WEINBERG, W.H. (1980), J. Chem. Phys., 72, 4885.

IBOK, E.E. and OLLIS, D.F. (1980), J. Catal., 66, 391.

ISAACS, B.H. and PETERSEN, E.E. (1982), J. Catal., 77, 43.

JACKSON, S.D., WELLS, P.B., WHYMAN, R. and WORTHINGTON, P. (1981), Catalysis (London), 75, 4.

JENKINS, J.W., MCNICOL, B.D. and ROBERTSON, S.D. (1977), Chem. Tech., 7, 316.

JOYNER, R. and MEEHAN, P. (1983), Vacuum, 33, 691.

KANTSCHEWA, M., ALBANO, E.V., ERTL, G. and KNOEZINGER, J. (1983), Appl. Catal., 8, 71.

KARPINSKII, Z. and CLARKE, J.K.A. (1975), J. Chem. Soc. Faraday Trans.1, 71, 2310.

KAWASAKI, K., KODANA, T., MIHI, H. and KIOKA, T. (1977), Surf. Sci., 64, 349.

KERKOF, F.P.J.M. and MOULIJN, J.A. (1979), J. Phys. Chem., 83, 1612.

KESMODEL, L.L., DUBOIS, L.H. and SOMORJAI, G.A. (1979), J. Chem. Phys., 70, 2180.

KING, D.A. (1975), Surf. Sci., 47, 384.

KIP, B.J., VAN GRONDELLE, J., MARTENS, J.H.A. and PRINS, R. (1986a), Appl. Catal., 26, 353.

KIP, B.J., DUIVENVOORDEN, F.B.M., KONINGSBERGER, D.C. and PRINS, R. (1986b), J. Am. Chem. Soc., 108, 5633.

KOESTNER, R.J. FROST, J.C., STAIR, P.C., VAN HOWE, M.A. and SOMORJAI, G.A. (1982), Surf. Sci., 116, 85.

KOMERS, R., AMENOMIYA, Y. and CVETANOVIC, R.J. (1969), J. Catal., 19, 293.

KONVALINKA, J.A., VAN OEFFELT, P.H. and SCHOLTEN, J.J.F. (1981), Appl. Catal., 17, 141.

KONVALINKA, J.A. and SCHOLTEN, J.J.F. (1977), J. Catal., 48, 374.

KRAMER, R. and ANDRE, M. (1979), J. Catal., 58, 287.

KRIER, C.A. and JAFFEE, R.I. (1973), J. Less-Comm. Met., 5, 411.

KRISHNAMURTHY, S., LANDOLT, G.R. and SCHOENNAGEL, H.J. (1982), J. Catal., 78, 319.

KRUPAY, B.W. and AMENOMIYA, Y. (1981), J. Catal., 67, 362.

KUIJERS, F.J. and PONEC, V. (1978), Appl. Surf. Sci., 2, 43.

KUNIMORI, K., IKEDA, Y., SOMA, M. and UCHIJIMA, T. (1983), J. Catal., 79, 185.

KUNIMORI, K., MAEZAWA, I. and UCHIJIMA, T. (1985), J. Chem. Soc. Chem. Comm., (9), 568.

KUNIMORI, K., OKOUCHI, T. and UCHIJIMA, T. (1980), Chem. Lett., (12), 1513.

LANG, B., JOYNER, R.W. and SOMORJAI, G.A. (1972), Surf. Sci., 30, 454.

LEE, T.J. and KIM, Y.G. (1984), J. Catal., 90, 279.

LESTER, G.R. (1969), J. Catal., 13, 187.

LEWIS, R.T. and KELLY, M.A. (1980), J. Elec. Spec. Rel. Phen., 20, 105.

LIAO, P.C., CARBERRY, J.J., FLEISCH, T.H. and WOLF, E.E. (1982), J. Catal., 74, 307.

LIESKE, J., LIETZ, G., SPINDLER, H. and VOELTER, J. (1983), J. Catal., 81, 8.

LIESKE, H. and VOELTER, J. (1984), Z. Anorg. Allg. Chem., 512, 65.

LIETZ, G., LIESKE, H., SPINDLER, H., HANEKE, W. and VOLTER, J. (1983), J. Catal., 81, 17.

LITTLE, L.H. and AMBERG, C.H. (1962), Can. J. Chem., 40, 1997.

LU, K.E. and RYE, R.R. (1974), Surf. Sci., 45, 677.

MADEY, T.E., WAGNER, C.D. and JOSHI, A. (1977), J. Elec. Spec. Rel. Phen., 10, 359.

MASON, M.G. (1983), Phys. Rev. B., 27, 748.

MCCABE, R.W. and SCHMIDT, L.D. (1976a), Surf. Sci., 65, 189.

MCCABE, R.W. and SCHMIDT, L.D. (1976b), Surf. Sci., 60, 85.

MCKERY, M.A., ROONEY, J.J. and SAMMAN, N.G. (1973), J. Catal., 30, 330.

MCNICOL, B.D. (1977), J. Catal., 46, 438.

MCVICKER, G.B., BAKER, R.T.K., GARTEN, R.L. and KUGLER, E.L. (1980), J. Catal., 65, 207.

MCVICKER, G.B., COLLINS, P.J. and ZIEMIAK, J.J. (1982), J. Catal., 74, 156.

MCVICKER, G.B., GARTEN, R.L. and BAKER, R.T.K. (1978), J. Catal., 54, 129.

MCVICKER, G.B. and ZIEMIAK, J.J. (1985), Appl. Catal., 14, 229.

MCVICKER, G.B. and ZIEMIAK, J.J. (1985), J. Catal., 95, 473.

MENON, P.G. and FROMENT, G.F. (1979), J. Catal., 59, 138.

MENON, P.G. and FROMENT, G.F. (1981), Appl. Catal., 1, 31.

MIEVILLE, R.L. (1984), J. Catal., 87, 437.

MILLS, G.A., HEINEMANN, H., MILLIKEN, T.H. and OBLAD, A.G. (1953), Ind. Eng. Chem., 45, 134.

MIMEAULT, V.J. and HANSEN, R.S. (1966), J. Chem. Phys., 45, 2240.

MINOT, C., BIGOT, B. and HARITI, A. (1986), J. Am. Chem. Soc., 108, 196.

MINTSA-EYA, V., HILAIRE, L., TOUROUDE, R., GAULT, F.G., MORAWECK, B. and RENOUPREZ, A. (1982), J. Catal., 76, 169.

MOSS, R.L. (1976), "Experimental Methods in Catalytic Research", 2, p.43.

NIEMANTSVERDRIET, J.W., VAN KAAM, J.A.C., FLIPSE, C.F.J. and VAN DER KRAAN, A.M. (1985), J. Catal., 96, 58.

NIEUWENHUYS, B.E., HAGEN, D.I., ROVIDI, G and SOMORJAI, G.A. (1976), Surf. Sci., 59, 155.

NIEUWENHUYS, B.E. and SOMORJAI, G.A. (1977), J. Catal., 46, 259.

NIEUWENHUYS, B.E. and SOMORJAI, G.A. (1978), Surf. Sci., 72, 8.

NORTON, P.R. and GOODALE, J.W. (1979), Solid State Commun., 31, 223.

ONUFERKO, J.H., SHORT, D.R. and KELLEY, M.J. (1984), Appl. Surf. Sci., 19, 227.

DEN OTTER, G.J. and DAUTZENBERG, F.M. (1978), J. Catal., 53, 116.

PAAL, Z. (1980), Adv. Catal., 29, 273.

PAAL, Z. and TETENYI, P. (1973), J. Catal., 30, 350.

PAAL, Z. and TETENYI, P. (1982), Catalysis (London), 5, 80.

PAAL, Z. and THOMSON, S.J. (1973), J. Catal., 30, 96.

PARERA, J.M., JABLONSKI, E.L., CABROL, R.A., FIGOLI, N.S., MUSSO, I.C. and VERDERONE, R.J. (1984), Appl. Catal., 12, 125.

PARKYNS, N.D. (1969), J. Chem. Soc. A., 410.

PARKYNS, N.D. (1971), J. Phys. Chem., 75, 526.

PARYJCZAK, T., JEZWIAK, K.W. and GORALSKI, J. (1982), React, Kinet. Catal. Lett., 21, 377.

PENN, D.R. (1976), J. Elec. Spec. Rel. Phen., 9, 29.

PEREZ, O.L., ROMAN, D. and YACAMAN, M.J. (1983), J. Catal., 79, 240.

PERI, J.B. (1975), J. Phys. Chem., 79, 1582.

PICK, W.C.S., WANKE, S.E. and KLENGLER, U. (1983), Prepr.-Am. Chem. Soc., Div. Pet. Chem., 28, 429.

PONCELET, G., GRANGE, P. and JACOBS, P.A. (1983), (Eds.) Stud. Surf. Sci. Catal. Vol.16.

PONEC, V. (1983), Adv. Catal., 32, 149.

RAGAINI, S.V. and CATTANIA-SABBADINI, M.G. (1985), J. Catal, 93, 161.

RAMASWAMY, A.V., RATVASAMY, P., SWASANKER, S. and LEONARD, A.J. (1976), Proc. 6th Int. Congr. Cat., London, p.855.

RASSER, J.C. (1977), Ph.D. Thesis, Delft University.

RASSER, J.C., BEINDORFF, W.H. and SCHOLTEN, J.J.F. (1979), J. Catal., 59, 211.

RAUBE, E. (1959), J. Less-Comm. Met., 1, 3.

RAUBE, E. and PLATE, W. (1956), Z. Metallkd, 47, 688.

RETHWISCH, D.G. and DUMESIC, J.A. (1986), Langmuir, 2, 73.

RICE, R.W. and LU, K. (1982), J. Catal., 77, 104.

ROBERTSON, S.D., MCNICOL, B.D., DE BAAS, J.H., KLOET, S.C. and JENKINS, J.W. (1975), J. Catal., 37, 424.

ROUCO, A.J., HALLER, G.L., OLIVER, J.A. and KEMBALL, C. (1983), J. Catal., 84, 297.

ROZANOV, V.V., GLAND, J. and SKLYAROV, A.V. (1979), Kinet. Katal., 20, 1030.

ROZANOV, V.V. and SKLYAROV, A.V. (1978), Kinet. Katal., 19, 1246.

ROZANOV, V.V., VLASENKO, A.G. and SKLYAROV, A.V. (1982), Kinet. Katal., 23, 1087.

RUCHENSTEIN, E. and DADYBURJOR, D.B. (1977), J. Catal., 48, 73.

RUCHENSTEIN, E. and DADYBURJOR, D.B. (1983), Rev. Chem. Eng., 1, 251.

RUCHENSTEIN, E. and PULVERMACHER, B. (1973), J. Catal, 29, 224.

SACHTLER, W.M.H. and VAN SANTEN, R.A. (1977), Adv. Catal., 26, 69.

SACHTLER, W.M.H. and VAN SANTEN, R.A. (1979), Appl. Surf. Sci., 3, 121.

SALMERON, M. and SOMORJAI, G.A. (1982), J. Phys. Chem., 86, 341.

SANTACESARIA, E., CARRA, S. and ADAMI, I. (1977), Ind. Eng. Chem. Prod. Res. Dev., 16, 41.

SAYERS, C.M. (1984), Surf. Sci., 143, 411.

SCHARPEN, L.H. (1974), J. Elec. Spec. Rel. Phen., 5, 369.

SCHWEIZER, A.E. and KERR, G.T. (1978), Inorg. Chem., 17, 2326.

SCOFIELD, J.H. (1976), J. Elec. Spec. Rel. Phen., 8, 129.

VAN SENDEN, J.G., VAN BROEKHOVEN, E.H., WEESMAN, C.T.J. and PONEC, V. (1984), J. Catal., 87, 468.

SEXTON, B.A., HUGHES, A.E. and FOGER, K. (1982), J. Catal., 77, 85.

SEXTON, B.A., HUGHES, A.E. and FOGER, K. (1984), J. Catal., 88, 466.

SHARAN, K.M. (1984), Cat. Rev. Sci. Eng., 26, 141.

SILVESTRI, A.J., NARO, P.A. and SMITH, R.L. (1969), J. Catal., 14, 386.

SINFELT, J.H. (1973), Adv. Catal., 23, 91.

SINFELT, J.H. (1983), "Bimetallic Catalysts - Discoveries, Concepts and Applications", J. Wiley and Sons, N.York.

SINFELT, J.H. and VIA, G.H. (1979), J. Catal., 56, 1.

SINFELT, J.H., VIA, G.H. and LYTLE, F.W. (1982), J. Chem. Phys., 76, 2779.

SKLYAROV, A.V., KRYLOV, O.V. and KEULKS, G. (1977), Kinet. Katal., 18, 1213.

SKLYAROV, A.V., ROZANOV, V.V. and KISLYUK, M.V. (1978), Kinet Katal., 19, 328.

SMUTEK, M., CERRY, S. and BUZEK, F. (1975), Adv. Ctal., 24, 343.

STEINIGER, H., IBACH, U. and LEHWALD, S. (1982), Surf. Sci., 117, 685.

STEPHAN, J.J., PONEC, V. and SACHTLER, W.M.H. (1975), J. Catal., 37, 81.

SUMMERS, J.C. and AUSEN, S.A. (1978), J. Catal., 52, 445.

SZUROMI, P.D., ENGSTROM, J.R. and WEINBERG, W.H. (1984), J. Chem. Phys., 80, 508.

SZUROMI, P.D. and WEINBERG, W.H. (1985), Surf. Sci., 149, 226.

TANG, R.Y., WU, R. and LIN, L. (1984), Appl. Catal., 10, 163.

TARDY, B., CHARCOSSET, H., ABOV, M. and BERGERET, G. (1979), Thermo. Chim. Acta., 28, 71.

TAUSTER, S.J. and FUNG, S.C. (1978), J. Catal., 55, 29.

TAUSTER, S.J., FUNG, S.C. and GARDEN, R.L. (1978), J. Am. Chem. Soc., 100, 170.

TAUSZIK, G.R., LEOFANTI, G. and GALVAGNO, S. (1984), J. Mol. Catal., 25, 357.

TSAI, M.C., MUETTERTIES, E.L. (1982a), J. Am. Chem. Soc., 104, 2534.

TSAI, M.C., FREIND, C.M. and MUETTERTIES, E.L. (1982b), J. Am. Chem. Soc., 104, 2539.

TSAI, M.C., MUETTERTIES, E.L. (1982c), J. Phys. Chem., 86, 5067.

TSUCHIYA, S., AMENOMIYA, Y. and CVETANOVIC, R.J. (1970), J. Catal., 19, 245.

TURNER, N.H., DUNLAP, B.I. and COTTON, R.J. (1984), Anal. Chem., 56, 373R.

VERBEEK, H. and SACHTLER, W.H. (1976), J. Catal., 42, 257.

VIS, J.C., VAN'T BLIK, H.F.J., HUIZINGA, T., VAN GRONDELLE, J. and PRINS, R. (1985), J. Catal., 95, 333.

DE VRIES, J.E., YAO, H.C., BAIRD, R.J. and GANDHI, H.S. (1983), J. Catal., 84, 8.

WAGNER, C.D., RIGGS, W.N., DAVIS, L.E., MOULDER, J.F. and MULLENBERG, J.E. (1979), "Handbook of X-ray Photoelectron Spectroscopy", Perkin Elmer.

WAGSTAFF, N. and PRINS, R. (1979a), J. Catal., 59, 434.

WAGSTAFF, N. and PRINS, R. (1979b), J. Catal., 59, 446.

WAGSTAFF, N. and PRINS, R. (1981), J. Catal., 67, 255.

WALKOV, W., GENKIN, M.W., SKLYAROV, A.W. and VOLTER, J. (1977), Z. Phys. Chem. (Leip)., 258, 156.

WANG, P.K., SLICHTER, C.P. and SINFELT, J.H. (1985), J. Phys. Chem., 89, 3606.

WANG, T. and SCHMIDT, L.D. (1980), J. Catal., 66, 301.

WANG, T. and SCHMIDT, L.D. (1981), J. Catal., 71, 411.

WANG, X.K. and SCHWARZ, J.A. (1985), Appl. Catal., 18, 147.

WEATHERBEE, G.D. and BARTHOLOMEW, C.H. (1984), J. Catal., 87, 55.

WEISANG, F. and GAULT, F.G. (1979), J. Chem. Soc. Chem. Comm., 519.

WELLER, S.W. and MONTAGNA, A.A. (1971), J. Catal., 21, 303.

WELLS, P.B. (1978), J. Catal., 52, 498.

WILLIAMS, F.L. and NASON, D. (1974), Surf. Sci., 45, 377.

WIMBER, R.T. and KRAUS, H.G. (1974), Metall. Trans., 5, 1565.

WITTRIG, T.S., SZUROMI, P.D. and WEINBERG, W.H. (1982a), J. Chem. Phys., 76, 716.

WITTRIG, T.S., SZUROMI, P.D. and WEINBERG, W.H. (1982b), J. Chem. Phys., 76, 3305.

WITTRIG, T.S., SZUROMI, P.D. and WEINBERG, W.H. (1982c), Surf. Sci., 116, 414.

WONG, T.K., BROWN, L.F., HALLER, G.L. and KEMBALL, C. (1981), J. Chem. Soc. Faraday Trans.1, 77, 519.

YACAMAN, M.J., ZENITH, J. and CONTRERAS, J.L. (1980), Appl. Surf. Sci., 6, 71.

YAO, U.C., SIEG, M. and PLUMMER, H.K. (1979), J. Catal., 59, 365.

ZIMMER, U., ROZANOV, V.V., SKLYAROV, A.V. and PAAL, Z. (1982), Appl. Catal., 2, 51.